UNIVERSIDAD NACIONAL AUTÓNOMA DE MÉXICO

PROGRAMA DE POSGRADO EN
CIENCIAS DE LA TIERRA
INSTITUTO DE GEOFISICA

MODELOS TERMOMECÁNICOS PARA LAS ZONAS DE SUBDUCCIÓN DE GUERRERO Y KAMCHATKA

TESIS
Para obtener el grado de
DOCTOR EN GEOFÍSICA
(SISMOLOGÍA Y FÍSICA DEL INTERIOR DE LA TIERRA)

PRESENTA

Vlad Constantin Manea

2004

A Dr. Vladimir Kostoglodov,

por todo el apoyo que me ha brindado desde mi llegada al

Departamento de Sismología

y

por haber puesto su confianza en mí.

Gracias por su amistad.

Agradecimientos

Agradezco a los coordinadores del programa de Posgrado, Drs. Blanca Mendoza Ortega y Oscar Campos-Enríquez, por todo el apoyo que me otorgaron.

Agradezco a mi comité de sinodales quienes lograron enriquecer este trabajo con sus comentarios muy atinados, a los Drs. Singh Krishna Singh, Rosa María Prol Ledesma, Juan Manuel Espíndola Castro, Iouri Taran Sobol, Luca Ferrari Pedraglio y Luis Delgado Argote.

Gracias a la beca que me otorgo la DGEP y al apoyo que me otorgaron PAEP, CONACYT (G25842-T, 37293-T), y PAPIIT (IN104801) pude finalmente concluir el doctorado con este trabajo de investigación.

Mucho aprecio al Dr. Granville Sewell por toda su ayuda en la aplicación de los métodos numéricos y por su amistad.

Muchas gracias a Dr. Carlos Mortera Gutiérrez por todo el apoyo que me brindó y por su amistad.

Muchas gracias a Drs. Carlos Valdez y Raul Valenzuela Wang por todo el apoyo y los buenos consejos que me dieron.

Muchas gracias a Dr. Arturo Iglesias que estuvo siempre cerca como buen compañero y amigo. Muchas gracias a ing. Manuel Velásquez por todo su apoyo en todos los problemas técnicos que ocurrieron y por su amistad.

Agradezco a Araceli y a Mónica del Posgrado en Ciencias de la Tierra y a Paty y Adriana del Departamento de Sismologia, por toda su ayuda con los tramites burocráticos.

Asimismo, quiero agradecer a Drs. Gillian Foulger, Taras Gerya, Bradely Hacker, Peter van Keken, Jeffery Park, Dean Presnall, Harro Schmeling, Jeroen van Hunen y Steven Ward quienes apoyaron en la revisión de los tres articulos que forman parte de esta tesis.

Sinceramente me siento afortunado por haber tenido la oportunidad de estudiar en el Posgrado en Ciencias de la Tierra de la UNAM y por haber convivido con excelentes profesores y compañeros.

INDICE

RESUMEN

La temperatura es una de las propiedades físicas de mayor importancia en la zona de subducción. La distribución de la temperatura con la profundidad y la distancia desde la trinchera depende principalmente de los siguientes parámetros: la forma de la placa subducida y la edad de la misma, la velocidad de convergencia y los parámetros térmicos de las rocas. Dentro de estos parámetros, la geometría de la placa subducida es uno de gran importancia. En el mundo existen básicamente dos tipos de geometrías para la placa subducida: una que contiene un segmento subhorizontal antes de entrar en la astenósfera (México, Chile) y otra que buza en la astenósfera a un ángulo de echado mayor y sin tener este segmento subhorizontal (México, Cascadia, Nicaragua, Costa Rica, Kamchatka). En este trabajo se han considerado dos placas oceánicas de subducción con geometrías, edades y velocidades de convergencia diferentes: una joven de ca. 14 Ma (placa de Cocos frente al estado de Guerrero) y la otra vieja de ca. 70 Ma (placa Pacífico subducida debajo de la península de Kamchatka).

Los modelos de temperatura asociados con la zona de subducción son muy útiles para estudiar fenómenos asociados a la sismicidad y el volcanismo. La sismicidad debajo de la costa esta relacionada con la temperatura, debido a que los terremotos en esta región ocurren en donde se encuentra el rango de temperatura de 100 °C - 250 °C. También los modelos térmicos son de gran interés para estudiar los reciéntemente descubiertos terremotos "*lentos*" en Guerrero (de hecho, los terremotos "*lentos*" representan una deformación que dura varios meses y es similar a la deformación observada durante un sismo normal que dura segundas) que ocurren en un rango de temperaturas de 250 °C - 450 °C. Además, en el presente estudio, a partir de la estructura térmica, se presenta un modelo de los esfuerzos termoelásticos en la placa de Cocos subducida debajo la placa de Norteamérica que podría explicar los eventos sísmicos con mecanismo normal intraplaca, que ocurren a una mayor profundidad dentro de la placa

oceánica subducida. Usando la relación entre la presión y la temperatura para basalto (diagrama de fase para basalto) y la temperatura en la superficie de la placa subducida (geoterma), obtenida a través de los modelos térmicos, se puede proporcionar información sobre los tipos de materiales (secuencias metamórficas) involucrados en el contacto entre la placa subducida y la placa continental. Otra rama de estudio derivada del conocimiento del campo térmico es el volcanismo a través de los modelos físicos para el transporte de magma en la cuña del manto (*Cap. III*).

La estructura térmica de una zona de subducción puede ser obtenida usándose el modelado numérico. Para el modelado térmico se usó un esquema numérico 2D que resuelve un sistema de ecuaciones compuesto por las ecuaciones Stokes y la ecuación del flujo de calor. El principal mineral que entra en la composición mineralogica de la cuña del manto es el olivino, así que en la preparación de los modelos termomecánicos se tomo en cuenta la reología del olivino seco. Finalmente, el sistema de ecuaciones fue resuelto con la ayuda del método de elementos finitos.

En el caso de la estructura térmica de la zona de subducción de México central, debajo del estado de Guerrero se determinó la distribución de la temperatura hasta una profundidad de 250 km para un perfil normal a la Trinchera Mesoaméricana que pasa por Acapulco y que se extiende ~ 600 km dentro del continente. Los resultados indican que la zona de fuerte acoplamiento debajo de la costa, en donde ocurren los terremotos de contacto entre las placas, corresponde a un intervalo de temperatura de 100 ° - 250 °C y se extiende hasta una distancia de ~ 80 km desde la trinchera. Los modelos de deformación que se ajustan bien a los datos de GPS, muestran que la zona acoplada debajo de Guerrero se extiende hasta una distancia, de ~ 200 km a partir de la trinchera. Después de esta región acoplada, los modelos muestran que la Placa de Cocos subducida y la Placa de Norteamérica están completamente desacopladas. Según datos experimentales, la temperatura de 450 °C representa la transición hacia un régimen de deslizamiento libre (*Cap. II*).

Posteriormente, con la ayuda del diagrama de fases para basalto se identificaron y localizaron las secuencias metamórficas en la corteza oceánica subducida. Se pudo observar que debido a los cambios metamórficos, una fuerte deshidratación ocurre a lo largo del contacto entre las dos placas, liberando hasta ~ 4 wt% de H_2O. Se observó una buena correlación entre los cambios metamórficos y los elementos con una cierta cantidad de acoplamiento de los modelos de deformación. La región en donde los terremotos lentos ocurren (aproximadamente 80 - 200 km desde la trinchera) corresponde a la facies metamórfica de esquitos azules. Junto con la liberación de agua por deshidratación, la facies de esquitos azules parece ser responsables de la ocurrencia de los eventos sísmicos lentos.

La estructura térmica debajo del volcán Popocatépetl muestra una temperatura máxima de ~ 1300 °C en la cuña del manto, que es suficiente para fundir la peridotita hidratada con agua que provendría de las reacciones de deshidratación en la placa subducida. La geoterma de la superficie de la placa subducida intercepta la curva del "*solidus*" para basalto a una profundidad de ~ 70 km y para sedimentos saturados a ~ 50 km. Esto sugiere que hay tres fuentes para producir material magmático debajo de la Faja neo volcánica mexicana: la peridotita, la placa basáltica y los sedimentos subducidos.

A continuación se desarrolló un modelo físico para el transporte de magma hasta la base de la corteza continental. En el modelo se propone que el magma es producido y se acumula en la proximidad de la superficie de la placa subducida debajo de la faja volcánica formando burbujas con diversos diámetros y viscosidades. Los resultados muestran que algunas burbujas nunca suben a la superficie, principalmente debido al diámetro pequeño (~ 0.6 km). Al aumentar el diámetro a ~ 1 km las burbujas pueden llegar hasta el Moho a través de una trayectoria sinuosa por la cuña del manto. Las burbujas llegan en lugares distintos, dependiendo de su diámetro y viscosidad. Si el diámetro aumenta hasta 10 km, todas las burbujas llegan al mismo punto justamente arriba del punto de formación.

En el capitulo IV, el mismo esquema numérico fue aplicado para la zona de subducción muy vieja (> 70 Ma) de Kamchatka. El perfil para el modelado de esta región está ubicado en el sur de Kamchatka, lejos del contacto entre la trinchera de Kamchatka y el arco de Aleutianas en donde hay una anomalía térmica muy fuerte. Los modelos muestran una temperatura > 1300 °C debajo del área volcánica, suficiente para producir los magmas calcialcalinos comunes en Kamchatka. Un problema complejo es obtener la distribución de la temperatura en la cuña del manto. En ese sentido es de gran ayuda la tomografía sísmica. En la parte sur de Kamchatka se usó una relación entre la atenuación de las ondas sísmicas y la temperatura de fusión del olivino para obtener un modelo de anomalías de velocidad debajo de la faja volcánica a partir de un modelo térmico. La anomalía de velocidad obtenida con este método para el Sur de Kamchatka muestra una anomalía negativa de 7% debajo del área volcánica. Este resultado concuerda con la anomalía de velocidad en la tomografía sísmica con atenuación de 7%. Aunque la forma de la anomalía de velocidad es diferente, una buena correlación con la magnitud podría darnos una indicación sobre una buena estimación de la magnitud de la temperatura en la cuña del manto. El modelo de las burbujas flotantes también se utilizó para el sur de Kamchatka, pero en este caso se calculó numéricamente la historia térmica de una burbuja de 10 km en diámetro que sube hasta el Moho en 2.6 Ma. El esquema numérico utiliza el mecanismo de transferencia del calor por conducción entre la burbuja y el manto. Los resultados muestran que la burbuja alcanza el Moho sin solidificarse, teniendo para el 90% de ella una temperatura mayor a 900 °C. Este resultado sugiere la posibilidad de acumulación de estas burbujas en la base del Moho, probablemente formando una cámara magmática profunda debajo del área volcánica.

Una característica adicional de la zona de subducción en la parte central de México, es la presencia exclusiva de terremotos cuyos mecanismos focales son normales (extensión) dentro de la placa oceánica subducida. Como la mayor parte de estos eventos normales se ubica dentro de la parte subhorizontal de la placa, hay muy poca influencia en el campo de esfuerzos debido al doblamiento de la

placa. La disponibilidad de un modelo térmico para Guerrero se usó para determinar los esfuerzos termoelásticos dentro de la litosfera oceánica (*Cap V*).

El esquema numérico usa las ecuaciones clásicas de la teoría de termoelasticidad en placas delgadas. Los resultados muestran una distribución de los esfuerzos termoelásticos que consiste en tres capas: una capa central caracterizada por esfuerzos termoelásticos de tensión máximos de 0.3 kbar y dos capas externas con esfuerzos termoelásticos de compresión máximos de 0.65 kbar. La capa inferior con esfuerzos de compresión se desvanece cuando en la base de la litosfera se incluye una ley de decaimiento exponencial de los esfuerzos debido a temperaturas mayores de 700 °C. También, incluyendo un momento de torsión para la parte horizontal de la placa subducida, la capa superior de esfuerzos de compresión se desvanece. Este momento de torsión se produce porque la placa subducida baja en la astenósfera. De este manera se queda nada mas una capa de esfuerzos de extensión con una magnitud de 0.5 kbar en donde la mayoría de los sismos de extensión se encuentran. La ubicación de la isoterma de 700°C concuerda bien con la profundidad máxima de los terremotos intraplaca y se puede considerar como una temperatura de corte. Para temperaturas mayores a este valor de corte, los terremotos no pueden existir debido al comportamiento dúctil de la placa oceánica subducida.

Este estudio demuestra que los modelos térmicos para la zona de subducción proporcionan informaciones útiles para los estudios geodinámicos relacionados con los eventos sísmicos lentos, la sismicidad entre las placas y la sismicidad dentro de la placa subducida, a través de los esfuerzos termoelásticos. También, los modelos de flujo en la cuña del manto permiten estudiar el comportamiento de los magmas en su trayecto hacia la base de la corteza continental.

I INTRODUCCIÓN

Una de las características más importantes de la zona de subducción mexicana es la forma subhorizontal de la placa subducida en la parte central, debajo del estado de Guerrero (*Kostoglodov et al., 1996*). Otra particularidad importante de esta area es la presencia de la brecha sísmica de Guerrero, que se extiende ~ 120 km desde Acapulco hacia el NE, no ha producido ninguna ruptura desde 1911, mientras que en las zonas cercanas han ocurrido grandes terremotos de mecanismo inverso.

Observaciones recientes de GPS en Guerrero muestran que el acoplamiento intraplaca durante el periodo intersísmico es anormalmente largo, con una extensión desde la trinchera, entre 180 y 220 km hacia el continente (*Kostoglodov et al., 2003*). Algunos modelos térmicos propuestos para la zona de subducción de Guerrero (*Currie et al., 2002*), no toman en cuenta la zona de acoplamiento de ~ 200 km debido a la falta de esa información en aquellos tiempos.

Usando la geometría de la placa subducida de *Kostoglodov et al. (1996)* y una área grande parcialmente acoplada de cerca de 220 km desde la trinchera, el modelo de dislocación de *Kostoglodov et al. (2003)* se ajusta bien con los datos de deformación observados. Haciendo la comparación del modelo de la dislocación que usa la geometría de la placa de *Currie et al. (2002)* con las deformaciones observadas en la superficie, no se puede observar una buena correlación debido a la geometría de la placa subducida y a la extensión limitada de la zona parcialmente acoplada. Nuevos estudios son necesarios para refinar los modelos existentes y para explicar la zona de acoplamiento de gran extensión (~ 200 km) desde la trinchera. También, estudios adicionales son necesarios para verificar una posible correlación entre los cambios metamórficos a lo largo del contacto entre las placas de Cocos y Norteamérica y las zonas con diversos grados de acoplamiento que satisfacen los modelos de deformación de *Kostoglodov et al. (2003)*.

Los pocos modelos térmicos que hay para la zona de subducción de México (*Currie et al., 2002; Manea et al., 2004a*) no presentan una estructura térmica detallada y confiable porque no toman en la cuenta la reología de la astenósfera. Los modelos termomecánicos de la cuña del manto con reología dependiente de la temperatura y/o la tasa de deformación están desarollandose (*Furukawa, 1993; Conder et al., 2002; Van Keken et al., 2002; Kelemen et al, 2003*). La dinámica de la cuña del manto y la estructura térmica de las zonas de subducción subhorizontales someras han sido investigadas recientemente por *van Hunen et al. (2002)*.

El modelo térmico previo para la zona de subducción de Guerrero con una interfaz somera de la placa usando una expresión analítica predefinida para el flujo en el rincón del manto (*Currie et al., 2002*), predice una temperatura de ~ 900°C para la astenósfera debajo del frente volcánico (por ejemplo, el volcán Popocatépetl), considerada muy baja para producir fundido. En este modelo, el componente basáltico de la placa subducida tampoco alcanza la temperatura del fundido. Como consecuencia, este modelo no puede explicar la fuente del magma para el Cinturón Volcánico Trans-Mexicano (CVTM) en su parte central.

El CVTM es un arco volcánico neógeno construido sobre el borde sur de la placa de Norteamérica (*Ferrari et al., 1999*). *Moore et al. (1994)* es el primero en sugerir la presencia de una pluma del manto debajo Guadalajara. Este modelo ha sido expandido mas tarde por *Márquez el al. (1999)*. Ellos proponen que todo el CVTM esta relacionado con una pluma del manto que impactó la parte oeste de México en el Mioceno tardío. En el modelo de *Márquez et al.(1999)* la pluma corta primero la placa subducida que, a su turno, puede cortar la cabeza de la pluma. Los dos modelos se apoyan en los datos de geoquímica y no ajustan con la geología y tectonica del CVTM. En un comentario por *Ferrari y Rosas (1999)*, acerca del trabajo de *Marquez et al. (1999)* se señala que: ni el rifting ni los magmas tipo OIB (Ocean Island Basalt) no presentan el aumento de la edad requerido por el modelo de la pluma; también, en el oeste de México, en donde la pluma podría impactar, no hay ninguna evidencia de levantamiento regional;

asimismo, el volumen de los magmas OIB en el CVTM representa nada mas una fracción del volcanismo relacionado con la subducción, y mucho más pequeña que los flujos basalticos continentales típicos.

Sheth et al. (2000) y *Verma (2002)* han hecho recientemente comentarios sobre el papel de la subducción en la génesis del CVTM y propusieron que el rifting continental encima del manto heterogéneo podría ser el mecanismo de formación. El rechazo de la influencia de la subducción sobre la génesis del CVTM se fundamenta por lo general en las bases petrológicas y de estadística geoquímica, con la ayuda de una interpretación sencilla acerca de la falta de sismicidad debajo del arco. En este estudio se aclara que la falta de sismicidad debajo el CVTM es debido a las temperaturas muy altas (> 700 °C) en la placa subducida de Cocos.

Recientemente, *Cervantes y Wallace (2003)* analizaron los elementos mayores y de traza en las inclusiones fundidas en algunos conos de ceniza en Sierra Chichinautzin. Encontraron lavas con alto contenido de agua, señalando que los fluidos de subducción penetran el manto debajo de CVTM. *Gómez-Tuena et al. (2003)* encontraron la presencia de un cinturón WNW-ESE con una firma adakitica, sugiriendo que parte de la placa subducida debajo del CVTM está fundida. Esta es otra evidencia sobre la influencia de la subducción debajo el CVTM.

Un modelo reciente por *Ferrari (2004)* propone un mecanismo basado en el desprendimiento de la placa subducida y unas infiltraciones de la astenósfera enriquecida con el fin de explicar la ocurrencia de los magmas de tipo OIB.

Estudios geológicos recientes (*Luhr, 1997; Márquez et al., 1999a*) sugieren que hay un manto complejo debajo del CVTM. Sin embargo, el origen de los basaltos tipo OIB no es muy claro todavía. La advección en el manto astenosférico debido al buzamiento de la Placa de Cocos ha sido propuesta como una fuente posible de los magmas tipo OIB (*Wallace y Carmichael, 1999*). Hay algunos estudios mineralógicos y geoquímicos sobre el CVTM (*e.g. Márquez y De Ignacio, 2002*) que sugieren la existencia de dos tipos primitivos de magmas máficos: uno

con un componente *"astenosférico"* tipo OIB y el otro con un componente *"litosférico"*. Aunque la corelación entre el volcanismo y la Placa de Cocos es conocida (*e.g. Pardo y Suárez, 1995; Wallace y Carmichael, 1999*) hay hipótesis diferentes con respecto al origen del volcanismo en esta área como: la extensión del sistema de fallas del Golfo de California (*Ferrari et al., 1994*), una zona de corteza vieja debilitada (*Cebull y Schubert, 1987*), mecanismos de transpresión de la corteza (*Shubert y Cebull, 1984; Ferrari et al., 1990*) y rifting (*Luhr, 1997; Márquez et al., 1999a,b*).

También, la fuente de los fluidos que metasomatizan el manto no es clara. Hay tres posibilidades propuestas como explicación para el manto metasomatizado (*Márquez et al., 1999c; Wallace y Carmichael, 1999; Verma, 1999; 2000*): a) la cuña del manto afectada por los fluidos generados por la deshidratación de la Placa de Cocos subducida; b) el manto litosférico viejo, enriquecido; c) el manto metasomatizado por los volátiles de los plumas del manto. Es imposible obtener evidencias directas acerca de la cuña del manto metasomatizada por los fluidos liberados de la placa oceánica subducida, aunque eventualmente, los xenolitos del manto son raras veces encontrados en las lavas de los arcos volcánicos. En el CVTM las andesitas hornbléndicas cuaternarias que irrumpen en la proximidad del área de El Peñón (ver la *Fig.1, pp.87*) contienen xenolitos de 1 - 2 cm, ricos en fenocristales de hornblenda y con matriz andesítica empobrecida en plagioclasa (*Blatter y Carmichael, 1998*). Todas estas observaciones sugieren un flujo de volátiles, que provienen de la placa subducida, en la cuña del manto.

Debajo del CVTM la subida del magma hacia la superficie produce grandes estratovolcanes y volcanes monogéneticos más pequeños esparcidos en áreas grandes. En su parte central, el CVTM contiene algunos estratovolcanes como Popocatépetl, Iztaccíhuatl y Nevado de Toluca. Los volcanes monogéneticos están representados en general por conos de lava, conos de ceniza, así como domos y flujos de lava. Mientras los estratovolcanes se caracterizan por la periodicidad de sus erupciones, los volcanes monogéneticos presentan un solo evento eruptivo y

por esto, tienen menor tamaño. *Takada (1989, 1994)* proponen un mecanismo doble que relaciona el aporte de magma y el esfuerzo regional.

El relleno sedimentario en la trinchera Mesoamericana es muy pequeño, sugiriendo que ~ 95% de esto sedimentos entran en subducción (*Manea et al., 2003*). Un flujo de volátiles de la placa oceánica metamorfizada y de los sedimentos puede iniciar la fusión parcial de la peridotita en la proximidad de la placa subducida (*Tatsumi, 1986; Davies y Stevenson, 1992*). *Gerya y Yuen (2003)* proponen que una instabilidad Raileigh-Taylor desarrollada en la superficie de la placa subducida puede generar burbujas flotantes hasta de 10 km de diámetro que pueden penetrar la cuña del manto. *Gerya y Yuen (2003)* sugieren que la composición química de estas burbujas está relacionada con el fundido parcial de la corteza oceánica basaltica y gabroica, el fundido parcial del manto hidratado y con los sedimentos oceanicos fundidos.

Además de las características de la zona de subducción de Guerrero relacionadas con la forma de la placa y la extensión de la zona acoplada, hay otra característica importante: todos los terremotos intraplaca en la zona de Guerrero tienen mecanismo normal, ocurriendo a partir de ~ 85 km de la trinchera.

Se ha aceptado que la litósfera oceánica fría que se subduce, entra en el manto más caliente produciendo esfuerzos termoelásticos importantes que pueden generar terremotos intraplaca. La distribución de los esfuerzos termoelásticos ha sido propuesta como una explicación para un doble plano de falla en varias zonas de subducción como Japón y Kamchatka (*Hamaguchi et al., 1983, Gorbatov et al., 1997*). La distribución de los esfuerzos termoelásticos según *Hamaguchi et al. (1983)* muestra esfuerzos de compresión muy grandes (hasta 10 kbars) para la parte superior e inferior de la placa subducida, y esfuerzos de tensión (hasta 7.5 kbars) para la parte central de la placa. Estos valores son con ~ 2 órdenes de magnitud mayores que la caída de esfuerzos durante los terremotos intraplaca (~ 0.1 kbars).

Estos valores muy grandes de los esfuerzos termo-elásticos están relacionados con un gran contraste de temperatura de hasta $\Delta T = 1000°C$ dentro

de la placa subducida. La estructura simplificada de la cuña del manto propuesta por *Hamaguchi et al. (1983)* está representada por un gradiente térmico de 10°C/km hasta 100 km de profundidad y 5°C/km hasta 150 km de profundidad. Los modelos termomecánicos más recientes para la cuña del manto con una reología dependiendo de temperatura y/o esfuerzo (*Furukawa, 1993; Conder et al., 2002; Van Keken et al., 2002; van Hunen et al., 2002; Kelemen et al, 2003, Manea et al., 2004b*) muestran una distribución más complicada de la temperatura. De este modo, el contraste de temperatura dentro de la placa subducida está controlado por la estructura térmica de la cuña del manto.

Nuevos estudios acerca del campo de esfuerzos termoelásticos en la zona de subducción mexicana son necesarios y esto se puede realizar usando los modelos térmicos recientes, desarrollados para una viscosidad en la cuña del manto, dependiendo muy fuerte de la temperatura

Además, es necesario un estudio para investigar la relación entre los esfuerzos termoelásticos y los terremotos normales intraplaca debajo de la zona de subducción de Guerrero.

Otra zona de subducción importante, considerada como vieja, es la zona de subducción de Kamchatka. Hasta la fecha no hay un estudio de la distribución del campo térmico asociado al fenómeno de subducción en esta región, aunque hay muchos estudios con respecto a la composición del magma a lo largo de la península (por ejemplo *Graybill et al., 1999*).

Para investigar con detalle la distribución del campo térmico debajo del centro del CVTM y sur de Kamchatka, nuevos modelos termomecánicos son necesarios, incluyendo la reología del olivino (el mineral más abundante en el manto superior). Además, para proporcionar más información acerca de la fuente del magma un modelo de propagación del magma a través de la cuña del manto permitirá mejorar nuestro conocimiento sobre la relación entre el volcanismo y la dinámica de la zona de subducción.

Las metas principales del presente estudio son:

-Estudiar la relación entre el campo térmico y la ocurrencia de los eventos sísmicos lentos en México;

-Examinar una posible dependencia entre los cambios metamórficos a lo largo del contacto entre las placas de Cocos y Norteamérica y los modelos de deformación existentes;

-Obtener la distribución del campo térmico y convectivo debajo del CVTM y de la parte sur de Kamchatka;

-Estudiar la relación entre las condiciones de *P-T* debido a los modelos térmicos y la composición química de los productos volcánicos en superficie;

-Estudiar uno de los posibles mecanismos de transporte del magma desde la superficie de las placas subducidas (Placa de Cocos y Placa de Norteamérica) hasta el Moho.

Adicionalmente, este estudio trata de:

-Obtener una imagen tomográfica a partir de los modelos térmicos debajo del sur de Kamchatka y compararla con la imagen tomográfica ya existente obtenida a partir de la atenuación de las ondas sísmicas P;

-Calcular los esfuerzos termoelásticos en la Placa de Cocos debajo del estado de Guerrero y compararlos con la distribución de los sismos intraplaca en la región.

En el capítulo II se presenta un estudio que determinan las relaciones entre el modelo térmico y la ocurrencia de los terremotos lentos en México. Además, con la ayuda del diagrama de fases para basalto se investiga la correlación entre los cambios metamórficos a lo largo del contacto entre las placas y los resultados del modelado de deformación que satisfacen los datos observados. El capítulo III se enfoca en la distribución del campo térmico y de velocidades debajo del CMVB. Se analiza también la propagación del magma hacia el Moho usando un modelo

físico de burbujas flotantes en un manto convectivo. En el capítulo IV se aplica el mismo esquema numérico para obtener la distribution de la temperatura para el sur de Kamchatka. Además, el modelo de burbujas flotantes se desarrolla con mayor detalle para tener un mejor conocimiento sobre la evolución térmica de las burbujas a través del manto. En este capítulo, la disponibilidad de una tomografía sísmica para el sur de Kamchatka hace posible constreñir el campo térmico debajo del CVTM. En el capítulo V se calculan los esfuerzos termoelásticos inducidos por la distribución nouniforme de la temperatura en la Placa de Cocos debajo del estado de Guerrero. Se estudia también la correlación entre la distribución de los esfuerzos termoelásticos y la sismicidad intraplaca en la región. En el capítulo VI se presentan la discusión y las conclusiones del trabajo en su conjunto.

REFERENCIAS

Blatter, D.L., and Carmichael, I.S.E., 1998. Hornblende peridotite xenoliths from central Mexico reveal the highly oxidized nature of subarc upper mantle. *Geology, v. 26, no. 11, pp. 1035-1038.*

Carmichael, I.S.E., 2002. The andesite aqueduct: perspectives on the evolution of intermediate magmatism in west-central (105° 99' W) México. *Contribution Mineral Petrology, 143, 641-663.*

Cebull, S.E., and Schubert, D.H., 1987. Mexican Volcanic Belt-an intraplate transform. *Geofisica Internacional, v.26, pp. 1-13.*

Cervantes P., and Wallace P., 2003. Role of H2O in subduction zone magmatism: new insights from melt inclusions in high-Mg basalts form central México. *Geology, 31, 235-238.*

Conder, J.A., Weins, D.A., and Morris, J., 2002. On the decompression melting structure at volcanic arcs and back-arc spreading centers. *Geophysical Research Letters, vol. 29, 17-1-17-4.*

Currie, C.A., Hyndman, R.D., Wang, K., and Kostoglodov, V., 2002. Thermal models of the Mexico subduction zone: Implications for the megathrust seismogenic zone. *Journal of Geophysical Research, 107, no. B12, 2370, doi: 10.1029/2001JB000886.*

Davies, J.H., and Stevenson, D.J., 1992. Physical model of source region of subduction zone volcanism. *Journal of Geophysical Research, v. 97, p. 2037-2070.*

Ferrari, L., Pasquare, G., and Tybaldi, A., 1990. Plio-Quaternary tectonics on the central Mexican Volcanic Belt and some constraints on its rifting mode. *Geofisica Internacional, v. 29, pp. 5-18.*

Ferrari, L., Garduno, V., Innocenti, F., Manetti, P., Pasquere, G., and Vaggeli, G., 1994. Volcanic evolution of central Mexico: Oligocene to Present. *Geofisica Internacional, 33, 91-105.*

Ferrari L., and Rosas-Elguera, J., 1999. Alkalic (OIB type) and calc-alkalic volcanism in the Mexican Volcanic Belt: a case for plume-related magmatism and

propagating rifting at an active margin? Comment to the article by Marquez, A., Oyarzun, R., Doblas, M., Verma, S. P. *Geology, 27, 1055-1056.*

Ferrari L., Conticelli S., Vaggelli C., Petrone C., and Manetti P., 2000. Late Miocene mafic volcanism and intra-arc tectonics during the early development of the Trans-Mexican Volcanic Belt. *Tectonophysics, 318, 161-185.*

Ferrari L., 2004. Slab detachment control on volcanic pulse and mantle heterogeneity in Central Mexico. *Geology, v. 32, p. 77-80.*

Furukawa, F., 1993. Magmatic processes under arcs and formation of the volcanic front. *Journal of Geophysical Research, 98, 8309-8319.*

Gerya, T.V. and Yuen, D.A., 2003. Rayleigh-Taylor instabilities from hydration and melting propel 'cold plumes' at subduction zones. *Earth and Planetary Science Letters, v. 212, p. 47-62.*

Gómez-Tuena A., LaGatta A., Langmuir C., Goldstein S., Ortega-Gutierrez F., and Carrasco-Nuñez G., 2003. Temporal control of subduction magmatism in the eastern Trans-Mexican Volcanic Belt: mantle sources, slab contributions and crustal contamination. *Geochemistry, Geophysics and Geosystems, 4, DOI:10.1029/2003GC000524, 1-33.*

Gorbatov, A., Kostoglodov, V., Suárez, G., and Gordeev, E., 1997. Seismicity and structure of the Kamchatka subduction zone. *Journal of Geophysical Research, v. 102, no. B8, p. 17,883-17,898.*

Graybill, J., Brandon, M.T., and Kepezhinskas, P.K., 1999. Olivine lattive-preffered orientation in xenoliths from the mantle wedge beneath the southern Kamchatka volcanic arc (abstract). *Eos Trans. AGU, 80, F926.*

Hamaguchi, H., Goto, K., and Suzuki, Z., 1983. Double-planed structure of intermediate-depth seismic zone and thermal stress in the descending plate. *Journal of Physics of the Earth, 331, 329-347.*

Kelemen, P.B., Rilling, J.L., Parmentier, E.M., Mehl, L., and Hacker, B.R., 2003. Thermal Structure due to Solid-State Flow in the Mantle Wedge Beneath Arcs: in Inside the Subduction Factory, *Geophysical Monograph 138*, edited by Eiler, J., *AGU, Washington DC, p. 293-311.*

Kostoglodov, V., Bandy, W., Dominguez, J., and Mena, M., 1996. Gravity and seismicity over the Guerrero seismic gap, Mexico. *Geophysical Research Letters, 23, 3385-3388.*

Kostoglodov, V., Singh, S. K., Santiago, J. A., Franco, S. I., Larson, K. M., Lowry, A. R., and Bilham, R., 2003. A large silent earthquake in the Guerrero seismic gap, Mexico. *Geophysical Research Letters, 30(15), 1807,* doi:10.1029/2003GL017219.

Luhr, J.F., 1997. Extensional tectonics and the diverse primitive volcanic rocks in the western Mexican Volcanic Belt. *Canadian Mineralogy. 35: 473-500.*

Manea, M., Manea, V.C., Kostoglodov, V., 2003. Sediment fill of the Middle America Trench inferred from the gravity anomalies. *Geofisica Internacional, 42, (4), 603-612.*

Manea, V.C., Manea, M., Kostoglodov, Currie, C.A., and Sewell, G., 2004a. Thermal Structure, Coupling and Metamorphism in the Mexican Subduction Zone beneath Guerrero. *Geophysical Journal International, 158, 775–784 doi: 10.1111/j.1365 - 246X.2004.02325.x.*

Manea, V.C., Manea, M., Kostoglodov, V., Sewell, G., 2004b. *(in press)* Thermo-mechanical model of the mantle wedge in Central Mexican subduction zone and a blob tracing approach for the magma transport. *Physics of the Earth and Planetary Interiors.*

Márquez, A., Oyarzun, R., Doblas, M., Verma, S.P., 1999a. Alkalic (OIB-type) and calc-alkalic volcanism in Mexican volcanic belt: a case study of plume-related magmatism and propagating rifting at an active margin? *Geology, 27: 51-54.*

Márquez, A., Oyarzun, R., Doblas, M., Verma, S.P., 1999b. Replay to comment to: Alkalic (OIB-type) and calc-alkalic volcanism in Mexican volcanic belt: a case study of plume-related magmatism and propagating rifting at an active margin? *Geology, 27: 1055-1056.*

Márquez, A., Verma, S.P., Anguita, F., Oyarzun, R., Brandle, J.L., 1999c. Tectonics and volcanism of Sierra Chichinautzin: extension at the front of the

central Trans-Mexican Volcanic Belt. *Journal of Volcanology and Geotherm. Research, 93, 125-150.*

Márquez, A. and De Ignatio, C., 2002. Mineralogical and geochemical constrains for the origin and evolution of magmas in Sierra Chichinautzin, Central Mexican Volcanic Belt. *Lithos, 62, 35-62.*

Moore, G., Marone, C., Carmichael, I.S.E., and Renne, P., 1994. Basaltic volcanism and extension near the intersection of the Sierra Madre volcanic province and the Mexican Volcanic Belt. *GSA Bulletin, 106, 383-394.*

Pardo, M., and Suárez, G., 1995. Shape of the subducted Rivera and Cocos plates in southern mexico: seismic and tectonic implications. *Journal of Geophysical Research, 100, 12357-12373.*

Sheth, H., Torres-Alvarado, I., and Verma, S. P., 2000. Beyond subduction and plumes: A unified tectonic-petrogenetic model for the Mexican Volcanic Belt. *International Geology Review, 42, 1116-1132.*

Shubert, D.H., and Cebull, S.E., 1984. Tectonic interpretation of the Trans-Mexican volcanic belt. *Tectonophysics, 101, pp.159-165.*

Takada, A., 1989. Magma transport and reservoir formation by a system of propagating cracks. *Bulletin of Volcanology, v. 52, pp.118-126.*

Takada, A., 1994. The influence of regional stress and magmatic input on styles of monogenetic and polygenetic volcanism. *Journal of Geophysical Research, v. 99, pp. 13563-13573.*

Tatsumi, Y., 1986. Formation of the volcanic front in subduction zones. *Geophysical Research Letters, v. 13, p. 717-720.*

van Keken, P.E., Kiefer, B., and Peacock, S.M., 2002. High resolution models of subduction zones: Implications for mineral dehydration reactions and the transport of water into deep mantle. *G-cubed , 3, 10, 20.*

von Hunen, J., van den Berg, A., and Vlaar, N., 2002. On the role of subducting oceanic plateaus in the development of shallow flat subduction. *Tectonophysics, 352, 317-333.*

Verma, S.P., 1999. Geochemistry of evolved magmas and their relationship to subduction un-related mafic volcanism at the volcanic front of the central Mexican Volcanic Belt. *Journal of Volcanology and Geothermal Research, v.93, pp. 151-171.*

Verma, S.P., 2000. Geochemistry of subducting Cocos plate and the origin of subduction-unrelated mafic volcanism at volcanic front of central Mexican Volcanic Belt, in Delgado-Granados, H., Aquirre-Diaz, G.J., and Stock, J., eds., Cenozoic tectonics and volcanism of Mexico: Boulder Co., *Geological Society of America, Special Paper, 334 , pp. 195-222.*

Verma S.P., 2002. Absence of Cocos plate subduction-related mafic volcanism in southern Mexico: A unique case on Earth? *Geology, 30, 1095-1098.*

Wallace, P., Carmichael, I.S.E., 1999. Quaternary volcanism near the Valley of Mexico: implications for subduction zone magmatism and the effects of crustal thickness variations on primitive magma compositions. *Contribution to Mineral Petrology. 135, 291-314.*

II. ESTRUCTURA TÉRMICA, ACOPLAMIENTO Y METAMORFISMO EN LA ZONA DE SUBDUCCIÓN MEXICANA DEBAJO DEL ESTADO DE GUERRRO

THERMAL STRUCTURE, COUPLING AND METAMORPHISM IN THE MEXICAN SUBDUCTION ZONE BENEATH GUERRERO

V.C. Manea[1], M. Manea[1], V. Kostoglodov[1], C.A. Currie[2,3], and G. Sewell[4]

[1] Instituto de Geofísica, Universidad Nacional Autónoma de México (UNAM), México

[2] School of Earth and Ocean Sciences, University of Victoria, Victoria, B.C., Canada

[3] Pacific Geoscience Centre, Geological Survey of Canada, Sidney, B.C., Canada

[4] University of Texas, El Paso, USA

ABSTRACT.

Temperature is one of the most important factors that controls the extent and location of the seismogenic coupled, and transition, partially coupled segments of the subduction interplate fault. The width of the coupled fault inferred from the continuous GPS observations for the steady interseismic period and the transient width of the last slow aseismic slip event ($M_w \sim 7.5$) that occurred in the Guerrero subduction zone in 2001 - 2002, extends up to 180 km - 220 km from the trench. Previous thermal models do not consider this extremely wide coupled interface in Guerrero subduction zone that is characterized by shallow subhorizontal plate contact. In this study, a finite element model is applied to examine the temperature

constraints on the width of the coupled area. The numerical scheme solves a system of 2D Stokes equations and 2D steady state heat transfer equation.

The updip limit of the coupling zone is taken between 100°C and 150°C, while the downdip limit is accepted at 450°C as the transition from partial coupling to stable sliding. From the entire coupled zone, the seismogenic zone extends only up to ~ 82 km from the trench (inferred from the rupture width of large subduction thrust earthquakes), corresponding to the 250°C isotherm. Only a small amount of frictional heating is needed to fit the intersection of the 450°C isotherm and the subducting plate surface at 180 - 205 km from the trench.

The calculated geotherms in the subducting slab and the phase diagram for MORB are used to estimate the metamorphic sequences within the oceanic subducting crust. A certain correlation exists between the metamorphic sequences and the variation of the coupling along the interplate fault.

INTRODUCTION

The most crucial feature of the Mexican subduction zone is a shallow subhorizontal plate interface in its central part beneath the Guerrero state *(Kostoglodov et al., 1996)*. This particular configuration of the young subducting Cocos plate (~ 14 Myr) apparently creates some distinct geodynamic consequences, such as very thin continental lithosphere, relatively shallow intraslab seismicity, remote position of the volcanic front, etc. The Guerrero seismic gap extending ~ 120 km northwest from Acapulco (*Fig. 1*) has never ruptured since 1911, meanwhile the neighboring zones suffered large subduction thrust earthquakes.

Recent continuous GPS observations in Guerrero show that the interplate coupling during the steady-state interseismic period is abnormally wide, extending up to 180 - 220 km inland from the trench *(Kostoglodov et al., 2003)*. A few thermal models of the subduction zone in Guerrero have been proposed *(Currie et al., 2002)*, however they take no account of the ~ 200 km-wide coupled zone (because of the lack of this information at that time).

In a recent study of *Kostoglodov et al. (2003)*, the surface deformation inferred from GPS measurements during this last slow slip earthquake are compared with the results from the 2D forward dislocation model for an elastic half space *(Savage, 1983)*. The steady-state component of GPS site velocities is modeled as constant-velocity slip on the subduction interface. In this approach, a virtual slip or "*back-slip*" with magnitude and direction equal and opposite the relative plate motion, is used to represent frictional coupling on the megathrust. On any given discrete segment of the megathrust, it is assumed that the steady state slip rate is some fraction (coupling (α)) of the relative plate motion: $\alpha = S_b / S_{rpm}$, where $\alpha = [0 - 1]$; S_b is the back-slip rate; S_{rpm} is the relative slip between Cocos and North American plates (5.5 cm/yr from *NUVEL 1A* model of *DeMets et al., 1994*). When $\alpha = 0$, no coupling between the two plates is considered (perfectly

decoupled *"back-slip"* segment) and $\alpha = 1$ indicates a full coupling between the oceanic plate and the overriding continental plate (perfectly coupled *"back-slip"* segment).

Using the slab geometry from *Kostoglodov et al., (1996)* and a wide partially couple zone (~ 220 km from the trench), the dislocation model of *Kostoglodov et al. (2003)* show a reasonable well fit with the observations (*Fig. 2*). The best model fits the GPS measurements when the plate interface is partially locked on three segments. The first segment is located in the shallower part of the subducting plate with a coupling of $\alpha = 0.9$. It follows two partially coupled segments with $\alpha = 0.7$. The rest of the interface slips freely ($\alpha = 0.0$). In order to obtain a good fit with the observed data, the partially coupled segment was extended up to 215 km from trench.

A dislocation model with the slab geometry from *Currie et al. (2002)* do not offer a good fit with the observed surface deformations, because of the slab geometry and the limited extent of the partially coupled zone.

In the view of these new results for the Guerrero subduction zone, the motivation of the present paper is to review the previous published thermal structure for Guerrero, and to offer a possible explanation for the largest silent earthquake ever recorded. The largest slow aseismic slip event in Guerrero (2001-2002) has developed almost over the entire width of the previously coupled plate interface *(Kostoglodov et al., 2003)*. The discovery of this large slow aseismic event and the non-episodic occurrence of such extensive slow earthquake in Guerrero gap (*Fig. 1*), call for an examination of the controlling factors and physical conditions associated with these events.

It is assumed that pressure, temperature and rock composition provide the key controls on the extent and location of the seismogenic zone (*Peacock and Hyndman, 1999*). The main goal of this study is to analyze this wide subhorizontal coupled plate interface beneath Guerrero using a numerical modeling of the thermal structure in this subduction zone. The interplate geometry and coupling extension is better constrained (*Kostoglodov et al., 2003*) than in the previous

models (*Currie et al., 2002*). We developed the 2D steady - state thermal models using a numerical scheme with a system of 2D steady state heat transfer equation and 2D Stokes equations.

The updip and downdip limits of the interplate and slow slip earthquakes have been attributed to a certain temperature range. While, the seismogenic, coupled zone, where large interplate earthquakes often occur, is confined by 100 - 150°C and $\leq$ 350°C isotherms, the partially coupled, transient zone, is delimited by $\leq$ 350°C and 450°C isotherms (*Fig. 3) (Wang, 1980; Tse and Rice, 1986; Blanpied et al., 1985; Hyndman and Wang, 1993)*. The position of the updip limit of the seismogenic zone at 100 - 150°C has been attributed to the presence of the stable subducted sliding sediments (*Vrolijk, 1990*).

Since laboratory experiments (*Blanpied et al., 1995)* show that continental rocks exhibit a transition from velocity weakening to velocity strengthening at 325°C - 350°C, this temperature range was proposed to be the downdip limit of the seismogenic zone. However, the experiments were carried out on quartzo-feldspathic continental rock type, while the mineralogical composition of the subducting oceanic crust is quite different. Therefore the 325°C - 350°C temperature range for the dowdip limit of the seismogenic zone should not be considered so restrictive, it may be quite variable from one subduction zone to another.

The final intention of this study is to verify a possible relationship between the predicted metamorphic facies along the subducting oceanic plate (*Hacker et al., 2003)* and the width of the interplate coupling inferred from the modeling of the surface crustal deformations observed during the interseismic steady-state period and the last silent earthquake in Guerrero.

MODELING PROCEDURE

A system of 2D Stokes equations and the 2D steady state heat transfer equation are solved for the Guerrero cross section *(Fig. 1)* using the finite element solver PDE2D (*http://pde2d.com/*). The equations in an explicit form are:

$$
\begin{cases}
\dfrac{\partial\left(-P+2\eta\dfrac{\partial u}{\partial x}\right)}{\partial x} + \dfrac{\partial\left(\eta\left(\dfrac{\partial u}{\partial y}+\dfrac{\partial v}{\partial x}\right)\right)}{\partial y} = 0 \\[6mm]
\dfrac{\partial\left(\eta\left(\dfrac{\partial u}{\partial y}+\dfrac{\partial v}{\partial x}\right)\right)}{\partial x} + \dfrac{\partial\left(-P+2\eta\dfrac{\partial v}{\partial y}\right)}{\partial y} = -\rho\cdot g \\[6mm]
C_p\left(u\dfrac{\partial T}{\partial x}+v\dfrac{\partial T}{\partial y}\right) = \dfrac{\partial}{\partial x}\left(k\dfrac{\partial T}{\partial x}\right) + \dfrac{\partial}{\partial y}\left(k\dfrac{\partial T}{\partial y}\right) + Q + Q_{sh}
\end{cases}
\tag{1}
$$

where:

P - pressure (Pa),

η - mantle wedge viscosity (isoviscous mantle wedge) (Pa s),

u - horizontal component of the velocity (m/s),

v - vertical component of the velocity (m/s),

ρ - density (kg/m^3),

T - temperature (°C),

C_p - thermal capacity (MJ/m^3 °K),

k - thermal conductivity (W/m°K),

Q - radiogenic heat production (W/m^3),

Q_{sh} - volumetric shear heating (W/m^3).

Since this paper focuses on the forearc thermal structure, the present thermal models consider only an isoviscous mantle wedge. Models with strong

temperature-dependent viscosity and magma transport are presented in detail in a recent paper of *Manea et al. (2004)*.

The Stokes equations are solved only for the mantle wedge, while the heat transfer equation is solved for the entire model. The linear system solver used by the present numerical scheme is the frontal method, which represents an out-of-core version of the band solver (uses a reverse Cuthill - McKee ordering). In the present numerical scheme, the penalty method formulation is used, P being replaced by $P = -\alpha' \cdot \left(\frac{\partial u}{\partial x} + \frac{\partial v}{\partial y} \right)$, where α' is large, on the order of $\frac{\eta}{\sqrt{\varepsilon}}$ (ε is the machine relative precision). In other words, the material is taken to be "almost" incompressible, so that a large pressure results in a small decrease in volume, and the continuity equation $\left(\frac{\partial u}{\partial x} + \frac{\partial v}{\partial y} \right) = 0$ is almost satisfied.

The connection between the Stokes and heat transfer equations is the velocity field. In terms of displacements, the velocity of the oceanic plate is considered with reference to the continental plate. Thus the convergence rate of 5.5 cm/year between the Cocos and North American plates is used in our models *(DeMets et al., 1994)*. The velocities in the subducting Cocos slab beneath the volcanic arc are set of 5.5 cm/yr; therefore the interface with the mantle wedge is predefined. The boundary between the mantle wedge and overlying lithosphere is considered fixed.

The finite element grids extend from 20 km seaward of the trench up to 600 km landward. The lower limit of the grid follows the shape of the subducting plate upper surface *(Kostoglodov et al., 1996)* at 100 km depth distance. The thickness of continental crust of 40 km is assumed for the modeling, which is consistent with the values inferred from the seismic refraction surveys and gravity modeling *(Arzate et al., 1993; Valdes et al., 1986)*.

The modeled profile is subdivided in three regions: fore-arc, volcanic arc and back-arc. The continental crust in every region consists of two layers: the upper crust (15 km thick) and the lower crust (25 km thick). A summary of the

thermal parameters used in the models is presented in *Table 1* (compilation from: *Peacock and Wang, 1999; Smith et al., 1979; Ziagos et al., 1985; Vacquier et al., 1967; Prol-Ledesma et al., 1989).*

The average radioactive heat production in the upper continental crust reported by *Ziagos et al. (1985)* is about 1.3 ± 0.6 $\mu W/m^3$. It has an exponential decrease from the upper crust down to the lower crust. Since the slow slips occurrence is located in the forearc area, we center the attention to fit the modeled surface forearc heat flow to the observed heat flow data *(Fig. 1)*. Therefore, the radioactive heat production for the upper crust is taken of 0.7 $\mu W/m^3$ (this value is within the 95% confidence interval of *Ziagos et al. 1985's* estimate), while a value of 0.2 $\mu W/m^3$ is assumed for the lower crust. This reduction has a negligible effect on the thermal structure of the subduction interface.

The upper and lower boundaries of the model are maintained at constant temperatures of 0°C and 1,450°C (asthenosphere), correspondingly. The right (landward) vertical boundary condition (BC) is defined by a 20°C/km thermal gradient for the continental crust. This value is in agreement with the back arc thermal gradient of 17.8 - 20.2°C/km reported by *Ziagos et al. (1985)*. Although the conductive heat equation with internal heating does not produce a linear temperature increase with depth, the heat flow from the mantle controls the thermal gradient in the crust in the back arc zone. Furthermore, this landward boundary is located far away (~ 400 km) from the coupled plate interface and does not produce a significant effect on it (the heat transfer by conduction can be noticeable only to a relatively small distance). Therefore, we simplify this BC by a linear temperature increase with depth. It is considered that the temperature at Moho beneath arcs and backarcs is above 800°C (*Bostock et al., 2002*) and 1,450°C at 100 km depth in the asthenosphere. In our models we consider the Moho temperature in the backarc of 850°C, and a linear thermal gradient for the continental crust of 20°C/km. Given that in our models the Moho is located at 40 km depth, the mantle wedge right BC is represented by 10°C/km thermal gradient down to the depth of 100 km. Underneath 100 km depth no horizontal conductive heat flow is specified.

Beneath Moho, for the right boundary corresponding to the mantle wedge, the BCs are:

$$\begin{cases} \left(-P+2\cdot\eta\cdot\dfrac{\partial u}{\partial x}\right)\cdot\vec{n}_x + \eta\cdot\left(\dfrac{\partial u}{\partial y}+\dfrac{\partial v}{\partial x}\right)\cdot\vec{n}_y = GB1, \\[2mm] \eta\cdot\left(\dfrac{\partial u}{\partial y}+\dfrac{\partial v}{\partial x}\right)\cdot\vec{n}_x + \left(-P+2\cdot\eta\cdot\dfrac{\partial v}{\partial y}\right)\cdot\vec{n}_y = GB2, \end{cases}$$

which are obtained by balancing the internal (stress induced) forces against the external boundary forces, called tractions (*GB1* and *GB2*). Therefore, beneath Moho, where there is no "*external*" force applied, *GB1* = *GB2* = 0. Since the slab is considered as a rigid body, for the deepest part of the right boundary, the velocity of the subducting slab is used. The left (seaward) BC is a one-dimensional geotherm for the oceanic plate. This geotherm is calculated by allowing a conductive cooling of the zero age half-space during the time equal to the age of the oceanic plate at the trench. This geotherm is corrected for the time-dependent sedimentation history *(Wang & Davis, 1992)*, assuming a constant porosity - depth profile of the sediment column and a uniform sediment thickness of 200 m (*Moore et al., 1982*) at the trench. The calculated oceanic geotherm is shown in *Fig. 4*.

The plate age at the trench is of 13.7 Myr according to the interpretation of Pacific-Cocos seafloor spreading magnetic anomaly lineations by *Klitgord and Mammerickx (1982)*. The plate interface geometry is constrained by the local seismicity and the gravity anomalies modeling (*Kostoglodov et al., 1996*). The Cocos slab has an initial dip of < 15°, which steepens to as much as 35° near the coast and subsequently becomes subhorizontal beneath the overriding continental lithosphere. At 270 km from the trench the slab dips into the asthenosphere at 20° (*Fig. 3*). The two dense clusters of seismic events beneath the coast (small yellow circles in *Fig. 3*), representing the background seismic activity with low magnitude ($M_w \leq 4$), appear to be related with the sharp bending-unbending of the plate in this region at ~ 80 km and ~ 115 km from the trench. Important stress concentrations and pressure variations (up to some 100 MPa) along the thrust fault are likely to appear in this region.

Marine heat flow measurements at the Middle American trench (*Prol-Ledesma et al., 1989*) revealed anomalously low (*Fig. 1*) average values of ~ 30 mW/m², suggesting that the hydrothermal circulation might be active in the upper part of the oceanic crust near the trench. Unfortunately, the maximum depth as well as the extension of the hydrothermal circulation layer is unknown. Given all these uncertainties, our models do not include the cooling of the oceanic plate at the trench due to hydrothermal circulation. However, the effect of the hydrothermal circulation becomes insignificant at the distances greater than ~ 100 km from the trench. The hydrothermal circulation shifts the position of the 100°C - 150°C isotherms with less than 10 km landward (*Currie et al., 2002*), therefore introducing only a relatively small error in the estimate of the upper limit of the seismogenic zone.

The long term continuous sliding between the subducting and the continental plates along the thrust fault should produce frictional heating. We introduced in the models a small degree of frictional heating using the Byerlee's friction law (*Byerlee, 1978*). Frictional heating is limited to a maximum depth of 40 km, which corresponds to the contact between the oceanic plate and the mantle wedge. The pore pressure ratio, PPR (Pore Pressure Ratio, the ratio between the hydrostatic and lithostatic pressures; PPR ≤ 1; PPR = 1, means no frictional heating), is set in order to fit the extent of the coupled zone (450°C isotherm) at 180 km and 205 km from the trench.

The uncertainties in the forearc thermal models arise mainly from errors in the thermal constants of the continental crust and the oceanic lithosphere and plate geometry. Underneath the volcanic arc, the major uncertainties come from the thermal structure of the mantle wedge. Recent thermal models for Central Mexican Volcanic Belt (*Manea et al., 2004*), with strong temperature-dependent viscosity, show an increasing the temperature with < 200°C along the slab-wedge interface. A test with reasonably varied parameters show uncertainties in the thermal models of ±50 - ±100°C, with the lower limit for the forearc and the higher limit for the volcanic arc.

MODELING RESULTS

The main constraint on the thermal models is the observed surface heat flow *(Fig. 1).* The heat flow data show a steep increase in front of the Mexican volcanic arc that is common for the subduction zones. In our model the fore arc and the volcanic belt have a surface heat flow of 28 - 35 mW/m^2 and ~ 60 mW/m^2 respectively. The fore arc heat flow data, 13 - 38 mW/m^2, are slightly lower than those predicted by the thermal models, while for the volcanic arc the measured values are higher, 64 - 90 mW/m^2, than the modeled values. The low modeled heat flow in the fore arc region of 28 - 35 mW/m^2 is a consequence of the heat consumption from the overriding plate by the underlying cold subducting oceanic plate. Our models do not consider magma generation and transport, or temperature-dependent viscosity in mantle wedge; therefore the modeled surface heat flow beneath the volcanic arc is smaller than the observed values. The present study focuses only on the fore arc zone, the thermal structure beneath the volcanic arc does not influence significantly the thrust fault region (*Manea et al., 2004).* A recent paper of *Manea et al. (2004),* shows a better fit of the surface heat flow in the volcanic arc, due to the introduction of a strong temperature-dependence of the asthenospheric viscosity in the mantle wedge. Rayleigh - Taylor instabilities may arise at the slab-wedge interface as a consequence of hydration and partial melting, and compositionally positive buoyant diapirs start to rise toward the base of the continental lithosphere changing the thermal distribution and flow pattern in mantle wedge (*Gerya and Yuen, 2003).* All these effects are not included in the modeling here.

The examples of thermal models, which correspond to the main restrictions (e.g., location and extension of the coupled zones, local seismicity and the hypocenter location of the intraslab earthquakes etc.) are shown in *Fig. 5.* The model with PPR = 0.97 is in good agreement with a coupled zone extent up to 180 km from the trench, while the model with PPR = 0.98 better explains the coupled zone extent up to 220 km. The average shear stress along the thrust fault is 13

MPa or an effective coefficient of friction of 0.017 (*Wang et al., 1995*). A smaller value of PPR (< 0.97) would increase the amount of frictional heating along the thrust fault, and the position of the 450°C isotherm moves toward the trench. A greater value of PPR (> 0.98) would decrease the frictional heating, and therefore widening the coupling zone to distances superior to 205 km from the trench. Both thermal models are in agreement with the hypocenter location of the intraslab earthquakes (note that the hypocentral depth estimates of the intraplate earthquakes could have the errors up to 20 km). The models indicate that the seismogenic fault (limited by 150°C and 250°C isotherms) in the Guerrero subduction zone is in good agreement with the rupture width of large megathrust earthquakes (*Fig. 1*) inferred from the aftershock sequences and the models of seismic rupture (*Ortiz et al., 2000*). The position of the 450°C isotherm can account for the maximum extent of the coupled interplate zone in Guerrero. The slow aseismic slip events are usually occurring on the transient partially coupled plate interface limited by the 250°C and 450°C isotherms.

METAMORPHIC FACIES IN THE SUBDUCTING SLAB

Interplate coupling in the subduction zone should depend not only on the *P-T* conditions but also on the properties of the rock material at the plate contact. In our models the pressure is considered hydrostatic, although the non-hydrostatic stresses and pressures in subduction zones can reach several 100 MPa along the slab surface. The relationship between the metamorphic facies (*Hacker et al., 2003*) and the coupling degree along the subducting oceanic plate can be revealed using the results of our thermal modeling.

The calculated geotherms of the slab (*P-T* paths) are plotted on the phase diagrams for MORB and for harzburgite (*Hacker et al., 2003*) in order to determine the metamorphic sequences within the oceanic subducting slab, for our two models (*Fig. 6*). The eclogite facies is bounded by lawsonite-blueschist at low temperatures and by garnet-amphibolite and garnet-granulite facies at high temperatures. The main metamorphic facies in the Guerrero subduction zone are shown in *Fig. 7*. The crustal material of the subducting Cocos plate passes through zeolite, prehnite-pumpellyite-actinolite facies when $T < 250°C$, then it enters into lawsonite-blueschist-jaedite and epidote-blueschist facies at $T < 450°C$. The position of the hinge point (270 km from the trench) is in good agreement with the transition to the eclogitic facies.

The maximum depth of the intraslab earthquakes in Guerrero (~ 80 km) correlates with the depth of the stable hydrous phases suggesting that the occurrence of these earthquakes might be related with the dehydration process in the oceanic slab.

The change of metamorphic sequences along the plate interface on the Guerrero profile is consistent with the location and the extension of the coupled zones (*Fig. 8*). The shallow seismogenic zone with $\alpha = 0.9$, corresponds to the metamorphic facies of zeolite, prehnite - pumpellyite - actinolite, the intermediate partially coupled zone with $\alpha = 0.7$ corresponds to the metamorphic facies of lawsonite-blueschist, while the deeper zone with $\alpha = 0.0$ corresponds to the

metamorphic facies of jadeite - lawsonite - blueschist. The blueschist and associated facies (jadeite and lawsonite) in the range of temperature between 250°C and 450°C, and the pressure range of 0.6 - 1.3 GPa, tends to some ductility, and the slow transient slip events seem to be related with the properties of the blueschist facies.

The estimated variation of wt% H_2O content with depth along the subducting plate is presented in *Fig. 7 - inset.* 4 - 5 wt% H_2O may be released from the hydrous phases in the subducting slab through a process of dehydration at the depths between 20 km and 80 km. Very low shear-wave velocities in the cold forearc mantle have been discovered in the southern Cascadia subduction zone (*Bostock et al., 2002*). This is an evidence of a highly hydrated and serpentinized material in the forearc region. The same conditions should be expected in the Guerrero subduction zone, too. The presence of serpentine in the mantle wedge can be examined using the phase diagram for harzburgite (*Hacker et al., 2003*). The calculated geotherms plotted in the phase diagram for harzburgite show that the serpentine facies might exist in the mantle wedge *(Fig. 6-B).* The location of serpentinized mantle wedge tip is critical because it may control the down-dip coupling and slow slip limits.

DISCUSSION AND CONCLUSIONS

The numerical models of temperature distribution in the forearc for the central part of Guerrero subduction zone are constrained by: the surface heat flow data, the shape of the plate interface estimated from gravity modeling (*Kostoglodov et al., 1996*), seismicity data and recently estimated extension of the coupled interplate fault. The modeled seismogenic zone delimited by 100°C - 150°C and 250°C is in good agreement with the rupture width of large subduction thrust earthquakes in Guerrero. A small degree of frictional heating is required in order to adjust the downdip extension of the partially coupled zone (450°C isotherm) in accordance with the coupled zone width assessed from the deformation models. The flat subhorizontal plate interface at the distance between 115 and 270 km from the trench is essential in the model to fit the position of the 450°C isotherm at ~ 200 km distance from trench corresponding to the maximum extent of the plate coupling.

The change of the metamorphic sequences in the subducting crust apparently relates with the variation of the coupling along the interplate fault estimated from the observations of surface deformation during the interseismic period (*Fig. 8*). In the temperature range of 250°C - 450°C and the pressure of 0.6 - 1.3 GPa, the metamorphic facies are represented by jadeite - lawsonite - blueschist and epidote - blueschist. The blueschist and associated facies in this temperature and pressure range probably exposes a ductile behavior, which is responsible for the long-term partial coupling and the sporadic aseismic transient slip events. For temperatures superior of 200°C - 300°C the preexisting rock undergoes pronounced changes in texture and mineralogy. Pressure and heat are the main agents of metamorphism, the effect of the heat on a preexisting rock (basalt in our case) being the increased ductility and change in mineral assemblage. Foliated metamorphic rocks, like blueschist, present a layered texture, favoring the ductile behavior along the slab-overriding plate interface. Ductile deformation resulting from nonhydrostatic stress, which is characteristic for

subduction zones, is responsible for the development of imposed anisotropic fabrics in metamorphic rock like blueschist.

The slab surface geotherm of *Currie et al. (2002)* (*Fig. 6*) shows a different path. Although the metamorphic facies along the slab surface are basically the same, for depths grater than ~ 20 km the *P-T* limits between adjacent facies are different. At ~ 250°C, the slab surface geotherm enters in lawsonite - blueschist, then between ~ 370°C and ~ 450°C the epidote-blueschist facies is present. The jaedite - lawsonite - blueschist and zoisite - amphibole - eclogite are absent in the *Currie et al. (2002)* thermal model for Guerrero; instead jadeite - epidote - blueschist, lawsonite - amphibole - eclogite and amphibole - eclogite are present. Our models show a good correlation between the position of the hinge point (270 km from the trench) and the occurrence of the eclogitic facies in the subducted oceanic crust (*Fig. 7*). The thermal models of *Currie et al. (2002)*, illustrate the initiation of the eclogitic facies at greater depth of ~ 80 km, although the bending of the slab into the asthenosphere begins at ~ 50 km depth.

The down dip limit of the seismogenic zone proposed by *Currie et al. (2002)* extends up to 350°C. From the thermal models of *Currie et al. (2002)* and the phase diagram for MORB, between 250°C and 350°C lawsonite-blueschist facies is present. This temperature range represents half of the total width of the seismogenic zone. If blueschist and associated facies is responsible for the occurrence of the slow earthquakes in Guerrero, then it should not be present in the seismogenic zone. In our models, 250°C is in good agreement with the maximum extent of the seimogenic zone (~ 82 km from the trench) and with the onset of the blueschist and associated facies.

Since the model of *Currie et al. (2002)* is colder than our models, the serpentine is not present in the tip of the mantle wedge (*Fig. 6-B*). The proposed alternative for the downdip extension of the thrust zone by the presence of the serpentinezed forearc mantle wedge is not supported by the thermal model for Guerrero of *Currie et al. (2002)*. Alternatively, the thermal models proposed by this study reveal the presence of a significant amount of serpentine in the tip of the

mantle wedge (*Fig. 6-B* and *Fig. 7*), sustaining the alternative for the downdip extension of the thrust zone.

According to the phase diagrams for MORB, intensive dehydration in the subducting oceanic crust should occur (*Fig. 7* - inset) at $T = 250°C - 450°C$, and $P = 0.6 - 1.3$ GPa, more than 2 wt% H_2O being released during this phase transformation. The occurrence of the slow transient slip events may be related with this dehydration.

REFERENCES

Arzate, J.A., Mareschal, M. and Urrutia-Fucugauchi, J., 1993. A preliminary crustal model of the Oaxaca continental margin and subduction zone from magnetotelluric and gravity measurements. *Geofisica Internacional, 32, 441-45.*

Blanpied, M.L., Lockner, D.A. and Byerlee, J.D., 1995. Frictional slip of granote at hydrothermal conditions. *Journal of Geophysical Research, 100, 13,045-13,064.*

Bostock, M.G., Hyndman, R.D., Rondenay, S., and Peacock, S.M. 2002. An inverted continental Moho and serpentinization of the forearc mantle. *Nature, v. 417, p. 536-538.*

Byerlee, J.D., 1978. Friction of rocks. *Pure Applied Geophysics, 116, 615-626.*

Currie, C.A., Hyndman, R.D., Wang, K., and Kostoglodov, V., 2002. Thermal models of the Mexico subduction zone: Implications for the megathrust seismogenic zone. *Journal of Geophysical Research, 107, NO. B12, 2370, doi: 10.1029/2001JB000886.*

DeMets, C., Gordon, R., Argus, D. and Stein, S., 1994. Effect of recent revisions to the geomagnetic reversal time scale on estimates of current plate motions. *Geophysical Research Letters, 21, 2191-2194.*

Gerya, T.V. and Yuen, D.A., 2003. Rayleigh-Taylor instabilities from hydration and melting propel 'cold plumes' at subduction zones. *Earth and Planetary Science Letters, 212, 47-62.*

Hacker, B.R., Abers, G.A., and Peacock, S.M., 2003. Subduction Factory 1. Theoretical mineralogy, densities, seismic wave speeds, and H2O contents. *Journal of Geophysical Research, v. 108, 10.1029/2001JB001127.*

Hyndman, R.D. and Wang, K., 1993. Thermal constrains on the zone of major thrust earthquake failure: The Cascadia subduction zone. *Journal of Geophysical Research, 98, 2039-2060.*

Klitgord, K. and Mammerickx, J., 1982. J., Northern East Pacific Rise: Magnetic anomaly and bathymetric framework. *Journal of Geophysical Research, 87, 6725-6750.*

Kostoglodov, V., Bandy, W., Cominguez, J., and Mena, M., 1996. Gravity and seismicity over the Guerrero seismic gap, Mexico, *Geophysical Research Letters, 23, 3385-3388.*

Kostoglodov, V., Singh, S. K., Santiago, J. A., Franco, S. I., Larson, K. M., Lowry, A. R., and Bilham, R., 2003. A large silent earthquake in the Guerrero seismic gap, Mexico. *Geophysical Research Letters, 30(15), 1807, doi:10.1029/2003GL017219.*

Kostoglodov, V., and Pacheco, J. F., 1999. One hundred years of seismicity in Mexico, Instituto de Geofisica, Universidad Nacional Autónoma de México, México City.

Manea, V.C., Manea, M., Kostoglodov, V., Sewell, G., 2004 (in press). Thermo-mechanical model of the mantle wedge in Central Mexican subduction zone and a blob tracing approach for the magma transport. *Physics of the Earth and Planetary Interiors.*

Moore, J.C., Watkins, J.S., Shipley, T.H., McMillen, K.J., Bachman, S.B., and Lundberg, N., 1982. Geology and tectonic evolution of a juvenile accretionary terrane along a truncated convergent margin: Synthesis of results from Leg 66 of the Deep Sea Drilling Project, southern México. *Geological Society American Bulletin, 93, 847-861.*

Ortiz, M., Singh, S.K., Kostoglodov, V., and Pacheco, J., 2000. Source areas of the Acapulco-San Marcos, Mexico earthquakes of 1962 (M 7.1; 7.0) and 1957 (M 7.7), as constrained by tsunami and uplift records. *Geofisica Internacional, 39, 337-348.*

Peacock, S. M., and Hyndman, R. D., 1999. Hydrous minerals in the mantlewedge and the maximum depth of subduction thrust earthquakes. *Geophysical Research Letters, 26, 2517– 2520.*

Peacock, S.M., and Wang, K., 1999. Sesimic consequences of warm versus cool subduction metamorphism: Examples from southwest and northeast Japan. *Science, 286, 937-939.*

Prol-Ledesma, R.M., Sugrobov, V.M., Flores, E.L., Juarez, G., Smirnov, Y.B., Gorshkov, A.P., Bondarenko, V.G., Rashidov, V.A., Nedopekin, L.N. and Gavrilov, V.A., 1989. Heat flow variations along the Middle America Trench. *Marine Geophysical Research, 11, 69-76.*

Savage, J. C., 1983. A dislocation model of strain accumulation and release at a subduction zone. *Journal of Geophysical Research, 88 , 4984–4996.*

Smith, D.L., Nuckels, C.E., Jones, R.L. and Cook, G.A., 1979. Distribution of heat flow and radioactive heat generation in northern México. *Journal of Geophysical Research, 84, 2371-2379.*

Tse, S.T. and Rice, J.R., 1986. Crustal earthquake instability in relation to the depth variation of frictional slip properties. *Journal of Geophysical Research, 91, 9452-9472.*

Vacquier, V., Sclater, J.G., and Corry, C.E., 1967. Studies of the thermal state of Earth. The 21st paper: Heat-flow, eastern Pacific. *Bulletin of Earthquake Research Institute, 45, 375-393.*

Valdes, C.M., Mooney, W.D., Singh, S.K., Meyer, R.P., Lomnitz, C, Luetgert, J.H., Helsley, C.E., Lewis, B.T.R. and Mena, M., 1986. Crustal structure of Oaxaca, Mexico, form seismic refraction measurements. *Bulletin of Seismological Society of America, 76, 547-563.*

Vrolijk, P., 1990. On the mechanical role of smectite in subduction zones. *Geology, 18, 703–707.*

Wang, C. Y., 1980. Sediment subduction and frictional sliding in a subduction zone. *Geology, 8, 530– 533.*

Wang, K., and Davis, E.E., 1992. Thermal effect of marine sedimentation in hydrothermally active areas. *Geophysical Journal Internacional, 110, 70-78.*

Wang, K., Hyndman, R.D. and Yamano, M., 1995. Thermal regime of the southwest Japan subduction zone: Effects of age history of the subducting plate. *Tectonophysics, 248, 53-69.*

Ziagos, J.P., D.D. Blackwell, and F. Mooser, 1985. Heat flow in southern Mexico and the thermal effects of subduction. *Journal of Geophysical Research, 90, 5410-5420.*

FIGURE CAPTIONS

Figure 1.

Distribution of the heat flow data and the location of modeled cross-section in Guerrero. Large orange circles are continental heat flow measurements in mW/m^2 (*Ziagos et al., 1985*). Small light blue circles in the insets are ocean heat flow measurements in mW/m^2 (*Prol-Ledesma et al., 1989*). Yellow triangles show the location of active volcanoes in Mexico. Green squares are the major cities. Grey thick line is the modeled cross-section. Also, the rupture areas for megathrust earthquakes along the Mexican coast are shown (*Kostoglodov and Pacheco, 1999*). The extension of the seismic gap in Guerrero is ~ 120 km northwest from Acapulco.

Figure 2.

Dislocation model for the interseismic steady state deformations observed on the GPS stations. The interface is partially locked on three segments (thick lines; bold numbers indicating the fraction of locking). The rest of the interface slips freely. The model fits reasonably well the observed data. Displacement errors bars larger than 1σ are shown. Reproduced from *Fig. 4* of *Kostoglodov et al. (2003)*, copyright by the American Geophysical Union.

Figure 3.

The updip and downdip limits of the seismogenic and slow slip zones. The seismogenic zone (fine dashed black-pink line) is confined by 100 - 150°C and $\leq$ 350°C isotherms. The partially coupled zone, where slow earthquakes are proposed to occur, (coarse dashed black-pink line) is delimited by $\leq$ 350°C and 450°C isotherms. Beyond 450°C, the oceanic plate and the overriding plate are considered completely decoupled (continuous light blue line). Small yellow circles represent the background seismic activity with low magnitude ($M_w \leq 4$). The red circles represent intraslab earthquakes with magnitude $M_w \geq 5.9$.

Figure 4.

Boundary condition (BC) and thermal parameters used in the modeling. The upper and lower boundaries are maintained at the constant temperatures of 0°C and 1,450°C (asthenosphere), correspondingly. The right (landward) vertical BC is defined by 20°C/km thermal gradient in the continental crust and 10°C/km up to a depth of 100 km. Deeper, no horizontal conductive heat flow is specified. The left (seaward) BC (shown in the inset) is the one-dimensional geotherm for the oceanic plate. The oceanic geotherm is corrected for the time-dependent sedimentation history (*Wang & Davis, 1992*), assuming a constant porosity-depth profile of the sediment column and a uniform sediment thickness of 200 m at the trench. The oceanic plate is subducting at a constant rate of 5.5 cm/year while the continental crust is considered fixed.

The modeled profile is subdivided into three regions: fore-arc, volcanic arc and back-arc. In each region the continental crust consists of two layers: the upper crust and the lower crust. A summary of the thermal parameters used in the models is presented in *Table 1*.

Figure 5.

(A) Variations of the surface heat flow along the Guerrero profile. Red dots with vertical error bars are the heat flow measurements from *Ziagos et al. (1985)*. Blue solid line: the surface heat flow for the model without frictional heating. Red dashed line corresponds to the model with PPR = 0.97, and the blue solid line to the model with PPR = 0.97. PPR - Pore Pressure Ratio.

(B) The model of steady-state thermal structures for the 13.7 Myr oceanic lithosphere subducting at 5.5 cm/year beneath Guerrero. Frictional heating (PPR = 0.98) is introduced down to a maximum depth of 40 km. The shear stress along the fault is given by Byerlee's friction law *(Byerlee, 1978)*. Orange triangle - Popocatépetl volcano. Black dashed line is the Moho (40 km depth). The continuous black line indicates the top of the subducting oceanic slab. Short-dashed red segments delimit the seismogenic zone (between 100°C - 150°C and

250°C). Long-dashed pink segment (250°C - 450°C) shows the zone of partial coupling. The seismogenic zone is located between 32 km and 81 km from the trench. The coupling zone extends up to 205 km from the trench.

(C) Same as *(B)* with the frictional heating, PPR = 0.97. The seismogenic zone is between 32 km and 81 km. The coupling zone extends up to 180 km from the trench.

Figure 6.

(A). Phase diagram for MORB and maximum H_2O contents (*Hacker et al., 2003)*. Calculated geotherms: continuous blue line and dashed red line - *P-T* paths for the top of the subducting oceanic crust for PPR = 0.97 and PPR = 0.98, respectively; continuous green line - *P-T* path for the top of the subducting oceanic slab from *Currie et al. (2002).* 1 - Zeolite (4.6 wt%H_2O), 2 - Prehnite -Pumpellyite (4.5 wt% H_2O), 3 - Pumpellyite - Actinolite (4.4 wt% H_2O), 4 - Greenschist (3.3 wt% H_2O), 5 - Lawsonite - Blueschist (5.4 wt% H_2O), 6 - Epidote - Blueschist (3.1 wt% H_2O), 7 - Epidote - Amphibolite (2.1 wt% H_2O), 8 - Jadeite - Epidote - Blueschist (3.1 wt% H_2O), 9 - Eclogite - Amphibole (2.4 wt% H_2O), 10 - Amphibolite (1.3 wt % H_2O), 11 - Garnet - Amphibolite (1.2 wt% H_2O), 12 - Granulite (0.5 wt% H_2O), 13 - Garnet - Granulite (0.0 wt% H_2O), 14 - Jaedite - Lawsonite - Blueschist (5.4 wt% H_2O), 15 - Lawsonite - Amphibole - Eclogite (3.0 wt% H_2O), 16 - Jaedite - Lawsonite - Talc - Schist, (2.0 wt% H_2O), 17 - Zoisite -Amphibole - Eclogite (0.7 wt% H_2O), 18 - Amphibole - Eclogite (0.6 wt% H_2O), 19 - Zoisite - Eclogite (0.3 wt% H_2O), 20 - Eclogite (0.1 wt% H_2O), 21 - Coesite - Eclogite (0.1 wt% H_2O), 22 - Diamond - Eclogite (0.1 wt% H_2O).

(B) Phase diagram for harzburgite, and maximum $H2O$ contents (*Hacker et al., 2003)*. A - Serpentine - Chlorite - Brucite (14.6 wt% H_2O), B - Serpentine - Chlorite - Phase A (12 wt% H_2O), C - Serpentine - Chlorite - Dunite (6.2 wt% H_2O), D - Chlorite - Harzburgite (1.4 wt% H_2O), E - Talc - Chlorite - Dunite (1.7 wt% H_2O), F - Anthigorite - Chlorite - Dunite (1.7 wt% H_2O), G - Spinel - Harzburgite (0.0 wt% H_2O), H - Garnet - Harzburgite (0.0 wt% H_2O). Calculated geotherms are the same

as in *(A)*. The calculated geotherms plotted on the phase diagram for harzburgite, show that in both of our models the serpentine might exist in the mantle wedge.

Figure 7.

Metamorphic facies along the oceanic subducting crust. The metamorphic facies in the subducting Cocos plate pass through zeolite, prehnite-pumpellyite-actinolite at $T \leq 250°C$ then lawsonite-blueschist-jaedite and epidote-blueschist at $T \leq 450°C$. It can be seen from the histogram (inset) wt% H_2O *versus* the metamorphic sequences along the subducting plate that 4 - 5 wt% H_2O may be released from the hydrous phases in the subducting slab through the process of dehydration. The presence of the serpentine in the mantle wedge is predicted from the phase diagram for harzburgite *(Hacker et al., 2003) Fig. 6-B*. The dashed yellow line represents the onset of the eclogitic facies in the subducted oceanic crust.

Figure 8.

Metamorphic facies along the oceanic subducting crust in the forearc. Superimposed are the coupled segments from the best fitting dislocation model *(Fig. 2)*. The changes of the metamorphic sequences along the plate interface on Guerrero profile are consistent with the estimates of the location and the extension of the coupled zone.

Table 1.

Summary of the thermal parameters used in the models. (Compilation from: *Peacock and Wang, 1999; Smith et al., 1979; Ziagos et al., 1985; Vacquier et al., 1967; Prol-Ledesma et al., 1989).*

Geological Unit	Thermal Conductivity (W/m °K)			Heat production ($\mu W/m^3$)	Thermal Capacity (MJ/m^3 °K)
	Fore-arc	Volcanic-arc	Back-arc		
Oceanic sediments		1.00 -2.00[*]		1.00	2.50
Continental crust (0 -15 km)	2.00	3.00	2.50	0.65	2.50
Continental crust (15 - 40 km)	2.00	3.00	2.50	0.20	2.50
Continental mantle		3.10		0.01	3.30
Oceanic lithosphere		2.90		0.02	3.30

* *Increase linearly with distance from the deformation front up to a depth of 10 km.*
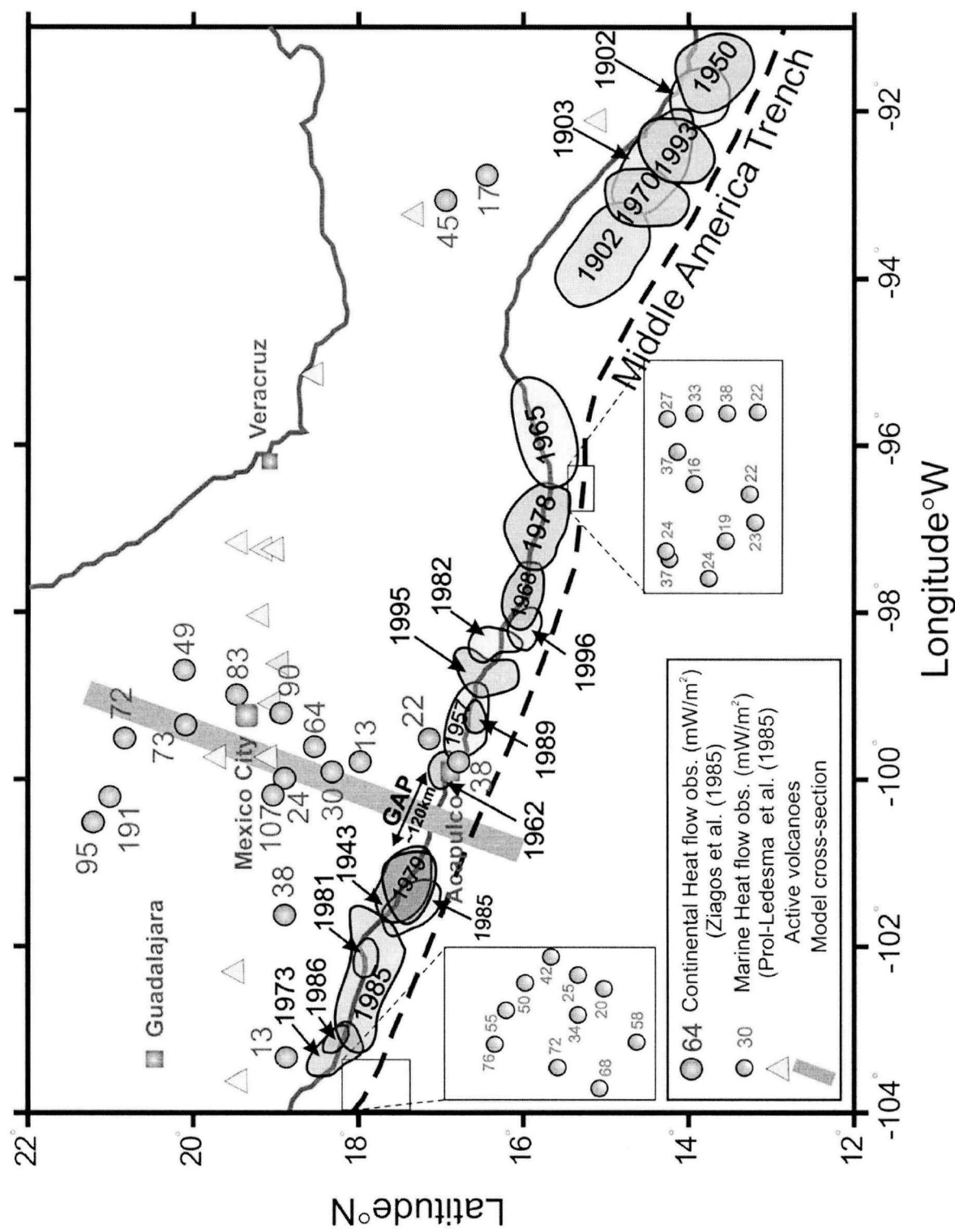
Figure 1
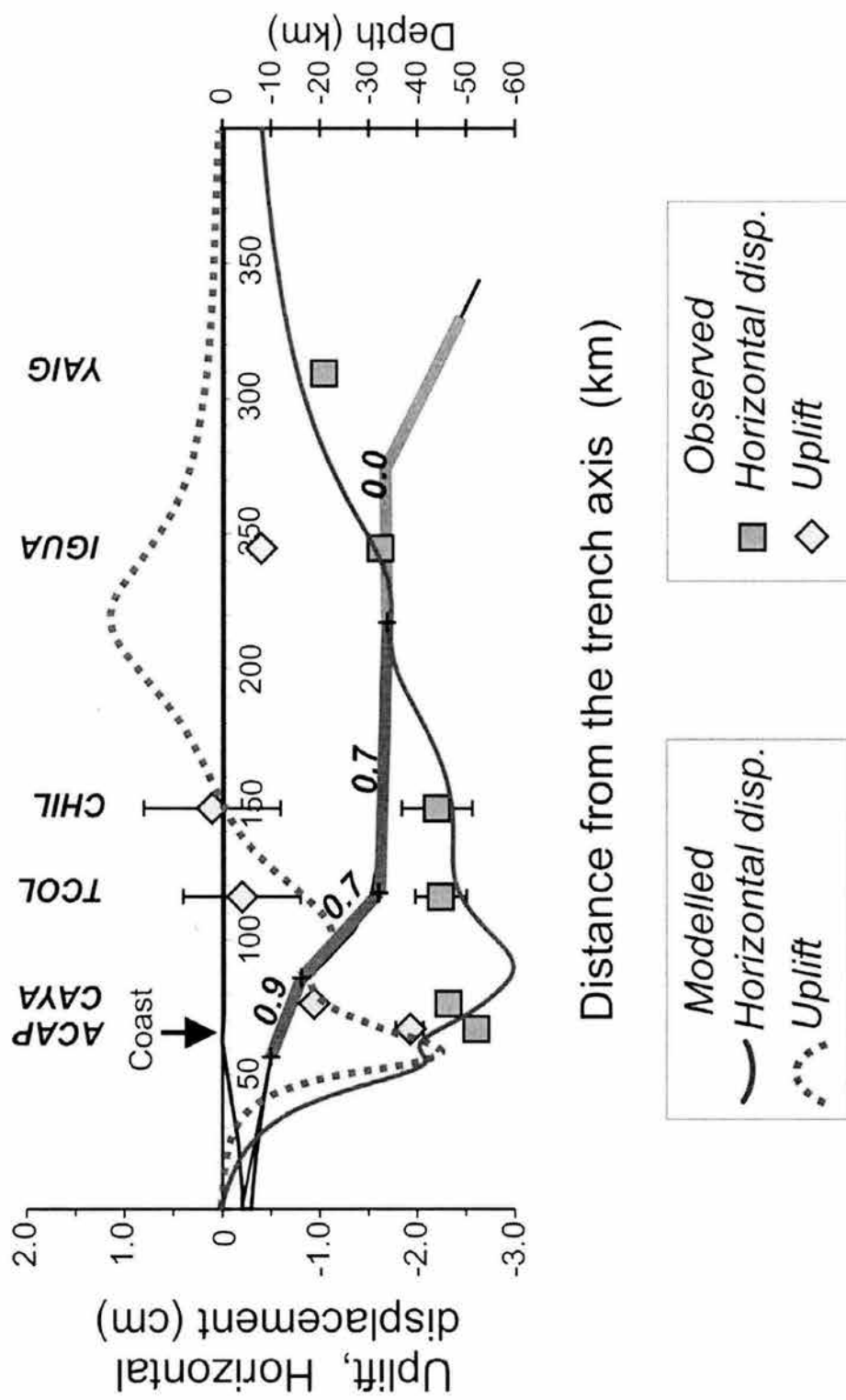
Figure 2
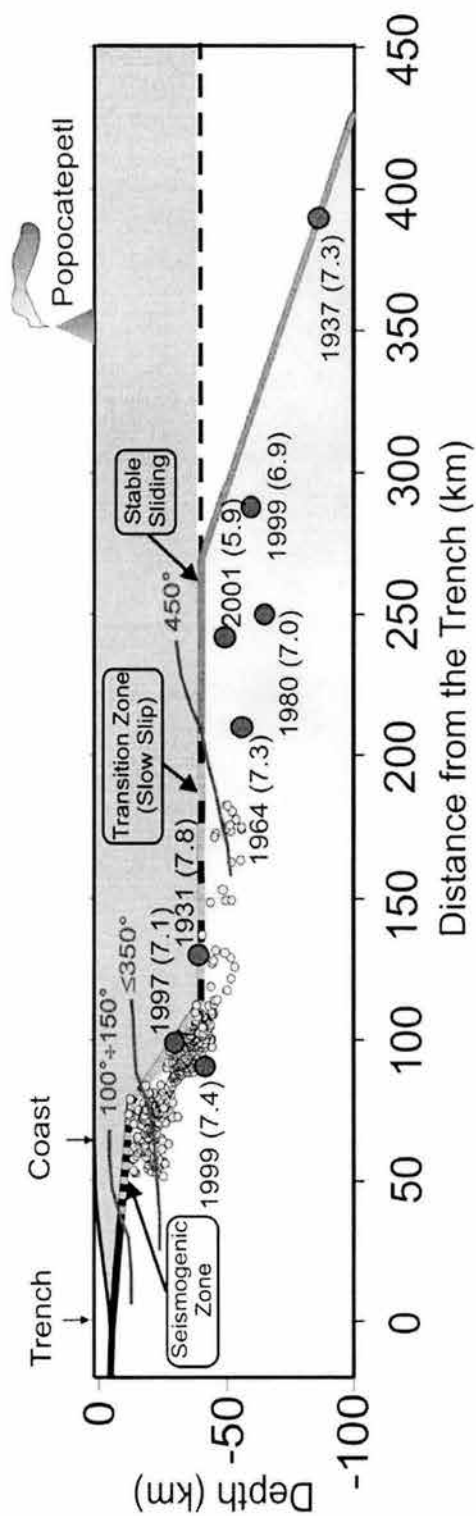
**Figure 3**
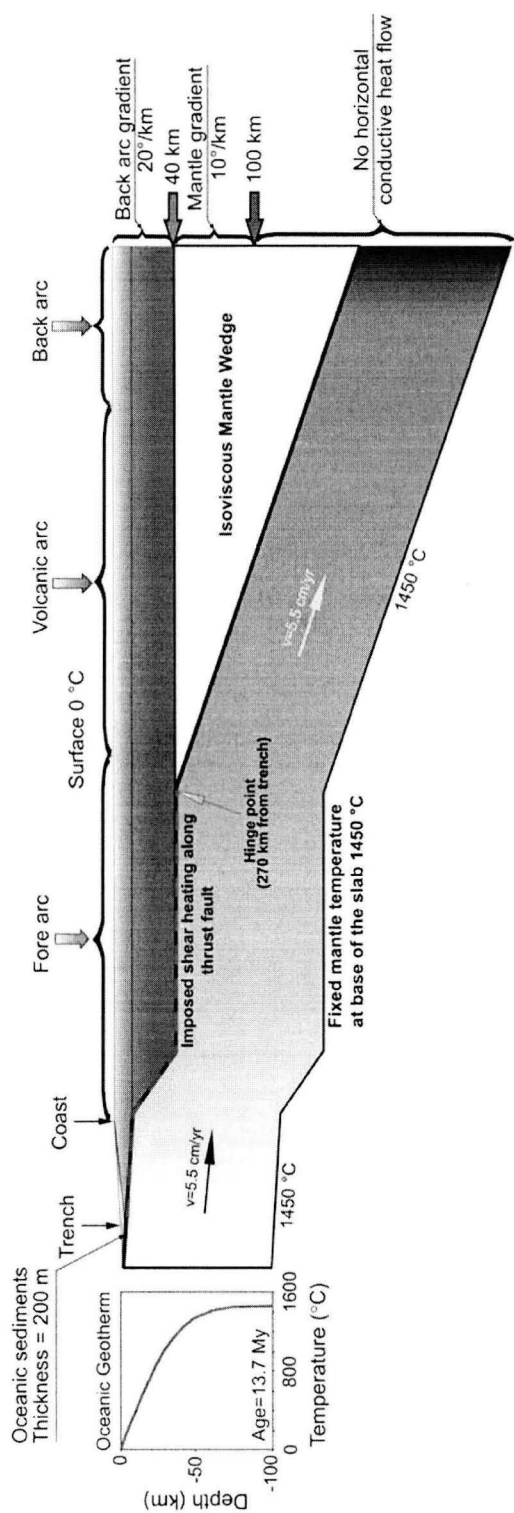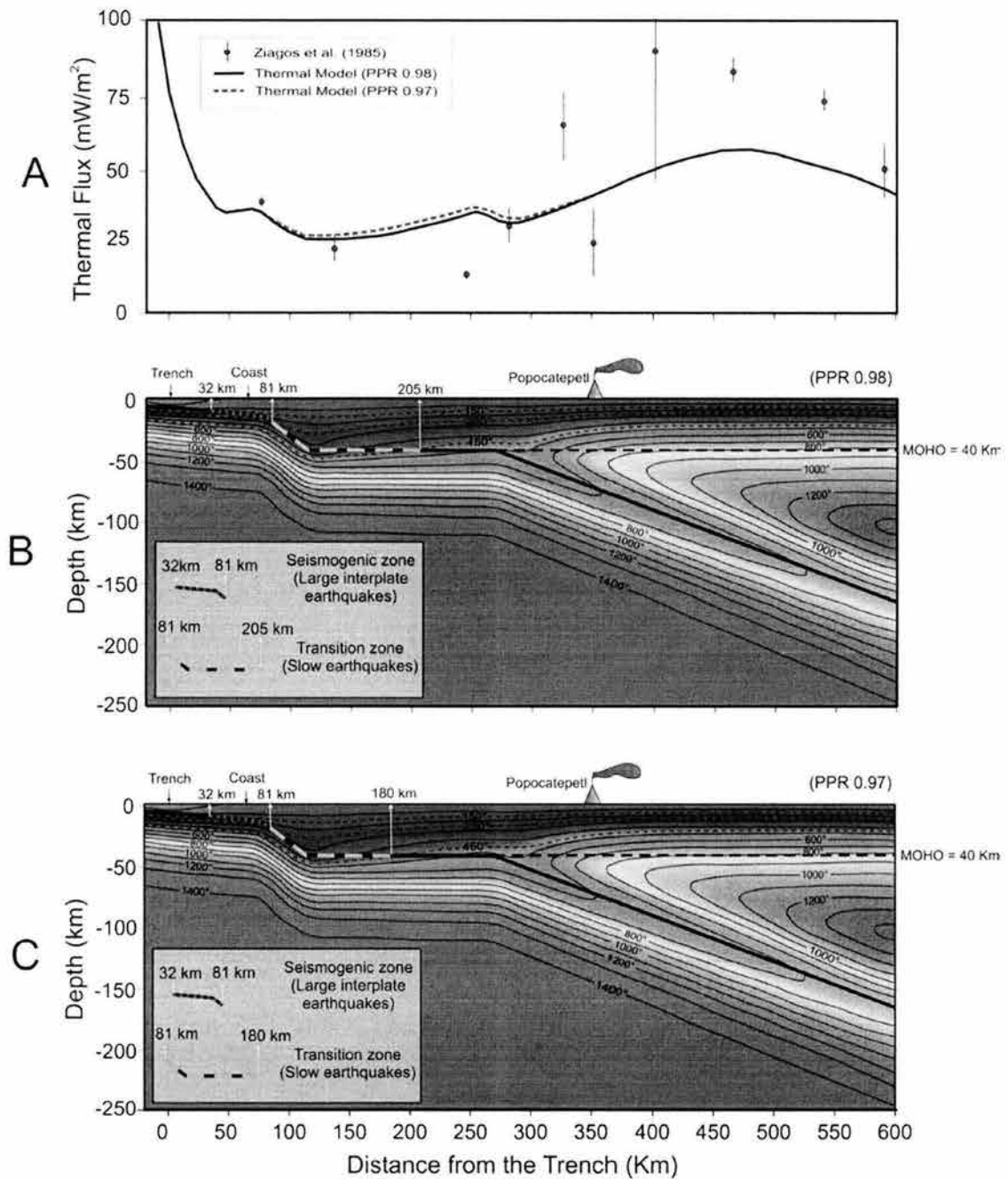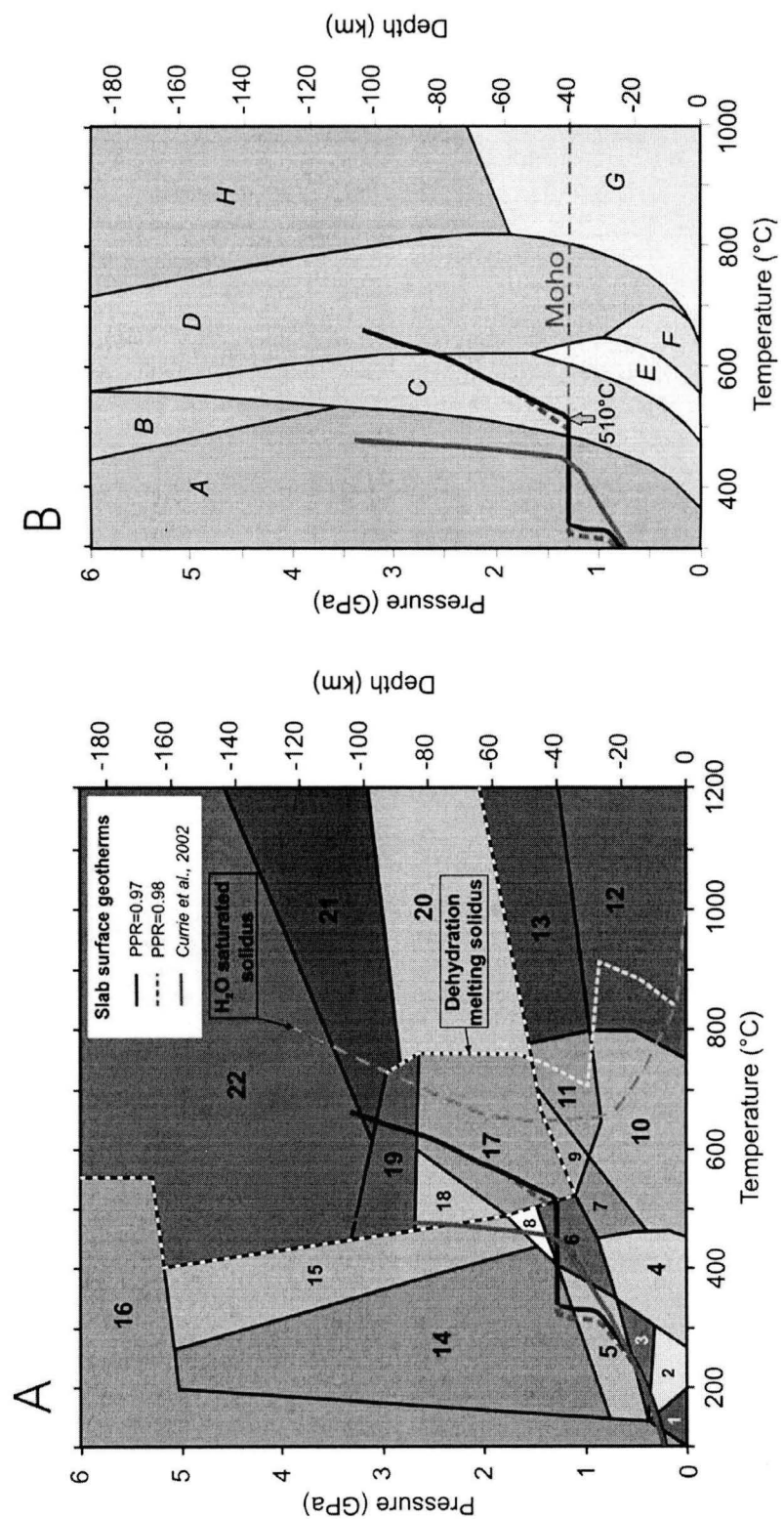
**Figure 4**
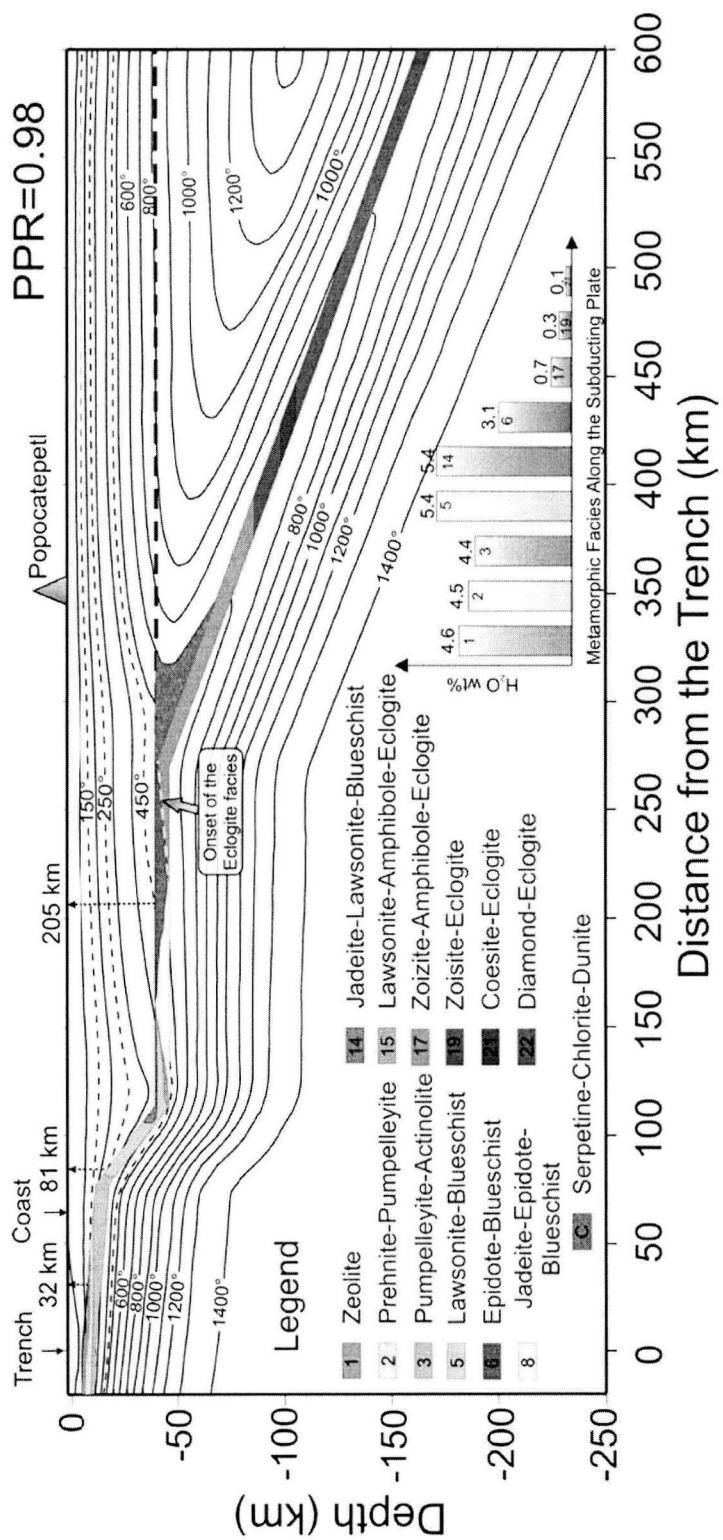
Figure 5
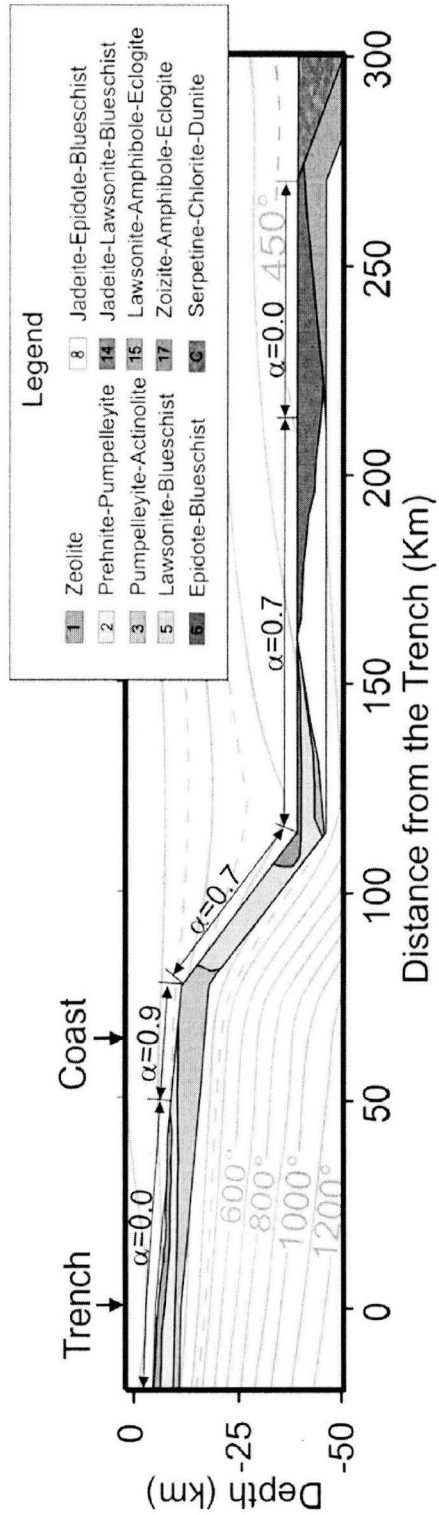
Figure 6

Figure 7

Figure 8

III. MODELO TERMOMECÁNICO DE LA CUÑA DEL MANTO EN LA ZONA DE SUBDUCCIÓN DEL CENTRO DE MÉXICO Y EL MECANISMO *"BLOB TRACING"* PARA EL TRANSPORTE DE MAGMA

In press at: Physics of the Earth and Planetary Interiors

THERMO-MECHANICAL MODEL OF THE MANTLE WEDGE IN CENTRAL MEXICAN SUBDUCTION ZONE AND A BLOB TRACING APPROACH FOR THE MAGMA TRANSPORT

V.C. Manea[1], M. Manea[1], V. Kostoglodov[1], G. Sewell[2]

[1] Instituto de Geofisica, Universidad Nacional Autónoma de México (UNAM), México
[2] University of Texas, El Paso

ABSTRACT

The origin of the Central Mexican Volcanic Belt (CMVB) and the influence of the subducting Cocos plate on the CMVB volcanism are still controversial. In this study, the temperature and mantle wedge flow models for the Mexican subduction zone are developed using the finite element method to investigate the thermal structure below CMVB. The numerical scheme solves a system of 2D Stokes equations and 2D steady state heat transfer equation.

Two models are considered for the mantle wedge: the first one with an isoviscous mantle wedge and the second one with a strong temperature-dependent viscosity. The first model reveals a maximum temperature of ~ 830 °C in the mantle wedge, which is not sufficient for melting wet peridotite. Also, the geotherm of the subducting plate upper surface does not intersect the dehydration-melting *solidus* for mafic minerals. The second model predicts temperatures of

more than 1,200°C beneath the CMVB for a wide range of rheological parameters (reference viscosity and activation energy). Up to 0.6 wt% H_2O can be released down to 60 km depth through metamorphic changes in the oceanic crust of the subducting slab. The melting of this oceanic crust apparently occurs in a narrow depth range of 50-60 km and also melting of the hydrated mantle wedge peridotite is now expected to take place beneath the CMVB.

Considering that the melting processes on and in the vicinity of the subducting plate surface generate most of the volcanic material, a dynamic model for the blob tracers is developed using Stokes flow at infinite Prandtl number. The blobs of 0.2 - 10.0 km in diameter migrate along different trajectories only at low wrapping viscosities ($\eta_w = 10^{14}$ - $5 \cdot 10^{17}$ Pa s). The modeling results show that the "fast" trajectories terminate at the same focus location at the base of the continental crust, while the arrival points of "slow" trajectories, which are common for the blobs of smaller size (~ 0.4 - 0.5 km), are scattered away from the average focus location. This observation may give us a hint on a possible mechanism of strato and mono volcanoes genesis. The rise time, which the blob detached from the subducted plate, needs to reach the bottom of the continental crust, is from 0.001 up to 14 Myr depending on the blob diameter and surrounding viscosity.

Keywords: Mexican subduction zone, thermal models, mantle wedge flow, blobs.

INTRODUCTION

Thermal and flow models in the mantle wedge can give us advance insights on the geodynamic processes in the forearcs as well as beneath the volcanic arcs. There are only a few thermal models of the subduction zone in Mexico (*Currie et al., 2002; Manea et al., 2004*), but none of them presents a reliable and detailed thermal structure beneath the volcanic arc considering the rheology of the asthenosphere. The present models are further developed based on previous study of the Mexican subduction zone in Guerrero in *Manea et al. (2004)*, which plausibly constrained the thermal structure for the forearc area only. The thermo - mechanical modeling of the mantle wedge with temperature and/or stress dependent rheology is proposed *(Furukawa, 1993; Conder et al., 2002; Van Keken et al., 2002; Kelemen et al, 2003)*. Mantle wedge dynamics and thermal structure of shallow flat subduction zones in general have been investigated recently by *van Hunen et al. (2002)*. In this study we explore the thermal structure of the mantle wedge in a specific subduction zone of the Central Mexico (Guerrero), which has an anomalously wide, subhorizontal plate interface and a distant volcanic arc. The models describe a stationary slab-induced convection, in the cases of the constant viscosity (isoviscous mantle) and strong temperature - dependent viscosity of the asthenosphere.

The previous thermal model for the Guerrero subduction zone with a shallow plate interface (*Currie et al., 2002*) with predefined analytical expression for the mantle corner flow, predicts the temperature of ~ 900°C in the asthenosphere beneath the volcanic front (Popocatépetl volcano). In Currie's model the basaltic component of the subducting plate crust does not reach the melting temperature.

Recent geological studies (*Luhr, 1997; Márquez et al., 1999a*) suggest the existence of a complex mantle beneath the CMVB. However the origin of the OIB-like basalts is still unclear there. Advection of the asthenospheric mantle caused by

sinking of the Cocos plate was proposed as a possible source of the OIB-like magmas (*Luhr, 1997; Wallace and Carmichael, 1999*).

There are several mineralogical and geochemical studies of the CMVB (*Márquez and De Ignacio, 2002*) suggesting the existence of two different primitive mafic magmas, one with an *asthenospheric* OIB-like component and another with a *lithospheric* component. Although the relationship between volcanism and the subduction of the Cocos plate is commonly recognized (*Pardo and Suárez, 1995, Wallace and Carmichael, 1999*), there are different hypothesis regarding the source of the volcanism in this area: the extension of the Gulf of California transform fault zone (*Ferrari et al., 1994*), an old weakened cortical zone (*Cebull and Schubert, 1987*), cortical transtension mechanisms (*Shubert and Cebull, 1984; Ferrari et al., 1990*) and rifting (*Luhr, 1997; Márquez et al., 1999a,b*).

The source of fluids that metasomatize the mantle is also unclear. There are three possibilities proposed to explain the metasomatized mantle (*Márquez et al., 1999c; Wallace and Carmichael, 1999; Verma, 1999; 2000*): a) the mantle wedge affected by the fluids originated from dehydration of the subducted Cocos plate; b) old enriched lithospheric mantle; c) mantle metasomatized by volatiles from a mantle plume. Direct evidences that the mantle wedge was metasomatized by fluids released from the down going oceanic slab is essentially difficult, because mantle xenoliths are rarely discovered in arc lavas. In the CMVB, Quaternary hornblende andesites erupted near the El Peñón area (see *Fig. 1*) contain xenoliths 1 - 2 cm in diameter. These xenoliths are rich in phenocrysts of hornblende and the host andesite is depleted in plagioclase phenocrysts (*Blatter and Carmichael, 1998*). All these observations suggest an influx of volatiles from the subducting slab into the mantle wedge.

Underneath the CMVB, the magma ascents toward the earth surface producing large strato-volcanic structures and smaller sized monogenetic volcanoes scattered in large areas. The CMVB includes several stratovolcanoes like Popocatépetl, Iztaccíhuatl and Nevado de Toluca (*Fig. 1*). The monogenetic volcanoes are basically cinder cones, lava cones, domes and lava flows. While

stratovolcanoes are characterized by a periodicity of magma eruptions, the monogenetic volcanoes present a single one eruptive event, and as a result have a smaller size compared with stratovolcanoes. *Fedotov (1981)* suggested that the occurrence of one or another type of volcanoes might be related with the magma supply. Other scientists (*Takada, 1989, 1994*) propose a dual mechanism related with both the magma supply and regional stress. While the alignment of the monogenetic volcanoes can be parallel to a main normal fault system, the arrangement of the large stratovolcanoes seems to be rather orthogonal to the volcanic belt (*Alaniz-Alvarez et al., 1998*).

Using the phase diagrams for mafics (e.g. *Hacker et al., 2002)* it is possible to investigate whether the mantle wedge is subjected to the hydration by fluids released from the subducting slab. A very thin sedimentary fill at the Mexican trench suggests that about of 95% of these sediments (~ 200 m) are subducted (*Manea et al., 2003*). An influx of volatiles from the metamorphosed oceanic crust and sediments might trigger partial melting of the peridotite just above the subducted slab (*Tatsumi, 1986; Davies and Stevenson, 1992*). *Gerya and Yuen (2003)* showed that a Rayleigh-Taylor instability developed above the subducting slab generates positively buoyant plumes up to 10 km in diameter that can penetrate the overlying mantle wedge.

Albeit various mechanisms of magma generation have been proposed (e.g. anhydrous decompression melting of peridotite (*Klein and Langmuir, 1987; Langmuir et al., 1992*); porous flow of hydrated partial melt (*Davies and Stevenson, 1992*)), in the present study, the magma generation and migration is assumed in a form of partially melted positively buoyant blobs. Regardless of the oversimplification of the blob properties, this model can help to understand the existence of different sources of the volcanism in the area. The buoyant blobs of different size and composition may be generated by melting of the Cocos plate and overlying mantle peridotite, when the pressure and temperature reach the *solidus* conditions *(e.g. Gerya and Yuen, 2003*).

It is important to estimate the viscosity range for the reasonable trajectories and average rise times for the blobs reaching the bottom of the continental crust. A recent study by *Gerya and Yuen* (*2003*) revealed that these plume - like blobs may be lubricated by the partially melted material of the subducted crust and hydrated mantle, thus producing a very low viscosity wraps around the blob structures. Burov et al. (*2000*), apply a similar extremely low viscosity, in order to model the exhumation in the continental lithosphere.

MODELING PROCEDURE

A system of 2D Stokes equations and 2D steady state heat transfer equation is solved for the Guerrero cross section (*Fig. 1*) using the finite element solver PDE2D (*http://pde2d.com/*). The system of equations in an explicit form is:

$$\begin{cases} \dfrac{\partial\left(-P+2\eta\dfrac{\partial u}{\partial x}\right)}{\partial x}+\dfrac{\partial\left(\eta\left(\dfrac{\partial u}{\partial y}+\dfrac{\partial v}{\partial x}\right)\right)}{\partial y}=0 \\[4mm] \dfrac{\partial\left(\eta\left(\dfrac{\partial u}{\partial y}+\dfrac{\partial v}{\partial x}\right)\right)}{\partial x}+\dfrac{\partial\left(-P+2\eta\dfrac{\partial v}{\partial y}\right)}{\partial y}=-\rho\cdot g-Ra\cdot T \\[4mm] C_p\left(u\dfrac{\partial T}{\partial x}+v\dfrac{\partial T}{\partial y}\right)=\dfrac{\partial}{\partial x}\left(k\dfrac{\partial T}{\partial x}\right)+\dfrac{\partial}{\partial y}\left(k\dfrac{\partial T}{\partial y}\right)+Q+Q_{sh} \end{cases} \tag{1}$$

where:

P - pressure (Pa),

$\eta=\eta_0\cdot e^{\left[\frac{E_a}{R\cdot T_0}\cdot\left(\frac{T_0}{T}-1\right)\right]}$ - the mantle wedge viscosity (Pa s).

Other parameters are:

η_0 -mantle wedge viscosity at the potential temperature T_0 (reference viscosity) (10^{17} -10^{21} Pa s),

T_0 -mantle wedge potential temperature (1,450°C),

Ea -activation energy for olivine (kJ/mol),

R -universal gas constant (8.31451 J/mol.K),

T -temperature (°C),

u -horizontal component of the velocity (m/s),

v -vertical component of the velocity (m/s),

ρ -density (kg/m^3),

C_p -thermal capacity (MJ/m^{3}K),

k -thermal conductivity (MJ/m^{3}K),

Q -radiogenic heating (W/m^3),

Q_{sh} -volumetric shear heating (W/m^3),

$$Ra = \frac{\rho \cdot \alpha \cdot g \cdot \Delta T \cdot L^3}{\eta_0 \cdot k}$$ -thermal Rayleigh number,

α -thermal expansion $3.5 \cdot 10^{-5}$ (1/°C),

L -length scale (330 km),

ΔT -temperature difference between the bottom and top model temperatures (1450 °C),

k -thermal diffusivity (10^{-6} m/s^2),

g -gravitational acceleration (9.81 m/s^2).

The Stokes equations are solved only for the mantle wedge, while the heat transfer equation is solved for the entire model. The linear system solver used by the present numerical scheme is the frontal method, which represents an out-of-core version of the band solver (uses a reverse Cuthill - McKee ordering). For the model with strong temperature-dependent viscosity, the system of equations becomes strongly nonlinear, therefore Picard iterations are applied, and in order to achieve a convergent solution a cut-off viscosity of 10^{24} Pa s for the temperature less than 1,100 °C is used. For such highly non-linear problems we constructed a one-parameter family of problems using a variable (V), such that for $V = 1$ the problems is easy (e.g. linear) and for $V > N$ (N is less NSTEPS = 20), the problem reduces to the original highly nonlinear problem. The nonlinear terms are multiplied by MIN(1.0,(V - 1.0)/N). With a wide viscosity range from 10^{17} Pa s to 10^{24} Pa s, the fully nonlinear viscosity formulation (e.g., temperature and stress dependence of the viscosity) presented significant numerical instabilities; therefore the strain-rate dependence is neglected in the present study.

In the present numerical scheme, the penalty method formulation is used, P being replaced by $P = -\alpha' \cdot \left(\dfrac{\partial u}{\partial x} + \dfrac{\partial v}{\partial y} \right)$, where α' is large, on the order of $\dfrac{\eta}{\sqrt{\varepsilon}}$ (ε is the machine relative precision). In other words, the material is taken to be "almost" incompressible, so that a large pressure results in a small decrease in volume, and the continuity equation $\left(\dfrac{\partial u}{\partial x} + \dfrac{\partial v}{\partial y} \right) = 0$ is almost satisfied.

The finite elements grid extends from 25 km seaward of the trench up to 600 km landward of it, and consists of 12,000 triangular elements with the higher resolution in the tip of the wedge (*Fig. 2*). The triangles have the height to width ratio equal to 1. A benchmark with different grid resolutions is done to quantify the numerical error introduced by the present numerical scheme. The lower limit of the grid follows the shape of the subducting plate upper surface (*Kostoglodov et al., 1996*) at 100 km depth distance. The top of the model has a fixed temperature of 0°C. The temperature at the bottom of the model is of 1,450°C which represents the mantle temperature at ~ 100 km depth *(Fig. 3)*.

The continental lithosphere in Guerrero is defined mostly by the crust, which thickness is 40 km in the model. This is consistent with the values inferred from the seismic refraction surveys and gravity modeling (e.g. *Valdes et al., 1986, Arzate et al., 1993*). The bending geometry of the subducting slab (up to the hinge point: 270 km) is well constrained by gravity modeling (*Kostoglodov et al., 1996*), seismicity data and recently estimated extension of the coupled plate interface inferred from GPS measurements during the last slow slip event in Guerrero (2001-2002) (*Kostoglodov et al., 2003*).

A dip of the subducting plate beneath the volcanic arc is poorly constrained because of a very limited number of intraslab earthquakes. The dip of 20° and a hinge point at 270 km from the trench match better the hypocenter locations of the intraslab events (*Fig. 4*) and as a result, these are enveloped by the modeled "*seismicity cut-off*" temperature of T ~ 800°C (*Gorbatov and Kostoglodov, 1997*). The continental crust consists of two layers: the upper crust of 15 km and the lower

crust of 25 km. A summary of the thermal parameters used in the models is presented in *Table 1* (compilation from: *Peacock and Wang, 1999; Smith et al., 1979; Ziagos et al., 1985; Vacquier et al., 1967; Prol-Ledesma et al., 1989*).

The radiogenic heat generation in the continental crust decreases exponentially from 1.3 $\mu W/m^3$ in the uppermost crust down to 0.2 $\mu W/m^3$ in its lowermost part (*Ziagos et al., 1985*). The radiogenic heat production in the models is taken as 50% from the above values to fit the surface heat flow with the observed heat flow data (*Fig. 5*). This reduction has a minor effect on the thermal structure of the subduction interface and mantle wedge.

A long term sliding between the subducting and the continental plates along the thrust fault should produce frictional heating. We introduced in the models a small degree of volumetric frictional heating using the Byerlee's friction law (*Byerlee, 1978*). Frictional heating is ceased at a maximum depth of 40 km, which corresponds to the contact between the oceanic plate and the mantle wedge (*Fig. 3*). The volumetric shear heating is calculated as follows:

$$Q_{sh} = \frac{\tau \cdot v}{w}, \tag{2}$$

where:

Q_{sh} -volumetric shear heating (mW/m^3),

τ -shear stress $\begin{cases} \tau = 0.85 \cdot \sigma_n \cdot (1-\lambda) & \text{for } \sigma_n \cdot (1-\lambda) \leq 200 MPa \\ \tau = 50 + 0.6 \cdot \sigma_n \cdot (1-\lambda) & \text{for } \sigma_n \cdot (1-\lambda) > 200 MPa \end{cases}$

σ_n -lithostatic pressure (MPa),

λ -pore pressure ratio, (the ratio between the hydrostatic and lithostatic pressures. $\lambda = 0.98$ in the present study. The maximum value, $\lambda = 1$, means no frictional heating),

v -convergence velocity (5.5 cm/yr),

w -thickness of the oceanic crust involved in friction (200 m).

The right landward vertical boundary condition is defined by 20°C/km thermal gradient in the continental crust. This value is in agreement with the back-arc thermal gradient of 17.8 - 20.2°C/km reported by *Ziagos et al.* (*1985*).

Underneath Moho (40 km), the right boundary condition is represented by 10°C/km thermal gradient down to the depth of 100 km. Below 100 km, no horizontal conductive heat flow is specified. Below 100 km, no horizontal conductive heat flow is specified. Beneath Moho (40 km depth), for the right boundary corresponding to the mantle wedge, the boundary conditions are:

$$\begin{cases} \left(-P+2\cdot\eta\cdot\dfrac{\partial u}{\partial x}\right)\cdot\vec{n}_x+\eta\cdot\left(\dfrac{\partial u}{\partial y}+\dfrac{\partial v}{\partial x}\right)\cdot\vec{n}_y=GB1, \\[4mm] \eta\cdot\left(\dfrac{\partial u}{\partial y}+\dfrac{\partial v}{\partial x}\right)\cdot\vec{n}_x+\left(-P+2\cdot\eta\cdot\dfrac{\partial v}{\partial y}\right)\cdot\vec{n}_y=GB2, \end{cases} \tag{3}$$

which are obtained by balancing the internal (stress induced) forces against the external boundary forces, called tractions (*GB1* and *GB2*). Therefore, beneath Moho, where there is no "*external*" force applied, *GB1* = *GB2* = 0.

At the intersection between the subducted slab and the right boundary, the velocity of the subducting slab is used.

The left seaward boundary condition is a one-dimensional geotherm calculated for the oceanic plate by allowing a half-space to cool from zero age to the oceanic plate age at the trench. This geotherm is obtained using a time-dependent sedimentation history (*Wang and Davis, 1992*) and assuming a constant porosity-depth profile of the sediment column with a uniform sediment thickness of 200 m (*Moore et al., 1982*) at the trench (*Fig. 3*). The sedimentation history and the porosity-depth profile are used only to calculate the oceanic geotherm and are not included in the modeling procedure.

In terms of displacements, the velocity of the oceanic plate is considered with reference to the continental plate. Thus the convergence rate of 5.5 cm/yr between the Cocos and North American plates is used for the Guerrero subduction

zone (*DeMets et al., 1994*). The velocities in the subducting Cocos slab are set of 5.5 cm/yr; therefore the interface with the mantle wedge is predefined. The boundary between the mantle wedge and overlying lithosphere is considered fixed.

The Cocos plate age at the trench is 13.7 Myr according to the interpretation of Pacific-Cocos seafloor spreading magnetic anomaly lineations (*Klitgord and Mammerickx, 1982, Kostoglodov and Bandy, 1995*). The forearc thermal model constraints are described in detail by *Manea et al., 2004*. The present study is focusing mostly on the mantle wedge thermal and velocity structure.

Based on the velocity field obtained in the case of temperature dependent viscosity, a dynamic model for the blob tracers is developed using Stokes flow at infinite Prandtl number (*Turcotte and Schubert, 1982*). The blob moves under the action of drag, mass, and buoyancy forces in the mantle wedge stationary velocity field generated in the previous model (1). To investigate the mere dynamic effect of the mantle wedge convection on the hypothetical blobs rising from the subducted plate up to the base of the continental lithosphere, the following main assumptions are done:

-The motion of the asthenosphere is described by the above 2D Stokes equations (1);
-The blobs are spherical and the drag force is assumed to be similar to that of non-deforming spheres;
-The velocity field is steady state and the liquid acceleration is negligible because the related forces have small magnitude compared to the steady drag force;
-The influence of the blob motion on the mantle wedge circulation is irrelevant and there is not interaction between individual blobs.

According to these assumptions the total force acting on the blob is:

$$\vec{F} = \vec{F}_g + \vec{F}_A + \vec{F}_D \tag{4}$$

where:

$$\vec{F} = \frac{4 \cdot \pi \cdot r^3}{3} \cdot \rho_b \cdot \frac{d\vec{v_b}}{dt}$$ -resultant force

$$\vec{F_g} = \frac{4}{3} \cdot \pi \cdot r^3 \cdot \rho_b \cdot \vec{g}$$ -buoyancy force ($\vec{F_A} - \vec{F_g}$),

$$\vec{F_A} = -\frac{4}{3} \cdot \pi \cdot r^3 \cdot \rho_a \cdot \vec{g}$$

$$\vec{F_D} = \frac{1}{2} \cdot \pi \cdot r^2 \cdot \rho_a \cdot C_D(\text{Re}) \cdot (\vec{v_a} - \vec{v_b}) \cdot |\vec{v_a} - \vec{v_b}|$$ -steady drag force,

$$C_D(\text{Re}) = \frac{24}{\text{Re}}$$ -drag force coefficient

$$\text{Re} = \frac{2 \cdot r \cdot |\vec{v_a} - \vec{v_b}|}{\eta_w / \rho_a}$$ -Reynolds number,

$\vec{v_b}$ -blob velocity,

$\vec{v_a}$ -mantle wedge velocity,

r -blob radius (0.1 - 5.0 km),

ρ_b -blob density (3,000 kg/m^3),

ρ_a -mantle wedge density (3,200 kg/m^3),

$\vec{g}$ -gravitational acceleration (9.81 m/s^2),

η_w -the blob's wrapping viscosity (Pa s).

Using the expressions for forces, the equation of the blob motion has the following form:

$$\frac{d\vec{v_b}}{dt} = \vec{g} - \frac{\rho_a}{\rho_b}\vec{g} + \frac{3\rho_a C_D(\text{Re})}{8r\rho_b}(\vec{v_a} - \vec{v_b}) \cdot |\vec{v_a} - \vec{v_b}| \qquad (5)$$

The equations of the blob motion can be written as a system of four ordinary differential equations, two equations for the coordinates and two for the velocity. Then the system is solved using PDE2D.

The time step size will be chosen adaptively, between an upper limit of DTMAX = TF/NSTEPS and a lower limit of 0.0001·DTMAX. NSTEPS represents the minimum number of steps (NSTEPS = 5) and TF represents the time necessary for a blob to touch the base of the continental crust. Each time step, two steps of size DT/2 are taken, and that solution is compared with the result when one step of size DT is taken. If the maximum difference between the two answers is less than the relative tolerance (0.001), the time step DT is accepted. Then, the next step DT is doubled, if the agreement is "too" good; otherwise DT is halved and the process is repeated. As the tolerance is decreased, the global error decreases correspondingly. The Crank-Nicolson scheme is used to discretize the time. The steady mantle wedge velocity ($\vec{v_a}$) field is obtained previously, for the model with temperature dependent viscosity (1).

The trajectories of blobs with the diameters varying between 0.2 and 10.0 km are calculated for different values of η_w. The total rise times that the blobs require to reach the base of the continental crust are also estimated.

MODELING RESULTS

The thermal models which, correspond to the isoviscous mantle wedge and to the temperature-dependent viscosity, are presented in *Fig. 4, Fig. 6 and Fig. 7*. The isoviscous mantle wedge model predicts temperatures of ~ 830°C in the asthenosphere (*Fig. 4*), beneath the Popocatépetl volcano, indicating that melting should not occur at least for dry olivine. The geotherm of the oceanic plate surface does not intersect the *solidus* for basalt (*Fig. 8-A*), suggesting that the oceanic plate does not suffer melting as well. The temperature at the base of the continental crust is also low, reaching values of ~ 800°C, which is not sufficient to produce melting. The back flow velocity field from the mantle wedge (the inflow into the mantle wedge) is relatively small, ~ 1.5 cm/yr. It is evident that simple model with the isoviscous mantle wedge cannot create any source of the volcanic material beneath the CMVB.

A series of benchmark tests with different grid resolutions have been done to verify the accuracy of numerical scheme realized in the present study. The slab-mantle wedge interface is the area where the isotherms have a very small incidence angle with this interface, thus significant errors might appear along this boundary. The benchmark tests on this boundary quantify the numerical errors as a function of mesh resolution. Grids with a systematic increase in element number from 4,000 to 12,000 elements in steps of 2,000 elements are used for this benchmark.

The benchmark results are presented in *Fig. 9*. Large temperature fluctuations (up to 22°C) close to the tip of the wedge occur for grids with 4,000 and 6,000 elements. Increasing the mesh resolution (8,000 and 10,000 triangles), this fluctuation are diminished and the maximum temperature fluctuation along the slab-wedge interface is of ~ 7°C. Increasing the grid resolution to 12,000 triangles, the numerical error is less then 5°C. We stop the benchmark at this point because the computing time is increasing exponentially with the grid resolution (from half of hour for 4,000 triangles to more than 10 hours for a model with 12,000 elements,

running on a Pentium 4 PC at 3 Ghz and 2 Gb RAM memory). To obtain final results we used the 12,000 elements grid, thus our thermal models have the numerical error < 5°C.

The temperature dependent viscosity case has been investigated for a systematic variation of the rheological parameters η_0 and Ea. Hirth and Kohlstedt (*2003*) showed that the viscosities experimentally estimated for olivine at upper mantle pressures and temperatures are in the range of 10^{17} - 10^{21} Pa s. Consequently, the reference viscosity, η_0, has been varied in our model from 10^{17} Pa s up to 10^{21} Pa s. The modeling results are presented in *Fig. 6*. The activation energy for diffusion creep in olivine is fixed at 300 kJ/mol (*Karato and Wu, 1993*). For the viscosity, η_0, in the range from 10^{17} Pa s to 10^{20} Pa s, only a small increase of temperature (< 1 °C) is observed beneath Popocatépetl (*Fig. 10*). The maximum temperature underneath the Popocatépetl is around 1,260 °C. On the other hand, for the reference viscosity of $\eta_0 = 10^{21}$ Pa s, a significant decrease of temperature (~ 200°C) occurs. For this case a maximum temperature below Popocatépetl is ~ 1,170°C. The viscosity distributions in the mantle wedge for $\eta_0 = (10^{17} - 10^{21}$ Pa s) are presented in *Fig. 11*.

Experimentally obtained values of the activation energy for diffusion creep in olivine are of 300 kJ/mol (*Karato and Wu, 1993*) and of 315 kJ/mol (*Hirth and Kohlstedt, 1995*). The thermal models with variable activation energy from 150 kJ/mol up to 350 kJ/mol are presented in *Fig. 7*. Since the variation of the reference viscosity has a little effect on the overall thermal distribution (except for $\eta_0 = 10^{21}$ Pa s), the modeling is done for constant $\eta_0 = 10^{20}$ Pa s. Increase of the activation energy from 150 kJ/mol up to 300 kJ/mol results in a relatively small increase of temperature (< 25°C). For higher activation energies (~ 350 kJ/mol) an important increase in temperature (up to 70°C) is observed, and the maximum temperature below the Popocatépetl volcano reaches ~ 1,330 °C (*Fig. 12*). The mantle wedge viscosity distributions for $E_a = (150 - 350$ kJ/mol) are presented in *Fig. 13*.

The geotherms along the slab surface are presented in the phase diagram for mafics and harzburgite (*Hacker et al., 2002*) for a variable reference viscosity, η_0, in *Fig. 8*, and for variable activation energy, *Ea*, in *Fig. 14*. The slab geotherm intersects the dehydration melting *solidus* for basalt at 50 - 60 km for the reference viscosities $\eta_0 =(10^{17} - 10^{20}$ Pa s) and the activation energy *Ea* = (150 - 300 kJ/mol) (*Fig. 8-A and Fig. 14-A*).

The effect of the mantle wedge flow on the blob's trajectory is an interesting aspect of the volcanic magma source problem. We selected an initial point for the blob trajectories at the depth of 70 km on the surface of the subducted slab. This initial point corresponds to the geometric vertical projection of the Popocatépetl volcano on the subducting Cocos plate. Estimated blob trajectories are presented in *Fig. 15* for different wrapping viscosities ($10^{14} - 5 \cdot 10^{17}$ Pa s) and blob diameters (0.2 - 10.0 km).

For a wide range of activation energies (150 - 350 kJ/mol) and reference viscosities ($10^{17} - 10^{20}$ Pa s), the blob trajectories and rising times are practically indistinguishable (*Fig. 16*). Only for the reference viscosity of 10^{21} Pa s, an ~ 1 Myr increase in rising time is obtained due to lower velocities in the mantle wedge. A very low wrapping viscosity is essential to let the blob to rise up to the continental crust. Such low viscosity could result from the lubricating wrap around the blob. The source of the wrapping is apparently the melted material coming from the subducting slab, including the melted subducted sediments. Indeed, the water saturated sediments are likely to melt at a depths of 50 - 58 km for $\eta_0 =(10^{17} - 10^{21}$ Pa·s) (*Fig. 17-A*), and of 45 - 50 km for *Ea* = (150 - 350 kJ/mol) (*Fig. 17-B*).

For the blobs of 2 km size (*Fig. 15-C*) and the wrapping viscosity, $\eta_w >$ $2 \cdot 10^{16}$ Pa s, the drag force is predominant and the blob cannot rise. Decreasing the viscosity the drag force is less significant and at the depth of ~ 110 km the blob intercepts the mantle wedge back flow, which returns it toward the tip of the wedge. Finally the blob rises up and touches the continental crust after ~ 8 Myr. For the lower viscosity (< $9 \cdot 10^{15}$ Pa s) the blobs are rising faster (*Fig. 16*) and pop up at approximately the same point below the Popocatépetl volcano (~ 350 km from the

trench). The larger is the blob's size the less time is necessary to reach the continental crust. Any blob of the size > 0.6 km will touch the bottom of the continental crust in less then 4 Myr when the wrapping viscosity is of $1 \cdot 10^{15}$ Pa s *(Fig. 15-A)*. For the blob with the diameter of ~ 2 km, ~ 1 Myr is necessary to pop up if the $\eta_w < 3 \cdot 10^{15}$ Pa s. The buoyancy force of large size blobs becomes more dominant than the drag force and this yields a substantially upright trajectory. A 10 km blob touches the Moho in almost the same location for $\eta_w < 10^{17}$ Pa s *(Fig. 15-B)*. On the other hand, 10 km blobs with the $\eta_w > 5 \cdot 10^{17}$ Pa s would never rise up to the continental crust *(Fig. 15-D)*. For a η_w fixed at 10^{17} Pa s, blobs with diameters grater than 4 km will be able to traverse the mantle wedge flow and to go up toward the surface.

DISCUSSION AND CONCLUSIONS

Numerical models of temperature and velocity fields in the mantle wedge can contribute to our understanding of the magma generation, dynamics and volcanic sources in very atypical subduction zone of Central Mexico. In particular, the models, allowing for the ascending of buoyant material melted from the subducted slab and mantle in the form of plumes or blobs, can reveal the mechanisms of magma transport to the bottom of the continental plate.

Two basic thermo-mechanical models for the mantle wedge in the Central Mexico are considered in this study. The first model is restricted with the isoviscous mantle wedge whereas the second one is advanced with the temperature-dependent mantle viscosity. The first model (*Fig. 4*) does not predict any melting conditions in the asthenosphere, beneath the CMVB, at the base of the continental crust and on the surface of the subducting slab. The slab surface geotherm intersect neither the dehydration melting *solidus* for basalt (*Fig. 8-A*) nor the *solidus* for H_2O saturated sediments (*Fig. 17-A*). The vertical temperature profile just beneath the Popocatépetl volcano through the mantle wedge does not encounter the wet peridotite *solidus* (*Fig. 8-B*), thus the melting of the hydrated peridotite should not occur.

The temperature and velocity fields in the second model depend on the rheological parameters, the reference viscosity, η_0, and the activation energy, *Ea*. Variation of the reference viscosity, η_0, from 10^{17} Pa s to 10^{20} Pa s causes a slight temperature increase (< 15°C) close to the tip of the wedge (*Fig. 10*). Increasing the reference viscosity up to $\eta_0 = 10^{21}$ Pa s provokes a significant drop of the tip temperature of about 200°C. The phase diagram for mafic minerals shows (*Fig. 8-A*) that the melting of basaltic oceanic crust might take place at the depths of ~ 58 km for $\eta_0 = (10^{17} - 10^{20}$ Pa s), and at ~ 80 km for $\eta_0 = 10^{21}$ Pa s. The water saturated sediments start to melt at shallower depths, between 50 km and 55 km (*Fig. 17-A*). The vertical temperature profile beneath the Popocatépetl volcano achieves the temperature which is high enough to melt the wet peridotite (*Fig. 8-B*).

The thermal models show that basalt melting initiates at ~ 60 km depth for the activation energy, Ea = 150 - 300 kJ/mol, and at ~ 50 km depth for Ea = 350 kJ/mol (*Fig. 14-A*). In the range of reference viscosity values (10^{17} - 10^{21} Pa s), the saturated sediments may melt at the depth between 45 km and 50 km (*Fig. 14-B*). The temperature below the Popocatépetl volcano is well beyond the wet peridotite *solidus* for the whole range of activation energies applied in this study (150 - 350 kJ/mol).

The modeling results ascertain that the melting of the oceanic crust is likely to occur in a narrow depth range of 50 - 60 km (except for a reference viscosity of 10^{21} Pa s which predicts the melting at ~ 80 km depth). The subducted sediments begin to melt at shallower depths of 45 - 55 km for the entire range of η_0 and Ea.

As the oceanic crust melting starts, at first, the dacitic-rhyolitic magma is formed; afterward as it ascends and interacts with the mantle wedge, the adakitic magma might be formed. The oceanic slab contribution to the volcanism in Eastern Mexican Volcanic Belt has been reported by *Gomez-Tuena et al. (2003)*. Magmatic rocks with the adakitical signature have been found recently in the Quaternary series in CMVB. The stratovolcano Nevado de Toluca shows evidences of the same adakitic mark as well (*Gomez-Tuena - personal communication*).

The temperature of the hydrated peridotite below the CMVB is beyond wet peridotite *solidus*, but it is still lower the dry *solidus*. This suggests that the hydration of the mantle wedge by fluids released from the subducted Cocos plate is a necessary condition for the partial melting of the mantle. Indeed, the metamorphic dehydration predicted by our thermal models might occur down to 80 km depth. The estimated variation of wt% H_2O content with the depth along the subducting plate is presented in *Fig. 8-A* - inset. By the transformation of zoisite and amphibole into eclogite, ~ 0.6 wt% H_2O may be released into the mantle wedge from the hydrous phases in the subducting slab through a dehydration at the depths between 40 km and 60 km.

Mantle xenoliths (oxidized peridotite) have been found in Mexico near El Peñón (*Fig. 1*), suggesting an important flux of volatiles from the subducting Cocos

slab (*Blatter and Carmichael, 1998*). This dehydration would drop down the mantle viscosity in the tip of the wedge. This effect is not included in the present thermal models. The amount of serpentine in the tip of the wedge is much smaller for the model with temperature dependent viscosity (*Fig. 8-B* -upper left inset) than for the model with the isoviscous mantle wedge (*Fig. 8-B* -upper right inset). Furthermore, the amount of serpentine decreases as the activation energy increases (*Fig. 14-B* - upper insets). The serpentinized tip of the mantle wedge may have bearing on the down dip limit of the forarc coupled plate interface that controls an extension of aseismic slow slip transients (*Kostoglodov et al., 2003; Manea et al., 2004*).

The calcalkaline rocks are the most common series in the CMVB. This series includes the igneous rocks from basalts up to rhyolites, and is characterized by depletion of *Fe*. The depletion probably occurs because of the *Fe* and *Ti* oxides crystallization, which initially might be facilitated by the presence of fluids in the magma. The influx of volatiles from the metamorphosed oceanic crust and sediments triggers partial melting of peridotite above the subducted slab (*Tatsumi, 1986; Davies and Stevenson, 1992*). The majority of the calcalkalines in the CMVB is represented by the rocks with high content of K_2O and Na_2O, which originally might represent low degrees of partial melting in the mantle wedge. In fact, the wet *solidus* conditions for peridotite (*Wyllie, 1979*) are developed close to the slab surface (see *Fig. 7-A*).

Felsic magma formations were found in the monogenetic volcanic field of Chichinautzin (*Márquez and De Ignacio, 2002*). The models with the temperature-dependent viscosity show that at the base of the continental crust, the temperature exceeds 1,100°C (*Fig. 6 and Fig. 7*). That may create felsic magma sources in Sierra Chichinautzin by partial melting of the basaltic lower crust under low water fugacity conditions.

Recent paper of *Gerya and Yuen* (*2003*) demonstrates that Rayleigh-Taylor instabilities can develop and rise up from the surface of the cold subducting slab. They also suggest that the plumes detached from the slab might be lubricated by partially melted, low viscosity material of the subducted crust and hydrated mantle.

The modeling of the blob motion in the mantle wedge viscous flow induced by the subducting slab shows that this simple approach may help to understand the origin of the volcanism in the CMVB. The plume like blobs might origin at the slab-mantle wedge interface as a consequence of thermal instability. It appears that the detachment area along the subducted slab from which the blobs might emerge is not very large. Within the wide range of values of the rheological parameters, the sediment and oceanic crust melting, and metamorphic dehydration is expected to occur in the present models at depths of 45 - 60 km.

A certain distance along the slab surface is necessary for the melted material to accumulate and to form the blob. Nevertheless, the same blob detachment point in the present model is selected on the subducted slab surface, just below the main volcanic structure, Popocatépetl volcano (70 km depth). In reality, the spatial (and temporal) variation of the composition of the material transferred from the subducted Cocos plate into the overlying mantle wedge is expected. Therefore the volcanic arc lavas may be enriched with incompatible elements and volatiles, and highly variable composition of the subducted-related lavas is probable. The proposed positively buoyant blobs might have a complex composition of melted H_2O saturated peridotite, melted sediments and oceanic crust.

Two parameters control the trajectories of the blob structures rising from the slab: the diameter of the blob and the wrapping viscosity. Very low values of the wrapping viscosity (10^{14} - $5 \cdot 10^{17}$ Pa s) are necessary to reduce the drag force, which is critical for the blob to pop up. The lowest dynamic viscosity reported for dry mantle is ~ 10^{17} Pa s (*Moore et al., 1998*). On the other hand, the viscosity of hydrated, partially molten blobs might be as low as 10^{14} Pa s (*Gerya and Yuen, 2003*). Since the viscosity of the surrounding dry mantle controls the propagation of the blob, a certain mechanism is responsible for the occurrence of the low wrapping viscosity.

As the blob ascents through the mantle wedge, porous flow (*Davies and Stevenson, 1992*) of the melt and fluid might penetrate the mantle around the blob,

dropping there the viscosity down to 10^{14} Pa s. The rate of this penetration by porous flow has to be at least the same as the ascending rate of the blob. Recent laboratory experiments by *Hall and Kincaid* (*2001*) show that the positively buoyant blobs might pass through the low-viscosity, low-density paths created by previous blobs. The mechanism that produces the low wrapping viscosities may be a combination of the porous flow and a low viscosity conduit left by previous blobs.

Since the rigid sphere approximation is used to estimate the drag force applied to weak partially molten blobs, the estimates of wrapping viscosity in the present study should be considered as rather approximate. The blobs of 10 km diameter reach the base of the continental crust in ~ 6 Myr when the wrapping viscosity is of ~ $3 \cdot 10^{17}$ Pa s. Since this viscosity value is in the lower range reported for dry mantle (*Moore et al., 1998*), no wrapping viscosity mechanism is needed in this case. The blobs of such big size can affect locally the mantle wedge flow pattern and the effective viscosity distribution (*Gerya and Yuen, 2003*), especially for the temperature and strain-rate dependent viscosity (*Ranalli, 1995*). These effects are not included in the present models.

The time required for the blob of 1 km diameter to rise from the slab surface up to the continental crust varies between 0.001 Myr and 14 Myr for the viscosity between 10^{14} Pa s and $5 \cdot 10^{17}$ Pa s respectively. In general, the blob rising time decreases nonlinearly as its diameter increases and the wrapping viscosity is diminishing (*Fig. 16*). The reference viscosity, $\eta_{0,}$ in the range up to 10^{20} Pa s, has a negligible effect on the blob trajectory. The effect can be noticed for the higher values of the reference viscosity (10^{21} Pa s) when the raising time is more than ~ 2 Myr (*Fig. 16*).

The blob tracing dynamic model in the mantle wedge velocity field shows that the *"fast"* trajectories end at the same focus location (below the Popocatépetl volcano, ~ 350 km from trench) on the base of the continental crust (*Fig. 15*). This result may be interpreted as a possible condition for the development of the stratovolcanoes. The ending points of *"slow"* trajectories, which are common for the blobs of smaller size (~ 0.4 - 0.6 km), are scattered from the focus location (*Fig.*

15-A). This observation may give us a hint on a possible mechanism of monovogenic volcanism.

Recent studies (Lucia Capra – 2004, personal communication) revealed at least two magmatic pulses with a time span of ~ 1 Myr on the stratovolcano Nevado de Toluca. The maximum volume of each of these magmatic events is of 3.5 km^3 (equivalent blob diameter is ~ 2 km). It is interesting that both pulses started with a magmatic signature of melted sediments (*Ce* anomaly). These new studies will provide an important constrains on the blob size, rising time and the blob composition. From our model (*Fig. 15*), a blob of 2 km in diameter reaches the base of the continental crust in 1 Myr, if the wrapping viscosity is of ~ 2·10^{15} Pa s. The low viscosity is essential for the smaller size blobs to rise to the base of the continental crust.

The average volume of a monogenic cinder cone in the CMVB is less than 1 km^3 (*Hasenaka, 1994*), which corresponds to blob diameters of ~ 1.3 km. If the origin of monogenic cones are described by the blob tracing model, then the wrapping viscosity should be of η > 5·10^{15} Pa s to produce the "*slow*" trajectories. We need further model enhancement to verify the relation between the blob (or plume) hypothesis and the origin of the strato and monogenic volcanism in the CMVB.

REFERENCES

Alaniz-Alvarez, S.A., Nieto-Santiago, A.F., Tolson, G., 1998. A graphical technique to predict slip along a preexisting plane of weakness. *Engineering Geology, v. 49, pp.53-60.*

Arzate, J.A., Mareschal, M. and Urrutia-Fucugauchi, J., 1993. A preliminary crustal model of the Oaxaca continental margin and subduction zone from magnetotelluric and gravity measurements. *Geofísica Internacional, 32, 441-45.*

Blatter, D.L., and Carmichael, I.S.E., 1998. Hornblende peridotite xenoliths from central Mexico reveal the highly oxidized nature of subarc upper mantle. *Geology, v. 26, no. 11, pp. 1035-1038.*

Burov, E., Jolivet, E., Le Pourhiet, L. and Poliakov, A., 2000. A thermomechanical model of exhumation of high pressure (HP) and ultra-high pressure (UHP) metamorphic rocks in Alpine-type collision belts. *Tectonophysics, 342: 113-136.*

Byerlee, J.D., 1978. Friction of rocks. *Pure Applied Geophysics, 116, 615-626.*

Cebull, S.E., and Schubert, D.H., 1987. Mexican Volcanic Belt-an intraplate transform. *Geofisica Internacional, v.26, pp. 1-13.*

Conder, J.A., Weins, D.A., and Morris, J., 2002. On the decompression melting structure at volcanic arcs and back-arc spreading centres. *Geophysical Research Letters,29, 17-1-17-4.*

Currie C.A., Hyndman, R.D., Wang, K. and Kostoglodov, V., 2002. Thermal models of the Mexico subduction zone: Implications for the megathrust seismogenic zone. *Journal of Geophysical Research, 107, NO. B12, 2370, doi:10.1029/2001JB000886*

Davies, J.H., and Stevenson,D.J., 1992. Physical model of source region of subduction zone volcanism. *Journal of Geophysical Research, 97, 2037-2070.*

DeMets, C., Gordon, R., Argus, D. and Stein, S., 1994. Effect of recent revisions to the geomagnetic reversal time scale on estimates of current plate motions. *Geophysical Research Letters, 21, 2191-2194.*

Fedotov, S.A., 1981. Magma rates in feeding conduits of different volcanic centres. *Journal of Volcanology and Geothermal Research, v. 9, pp. 379-394.*

Ferrari, L., Garduno, V., Innocenti, F., Manetti, P., Pasquere, G., and Vaggeli, G., 1994. Volcanic evolution of central Mexico: Oligocene to Present. *Geofisica Internacional, 33, 91-105.*

Ferrari, L., Pasquare, G., and Tybaldi, A., 1990. Plio-Quaternary tectonics on the central Mexican Volcanic Belt and some constraints on its rifting mode. *Geofisica Internacional, v. 29, pp. 5-18.*

Furukawa, F., 1993. Magmatic processes under arcs and formation of the volcanic front. *Journal of Geophysical Research, 98, 8309-8319.*

Gerya, T.V. and Yuen, D.A., 2003. Rayleigh-Taylor instabilities from hydration and melting propel 'cold plumes' at subduction zones. *Earth and Planetary Science Letters, 212, 47-62.*

Gomez-Tuena A., LaGatta, A.B., Langmuir, C.H., Gutierrez, F.O., Carrasco-Nunez, G., 2003. Temporal control of subduction magmatism in the eastern Trans-Mexican Volcanic Belt: Mantle sources, slab contributions, and crustal contamination. *G-cubed, vol.4, no. 8.*

Gorbatov A., and V. Kostoglodov, 1997. Maximum depth of seismicity and thermal parameter of the subducting slab: worldwide empirical relation and its application. *Tectonophysics, 227, 165-187*

Hacker, B.R., Abers, G.A., and Peacock, S.M., 2003, Subduction Factory 1. Theoretical mineralogy, densities, seismic wave speeds, and H2O contents. *Journal of Geophysical Research, v. 108, 10.1029/2001JB001127.*

Hall, P., and Kincaid, C., 2001. Diapiric flow at subduction zones: a recipe for rapid transport. *Science, 292, 2472-2475.*

Hasenaka, B.R., 1994. Size, distribution, and magma output rate for shield volcanoes of the Michoacan-Guanajuato volcanic field, central México. *Journal of Volcanalogy and Geothermal Res., 63, 13-31.*

Hirth, G., and Kohlstedt, D.L., 1995. Experimental constraints on the dynamics of the partially molten upper mantle: Deformation in the diffusion creep regime. *Journal of Geophysical Research, 100, 1981-2001.*

Hirth, G., and Kohlstedt, D.L., 2003. Rheology of the mantle wedge: in Inside the Subduction Factory, *Geophysical Monograph 138*, edited by J. Eiler, *AGU, Washington DC, p. 83-105.*

Karato, S., and Wu, P., 1993. Rheology of the upper mantle: a synthesis. *Science, 260, 771-778.*

Kelemen, P.B., Rilling, J.L., Parmentier, E.M., Mehl, L., and Hacker, B.R.,2003. Thermal Structure due to Solid-State Flow in the Mantle Wedge Beneath Arcs, in Inside the Subduction Factory, *Geophysical Monograph 138*, edited by J. Eiler, *AGU, Washington DC, pp. 293-311.*

Klein, E.M., and Langmuir, C.H., 1987. Global correlations of ocean ridge basalt chemistry with axial depth and crustal thickness. *Journal of Geophysical Research, 92, 8089-8115.*

Klitgord, K. and Mammerickx, J., 1982. Northern East Pacific Rise: Magnetic anomaly and bathymetric framework. *Journal of Geophysical Research, 87, 6725-6750.*

Kostoglodov V. and W. Bandy, 1995. Seismotectonic constraints on the convergence rate between the Rivera and North American plates. *Journal of Geophysical Research, 100, 17,977-17,989.*

Kostoglodov V., W. Bandy, J. Domínguez, and M. Mena, 1996. Gravity and seismicity over the Guerrero seismic gap, México. *Geophysical Research Letters, 23, 3385-3388.*

Kostoglodov, V., Singh, S. K., Santiago, J. A., Franco, S. I., Larson, K. M., Lowry, A. R., and Bilham, R., 2003. A large silent earthquake in the Guerrero seismic gap, Mexico. *Geophysical Research Letters, 30(15), 1807, doi:10.1029/2003GL017219.*

Langmuir, C.L., Klein, E.M., and Plank, T., 1992. Petrological systematics of mid-ocean ridge basalts: Constraints on melt generation beneath ocean ridges, in

Mantle flow and melt generation at mid-ocean ridges. *AGU Monograph 71*, edited by J. Phipps Morgan, D.K. Blackman, and J.M. Sinton, pp. 183-280, *AGU, Washington DC.*

Luhr, J.F., 1997. Extensional tectonics and the diverse primitive volcanic rocks in the western Mexican Volcanic Belt. *Canadian Mineralogy, 35: 473-500.*

Manea, M., Manea, V.C., Kostoglodov, V., 2003. Sediment Fill of the Middle America Trench Inferred from the Gravity Anomalies. *Geofisica Internacional, 42, (4), 603-612.*

Manea, V.C., Manea, M., Kostoglodov, Currie, C.A., and Sewell, G., 2004. Thermal Structure, Coupling and Metamorphism in the Mexican Subduction Zone beneath Guerrero. *Geophysical Journal International, 158, 775–784 doi: 10.1111/j.1365 - 246X.2004.02325.x.*

Márquez, A., Oyarzun, R., Doblas, M., Verma, S.P., 1999a. Alkalic (OIB-type) and calc-alkalic volcanism in Mexican volcanic belt: a case study of plume-related magmatism and propagating rifting at an active margine? *Geology, 27: 51-54.*

Márquez, A., Oyarzun, R., Doblas, M., Verma, S.P., 1999b. Replay to comment to: Alkalic (OIB-type) and calc-alkalic volcanism in Mexican volcanic belt: a case study of plume-related magmatism and propagating rifting at an active margine? *Geology, 27: 1055-1056.*

Márquez, A., Verma, S.P., Anguita, F., Oyarzun, R., Brandle, J.L., 1999c. Tectonics and volcanism of Sierra Chichinautzin: extension at the front of the central Trans-Mexican Volcanic Belt. *Journal of Volcanology and Geothermal Research, 93, 125-150.*

Márquez, A. and De Ignatio, C., 2002. Mineralogical and geochemical constrains for the origin and evolution of magmas in Sierra Chichinautzin, Central Mexican Volcanic Belt. *Lithos, 62, 35-62.*

Moore, J.C., J.S. Watkins, T.H.Shipley, K.J. McMillen, S.B. Bachman, and N. Lundberg, 1982. Geology and tectonic evolution of a juvenile accretionary terrane along a truncated convergent margin: Synthesis of results from Leg 66 of the Deep

Sea Drilling Project, southern México. *Geological Society American Bulletin, 93,* *847-861.*

Moore, W. B., Schubert, G., and Tackley, P. J., 1998. Three-Dimensional Simulations of Plume-Lithosphere Interaction at the Hawaiian Swell. *Science, 279,* *1008-1011.*

Nichols, G.T., Wyllie, P.J., and Stern, C.R., 1994. Subduction zone melting of pelagic sediments constrained by melting experiments. *Nature, 371, 785-788.*

Pardo, M. Suárez, G., 1995. Shape of the subducted Rivera and Cocos plates in southern mexico: seismic and tectonic implications. *Journal of Geophysical Research, 100, 12357-12373.*

Peacock, S.M., and K. Wang, 1999. Sesimic consequences of warm versus cool subduction metamorphism: Examples from southwest and northeast Japan. *Science, 286, 937-939.*

Prol-Ledesma, R.M., Sugrobov, V.M., Flores, E.L., Juarez, G., Smirnov, Y.B., Gorshkov, A.P., Bondarenko, V.G., Rashidov, V.A., Nedopekin, L.N. and Gavrilov, V.A., 1989. Heat flow variations along the Middle America Trench. *Marine Geophysical Research, 11, 69-76..*

Ranalli, G., 1995. Rheology of the Earth, 2nd edition, *Chapman and Hall, London,* *413pp.*

Shubert, D.H., and Cebull, S.E., 1984. Tectonic interpretation of the Trans-Mexican volcanic belt. *Tectonophysics, 101, pp.159-165.*

Smith, D.L., Nuckels, C.E., Jones, R.L. and Cook, G.A., 1979. Distribution of heat flow and radioactive heat generation in northern Mexico, *Journal of Geophysical Research, 84, 2371-2379.*

Takada, A., 1989. Magma transport and reservoir formation by a system of propagating cracks. *Bulletin of Volcanology, v. 52, pp.118-126.*

Takada, A., 1994. The influence of regional stress and magmatic input on styles of monogenetic and polygenetic volcanism. *Journal of Geophysical Research, v. 99,* *pp. 13563-13573.*

Tatsumi, Y., 1986. Formation of the volcanic front in subduction zones. Geophysical Research Letters, *13, 717-720.*

Turcotte, D.L., and Schubert, G., 1982. Geodynamics, Applications of continuum Physics to Geological Problems. *Wiley, New York, NY.*

Vacquier, V., J.G. Sclater, and C.E. Corry, 1967. Studies of the thermal state of Earth. The 21st paper: Heat-flow, eastern Pacific. *Bulletin of Earthquake Research Institute, 45, 375-393.*

Valdes, C.M., Mooney, W.D., Singh, S.K., Meyer, R.P., Lomnitz, C, Luetgert, J.H., Helsley, C.E., Lewis, B.T.R. and Mena, M., 1986. Crustal structure of Oaxaca, Mexico, form seismic refraction measurements. *Bulletin of Seismological Society of America, 76, 547-563.*

van Hunen, J., van den Berg, A., and Vlaar, N., 2002. On the role of subducting oceanic plateaus in the development of shallow flat subduction. *Tectonophysics, 352, 317-333.*

van Keken, P.E., Kiefer, B., and Peacock, S.M., 2002. High resolution models of subduction zones: Implications for mineral dehydration reactions and the transport of water into deep mantle. *G-cubed, 3, 10, 20.*

Verma, S.P., 1999. Geochemistry of evolved magmas and their relationship to subduction un-related mafic volcanism at the volcanic front of the central Mexican Volcanic Belt. *Journal of Volcanology and Geothermal Research, v.93, pp. 151-171.*

Verma, S.P., 2000. Geochemistry of subducting Cocos plate and the origin of subduction-unrelated mafic volcanism at volcanic front of central Mexican Volcanic Belt, in Delgado-Granados, H., Aquirre-Diaz, G.J., and Stock, J., eds., Cenozoictectonics and volcanism of Mexico: Boulder Colorado, *Geological Society of America, Special Paper, 334, pp. 195-222.*

Wallace, P., Carmichael, I.S.E., 1999. Quaternary volcanism near the Valley of Mexico: implications for subduction zone magmatism and the effects of crustal thickness variations on primitive magma compositions. *Contribution to Mineral Petrology. 135, 291-314.*

Wang, K. and Davis, E.E., 1992. Thermal effect of marine sedimentation in hydrothermally active areas. *Geophysical Journal International, 110, 70-78.*

Wyllie, P.J., 1979. Magmas and volatile components, *American Mineralogy, 654, 469-500.*

Ziagos, J.P., D.D. Blackwell, and F. Mooser, 1985. Heat flow in southern Mexico and the thermal effects of subduction, *Journal of Geophysical Research, 90, 5410-5420.*

Table 1. Summary of the thermal parameters used in the models. (Compilation from: *Peacock and Wang, 1999; Smith et al., 1979; Ziagos et al., 1985; Vacquier et al., 1967; Prol-Ledesma et al., 1989).*

Geological Unit	Density (kg/m³)	Thermal Conductivity (W/mK)	Radiogenic heat production (µW/m³)	Thermal Capacity (MJ/m³K)
Oceanic sediments	2200	1.00 – 2.00*	1.00	2.50
Upper continental crust (0-15 Km)	2700	2.00	0.65	2.50
Lower continental crust (15-40 Km)	2700	2.00	0.15	2.50
Mantle wedge	3100	3.10	0.01	3.30
Oceanic lithosphere	3000	2.90	0.02	3.30

* *Increase linearly with distance from the deformation front up to a depth of 10 Km.*

FIGURE CAPTIONS

Figure 1.

Tectonic setting and position of the modeled cross-section (straight line), in Guerrero. Triangles show the location of active volcanoes in Mexico. Dashed ellipse is the CMVB - Central Mexican Volcanic Belt. Light blue rectangle represents the El Peñón area, where mantle xenoliths have been found. Arrows show convergence velocities between the Cocos and North American plates (*DeMets et al., 1994*).

Figure 2.

The grid with 12,000 elements used to solve the numerical models. This particular shape of the grid is designed to better resolve the velocity field nearby the tip of the mantle wedge.

Figure 3.

Boundary conditions and parameters used in the modeling. The upper and lower boundaries have constant temperatures of 0°C and 1,450°C, accordingly. The continental plate is fixed. The right (landward) vertical boundary: 20°C/km thermal gradient in the continental crust (down to 40 km); between 40 km and 100 km depth the thermal gradient is of 10°C/km; no horizontal conductive heat flow is specified beneath 100 km depth. Zero traction is considered beneath Moho (40 Km), at the boundary, which belongs to the mantle wedge. The convergence velocity is specified for the intersection between the right boundary and the subducting slab. The left (seaward) boundary condition is a one-dimensional geotherm for the oceanic plate. The Cocos plate motion is referred to the North American plate with the convergence velocity of 5.5 cm/yr. Volumetric shear heating is imposed along the plate interface up to a maximum depth of 40 km, using the Byerlee's friction law (*Byerlee, 1978*).

Figure 4.

Calculated steady-state thermal field for the isoviscous mantle wedge. Horizontal black dashed line shows the Moho (40 km depth). The hinge point is at 270 km from the trench. Thick violet solid line denotes the top of the subducting slab. Orange triangles are the two principal stratovolcanoes in CMVB: Nevado de Toluca and Popocatépetl. The maximum temperature beneath Popocatépetl volcano is about of 830°C. The lower left inset is the magnified thermal structure close to the tip of the mantle wedge. Thin dark blue arrows in the mantle wedge represent the velocity field. The intraslab earthquakes with magnitudes, $M_w \geq 5.5$, are represented by the focal mechanisms. The two brown clouds of hypocenters beneath the coast denote the smaller magnitude seismicity associated probably with the bending of the subducted plate.

Figure 5.

Variation of the surface heat flow along the Guerrero profile. The dots with vertical error bars are heat flow data reported by *Ziagos et al. (1985)*.

(A). Surface heat flow for steady-state thermal models reference viscosities $\eta_0 = 10^{17} - 10^{21}$ Pa s and Ea = 300 kJ/mol.

(B). Surface heat flow for steady-state thermal models activation energies $Ea = 150 - 350$ kJ/mol and $\eta_0 = 10^{20}$ Pa s.

Figure 6.

Steady-state thermal models with strong temperature-dependent viscosity in the mantle wedge. The reference viscosity, η_0, varies from 10^{17} Pa s (A) up to 10^{21} Pa s (E). The activation energy for olivine of 300 kJ/mol is used. Note an important increase of the temperature close to the tip of the wedge (A-D). NP and P represent the Nevado de Toluca and Popocatépetl volcanoes. The maximum temperature beneath the Popocatépetl volcano is about of 1,230°C. Other notations are the same as in *Fig. 4*.

Figure 7.

Steady-state thermal models with strong temperature-dependent viscosity in the mantle wedge for activation energies, *Ea*, from 150 kJ/mol (A.) to 350 kJ/mol (E). The reference viscosity of 10^{20} Pa s is used. The maximum temperature beneath the Popocatépetl volcano is about of ~ 1,250°C (A - D) and more than 1 300°C (E). Other notations are the same as in *Fig. 4*.

Figure 8.

(A). Phase diagrams for the MORB (*Hacker et al., 2002*). 1 - Zeolite (4.6 wt% H_2O), 2 - Prehnite - Pumpellyite (4.5 wt% H_2O), 3 - Pumpellyite - Actinolite (4.4 wt% H_2O), 4 - Greenschist (3.3 wt% H_2O), 5 - Lawsonite - Blueschist (5.4 wt% H_2O), 6 - Epidote - Blueschist (3.1 wt% H_2O), 7 - Epidote - Amphibolite (2.1 wt% H_2O), 8 - Jadeite - Epidote - Blueschist (3.1 wt% H_2O), 9 - Eclogite - Amphibole (2.4 wt% H_2O), 10 - Amphibolite (1.3 wt% H_2O), 11 - Garnet - Amphibolite (1.2 wt% H_2O), 12 - Granulite (0.5 wt% H_2O), 13 - Garnet - Granulite (0.0 wt% H_2O), 14 - Jaedite - Lawsonite - Blueschist (5.4 wt% H_2O), 15 - Lawsonite - Amphibole - Eclogite (3.0 wt% H_2O), 16 - Jaedite - Lawsonite - Talc - Schist, 17 - Zoisite - Amphibole - Eclogite (0.7 wt% H_2O), 18 - Amphibole-Eclogite (0.6 wt% H_2O), 19 - Zoisite-Eclogite (0.3 wt% H_2O), 20 - Eclogite (0.1 wt% H_2O), 21 - Coesite - Eclogite (0.1 wt% H_2O), 22 - Diamond - Eclogite (0.1 wt% H_2O). Slab surface geotherms are calculated for the reference viscosity range: 10^{17} - 10^{21} Pa s (see inset).

(B). Phase diagram for harzburgite (*Hacker et al., 2002*). A - Serpentine - Chlorite - Brucite (14.6 wt% H_2O), B - Serpentine - Chlorite - Phase A (12 wt% H_2O), C - Serpentine - Chlorite - Dunite (6.2 wt% H_2O), D - Chlorite - Harzburgite (1.4 wt% H_2O), E - Talc - Chlorite - Dunite (1.7 wt% H_2O), F - Anthigorite - Chlorite - Dunite (1.7 wt% H_2O), G - Spinel - Harzburgite (0.0 wt% H_2O), H - Garnet - Harzburgite (0.0 wt% H_2O). Calculated geotherms for the slab surface are the same as in A. The vertical temperature profile beneath the Popocatépetl volcano are the same as in *Fig. 10*. The amount of serpentine (green-yellow hatched insets) in the tip of the mantle wedge is noticeably smaller for the model with

temperature dependent viscosity (upper left inset) than for the model with the isoviscous mantle wedge (upper right inset).

Figure 9.

The results of benchmark test with different grid resolutions: 4,000, 6,000, 8,000, 1,000 and 12,000 triangles. The temperature differences between two subsequent models are calculated along the slab-wedge interface. Note the temperature fluctuation up to 22°C for low grid resolution (blue curve). Less than 5°C numerical error results when the grid with 12,000 triangles is used (red curve).

Figure 10.

Vertical temperature profile (A-A') for the mantle wedge thermal models with the reference viscosities of 10^{17} - 10^{21} Pa s. The activation energy is fixed at 300 kJ/mol. The temperature profile for the model with the isoviscous mantle is also shown as a dashed line.

Figure 11.

Distribution of the mantle wedge viscosity for steady-state thermal (*Fig. 4*) models with strong temperature-dependent viscosity. The reference viscosity, η_0, is from 10^{17} Pa s (A) up to 10^{21} Pa s (E).

Figure 12.

Vertical temperature profile (A-A') through the mantle wedge. The thermal modeling is done for activation energies of 150 - 350 kJ/mol. The reference viscosity is fixed at 10^{20} Pa s. Dashed line shows, for a comparison, the temperature profile for the model with the isoviscous mantle wedge.

Figure 13.

Distribution of mantle wedge viscosity with strong temperature-dependence for steady-state thermal models (*Fig. 12*). Activation energies, *Ea*, are from 150 kJ/mol up to 350 kJ/mol.

Figure 14.

(A). Phase diagrams for the MORB and maximum H_2O contents (*Hacker et al., 2002*). Modeled slab surface geotherms are plotted for the activation energy range: 150 - 350 kJ/mol (see inset). The other notations are the same as in *Fig. 8*.

(B). Phase diagram for harzburgite, and maximum H_2O contents (*Hacker et al., 2002*). The calculated geotherms are the same as in A, as well as those from the vertical profile beneath Popocatépetl (see *Fig. 13*). The amount of serpentine (green-yellow hatch upper insets) in the tip of the wedge decreases as the activation energy increases.

Figure 15. Blob trajectories in the steady mantle wedge flow Initial points for all trajectories are selected on the surface of the slab, right below the Popocatépetl volcano at 70 km depth.

(A). The wrapping viscosity is fixed at 10^{15} Pa s. The blobs with the diameter less than 0.4 would never rise up to the continental crust.

(B). The blob diameter is fixed at 10 km. The trajectories corresponding to different wrapping viscosities of less than 10^{17} Pa s have the same final point below the Popocatépetl volcano. The blobs would never rise up to the continental crust if with the wrapping viscosities is $> 5 \cdot 10^{17}$ Pa s.

(C). The blob's diameter is fixed at 2 km. The trajectories corresponding to different wrapping viscosities of less than $9 \cdot 10^{15}$ Pa s, have the same final point below the Popocatépetl volcano. The blobs with the wrapping viscosities $> 2 \cdot 10^{16}$ Pa s would never rise up to the continental crust.

(D). The wrapping viscosity is fixed at 10^{17} Pa s. The trajectories correspond to different blob size (4 - 10 km). The blobs with the diameter less than 4 km would never rise up to the continental crust.

Figure 16.

Blob rising time as a function of the wrapping viscosity. For a wide range of rheological parameters ($\eta_0 = 10^{17}$ - 10^{20} Pa s and Ea = 150 - 350 kJ/mol) the blob trajectories and rising times are nearly identical (blue curves). For the reference viscosity of 10^{21} Pa s, the rising time becomes longer after ~ 1 Myr, for a given wrapping viscosity (dashed green curves). The curves annotated with the blob's diameter show that the rising time is decreasing for the bigger blobs and the lower viscosity. The blobs with the size of ~ 2 km can reach the continental crust in less than 1 Myr (black dashed line) at a wide range of low wrapping viscosities.

Figure 17.

(A). Calculated slab surface geotherms for models with reference viscosities in the range of 10^{17} - 10^{21} Pa s (see inset), and fluid saturated sediment *solidus* from (*Nichols et al., 1994*). The horizontal dashed arrows mark the depths where the sediment meting might occur. Dashed line represents the geotherm for the isoviscous mantle.

(B). Calculated slab surface geotherms for models with activation energy range: 150 - 350 kJ/mol (see inset) and fluid saturated sediment *solidus* from *Nichols et al., 1994*. The horizontal dashed arrows mark the depths where sediment meting might occur.
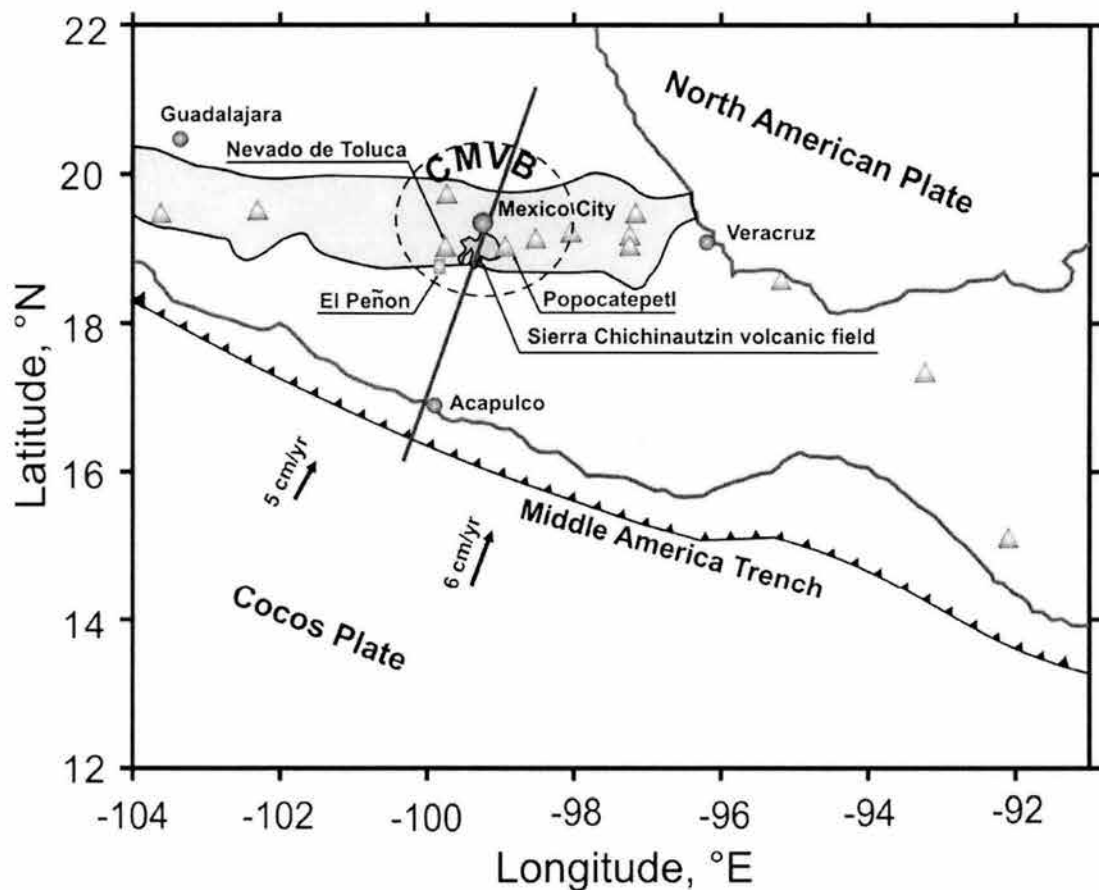
Figure 1
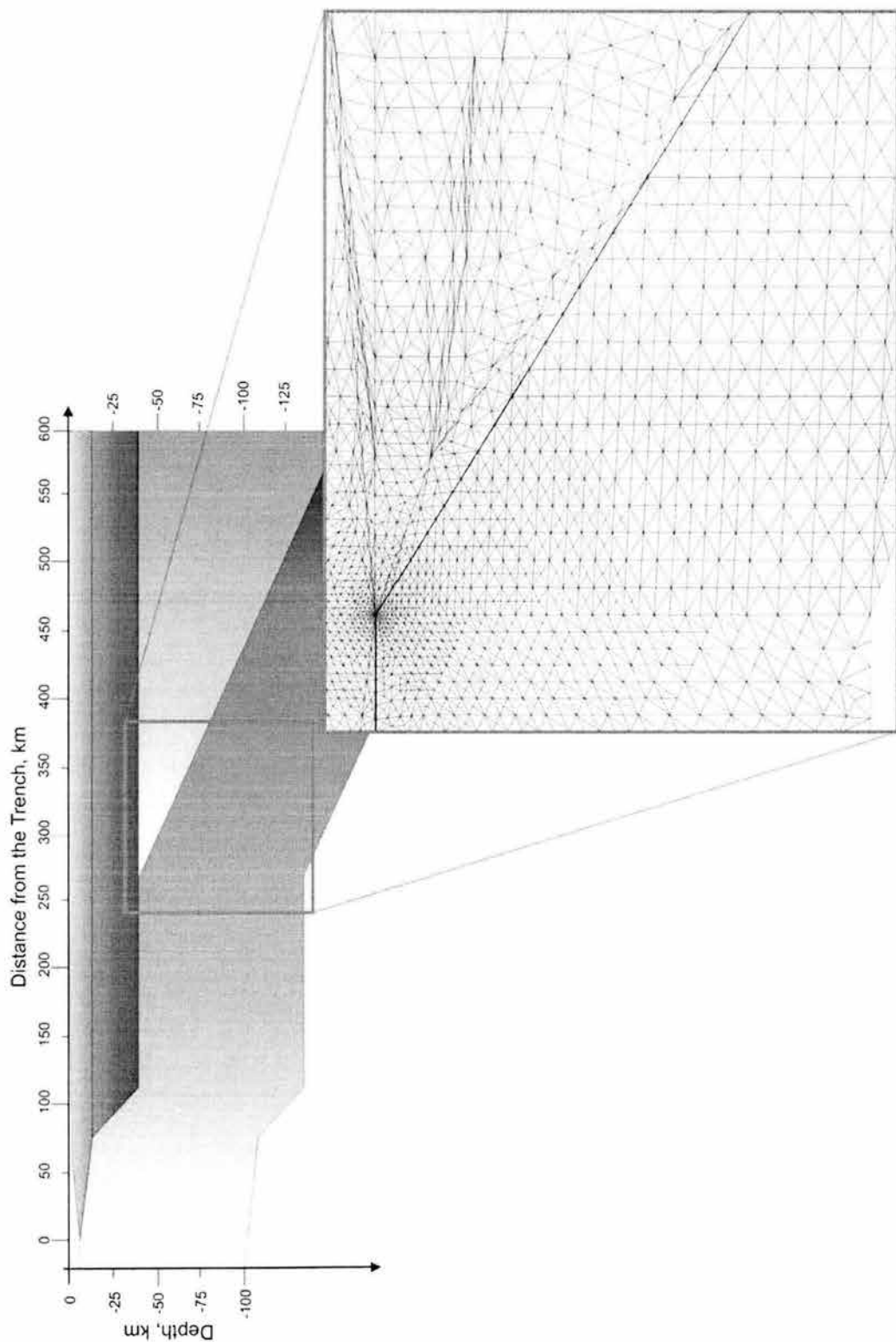
Figure 2
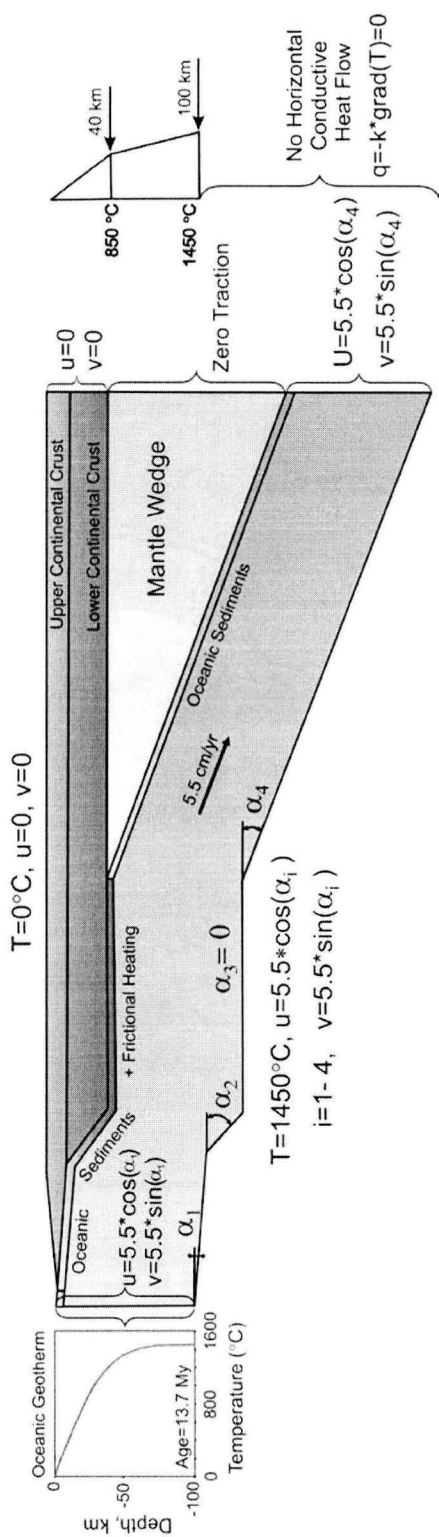
Figure 3
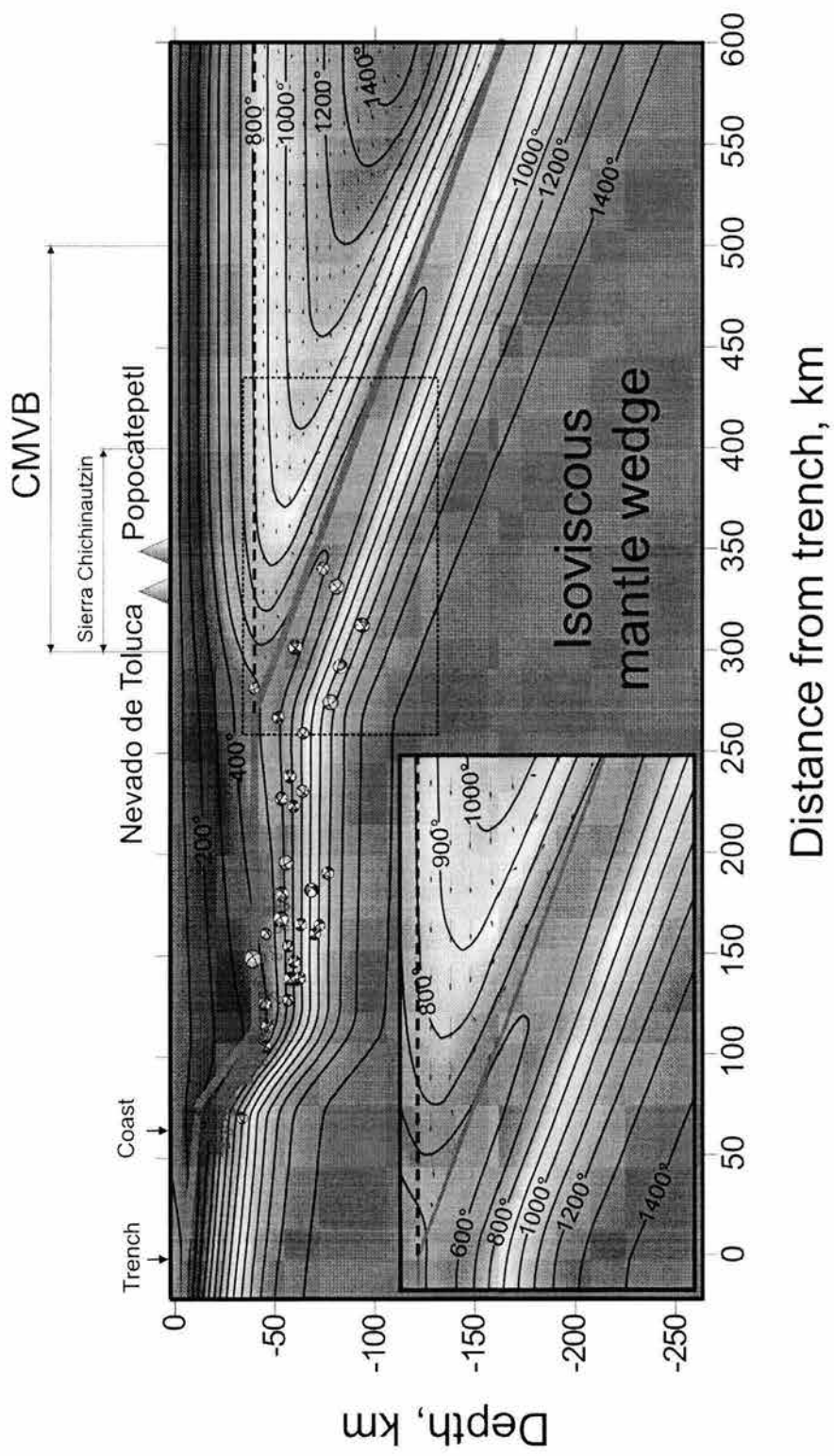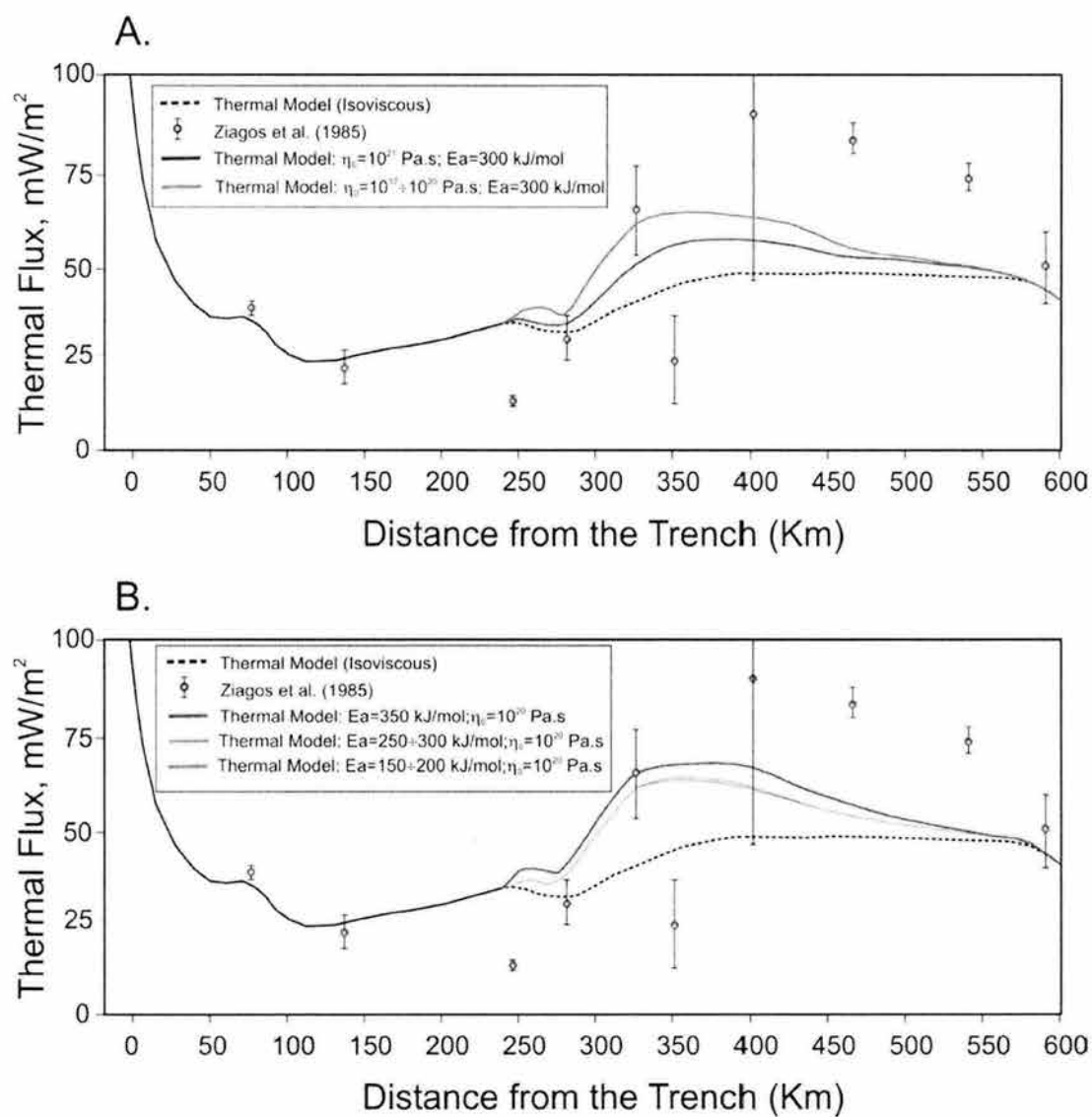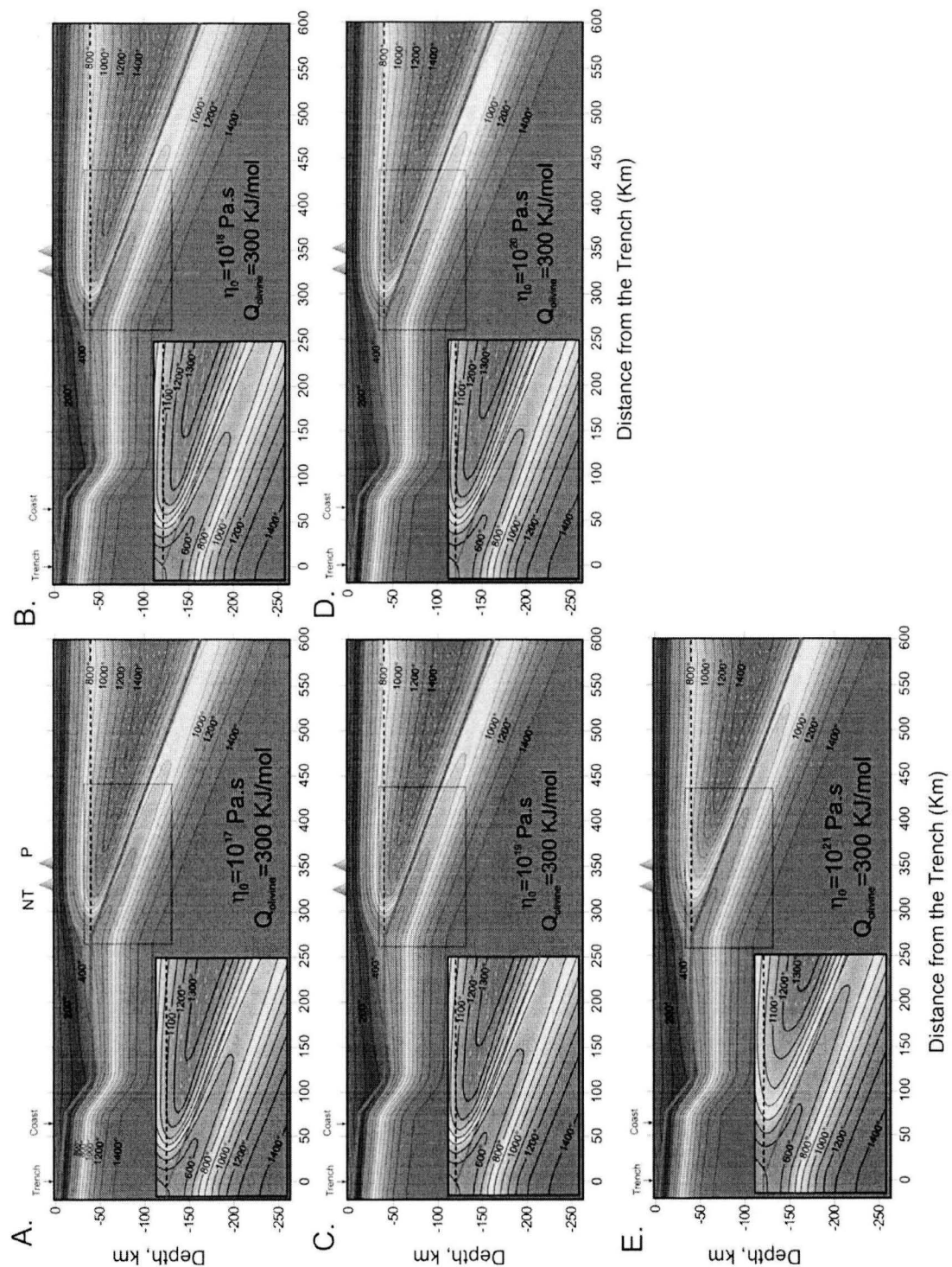
Figure 4
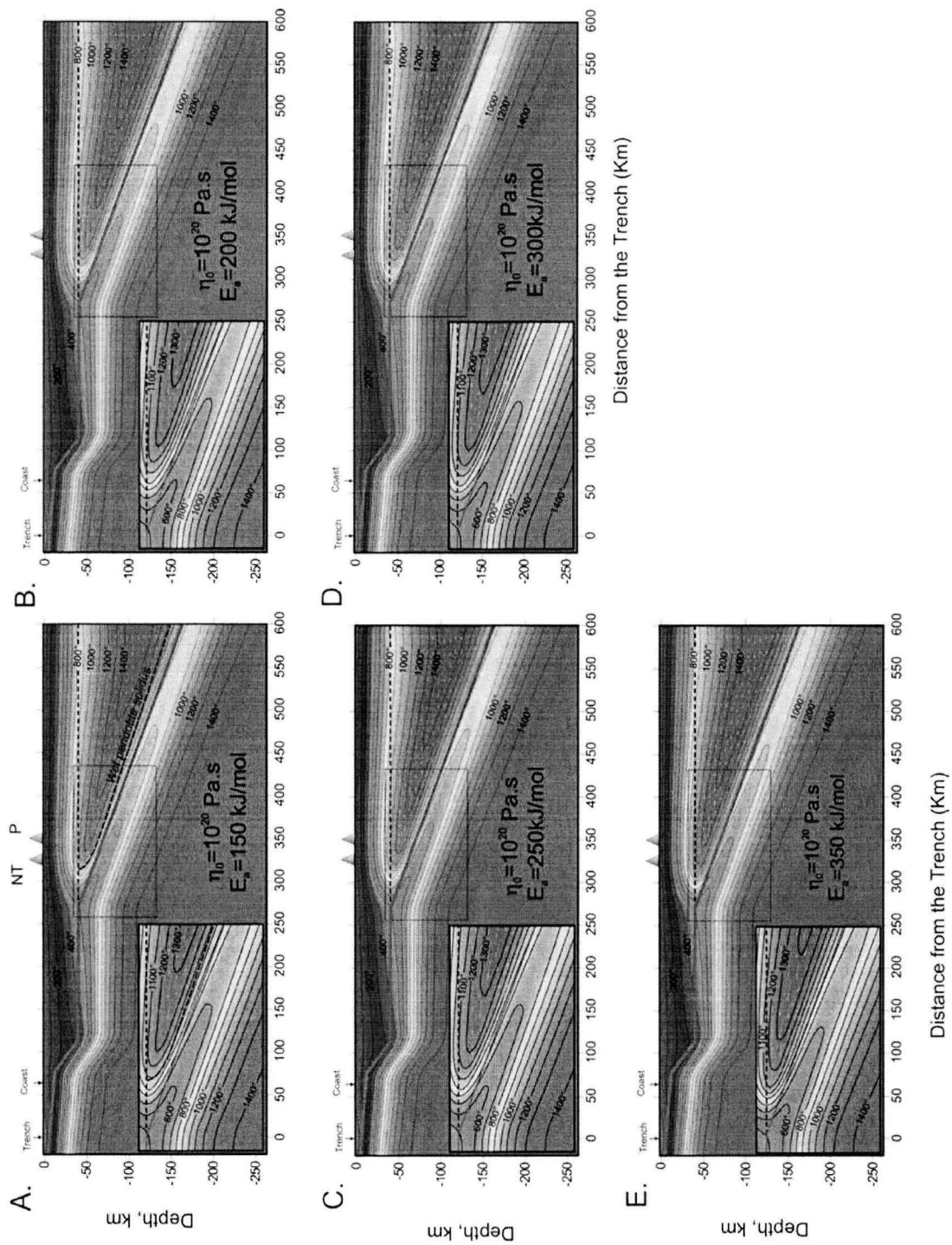
Figure 5
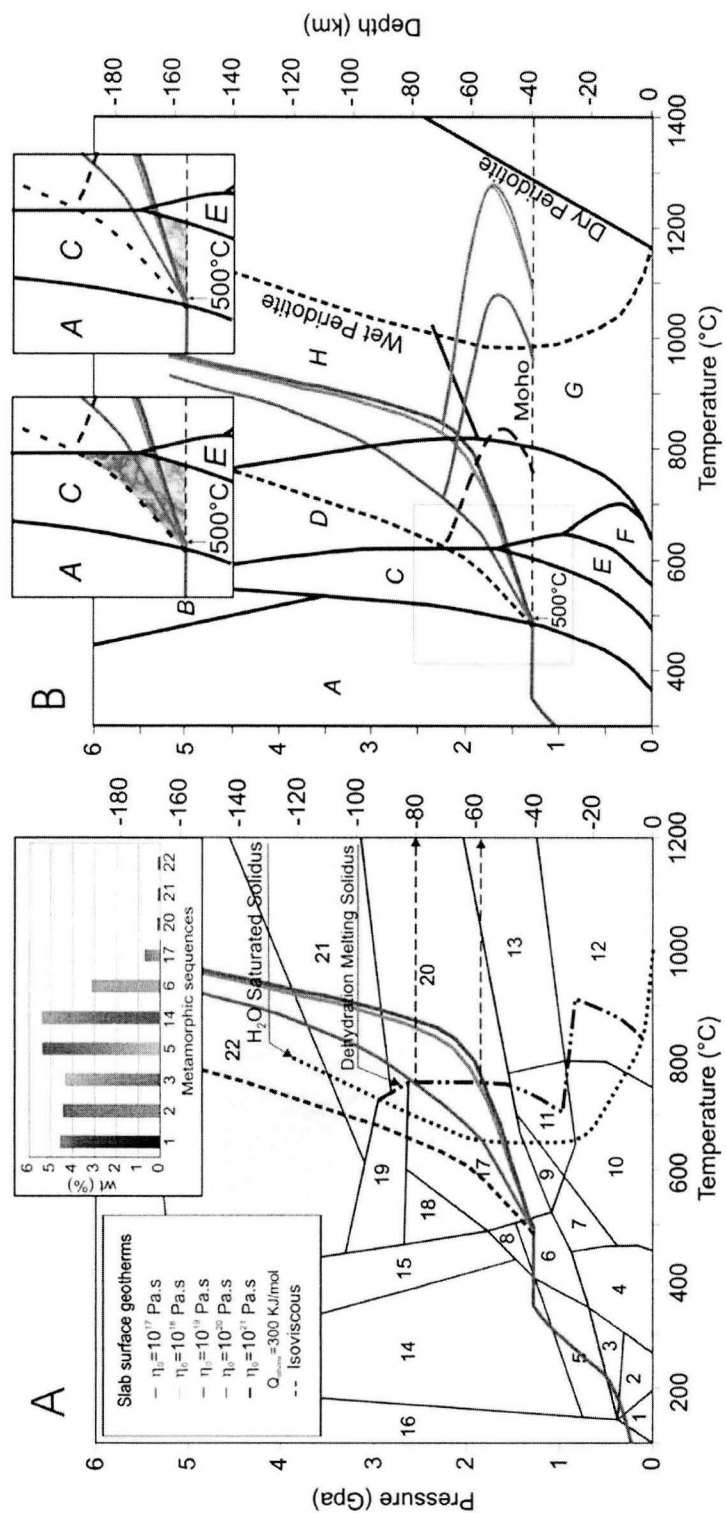
Figure 6
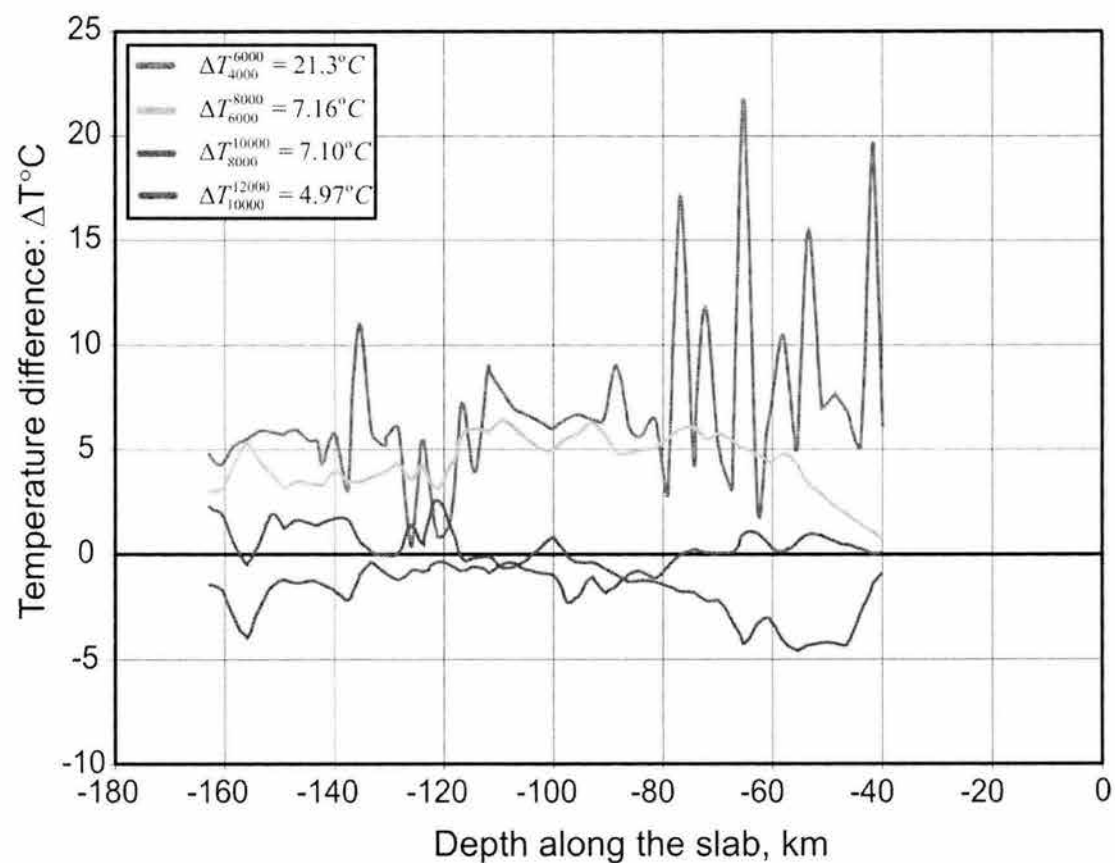
Figure 7
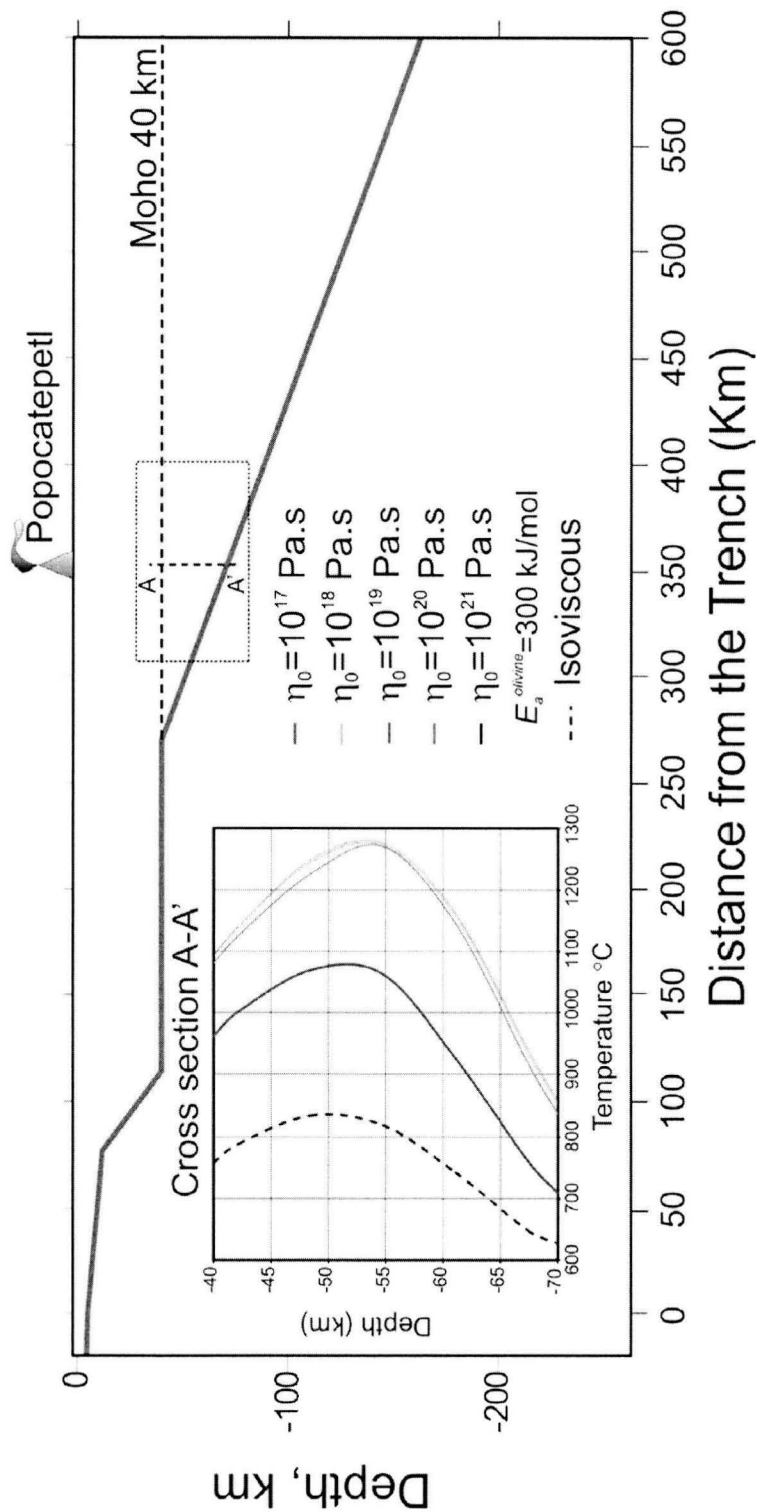
Figure 8
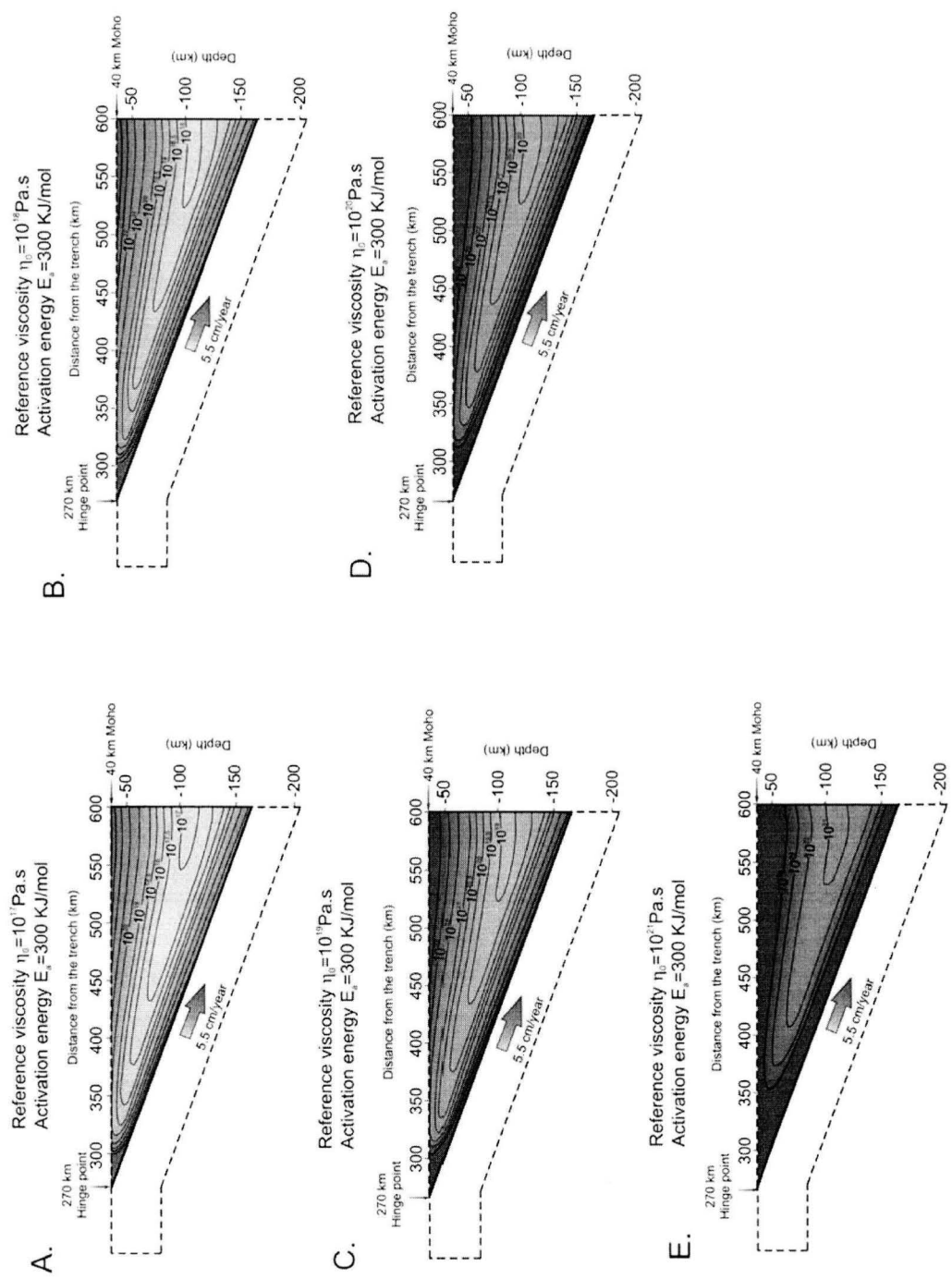
Figure 9
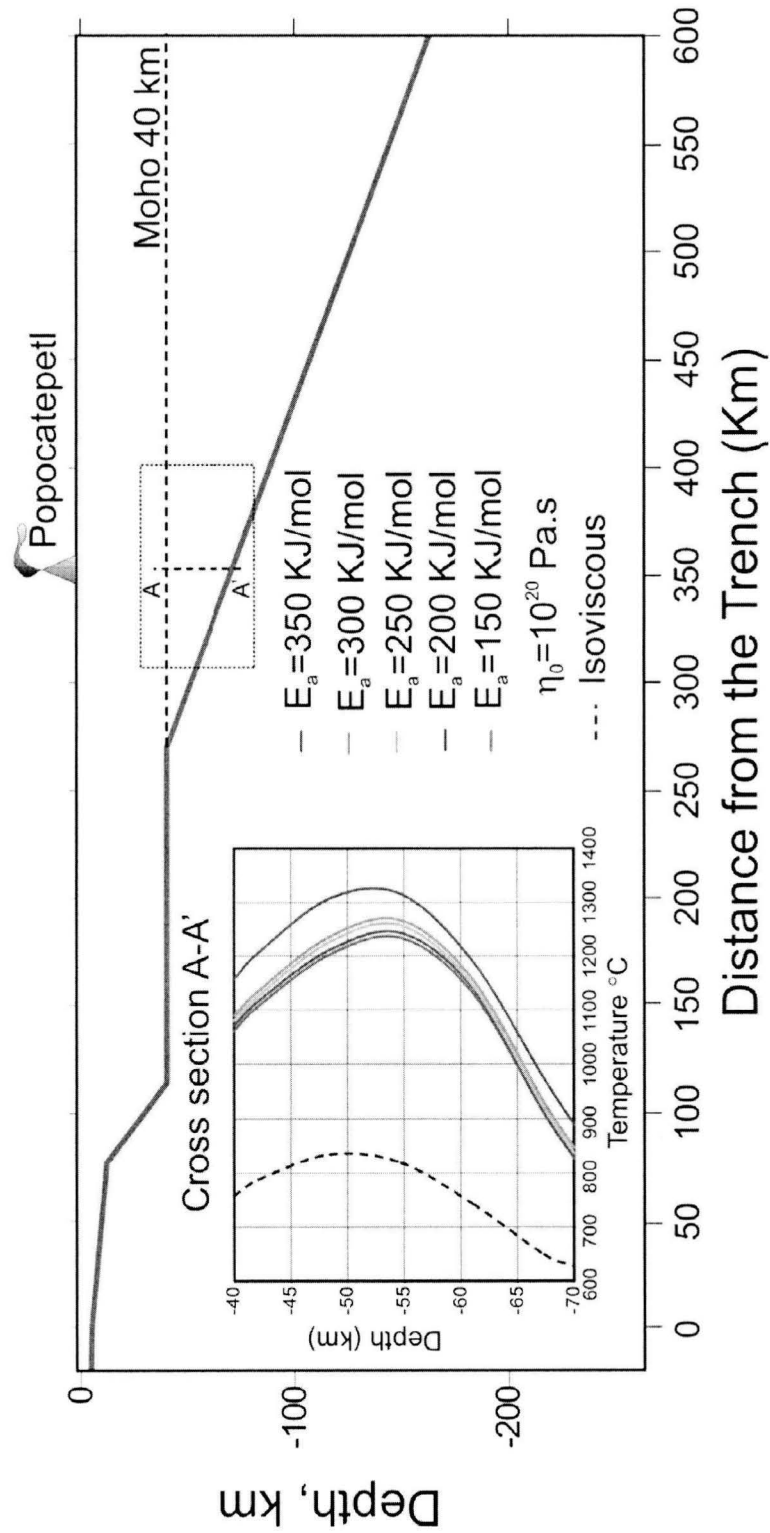
Figure 10
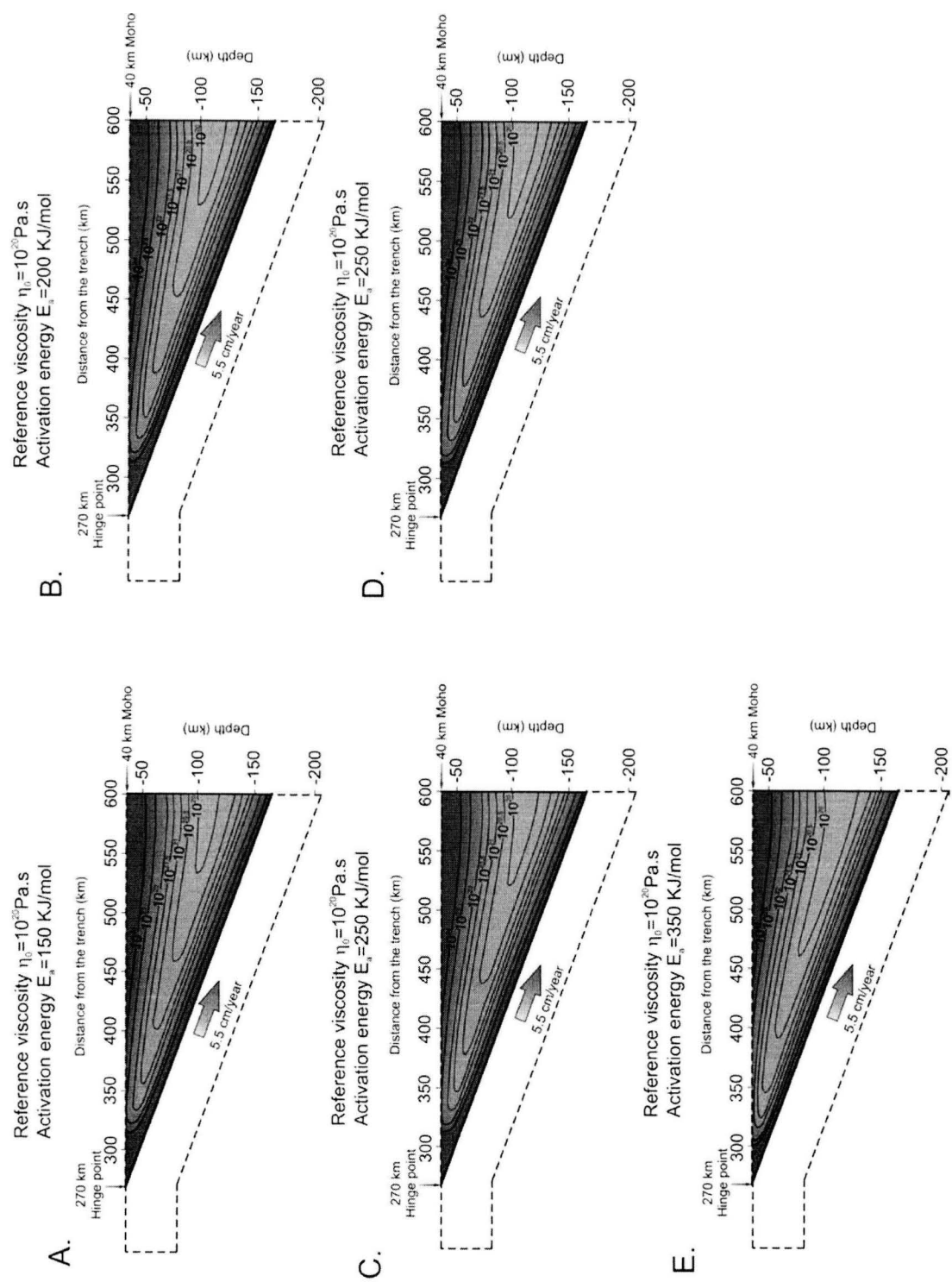
**Figure 11**
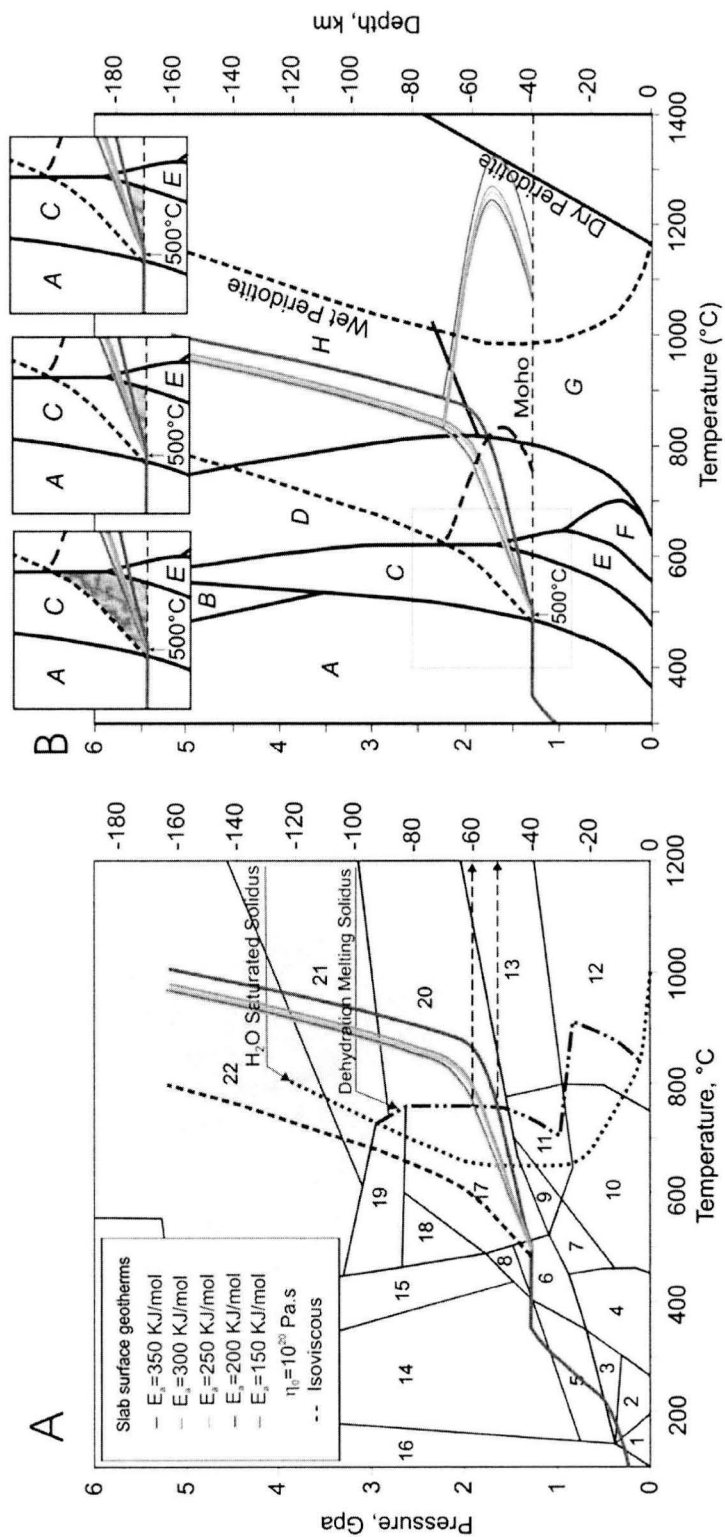
**Figure 12**
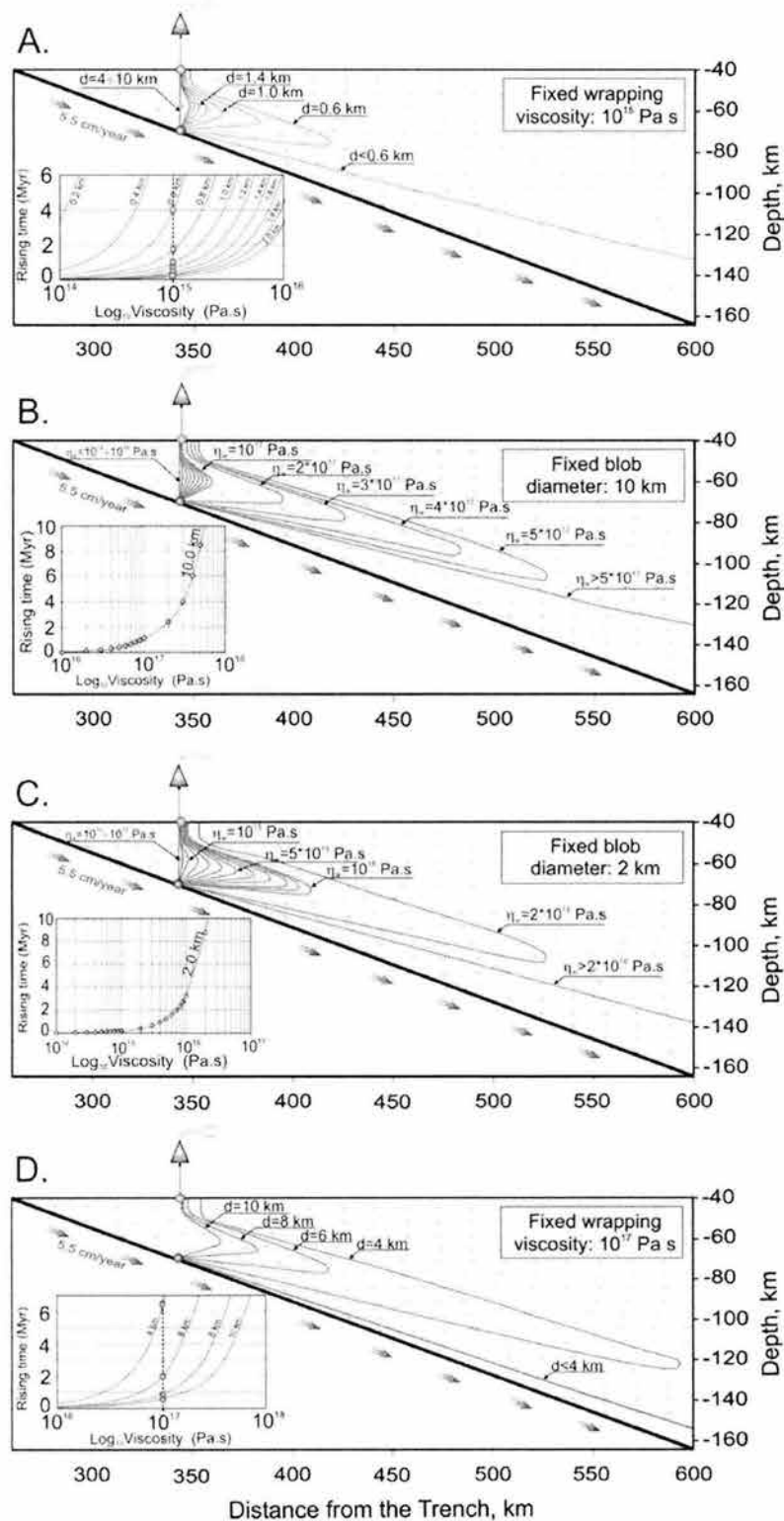
Figure 13

Figure 14

Figure 15
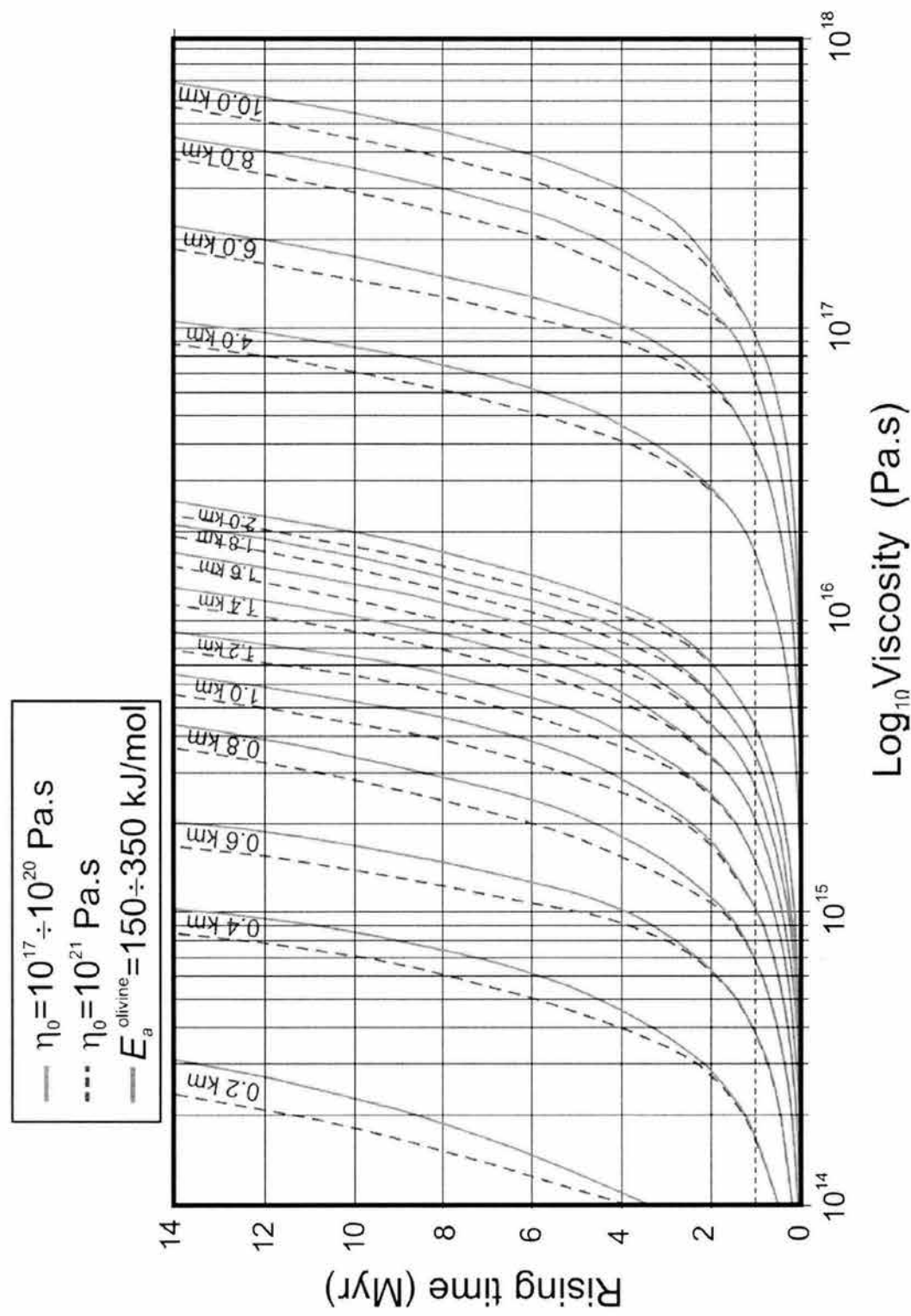
Figure 16
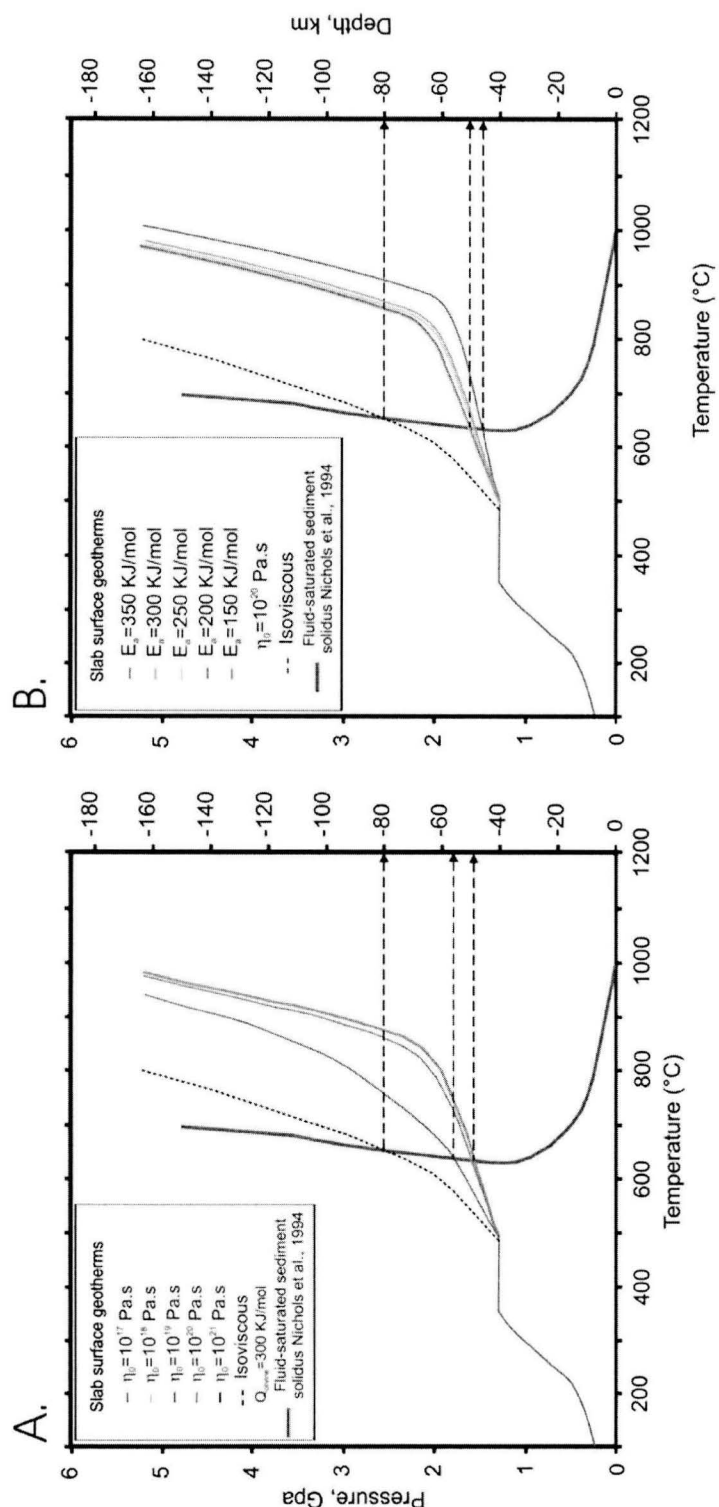
**Figure 17**

IV. MODELOS TÉRMICOS, TRANSPORTE DEL MAGMA Y ESTIMACIÓN DE LA ANOMALÍA DE VELOCIDAD DEBAJO DE KAMCHATKA MERIDIONAL

THERMAL MODELS, MAGMA TRANSPORT AND VELOCITY ANOMALY ESTIMATION BENEATH SOUTHERN KAMCHATKA

V.C. Manea[1], M. Manea[1], V. Kostoglodov[1], G. Sewell[2]

[1] Instituto de Geofisica, Universidad Nacional Autónoma de México (UNAM), México

[2] University of Texas, El Paso

ABSTRACT

A finite element method is applied to model the thermal structure of the subducted Pacific plate and overlying mantle wedge beneath the southern part of the Kamchatka peninsula. A numerical scheme solves a system of 2D Navier-Stokes equations and a 2D steady state heat transfer equation.

A model with isoviscous mantle exposed very low temperatures ($\sim 800°C$) in the mantle wedge, which cannot account for magma generation below the volcanic belt. Instead, a model with strong temperature-dependent viscosity shows a rise in the temperature in the wedge. At a temperature of more than $1300°C$ beneath the active volcanic chain, melting of wedge peridotite becomes possible. Although the subducting slab below the Kamchatka peninsula is rather old (~ 70 Myr), some frictional heating ($\mu = 0.034$) along the interface between the subducting oceanic slab and the overlying Kamchatka peninsula lithosphere would be enough to melt subducted sediments. Dehydration (> 5 wt% H_2O release) occurs in the subducting

slab because of metamorphic changes. As a consequence, hydration of the mantle wedge peridotite might produce melt, which may rise to the base of the continental crust as diapir-like blobs.

Considering that melting processes in the subducting plate generate most of the volcanic material, we developed a dynamic model which simulates the migration of partially melted buoyant material in the form of blobs in the viscous mantle wedge flow. Blobs with a diameter of 0.4 - 10.0 km rise to the base of the continental lithosphere within 0.002 - 10 Myr depending on the blob diameter and surrounding viscosity.

The thermal structure obtained in the model with temperature dependent viscosity is used to estimate seismic P-wave velocity anomalies (referenced to PREM) associated with subduction beneath Kamchatka. A low velocity zone (~ - 7% velocity anomaly) is obtained beneath the volcanic belt and a high velocity anomaly (~ 4%) for the cold subducted lithosphere. These results agree with seismic tomography results from P-wave arrivals.

GENERAL ASPECTS OF SUBDUCTION ZONE DYNAMICS

Mantle plumes are frequently assumed to come from the transition zone or from the core-mantle boundary. There is another place inside the Earth from where these thermal or chemical instabilities might develop: the top layer of the subducting slabs where strong dehydration and melting is expected. This chapter aims to study the subduction magmatism through numerical modeling of the mantle wedge thermal structure and magma transport with a diapir model.

The thermal structure of subduction zones provides important insight into the thermal and chemical exchange between subducted oceanic lithosphere and overlying mantle wedge, and on magma generation and transport. Various thermal models have been developed based on analytical approximations (*Davies, 1999; Molnar and England, 1995, 1990*), analytical solutions for wedge corner flow (*Peacock, 2002, 1996, 1991, 1990a, 1990b; Peacock and Hyndman, 1999; Peacock and Wang, 1999; Billen and Gurnis, 2001*), and recent models which incorporate temperature - and stress - dependence viscosity (*von Hunen, 2000, van Keken, 2002, Gerya and Yuen, 2003*).

The object of the present study is to model one of the oldest and most interesting subduction zones; the Kamchatka subduction zone (KSZ), in which thermal structure is poorly known up to now. Kamchatka thermal structure is analyzed in models with constant viscosity (isoviscosity) and strong temperature-dependent viscosity of the asthenosphere.

A distinctive feature of the thermal regime associated with subduction zones is the inverted thermal gradient just above the slab in the mantle wedge where the most important and intensive chemical and thermal exchanges occur. In this region the material transferred from the oceanic slab to the mantle wedge enriches the source region of arc lavas with incompatible elements and volatiles (*Plank and Langmuir, 1993; Stolper and Newman, 1994; Johnson and Plank, 1999; Eiler et al., 2000*). An influx of volatiles from metamorphosed oceanic crust and sediments triggers partial melting of peridotite above the subducted slab (*Tatsumi, 1986;*

Davies and Stevenson, 1992). Basically, three mechanisms of melt generation are expected: partial melting producing positively buoyant diapirs (*"blobs"* in the present paper) (*Tatsumi et al., 1983; Kushiro, 1990; Gerya and Yuen, 2003; Manea et al., 2004b);* anhydrous decompression melting of peridotite (*Klein and Langmuir, 1987; Langmuir et al., 1992*); porous flow of hydrated partial melt (*Gaetani and Grove, 2003*).

The latest insights revealed by new developed high-resolution dynamical models for subduction zones with 0.5 billion markers of *Gerya and Yuen (2003)* show that the hydration and related melting introduce a source of chemical buoyancy on the 1 - 10 km thick layer on top of the subducting slab. These plumes, with diameter up to 10 km, penetrate the hot mantle wedge with velocities of ~ 10 cm/yr.

Various mechanisms were proposed for rapid magma transport from the mantle wedge toward the surface: through channelized network (channels diameter of 1 - 100 m) (*Spiegelman and Kelemen, 2003*), through fractures and shear zones in the mantle (*Shaw, 1980*), through a fractal tree network (very thin channels with 1 - 4 mm diameter) (*Hart, 1993*) and the dike transport mechanism in the mantle (*Rubin, 1993*). The model of *Shaw (1980)* proposes fracture zones inside the mantle wedge. The presence of such fracture system is unlikely to exist in a very hot mantle wedge (> 1300°C). The mantle wedge peridotite behaves completely ductile for temperature above ~ 700°C. *Spiegelman and Kelemen (2003)* provide a model capable to explain the chemical and spatial variability of lava samples taken from mid ocean ridges. The geodynamics of subduction zones is quite different from the one of mid ocean ridges, basically the strong convection beneath the volcanic arcs represents one of the main differences. The applicability of this model with magma transport velocity of ~ 1.5 m/year through channels with diameters < 100 m proposed by *Spiegelman and Kelemen (2003)* needs to be further investigated in the presence of strong convecting systems as the mantle wedge beneath volcanic arcs. Although the other models *(Hart, 1993; Rubin, 1993)* predict fast magma transport toward the surface through very narrow channels,

they do not take into account the presence of strong mantle wedge convection which affect the continuation of these channels. For this reason, in the present study, for magma generation and propagation in the southern Kamchatka subduction zone, concept of positive buoyant diapirs (blobs) that migrate in the mantle wedge flow induced by the subducting slab is applied. We used for the modeling the numerical scheme *of Manea et al. (2004b)*.

Partial melting of fluid-saturated peridotite at low temperature on top of the subducted slab may generate H_2O-rich partial melt. In order for melt to progress, ascending blobs have to be efficiently heated as they move in the mantle wedge *(Gaetani and Grove, 2003)*. Conductive thermal evolution of these diapirs as they ascend toward the base of the continental crust is modeled.

Mantle wedge viscosity is an important factor that controls the migration of diapirs in the mantle wedge. Dissolved H_2O and the partial melt might lower mantle viscosity below 10^{18} Pa s *(Kelemen et al., 2003)*. Moreover, *Hirth and Kohlstedt (2003)* showed that experimentally measured viscosities for olivine at upper mantle pressures and temperatures are in the range 10^{17} - 10^{21} Pa s.

Thermal modeling is applied to investigate the possibility of melting slab fluid-saturated sediments (wet solidus from *Nichols et al., 1994*) and mantle-wedge wet peridotite (wet solidus from: *Mysen and Boettcher, 1975; Wyllie, 1979*), and dehydration along the slab-wedge interface beneath Kamchatka.

The main constraint on mantle-wedge temperature distribution could be P-wave seismic tomography. *Zhao et al. (1992, 1997)* observed a low-velocity zone (-6% P-wave velocity anomaly) beneath the Tonga and NE Japan volcanic arcs, which might be related to upper-mantle melting below the base of the continental crust. *Gorbatov et al. (1999)* detected a low-velocity zone (-7% P-wave velocity perturbation) beneath the active volcanic chain in Kamchatka. Tomography images of Northeast Japan (*Tamura et al., 2002; Zhao, 2001*) reveal a limited low velocity region that is in contact directly with the slab surface (-2 - 3% velocity anomaly) at depths of 80 - 100 km.

Following Karato (1993), the temperature dependence of seismic wave velocities can be used to estimate velocity anomalies from thermal models. An agreement between the velocity perturbation beneath the volcanic arc (shape and magnitude) observed in the seismic tomography anomaly and the tomography anomaly estimation from thermal modeling might be an indication of a satisfactory estimate of the thermal regime in the mantle wedge.

REGIONAL TECTONIC SETTINGS

The Kamchatka peninsula has one of the most active volcanic chains in the world and is a dynamic convergent margin where the Pacific plate (PAC) subducts beneath the North-American plate. The PAC subducts westward at a dip angle of ~ 55° from 50°N to 54°N, and at a rate of ~ 7.8 cm/year *(Gorbatov et al., 1999)*. The age of the subducting plate along the Kamchatka trench varies between 70 and 100 Myr. The dip of the Wadati-Benioff zone varies along the KSZ from ~ 55° in the south to ~ 35° in the north. Heat flow data *(Smirnov and Sugrobov, 1979; 1989a,b)* suggest that the thermal thickness of the subducted plate is up to 75% smaller in the north of the peninsula then in the south. Thus the effective age (thermally defined) is less there, because of the geological age *(Renkin and Sclater, 1988)*. In order to avoid the effect of oceanic plate rejuvenation in the north of the KSZ, the present paper explores a 2D profile normal to the trench in the southern part of Kamchatka *(Fig. 1)*, far from this important thermal anomaly. The seismicity and structure of the KZS was studied in detail by *Gorbatov et al. (1997)*. The volcanic front, from 50°N to 54°N, is trench-parallel and corresponds to a depth of the subducted slab of about 90 to 140 km.

Southern Kamchatka is separated into en eastern active volcanic chain and the western inactive tectonically and volcanically Sredinny Range *(Fedotov & Masurenkov, 1991)*. Numerous active and inactive volcanoes, which form the Eastern Volcanic Front (EFV), are situated above the subducting slab at depth where partial melting in the mantle wedge is induced by fluids from slab dehydration.

Observations of a slab-melt chemical signature are mainly restricted to the northern volcanoes as Sheveluch, which is the only active volcano with an adakite magma signature. The tectonic reconstruction of Kamchatka-Aleutian corner *(Park et al., 2002)* strongly suggests that the extinct subduction zone (just beyond the edge of the slab near the Aleutian junction) involved a shallow-dipping young slab. The melting of subducted slab and fluids from slab dehydration produced an

adakites type of arc volcanism. However, in southern Kamchatka no adakites were found, suggesting that in this region the slab is not melting. The lack of this style of volcanism would be a very important constraint on the subducting slab thermal structure. While melting of subducted basaltic crust is unlikely to occur beneath southern Kamchatka, there are evidences of sediment-melt chemical signature in Kamchatka, although this contribution is small (< 1%) compared with other volcanic arcs *(Park et al., 2002)*.

MODELING PROCEDURE

A system of 2D Navier-Stokes equations and the 2D steady state heat transfer equation are solved for the south Kamchatka cross section *(Fig. 1)* using the numerical scheme proposed by *Manea et al. (2004b)*. The strong temperature-dependence of viscosity imposed in the present modeling, corresponding to diffusion creep of olivine, has the following form:

$$\eta = \eta_0 \cdot e^{\left[\frac{E_a}{R \cdot T_0} \cdot \left(\frac{T_0}{T} - 1 \right) \right]}$$

(1)

where:

η -mantle wedge viscosity (Pa s),

η_0 -mantle wedge viscosity at the potential temperature T_0 (10^{20} Pa s),

T_0 -mantle wedge potential temperature (1,450°C),

E_a -activation energy for olivine (300 kJ/mol) (Karato and Wu, 1993),

R -universal gas constant (8.31451 J/mol °K),

T -temperature (°C).

A finite-element grid extends from 25 km seaward of the trench up to 375 km landward of it, and consists of 12,000 triangular elements with higher resolution in the tip of the wedge *(Fig. 2)*. A benchmark with various grid resolution of the present numerical scheme *(Manea et al., 2004b)* confirms that a numerical error of less than 5°C is introduced in the thermal models when 12,000 triangles are used. The lower edge of the grid follows the shape of the subducting plate upper surface at a constant distance of 100 km *(Fig. 3)*. The model consists of five thermo-stratigraphic units as follows: upper continental crust, lower continental crust, oceanic lithosphere, oceanic sediments, and mantle wedge.

A summary of the thermal parameters used is presented in *Table 1* (compilation from: *Peacock and Wang, 1999; Smith et al., 1979; Vacquier et al., 1967*). The continental crust in Kamchatka is divided into two layers: the upper crust (0 - 15 km depth) and lower crust (15 - 35 km depth). These depths are consistent with values inferred from 1D tomographic inversion by *Gorbatov et al. (2000).* A recent paper of *Levin et al. (2002)* shows a Moho depth range of 30 - 40 km across the entire Kamchatka peninsula. In this chapter we used a constant Moho depth of 35 km. The shape and dip of the subducting plate beneath the volcanic arc are constrained by earthquake hypocenter distribution. A 1.5 km-thick sediment layer is included in the model *(Dickinson, 1978; Selivestrov, 1983).*

The upper and lower boundaries are maintained at constant temperatures of 0°C at surface and of 1,450°C in the asthenosphere, respectively (*Fig. 3*). The left, landward vertical boundary condition is defined by an 18.5°C/km thermal gradient for the continental crust. Below the 35 km depth, the left boundary condition is represented by a low thermal gradient of 5.5°C/km down to the depth of 180 km. Beneath 180 km depth no horizontal conductive heat flow is specified. Underneath the Moho (35 km), for the left boundary, corresponding to the mantle wedge, zero traction is assumed. At the intersection between the subducted slab and the left boundary, the velocity of the subducting slab is assumed.

The right, seaward boundary condition is a one-dimensional geotherm calculated for the oceanic plate by allowing a half-space to cool from zero age to the oceanic plate age at the trench. This geotherm is obtained using a time-dependent sedimentation history (*Wang and Davis, 1992*) and assuming a constant porosity-depth profile of the sediment column with a uniform sediment thickness of 1.5 km at the trench.

Since the Stokes equations are applied only in the mantle wedge, the region between Moho and the slab surface is entirely involved in the flow induced by the subducting slab. This is consistent with the conclusion of *Levin et al. (2002),* suggesting that the mantle lithosphere beneath Kamchatka is actively deforming.

In terms of displacement, the velocity of the oceanic plate is taken with respect to the continental plate. Thus the convergence rate of 7.8 cm/year between the PAC and North American plates is used for the KSZ *(Renkin and Sclater, 1988)*. Although we assume the motion of the subducting slab as parallel to the dip, the slab can have an additional downward directed velocity component due to slab bending or slab rollback. On the other hand, slab can also have upward velocity component in case of swallowing of the subduction angle with time due to the slab unbending. In our models we are dealing with a steady state model and therefore, do not consider additional velocity component due to the slab bending/unbending. The PAC age at the trench is 72 Myr according the estimation of *Gorbatov and Kostoglodov (1997)*.

We consider two different models: the first has constant viscosity (isoviscosity) in the mantle wedge and the second one has strong temperature-dependent viscosity (diffusion creep of olivine). In the second model, the system of equations becomes strongly nonlinear. To deal with this difficulty Picard iterations are applied. In order to achieve a convergent solution a cut-off viscosity of 10^{24} Pa s fortemperature less than 1,000 °C is used.

A long-term continuous sliding between the subducting and continental plates along the thrust fault should produce frictional heating. We introduced into the models a small degree of frictional heating using Byerlee's friction law *(Byerlee, 1978)*. Frictional heating cease at a depth of 35 km, where the oceanic plate and the mantle wedge came into first contact *(Fig. 3)*. We impose this depth limitation of frictional heating because the contact between Moho (35 km) and the slab surface represents a maximum extent where interplate earthquakes might occur. The tip of the mantle wedge is subject of mantle serpentinization which has a completely ductile behavior and therefore decoupling the subducting and overriding plates. The location of serpentinized mantle wedge tip is critical because it controls the down-dip extension of the interplate earthquakes *(Manea et al., 2004a)*.

Volumetric shear heating is calculated as follows:

$$Q_{sh} = \frac{\tau \cdot v}{w} \quad , \tag{1}$$

where:

Q_{sh} -volumetric shear heating (mW/m^3),

τ -shear stress:
$$\tau = 0.85 \cdot \sigma_n \cdot (1-\lambda) \quad for \quad \sigma_n \cdot (1-\lambda) \leq 200 MPa$$
$$\tau = 50 + 0.6 \cdot \sigma_n \cdot (1-\lambda) \quad for \quad \sigma_n \cdot (1-\lambda) > 200 MPa$$

σ_n -lithostatic pressure (MPa),

λ -the pore pressure ratio, (PPR-the ratio between the hydrostatic and lithostatic pressures. $\lambda <= 1$. The maximum value, $\lambda = 1$, means no frictional heating),

v -convergence velocity (7.8 cm/year),

w -the thickness of a thin element layer (500 m) along the plate-interface, where frictional heating is formulated as body-heat source.

Based on the velocity field obtained in the case of temperature dependent viscosity, a dynamic model for the blob tracers is applied. A blob moves under the action of drag, mass, and buoyancy forces in the mantle wedge stationary velocity field generated in the previous model. The description of the modeling approach is given in (*Manea et al., 2004b*). The trajectories of positively buoyant blobs ($\Delta\rho = 200$ kg/m^3) with diameters between 0.4 and 10 km are calculated for different values of wrapping viscosity, η_w (10^{14} - 2.10^{17} Pa s). Very low wrapping viscosity around the blobs might be a consequence of viscous heating between the surrounding mantle and the blob (*Gerya and Yuen, 2003*). The total rise time that the blobs require to reach the base of the continental crust is also estimated.

During migration through the mantle wedge the blobs are heated first because of the inverted thermal gradient, and then cooled (normal thermal gradient) before approaching the base of the continental lithosphere. A blob is

assumed to be heated/cooled by conduction only. The following conduction equation is used to model blob thermal history:

$$C_p \cdot \frac{\partial T}{\partial t} + \nabla \cdot (-k \cdot \nabla T) = 0 \tag{2}$$

where:

C_p -thermal capacity 3.3 (MJ/m^3 °K),

T -temperature (°C),

t -time (Myr),

k -thermal conductivity 3.1 (W/m °K),

The equation is solved numerically inside the blob, with boundary conditions of mantle wedge temperature taken from the thermal modeling. We used 3,000 triangle elements to solve equation (2) inside the spherical blobs. The trajectory of the blobs and the time steps are taken from the dynamic model for the blob tracers described above.

Finally, a tomographic image is obtained using the thermal models and temperature dependence of seismic-wave velocities from (*Karato, 1993*). The seismic-velocity perturbations are calculated relative to the PREM model of *Dziewonski and Anderson (1981)*. The following equation (*Karato, 1993*) is used:

$$\frac{\partial \ln V}{\partial T} = \frac{\partial \ln V_0}{\partial T} - \left(\frac{Q_p^{-1}}{\pi} \cdot \frac{H}{R \cdot T^2} \right) \tag{3}$$

where:

V -velocity (km/s),

V_0 -the reference velocity (*Dziewonski and Anderson, 1981*),

T -temperature (°C),

$$\frac{\partial \ln V_0}{\partial T} = -\alpha \cdot \frac{\partial \ln V_0}{\partial \ln \rho} \tag{3.1}$$

with:

α pressure dependence of thermal expansion (*Stacey, 1977*),

$\dfrac{\partial \ln V_0}{\partial \ln \rho}$ from (*Chopelas, 1992*).

Q_p^{-1} - seismic anelasticity for compressional waves in peridotite (spinel lhezoite) determined by *Sato et al., 1988, 1989* as follows:

$$Q_p = Q_{pm} \cdot e^{[g' \cdot (\frac{T_m}{T} - a)]} \tag{3.2}$$

where:

Q_{pm} - is the Q_p at solidus temperature and it has the following form:

$$Q_{pm} = Q_1 + P/P_0, \tag{3.3}$$

with:

Q_1 =3.5
P_0 =73 MPa
P -lithostatic pressure (MPa),
$g' = 6.75$, $a = 1.00$ for $T_m/T < 1$,
$g' = 8.47$, $a = 1.00$ for $1 < T_m/T < 1.08$,

$g' = 13.3$, $a = 1.03$ for $T_m/T > 1.08$,

T_m -dry peridotite solidus (*Wyllie, 1979*),

H -activation enthalpy for olivine: 500 kJ/mol (*Karato and Spetzler, 1990*),

R -universal gas constant (8.31451 J/mol.K),

T -temperature (°C).

MODELING RESULTS

Thermal models

The thermal models that correspond to isoviscosity and temperature-dependent viscosity are presented in *Fig. 4* and *Fig. 5*. The isoviscous mantle wedge model predicts temperatures of ~ 950 °C in the asthenosphere, beneath the volcanic chain indicating that, at least for dry olivine, melting should not occur. The geotherm of the oceanic plate surface does not intersect the solidus (*Fig. 6-A*) neither for basalt nor for wet sediments (*Fig. 6-B*) indicating that the oceanic plate and the subducted sediments do not undergo melting. The mantle-wedge velocity field has a rather small back flow of ~ 3 cm/yr which is responsible for the low temperature in the wedge (*Fig. 7-A*). A small amount of frictional heating (a pore pressure ratio $\lambda = 0.96$ or an effective friction coefficient $\mu = 0.034$ and an average shear stress along the thrust fault $\tau \sim 14$ MPa) is added at the contact between the subducted slab and the overriding plate. Although the surface of the slab beneath the mantle wedge is heated by more than 150°C, this is not sufficient to melt the slab surface (*Fig. 6-A*). It is evident that this simple model with the isoviscous mantle wedge cannot create any source of the volcanic material.

Applying temperature-dependent viscosity in the mantle wedge produces an important increase of the temperature beneath the volcanic front. The maximum temperature then rises to more than 1,300°C (*Fig. 5*). The mantle wedge viscosity, η_0, at a potential temperature, T_0 (1,450°C), might be between 10^{17} Pa s and 10^{20} Pa s. A benchmark for the numerical scheme applied in this study (*Manea et al., 2004b*) shows a very small variation in temperature in the wedge of $\Delta T < 15$°C for $\Delta \eta_0 = 1,000$ Pa s (from 10^{17} Pa s up to 10^{20} Pa s). Therefore, a unique value for the mantle wedge viscosity at a potential temperature T_0 of $\eta_0 = 10^{20}$ Pa s is used, since its effect is negligible on the overall wedge thermal structure.

The velocity field (*Fig. 7-B*) has back-flow velocities of ~ 7.5 cm/yr, which are responsible for the higher temperature in the tip of the wedge. Without frictional heating, the geotherm of the subducting plate surface does not intersect the solidus neither for basalt nor for sediments *(Fig. 6-A)* therefore melting of the subducted sediments and basaltic oceanic crust does not occur for this model. The frictional heating fraction corresponding to λ = 0.96 might cause fluid-saturated melting of subducted sediments at a relatively shallow depth of ~ 35 km (*Fig. 6-B*). The same amount of frictional heating (λ = 0.96) is not sufficient to melt the basaltic subducted crust. For greater amounts of frictional heating (i.e. λ = 0.95) melting of basalt oceanic crust might be possible, but this is inconsistent with the lack adakites volcanism in southern Kamchatka.

Metamorphic sequences and dehydration within the descending oceanic crust

The estimated variation of wt% H_2O content with depth along the subducting plate for both models, with isoviscosity and temperature-dependent viscosity, with and without frictional heating, are presented in *Fig. 8* and *Fig. 9*. The isoviscous thermal model without frictional heating (*Fig. 8-A*) shows a fairly simple metamorphic structure: from Lawsonite - Blueschist facies, the oceanic crust enters at a depth of ~ 25 km into the stability field of Jaedite – Lawsonite - Blueschist; from ~ 55 km depth to ~ 85 km depth, the metamorphic facies is represented by Lawsonite - Amphibole - Eclogite. With a small amount of Zoisite - Eclogite from ~ 85 to ~ 100 km depth, the oceanic crust loses completely its hydrous phase entering finally into the Diamond - Eclogite stability field. Intensive dehydration occurs during these phase changes, more than 5 wt% H_2O being released into the overlying mantle up to a depth of ~ 100 km (*see Fig. 8-A – inset*). The same isoviscous thermal model, but with frictional heating included, predicts a more complicated metamorphic structure (*Fig. 8-B*). Up to the contact between the Moho and the subducted slab, the oceanic crust is represented by Lawsonite - Blueschist

(up to ~ 25 km depth), Epidote - Blueschist (25 - 28 km depth) and Epidote - Amphibolite (28 - 35 km depth) facies. Deeper, the metamorphosed structure is characterized by Eclogite - Amphibole (35 - 40 km depth), Zoisite - Amphibole - Eclogite (40 - 80 km depth), Zoisite - Eclogite (80 - 100 km depth) and from ~ 100 km by Diamond - Eclogite facies. Again, rigorous dehydration occur all the way through these phase changes, more than 5 wt% H_2O being released into the overlying mantle up to a depth of ~ 100 km (*see Fig. 8-B – inset*).

The thermal model with temperature-dependent viscosity and without frictional heating reveals a similar metamorphic pattern as the isoviscous model (without frictional heating): Lawsonite - Blueschist, Jaedite – Lawsonite - Blueschist, Jadeite - Epidote - Blueschist, Amphibole - Eclogite, Zoisite - Eclogite and Diamond - Eclogite (*see Fig. 9-A – inset*). Strong dehydration (more than 5%wt H_2O released) of wedge peridotite up to ~ 100 km depth is suggested by this model. The last thermal model proposed in this study, with temperature-dependence of viscosity and frictional heating (λ = 0.96 or μ = 0.034) exposes a slightly different and more complicated metamorphic arrangement along the oceanic crust: Lawsonite - Blueschist, Greenschist, Epidote - Amphibolite, Eclogite - Amphibole, Garnet - Amphibolite, Zoisite - Amphibole - Eclogite, Zoisite - Eclogite, Coesite - Eclogite and Diamond - Eclogite facies (*see Fig. 9-B - inset*). Hydration of mantle wedge peridotite is likely to occur up to ~ 90 km depth and melting of fluid-saturated oceanic sediments at shallower depth of ~ 40 km is suggested by this last thermal model (*Fig. 5-B* and *Fig. 6-B*).

Vertical thermal profiles (A-A') beneath the volcanic front (190 km from the trench) through the mantle wedge (*Fig. 4* and *Fig. 5*) illustrate that for the models with isoviscosity, mantle peridotite melting is not possible, while for both strong temperature-dependent viscosity models melting of wet peridotite is likely to occur (*Fig. 6-B*).

Diapiric ascent of melted material constrained by geochemical tracers

The thermal model with temperature dependent viscosity and frictional heating confirms the possibility of melting of fluid-saturated sediments and hydrated mantle wedge peridotite (*Fig. 6-B* and *Fig. 6-A*). A strong dehydration flux from the slab surface might lower the solidus of mantle wedge allowing the occurrence of partial melt of hydrated peridotite in the vicinity of the slab surface (< 10 km from the slab surface - *see Fig. 9*). Using the wet peridotite solidus from *Mysen & Bottcher (1975)* (i.e. 800°C at ~ 80 km) the wet peridotite solidus is even closer to the slab surface (~ 5 km).

Hydrated peridotite with a density lower than the asthenospheric density can develop buoyant plumes (*e.g., Gerya and Yuen, 2003*). *Gerya and Yuen (2003)* and *Manea et al. (2004b)* suggested that these blobs might be lubricated by a very low wrapping viscosity due to viscous heating against the surrounding mantle wedge. The source of the wrap is melted material coming from the subducting slab, including melted subducted sediments. Wrapping viscosities down to 10^{14} Pa s control diapiric ascent in the wedge. The surface geotherm of the subducted slab intersects the dehydration melting solidus at ~ 90 km (*Fig. 6-A*).

The blobs are not necessarily melts; they might be compositionally instabilities at the slab-wedge interface (*Gerya and Yuen, 2003*). Actually the blobs are not restricted to be melted, they need only positive buoyancy in order to detach from the slab surface. The origin of this positive buoyancy (low density) might be compositional and/or thermal. Consequently we selected an initial point to calculate blob trajectories at a depth of ~ 110 km on the slab surface, just below the EVF.

The blob trajectories are shown in *Fig. 10* for different wrapping viscosities (10^{14} - >10^{17} Pa s) and blob diameters (0.4 - 10.0 km). Very low viscosity is essential for the blob to rise to the base of continental crust. Extremely low viscosity (10^{14} - 10^{17} Pa s) is also essential to explain the high pressure and ultra-high pressure metamorphic rocks exhumation from great depths (*Burov et al., 2000*).

For blobs of 4 km diameter (*Fig. 10-A*) and wrapping viscosity $\eta > 3 \cdot 10^{16}$ Pa s, the drag force is predominant and the blob cannot rise. For lowered viscosity the drag force is less significant and at the depth of ~ 175 km the blob intercepts the mantle wedge back flow, which returns it toward the tip of the wedge. Finally the blob rises and impinges on the continental crust after ~ 8 Myr. For lower viscosity ($< 10^{16}$ Pa s) blobs rise faster (*Fig. 11*) and impact at approximately the same point below the volcanic chain.

The larger the blob size the less time is required to reach the continental crust (*Fig. 11*). The buoyancy force of large blobs becomes more dominant than the drag force and this yields a substantially upright trajectory (*Fig. 10-B*). At a wrapping viscosity of 10^{15} Pa s blobs with a diameter of less than ~ 0.8 never rise up to the continental crust. Blobs smaller than ~ 1 km reach the crust at some distance (up to 10 km), depending on the blob size. For a viscosity of $> 10^{17}$ Pa s, blobs with diameters ≥ 8 km are able to escape from the downward flow in the mantle and accumulate at the base of the continental crust.

An important constraint on the magma transport time through mantle wedge comes from U-series isotope disequilibria, ^{10}Be and fluid soluble trace elements as Th, Sr and Pb isotope studies.

U-series isotope disequilibria come from the mobility of U in aqueous fluids under oxidizing conditions. On the other hand Th in not mobile, therefore the timescale of such U-Th disequilibria might be used to infer the fluid-transfer and melt generation in the mantle wedge before surface eruptions.

Turner and Hawksworth (1997) proposed a very rapid ascent of magma (~ 1000 years) from the place where might be formed (near the slab surface) toward the earth surface through a channel network. *Regelous et al. (1997)* infer the magma transport rate from Th, Sr and Pb isotope data. They analyzed data from Tonga-Kermadec arc lavas, the same as *Turner and Hawksworth (1997)*. The final conclusion of *Regelous et al. (1997)* is that magmas are erupted at the surface < 350 kyr after the melts are generated in the mantle wedge. These results are quite different, clearly showing that this issue with U-Th isotope disequilibria and Th, Sr

and Pb isotope data used to infer the magma transport rates across the mantle wedge is an on going debate.

The cosmic ray produces [10]Be, which is subducted together with the ocean sediments. Studies of [10]Be show the Be can be transported from the trench through the mantle wedge and finally erupted in surface lavas over a period of ~ 7 Myr *(Brown et al. (1982); Morris et al. (1990))*. With a subduction velocity rate of 7.8 cm/yr it took ~ 1 Myr for the sediments to arrive at ~ 100 km depth beneath the EVF. Then the remaining ~ 6 Myr represents the residence time for Be in the mantle wedge.

The U series and [10]Be studies show contradictory estimates of the magma transport times through the mantle wedge, suggesting variable transport rates for different elements and/or real differences in transport times probably due to a variable melted volume generated in the wedge.

Whether we consider in our models the results of *Regelous et al. (1997)*, (350 kyr for magma transport), then from *Fig. 11* - inset can be seen that a magma transport mechanism as buoyant blobs still represents a reliable mechanism. The blobs with the size of less than 10 km can reach the continental crust in less than 350 kyr for wrapping viscosities less than ~ 10^{16} Pa s.

Assuming a residence time of magma of ~ 6 Myr (from [10]Be studies), then buoyant blobs with diameters of 0.4-10 km are allowed to travel through mantle wedge toward the Moho for a very wide range of wrapping viscosities of 10^{14} - > 10^{17} Pa s.

Thermal history of the blobs

Heat transfer accompanies the journey of cold buoyant blobs through the mantle wedge. A temperature-dependent viscosity thermal model was used for a 10-km diameter buoyant blob. The thermal history of this blob, which reaches the Moho in 2.6 Myr, is presented for nine time periods in *Fig. 12-A* relatively cold blob (~ 800°C) initiates its voyage through the inverted thermal gradient. Its top is

heated up to ~ 950°C by the surrounding mantle *(Fig. 12-A)*. After ~ 0.33 Myr, the blob has moved down few km from its initial position, being dragged by the vigorous mantle wedge flow. The top hot region grows in size and temperature (~ 1,170°C) while the cold core shrinks and becomes warmer (~ 810°C) *(Fig. 12-B)*. The downward trajectory of the blob continues, and after ~ 0.66 Myr inner temperatures between 1,000°C and 1,290°C are expected *(Fig. 12-C)*. From this point the blob starts to rise, being close from the maximum wedge temperature after ~1 Myr, when the temperatures inside the blob are from 1,180°C up to 1,330°C. Beyond this point the blob rises in a normal thermal gradient and after ~ 2.6 Myr reaches the base of the continental crust with a > 950°C hot core while the surrounding mantle has ~ 800°C *(Fig. 12-A-i)*. Assuming that the main composition of the blob is peridotite and using the wet peridotite solidus from *Mysen and Boettcher (1975)* (e.q. 850°C at 35 km depth) the main blob's volume is not solidified when touches the Moho due to hot core temperature above 950°C *(Fig. 12* and *Fig. 13)*.

Neither viscous heating around the diapir nor thermal convection inside are incorporated in this model. For a blob with d = 10 km diameter, with a minimum blob viscosity μ = 10^{17} Pas and a maximum thermal contrast of ΔT = 350°C *(see Fig. 12-A-b)*, the Rayleigh number is $Ra^{max} = \dfrac{\rho_b \cdot g \cdot \alpha \cdot \Delta T \cdot d^3}{\mu \cdot k}$ = 1,050 (other parameters for Ra^{max} calculation are: ρ_b = 3,000 kg/m^3, g = 10 m/s^2, α = 10^{-5} °C^{-1}, k = 10^{-6} m^2/s). Although Ra^{max} exceeds Ra^{cr} = 660 necessary for convection to begin in fluid layers heated from below (or above) *(Turcotte and Schubert, 2002)*, in the present study we do not incorporate the effect of thermal convection on the blob's thermal structure. Every parameter in the Rayleigh number is pretty well known except blob's viscosity, which can vary by orders of magnitude. Future investigations will focus on the effect of viscous heating and thermal convection over the thermal history of buoyant blobs.

Velocity anomaly estimation from thermal modeling

The tomographic image computed using the thermal model with temperature dependent viscosity is presented in *Fig. 14-A*. The high temperature in the mantle wedge beneath the volcanic chain (> 1,300°C) produces a strong negative velocity anomaly up to −7% (*Fig. 13*) (relative to PREM). The cold subducting slab produces a positive velocity anomaly up to +4%.

The tomographic image estimation from isoviscous thermal models revealed very low amplitude velocity perturbations in the mantle wedge, because of the thermal structure mainly controlled by the left boundary condition which is consistent with the PREM model.

The procedure applied to estimate the tomography anomaly from a thermal model applying *Karato (1993)* uses the dry solidus for peridotite (*Tm*). As is shown in *Fig. 6-B*, the wedge temperature is well above the wet solidus for peridotite but is below the dry solidus, therefore no partial melting effect is included in this tomography estimation. The thermal models with strong temperature dependence of viscosity show a temperature of ~ 1,300°C at ~ 90 km depth (*see Fig. 6-B*). This corresponds to ~ 90% of the dry peridotite solidus. Tomography anomalies are usually interpreted as indicating a partially molten asthenosphere, but *Sato et al. (1989)* shows that this may reflect instead a hot solid asthenosphere where the temperature approaches 90% of the dry peridotite solidus. Experimentally anelastic properties of peridotite determined by *Sato et al. (1989)* illustrate that the attenuation mechanism of peridotite might be the weakness (or "*softening*") of grain boundaries at high temperature below the solidus. This might be the case in southern Kamchatka too, since the wedge temperatures come close to ~ 90% of the peridotite dry solidus.

DISCUSSION AND CONCLUSIONS

Numerical models of steady-state temperature and velocity fields in the mantle wedge of the Kamchatka subduction zone are developed using the numerical scheme of *Manea et al. (2004b)*. Based on this, a dynamic model of buoyant blob migration in the mantle wedge velocity field is developed. The thermal history of a 10 km blob, which moves up through the mantle wedge thermal field is predicted. Finally, the thermal structure of the mantle wedge is used to estimate the seismic P-wave velocity anomalies (referenced to PREM) associated with subduction of the Pacific plate beneath Kamchatka. The velocity anomalies estimates are compared with a seismic tomography image inferred from P-wave arrivals for the same cross-section *(Gorbatov et al., 1999)*.

Four different models are considered, the first two with isoviscosity in the wedge (with and without frictional heating) and the second two with the temperature-dependent viscosity (with and without frictional heating). Both type of thermal models (isoviscous and with the temperature dependent viscosity), show a velocity inflow-outflow in the mantle wedge beneath Moho and the slab surface. This type of flow might induce elastic anisotropy in the wedge peridotite, which is consistent with the trench normal strike of the inferred anisotropic fast axes in southern Kamchatka *(Levin et al. 2002)*.

The isoviscous thermal models do not predict any melting in the asthenosphere beneath the volcanic chain *(Fig. 4)*. With a temperature > 1,300 °C *(Fig. 5)*, the model with temperature-dependent viscosity in the mantle wedge shows a significant increase in temperature beneath the volcanic arc. Two different sources of melt are possible: sediments and wedge peridotite beneath the volcanic front). A small amount of frictional heating (a pore pressure ratio $\lambda = 0.96$ or an effective friction coefficient $\mu = 0.034$ and an average shear stress along the thrust fault $\tau \sim 14$ MPa) is added at the contact between the subducted slab and the overriding plate *(Fig. 6-A)*. For larger amounts of frictional heating (i.e. $\lambda = 0.95$)

melting of basalt oceanic crust might become possible, but this is inconsistent with the lack adakites volcanism in southern Kamchatka.

Partial melting of peridotite in subduction zones is initiated by an influx of fluids derived from the metamorphosed slab and sediments *(Tatsumi, 1986; Davies and Stevenson, 1992)*. Major dehydration of the basaltic oceanic crust (> 5 wt% H_2O release) occurs just below the volcanic chain up to a depth of ~100 km (*Fig. 8* and *Fig. 9*). Despite the variation in parameters and model input, dehydration of the top of the slab is complete in all models at basically the same depth. This depth estimation is rather robust and does not depend on model parameters. The H_2O contents in the phase diagrams for mafics and harzburgite (*Hacker et al., 2003*) represent the maxima. Whether such H_2O contents are reached depends on pre-subduction alteration and fluid flow in the subducted slab. Experimental studies of fluid-saturated peridotite show a solidus as low as ~ 800 °C at pressures between 2-3 GPa *(Mysen and Boettcher, 1975)*. As a result, just above the subducting slab (~ 5 km) a layer of melted peridotite might exist, as is the case for the temperature-dependent viscosity thermal models in the present study. The existence of such a melted layer has been suggested by *Okada (1979)*. He deduced a low-velocity layer in the vicinity of the mantle wedge-slab interface from the efficient conversion of ScS and ScSp phases. *Gerya and Yuen (2003)* demonstrate that Rayleigh-Taylor instabilities can develop and rise up from the top of cold subducting slabs. They also suggest that plumes detached from the slab might be lubricated by partially melted, low-viscosity material from the subducted crust and hydrated mantle.

Modeling of blob motion in the mantle wedge viscous flow field induced by the subducting slab, shows that this simple approach may shed light on the origin of the volcanism beneath south Kamchatka. Two parameters control the trajectories of blobs rising from the slab: the diameter of the blob and the wrapping viscosity. Very low values of wrapping viscosity (10^{14} - 10^{17} Pa s) are necessary to counter out the drag and buoyancy forces, which is critical for the blob to rise.

Blob rise time decreases nonlinearly as its diameter increases and the wrapping viscosity diminishes (*Fig. 10*). The time required for a blob of 10 km diameter to rise from the slab surface up to the continental crust varies from < 2,000 yr up to 10 Myr for viscosities between 10^{14} Pa s and > 10^{17} Pa s respectively. For a diameter of $\geq$ 8 km and a viscosity of $\geq$ 10^{17} Pa s blobs rise upward until they reach the base of the continental lithosphere. This low value of viscosity is in the lowermost range experimentally determined for olivine at the upper mantle pressures and temperatures (*Hirth and Kohlstedt, 2003*).

Dynamic models of blob trajectories in the mantle wedge velocity field shows that "*fast*" trajectories terminate at the same location on the base of the continental lithosphere (*Fig. 10*), while the final points of "*slow*" trajectories, which are more common for the blobs of smaller size (< 1 km), are dispersed.

An important constraint on the magma transport time through mantle wedge comes from U-series isotope disequilibria, ^{10}Be and fluid soluble trace elements as Th, Sr and Pb isotope studies. *Turner and Hawksworth (1997)* proposed a very rapid ascent of magma (~ 1,000 years or ~ 60 m/yr) from the slab surface toward the earth surface through a channel network. On the other hand, *Regelous et al. (1997)* infer a magma transport rate of < 350 kyr (or ~ 17 cm/yr) from Th, Sr and Pb isotope data. These results are quite different but in a recent study for U-Th-Pa-Ra disequilibria for Kamchatka of *Dosseto et al. (2003)*, is discussed the existence of a dynamic melting model which does not require a high upwelling velocity (i.e. 1 m/yr) within the mantle wedge. A more contradictory conclusion comes from ^{10}Be studies, which show that residence time for Be in the mantle wedge is ~ 6 Myr before the surface eruption.

The U-Th-Pa-Ra, Th, Sr and Pb isotope disequilibria and ^{10}Be studies show very contradictory estimates of the magma transport times through the mantle wedge from < 350 kyr up to 6 Myr. Such high variability in magma transport suggests a very variable transport rates for different elements and/or real differences in transport times probably due to a variable melted volume generated in the wedge. Apart of its inherent simplicity, the advantage of a magma transport

model using buoyant blobs proposed in this chapter is its ability to cover the wide range of residence magma time inside the mantle wedge (*Fig. 11*).

The proposed positively buoyant blobs might have a complex composition of melted saturated peridotite and melted sediments. An H_2O-rich component (likely with sediments) resulting from dehydration penetrates overlying peridotites. Ascending into the hotter mantle, this material passes the wet solidus of peridotite (*see Fig. 14*). Partial melting starts and the buoyant blobs begin to move through the strong mantle wedge flow. Finally the blobs reach the base of the lithosphere and form a magmatic chamber beneath the volcanic chain.

Levin et al. (2002) proposes a scenario where the anisotropy in the top layer (~ 15 km beneath Moho) of the mantle wedge beneath EVF in southern Kamchatka is generated by melt lenses and/or sheeted diapirs. In this model, the anisotropy might be generated without the presence of a mantle wedge inflow beneath Moho. This model is in good agreement with the flow model presented in *Fig. 7-B*, where very small inflow velocities are obtained from the thermal model with strong temperature dependence of olivine. Moreover, the magma propagation model with buoyant blobs shows an accumulation area of melted blobs just beneath the volcanic arc at the base of Moho (*Fig. 10*).

One important control regarding the reality of buoyant blobs comes from a study of deformed peridotite xenoliths from Avachinscky volcano (*Fig. 1*) (*Graybill et al., 1999*). In this paper the xenoliths strains do not indicate a shear induced by a corner flow, rather they seems to belong from individual diapirs traveling through the mantle wedge.

The thermal evolution of the blobs was investigated by applying the heat conduction equation. Thermal convection inside a blob of 10 km diameter is not likely to occur because the Rayleigh number is very small (~ 2.7 for a viscosity of 10^{17} Pa s and a maximum thermal contrast of 300°C). Therefore, in the present study, the blob is heated/cooled only by conduction. After about 1 Myr, the cold blob (~ 800°C) moves toward the hotter region of the wedge where a temperature of more than 1,300°C is estimated (*Fig. 12* and *Fig. 14*). After being heated the

blob moves upwards toward the base of the continental lithosphere where it arrives with a hot core (> 900°C). According to the fluid-saturated peridotite solidus of *Mysen and Boettcher (1975),* most of the 10 km blob (*T* > 900°C at 1 GPa) is melted when arrives at the Moho base (*Fig. 12-A-i* and *Fig. 13*). The blobs may carry fluid-saturated melts (i.e. melted peridotite) and sediments from the subducted slab to the base of the continental lithosphere and therefore trace elements and the chemical signature finally might reach the earth's surface through volcanic eruptions. Although *Fedotov and Masurenkov (1991)* classified the active volcanoes in Kamchatka as calc-alkaline, *Tatsumi et al. (1994)* interpreted as tholeiitic the southern Kamchatka volcanoes. However, *Kelemen (1990)* shows that "*slow*" ascent of a tholeiitic melt through a hot mantle wedge produces calc-alkaline magmatism at the surface.

The thermal model with temperature-dependent viscosity and frictional heating is used to estimate a seismic tomography image below southern Kamchatka. The high temperatures in the mantle wedge beneath the volcanic chain (> 1,300°C) produce a strong negative velocity anomaly of up to –7 % (*Fig. 14-A*) (relative to PREM). On the other hand, the cold subducting slab produces a positive velocity anomaly up to +4%. Since the seismic tomography of *Gorbatov et al. (1999)* has a small uncertainty of ~ 10%, our estimation is in good agreement with the velocity anomalies obtained by *Gorbatov et al. (1999)* for a 2D profile identically located with our 2D cross sections. The shape of our tomographic image inferred from thermal modeling differs from the P-wave seismic tomography image of *Gorbatov et al. (1999),* especially for the continental lithosphere and the uppermost mantle beneath the volcanic chain (*Fig. 14-B*). This is likely due to the fact that the thermal models in this study do not consider the magma transport effect toward the surface. However, since the resolution of the seismic tomography is very low (50 km) the position of the low velocity zone beneath the EVF has very large uncertainties. Nevertheless, good agreement of the velocity perturbation beneath the volcanic arc (at least in magnitude) between the tomography image

from P-wave arrivals and our estimation from thermal modeling suggests satisfactory modeling the mantle wedge beneath southern Kamchatka.

REFERENCES

Billen, M.I., and Gurnis, M., 2001. A low viscosity wedge in subduction zones. *Earth Planetary Science Letters, v. 193, no. 1-2, p. 227-236.*

Brown, L., Klein, J., Middleton, R., Sacks, I.S., and Tera, F., 1982. [10]Be in island arc volcanoes and implications for subduction. *Nature, v. 299, p. 718-720.*

Burov, E., Jolivet, E., Le Pourhiet, L. and Poliakov, A., 2000. A thermomechanical model of exhumation of high pressure (HP) and ultra-high pressure (UHP) metamorphic rocks in Alpine-type collision belts. *Tectonophysics, v. 342, p. 113-136.*

Byerlee, J.D., 1978. Friction of rocks. *Pure Applied Geophysics, v. 116, p. 615-626.*

Chopelas, A., 1992. Sound velocities of MgO to very high compression. *Earth and Planetary Science Letters, v. 114, p. 185-192.*

Davies, J.H., and Stevenson,D.J., 1992. Physical model of source region of subduction zone volcanism. *Journal of Geophysical Research, v. 97, p. 2037-2070.*

Davies.J.H., 1999. The role of hydraulic fractures and intermediate-depth earthquakes in generating subduction-zone magmatism. *Nature, v. 398, p. 142-145.*

Dickinson, W.R., 1978. Plate tectonic evolution of north Pacific rim, in Geodynamics of the western Pacific. edited by Ueda, S., Murphy, R.W., and Kobayashi, K., p. 1-19, *Japan Scientific Societies Press, Tokyo, Japan.*

Dosseto, A., Bourdon, B., Joron, J.L., and Dupré, B., 2003. U-Th-Pa-Ra study of the Kamchatka arc: New constraints on the genesis of arc lavas. *Geochimica et Cosmochimica Acta, v. 67, no. 15, p. 2857-2877.*

Dziewonski, A.M., and Anderson, D.L., 1981. Preliminary reference Earth model. *Physics of the Earth and Planetary Interiors, v. 25, p. 297-356.*

Eiler, J.M., Crawford, A., Elliott, T., Farley, K.A., Valley, J.W., and Stolper, E.M., 2000. Oxygen isotope geochemistry of oceanic-arc lavas. *Journal of Petrology, v. 41, p. 229-256.*

Fedotov, S.A., and Masurenkov, Yu.P. (Eds.), 1991. Active Volcanoes of Kamchatka. *Nauka, Moscow, Russia.*

Gaetani, G.A., and Grove, T.L., 2003. Experimental Constraints on melt generation in the mantle wedge: in *Inside the Subduction Factory*, Geophysical Monograph 138, edited by J. Eiler, *AGU, Washington DC, p. 107-134.*

Gerya, T.V. and Yuen, D.A., 2003. Rayleigh-Taylor instabilities from hydration and melting propel 'cold plumes' at subduction zones. *Earth and Planetary Science Letters, v. 212, p. 47-62.*

Gorbatov, A., and Kostoglodov, V., 1997. Maximum depth of seismicity and thermal parameter of the subducting slab: general empirical relation and its application. *Tectonophysics, v. 277, p. 165-187.*

Gorbatov, A., Kostoglodov, V., Suárez, G., and Gordeev, E., 1997. Seismicity and structure of the Kamchatka subduction zone. *Journal of Geophysical Research, v. 102, no. B8, p, 17,883-17,898.*

Gorbatov, A., Dominguez, J., Suárez, G., Kostoglodov, V., and Gordeev, E. 1999. Tomographic imaging of the P-wave velocity structure beneath the Kamchatka peninsula. *Journal of Geophysical Research, v. 137, p. 269-279.*

Gorbatov, A., Widiyantoro, A., Fukao, Y., and Gordeev, E., 2000. Signature of remnant slabs in the North Pacific from *P*-wave tomography. *Geophysical Journal International, v. 142, p. 27-36.*

Graybill, J., Brandon, M.T., and Kepezhinskas, P.K., 1999. Olivine lattive-preffered orientation in xenoliths from the mantle wedge beneath the southern Kamchatka volcanic arc (abstract). *Eos Trans. AGU, 80, F926.*

Hacker, B.R., Abers, G.A., and Peacock, S.M., 2003. Subduction Factory 1. Theoretical mineralogy, densities, seismic wave speeds, and H2O contents. *Journal of Geophysical Research, v. 108, 10.1029/2001JB001127.*

Hart, S.R., 1993. Equilibration during mantle melting: a fractal tree model. *Proc.National Academy of Science, USA, v. 90, p. 11,914-11,918.*

Hirth, G., and Kohlstedt, D.L., 2003. Rheology of the mantle wedge: in Inside the Subduction Factory, *Geophysical Monograph 138*, edited by J. Eiler, *AGU, Washington DC, p. 83-105.*

Johnson, M.C., and Plank, T., 1999. Dehydration and melting experiments constrain the fate of subducted sediments. *G-cubed, 1.*

Karato, S., and Spetzler, H.A., 1990. Defect microdynamics and physical mechanisms of seismic wave attenuation and velocity dispersion in the Earth's mantle. *Review of Geophysics, v. 28, p. 399-421.*

Karato, S.I., 1993. Importance of anelasticity in the interpretation of seismic tomography. *Geophysical Research Letters, v. 20, p. 1623-1626.*

Karato, S., and Wu, P., 1993. Rheology of the upper mantle: a synthesis. *Science, v. 260, p. 771-778.*

Kelemen, P.B., 1990. Reaction between ultramafic rock and fractionating basaltic magma. I. Phase relations, the origin of calc-alkaline magma series, and the formation of discordant dunite. *Journal of Petrology, v. 31, p. 51-98.*

Kelemen, P.B., Rilling, J.L., Parmentier, E.M., Mehl, L., and Hacker, B.R., 2003. Thermal Structure due to Solid-State Flow in the Mantle Wedge Beneath Arcs: in Inside the Subduction Factory, *Geophysical Monograph 138*, edited by J. Eiler, *AGU. Union, Washington DC, p. 293-311.*

Klein, E.M., and Langmuir, C.H., 1987. Global correlations of ocean ridge basalt chemistry with axial depth and crustal thickness. *Journal of Geophysical Research, v. 92, p. 8089-8115.*

Kushiro, I., 1990. Partial melting of mantle wedge and evolution of island arc cruz. *Journal of Geophysical Research, 95, 15,929-12,939.*

Langmuir, C.L., Klein, E.M., and Plank, T., 1992. Petrological systematics of mid-ocean ridge basalts: Constraints on melt generation beneath ocean ridges. *In Mantle flow and melt generation at mid-ocean ridges, AGU Monograph 71*, edited

by J. Phipps Morgan, D.K. Blackman, and J.M. Sinton, *p. 183-280, AGU, Washington DC.*

Levin, V., Park, J., Brandon, M., Lees, J., Peyton, V., Gordeev, E., and Ozerov, A., 2002. Crust and upper mantle of Kamchatka from teleseismic receiver functions. *Tectonophysics, v. 358, p. 233-265.*

Manea, V.C., Manea, M., Kostoglodov, Currie, C.A., and Sewell, G., 2004a. Thermal Structure, Coupling and Metamorphism in the Mexican Subduction Zone beneath Guerrero. *Geophysical Journal International, 158, 775–784 doi: 10.1111/j.1365 - 246X.2004.02325.x.*

Manea, V.C., Manea, M., Kostoglodov, V., Sewell, G., 2004b. (in press) Thermo-mechanical model of the mantle wedge in Central Mexican subduction zone and a blob tracing approach for the magma transport. *Physics of the Earth and Planetary Interiors.*

Molnar, P., and England, P., 1990. Temperatures, heat flux, and frictional stress near Major thrust faults. *Journal of Geophysical Research, v. 95, p. 4883-4856.*

Molnar, P., and England, P., 1995. Temperatures in zones of steady state underthrusting of young oceanic lithosphere. *Earth and Planetary Science Letters, v. 131, p. 57-70.*

Morris, J., Leeman, W.P., and Tera, F., 1990. The subducted component in island arc magmas.: constraints from Be isotopes and B-Be systematics. *Nature, v. 344, p. 31-36.*

Mysen, B.O., and Boettcher, A.L., 1975. Melting of a hydrous mantle: I. Phase relations of natural peridotite at high pressures and temperatures with controlled activities of water, carbon dioxide, and hydrogen. *Journal of Petrology, v. 16, part 3, p. 520-548.*

Nichols, G.T., Wyllie, P.J., and Stern, C.R., 1994. Subduction zone melting of pelagic sediments constrained by melting experiments. *Nature, v. 371, p. 785-788.*

Okada, H., 1979. New evidences of the discontinuous structure of the descending lithosphere revealed by ScSp phase. *Journal of Physics of the Earth, v. 27, p. S53-S63.*

Park, J., V. Levin, M. T. Brandon, J. M. Lees, V. Peyton, E. Gordeev, and A. Ozerov, 2002. A dangling slab, amplified arc volcanism, mantle flow and seismic anisotropy near the Kamchatka plate corner. *in Plate Boundary Zones*, Stein, S., and Freymueller, J. (eds.), *AGU Geodynamics Series No. 30, AGU, Washington DC, p. 295-324.*

Peacock, S.M., 1990a. Fluid processes in subduction zone. *Science, v. 248 (4953), p. 329-337.*

Peacock, S.M., 1990b. Numerical simulation of metamorphic pressure-temperature-time paths and fluid production in subducting slabs. *Tectonics, v. 9(5).*

Peacock, S.M., 1991. Numerical simulation of subduction zone pressure-temperature-time paths: Constraints on fluid production and arc magmatism: in Phil. Trans. Roy. Soc. London A 335: *The Behavior and Influence of Fluids in Subduction Zones,* edited by Tarney, J., Pickering, K.T., Knipe, R.J., and Dewey, J.F., *p. 341-353, London, United Kingdom.*

Peacock, S.M., 1996. Thermal and petrologic structure of subduction zones, *in Subduction Zones, Top to Bottom: Geophysical Monograph 96,* edited by Bebout, G.E., Scholl, D.W., Kirby, S.H., and Platt, J.P., *p. 119-133, AGU, Washington DC.*

Peacock, S.M., and Hyndman, R.D., 1999. Hydrous minerals in the mantle wedge and the maximum depth of subduction thrust earthquakes. *Geophysical Research Letters, v. 26, p. 2517-2520.*

Peacock, S.M., and Wang, K., 1999. Sesimic consequences of warm versus cool subduction metamorphism: Examples from southwest and northeast Japan. *Science, v. 286, p. 937-939.*

Peacock, S.M., (in press) 2002. Thermal structure and metamorphic evolution of subducting slabs: in Eiler, J. (ed.) *The Subduction Factory, AGU Geophysical Monograph.*

Plank, T., and Langmuir, C.H., 1993. Tracing trace elements from sediment input to volcanic output at subduction zones. *Nature, v. 362, p. 739-743.*

Regelous, M., Collerson, K.D., Ewart, A., and Wendt, J.I., 1997. Trace element transport rates in subduction zones: evidence from Th, Sr and Pb isotope data for

Tonga-Kermandec arc lavas. *Earth and Planetary Science Letters, v. 150, p. 291-302.*

Renkin, M.L., and Sclater, J.G., 1988. Depth and age in the North Pacific. *Journal of Geophysical Research, v. 93, B4, p. 2919-2935.*

Rubin, A.M., 1993. Dikes vs. diapirs in viscoelastic rock. *Earth and Planetary Science Letters, v. 117, p. 653-670.*

Sato, H., Sacks, I.S., Takahashi, E., and Scarfe, C.M., 1988. Geotherms in the Pacific Ocean from laboratory and seismic attenuation studies. *Nature, v. 336, p. 154-156.*

Sato, H., Sacks, I.S., Murase, T., Muncill, G., and Fukuyama, H., 1989. Q_P-melting temperature relation in peridotite at high pressure and temperature: attenuation mechanism and implications for the mechanical properties of the upper mantle. *Journal of Geophysical Research, v. 94, p. 10,647-10,661.*

Selivestrov, N.I., 1983. Structure of the junction zone of the Kurile-Kamchatka and Aleutian island arcs according to data from continuous seismic profiling (in Russian). *Volcanology and Seismology, v. 2, p. 53-67.*

Shaw, B.E., 1980. The fracture mechanisms of magma transport from the mantle to the surface: In: Hargraves, R.B. (Eds.), *Physics of Magmatic Processes. Princeton Univ. Press, Princeton, p. 201– 264.*

Smirnov, Ya. B., and Sugrobov, V.M., 1979. Terrestrial heat flow in the Kurile-Kamchatka and Aleutian provinces. I. Heat flow and tectonics (in Russian). *Volcanology and Seismology, v. 1, p. 59-73.*

Smirnov, Ya. B., and Sugrobov, V.M., 1980a. Terrestrial heat flow in the Kurile-Kamchatka and Aleutian provinces. II. The map of measured and background heat flow (in Russian). *Volcanology and Seismology, v. 1, p. 16-31.*

Smirnov, Ya. B., and Sugrobov, V.M., 1980b. Terrestrial heat flow in the Kurile-Kamchatka and Aleutian provinces. III. Assessments of temperature at depth and thickness of the lithosphere (in Russian). *Volcanology and Seismology, v. 1, p. 16-31.*

Smith, D.L., Nuckels, C.E., Jones, R.L. and Cook, G.A., 1979. Distribution of heat flow and radioactive heat generation in northern México. *Journal of Geophysical Research, v. 84, p. 2371-2379.*

Spiegelman, M., and Kelemen, P.B., 2003. Extreme chemical variability as a consequence of channelized melt transport. *G-cubed, v. 4, no. 7, 1055, doi:10.1029/2002GC000336.*

Stacey, E.D., 1977. A thermal model of the Earth. *Physics of the Earth and Planetary Interiors, v. 15, p. 341-348.*

Stolper, E.M., and Newman, S., 1994. The role of water in the petrogenesis of Mariana trough magmas. *Earth and Planetary Science Letters, v. 121, p. 293-325.*

Tamura, Y., Tatsumi, Y., Zhao, D., Kido, Y., and Shukuno, H., 2002. Hot fingers in the mantle wedge: new insights into magma genesis in subduction zones. *Earth and Planetary Science Letters, v. 197, no. 1, p. 105-116.*

Tatsumi, Y., Sakuyama, M., Fukuyama, H., and Kushiro, I., 1983. Generation of arc basalt magmas and thermal structure of the mantle wedge in subduction zones. *Journal of Geophysical Research, v. 88, p. 5815-5825.*

Tatsumi, Y., 1986. Formation of the volcanic front in subduction zones. *Geophysical Research Letters, v. 13, p. 717-720.*

Tatsumi, Y., Furukawa, Y., Kogiso, T., Yamanaka, K., Yokoyama, T., and Fedotov, S.A., 1994. Unusual three volcanic chains in the Kamchatka: *Geophysical Research Letters, v. 21, p. 537-540.*

Turcotte, D.L., and Schubert, G., 2002. Geodynamics, 2nd edition, *Cambridge University Press, New York.*

Turner, S., and Hawkesworth, C., 1997. Constraints on flux rates and mantle dynamics beneath island arcs from Tonga-Kermadec lava geochemistry. *Nature, v. 389, p. 568-573.*

Vacquier, V., Sclater, J.G., and Corry, C.E., 1967. Studies of the thermal state of Earth: The 21st paper: Heat-flow, eastern Pacific. *Bulletin of Earthquake Research Institute, v. 45, p. 375-393.*

van Keken, P.E., Kiefer, B., and Peacock, S.M., 2002. High resolution models of subduction zones: Implications for mineral dehydration reactions and the transport of water into deep mantle. *G-cubed, v. 3, no. 10, p. 20.*

von Hunen, J., van den Berg, A.P., Vlaar, N.J., 2000. A thermo-mechanical model of horizontal subduction below an overriding plate. *Earth and Planetary Science Letters, v. 182, p. 157-169.*

Wang, K. and Davis, E.E., 1992. Thermal effect of marine sedimentation in hydrothermally active areas. *Geophysical Journal International, v. 110, p. 70-78.*

Wyllie, P.J., 1979. Magmas and volatile components. *American Mineralogy, v. 654, p. 469-500.*

Zhao, D., Hasegawa, A., and Horiuchi, S., 1992. Tomographic imaging of P and S wave velocity structure beneath northwestern Japan. *Journal of Geophysical Research, v. 97, no. 13, p. 19,909-19,928.*

Zhao, D., Yingbiao, X, Weins, D.A., Dorman, L., Hildebrand, J., and Webb, S., 1997. Depth extent of the Lau back-arc spreading center and its relation to subduction proceses. *Science, p. 254-257.*

Zhao, D., 2001. Seismological structure of subduction zones and its implications for arc magmatism and dynamics. *Physics of the Earth and Planetary Interiors, v. 3999, p. 1–18.*

Table 1. Summary of thermal parameters used in the models. (Compilation from *Peacock and Wang, 1999; Smith et al., 1979*)

Geological Unit	Density (g/cm³)	Thermal Conductivity (W/m °K)	Radiogenic heat production (μW/m³)	Thermal Capacity (MJ/m³ °K)
Oceanic sediments	2.20	1.00 – 2.00*	1.00	2.50
Upper continental crust (0-15 km)	2.70	2.00	1.3	2.50
Lower continental crust (15-35 km)	2.70	2.00	0.2	2.50
Mantle wedge and Blob	3.10	3.10	0.01	3.30
Oceanic lithosphere	3.00	2.90	0.02	3.30

- *Increases linearly with distance from the deformation front up to a depth of 10 km.*

FIGURE CAPTIONS

Figure 1.

Tectonic settings and position of the modeled cross-section (purple thick line) in Kamchatka. Orange triangles show the location of trench-side and back-arc volcanoes. Open, semi-transparent arrows show convergence velocities between the Pacific and North American plates.

Figure 2.

A grid with 12,000 triangles with ~ 2 km mesh resolution was used to solve the numerical thermal models. The green spherical mesh was used to solve the heat transfer equation (2) (*see text*) inside the blob and contains 3,000 triangles.

Figure 3.

Boundary condition and parameters used in the modeling. The upper and lower boundaries have constant temperatures of 0°C and 1,450°C, accordingly. The continetal plate is fixed. The left (landward) vertical boundary: 18.5°C/km thermal gradient in the continental crust (down to 35 km); between 35 km and 180 km depth the thermal gradient is of 5.5°C/km; underneath 180 km no horizontal conductive heat flow is specified. Zero tractions are considered beneath Moho (35 Km), at the boundary, which belongs to the mantle wedge. The right (seaward) boundary condition is a one-dimensional geotherm for the 70 Myr old oceanic plate. The PAC plate referred to the North American plate has the convergence velocity of 7.8 cm/yr. Volumetric shear heating is imposed along the plate interface up to a maximum depth of 35 km (red dashed line), using the Byerlee's friction law (*Byerlee, 1978*).

Figure 4.

(A). Calculated steady-state thermal field for the isoviscous mantle wedge. Horizontal dashed line shows the Moho (35 km depth). Thick solid magenta line denotes the top of the subducting slab. No frictional heating along the thrust zone is included in this model. A-A' is the vertical temperature profile in *Fig. 6-B*.

(B). The same as A., but frictional heating ($\lambda = 0.96$ or $\mu = 0.034$) along the thrust zone is included in this model.

Figure 5.

(A). Steady-state thermal field for strong temperature-dependent viscosity in the mantle wedge. Horizontal dashed line shows the Moho (35 km depth). Thick solid magenta line denotes the top of the subducting slab. No frictional heating along the thrust zone is included in this model. B-B' is the vertical temperature profile in *Fig. 6-B*.

(B). The same as A., but frictional heating ($\lambda = 0.96$ or $\mu = 0.034$) along the thrust zone is included in this model.

Figure 6.

(A). Phase diagrams for MORB and maximum H_2O contents (*Hacker et al., 2003*). Z - Zeolite (4.6 wt% H_2O), PP - Prehnite - Pumpellyite (4.5 wt% H_2O), PA - Pumpellyite - Actinolite (4.4 wt% H_2O), G - Greenschist (3.3 wt% H_2O), LB - Lawsonite - Blueschist (5.4 wt% H_2O), EpB - Epidote - Blueschist (3.1 wt% H_2O), EpA - Epidote - Amphibolite (2.1 wt% H_2O), JEpB - Jadeite - Epidote - Blueschist (3.1 wt% H_2O), EcA - Eclogite - Amphibole (2.4 wt.% H_2O), A - Amphibolite (1.3 wt% H_2O), GA - Garnet - Amphibolite (1.2 wt% H_2O), Gr - Granulite (0.5 wt% H_2O), GGr - Garnet - Granulite (0.0 wt% H_2O), JLB - Jaedite - Lawsonite - Blueschist (5.4 wt% H_2O), LAEc - Lawsonite - Amphibole - Eclogite (3.0 wt% H_2O), JLTS - Jaedite - Lawsonite - Talc - Schist, ZAEc - Zoisite - Amphibole - Eclogite (0.7 wt% H_2O), AEc - Amphibole - Eclogite (0.6 wt% H_2O), ZEc - Zoisite - Eclogite (0.3 wt% H_2O), Ec - Eclogite (0.1 wt% H_2O), CEc - Coesite - Eclogite (0.1 wt% H_2O), DEc -

Diamond - Eclogite (0.1 wt% H_2O). Calculated geotherms: dashed blue line - top of subducting oceanic crust for isoviscous mantle wedge and no frictional heating; solid blue line – top of subducting oceanic crust for strong temperature-dependent viscosity and no frictional heating; dashed pink/red line - top of subducting oceanic crust isoviscosity in the mantle wedge and frictional heating (λ = 0.96 or μ= 0.034); solid pink/red line - top of subducting oceanic crust for strong temperature-dependent viscosity and frictional heating (λ = 0.96 or μ = 0.034). The maximum depth of the stable hydrous phases in the oceanic slab is ~ 90 km in case of variable rheology in the wedge (and with frictional heating (λ = 0.96 or μ= 0.034)).

(B). Phase diagram for harzburgite, and maximum H_2O contents (*Hacker et al., 2003*). A - Serpentine - Chlorite - Brucite (14.6 wt% H_2O), B - Serpentine - Chlorite - Phase A (12 wt% H_2O), C - Serpentine - Chlorite - Dunite (6.2 wt% H_2O), D - Chlorite - Harzburgite (1.4 wt% H_2O), E - Talc - Chlorite - Dunite (1.7 wt% H_2O), F - Anthigorite - Chlorite - Dunite (1.7 wt% H_2O), G - Spinel - Harzburgite (0.0 wt% H_2O), H - Garnet - Harzburgite (0.0 wt% H_2O).

Continuous thick yellow line indicates the wet solidus for sediments from *Nichols et al. (1994)*. Calculated geotherms are the same as in A. The temperature profiles A-A' and B-B' (*Fig. 4* and *Fig. 5*) show that for an isoviscous mantle wedge thermal structure, melting of wet peridotite is not possible, while for temperature-dependent viscosity melting of wet peridotite beneath the volcanic chain is likely to occur. The wet and dry peridotite are taken from *Wyllie (1979)*.

Figure 7.

(A). The velocity field in the isoviscous mantle wedge. The maximum inflow velocity is about 3 cm/yr. The return flow (backflow) is horizontal.

(B). The velocity field with the strong temperature-dependent mantle wedge viscosity. Note that the maximum velocity of the inflow region is about 7.5 cm/yr that is comparable with the subducting slab velocity. The velocity field presents a diagonally upward pattern. Note the very low velocity (< 1 cm/yr) just beneath the Moho.

Figure 8.

(A). Metamorphic facies along the subducting oceanic crust corresponding to the isoviscous model without frictional heating. The inset represents the variation of wt% H_2O along the subducting crust as function of metamorphic sequence. More than 5 wt% H_2O may be released from hydrous phases in the subducting slab through continuous dehydration.

(B). The same as for *Fig. 8-A* but with frictional heating ($\lambda = 0.96$ or $\mu = 0.034$). More than 3 wt% H_2O may be released from hydrous phases in the subducting slab through continuous dehydration.

Figure 9.

(A). The same as *Fig. 8-A* but for the temperature-dependent viscosity model without frictional heating. More than 5 wt% H_2O may be released from hydrous phases in the subducting slab through continuous dehydration.

(B). The same as *Fig. 8-A* but for the temperature-dependent viscosity model with frictional heating ($\lambda = 0.96$ or $\mu = 0.034$). More than 3 wt% H_2O may be released from hydrous phases in the subducting slab through continuous dehydration.

Figure 10.

Blob trajectories in steady mantle wedge flow (*Fig. 7-B*). The initial point for all trajectories is at a depth of 110 km on the surface of the subducting slab below the trench-side volcanic belt.

(A). Blob diameter is fixed at 4 km. The trajectories, corresponding to different wrapping viscosities of less than 10^{16} Pa s, have the same final point below the volcanic chain.

(B). The wrapping viscosity is fixed at 10^{15} Pa s. The trajectories correspond to different blob size (0.8 - 10.0 km). Blobs with a diameter less than ~ 0.8 never rise to the continental crust.

Figure 11.

Blob rise time as a function of wrapping viscosity. The curves annotated with blob diameter show that the rise time decreases for bigger blobs and the lower viscosity. Blobs with a size of less than 10 km can reach the continental crust in less than 350 kyr for wrapping viscosities less than 10^{16} Pa s (*see inset*).

Figure 12.

(A). The thermal history of a 10-km blob which reaches the Moho in 2.6 Myr at nine time periods. The wrapping viscosity is 10^{17} Pa s. The circles represent the blob cross-section.

(B). The trajectory followed by the blob in a thermal structure for temperature-dependent viscosity (*Fig. 5-B*).

(C). The same as B. but zoomed.

Figure 13.

P-T Trajectory of the 10-km diameter blob (*see Fig. 12*) through the mantle wedge. Colour disks represent the blob at nine time periods from *Fig. 12*. The number inside the disks shows the rising time. Dark blue dashed line represents wet peridotite solidus from *Wyllie (1979)*. Green dashed line represents wet peridotite solidus from *Mysen and Boettcher (1975)* (limited to ~ 3 GPa).

Figure 14.

(A). Velocity anomaly estimation below south Kamchatka inferred from thermal models with temperature-dependent viscosity (*Fig. 5-B*). Red and blue colors reveal the slow and fast velocities according to the vertical scale.

**(B).** Seismic tomography of south Kamchatka inferred from P-wave arrivals from *Gorbatov et al. (1997)*.
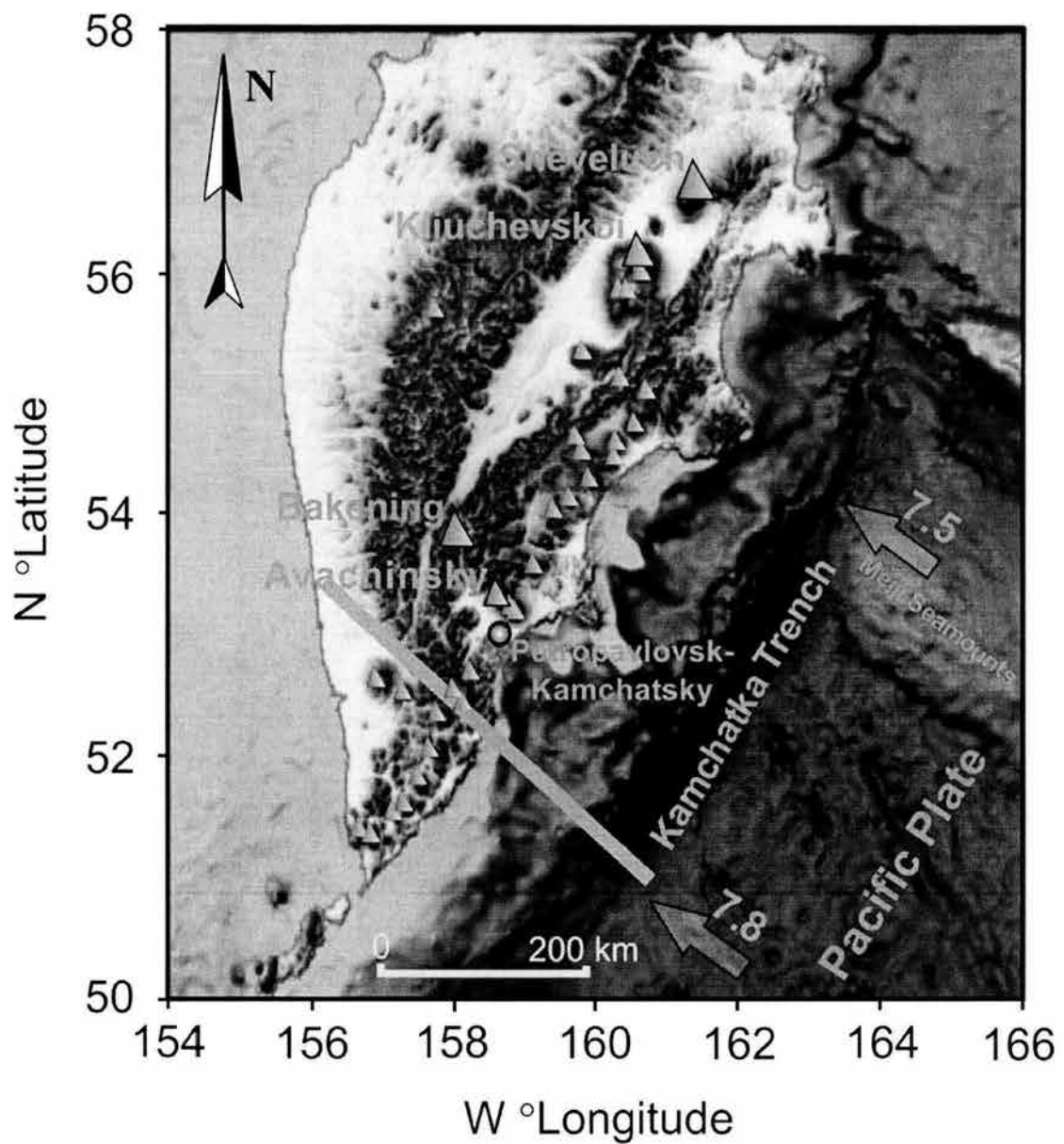
Figure 1
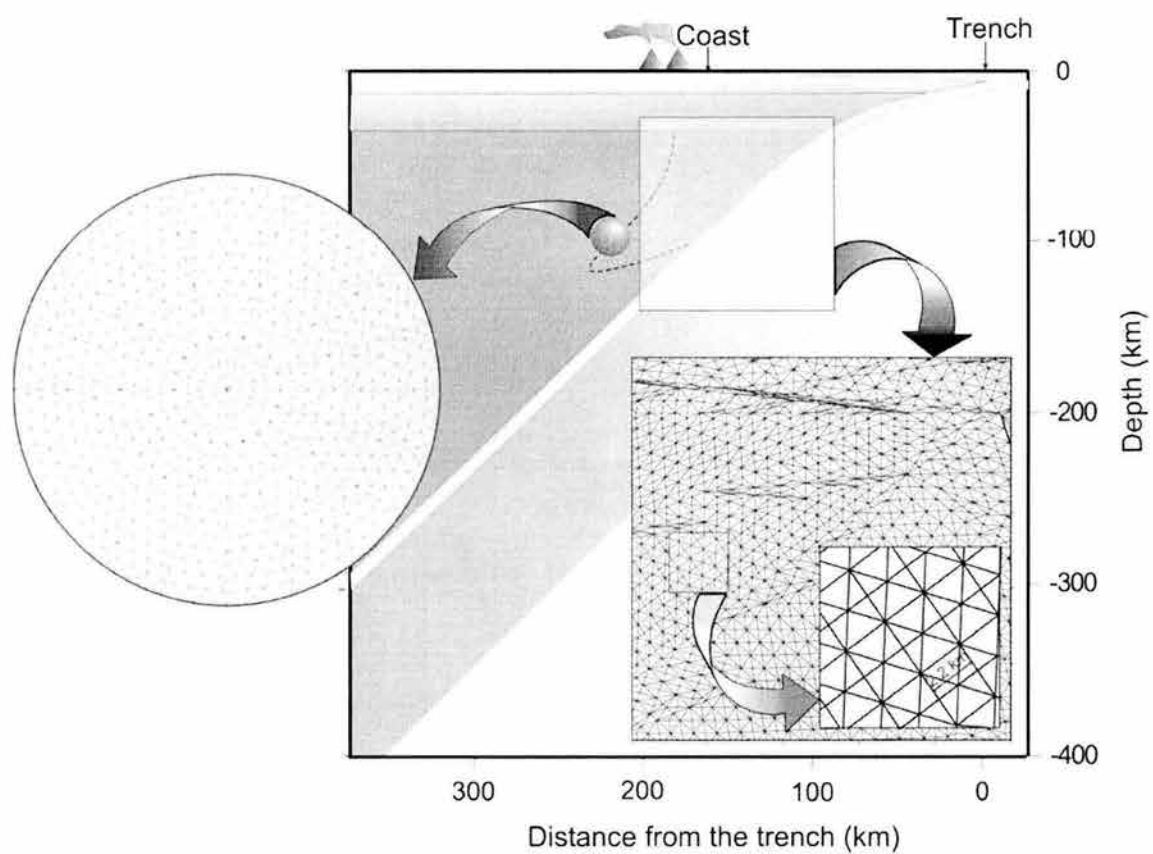
Figure 2
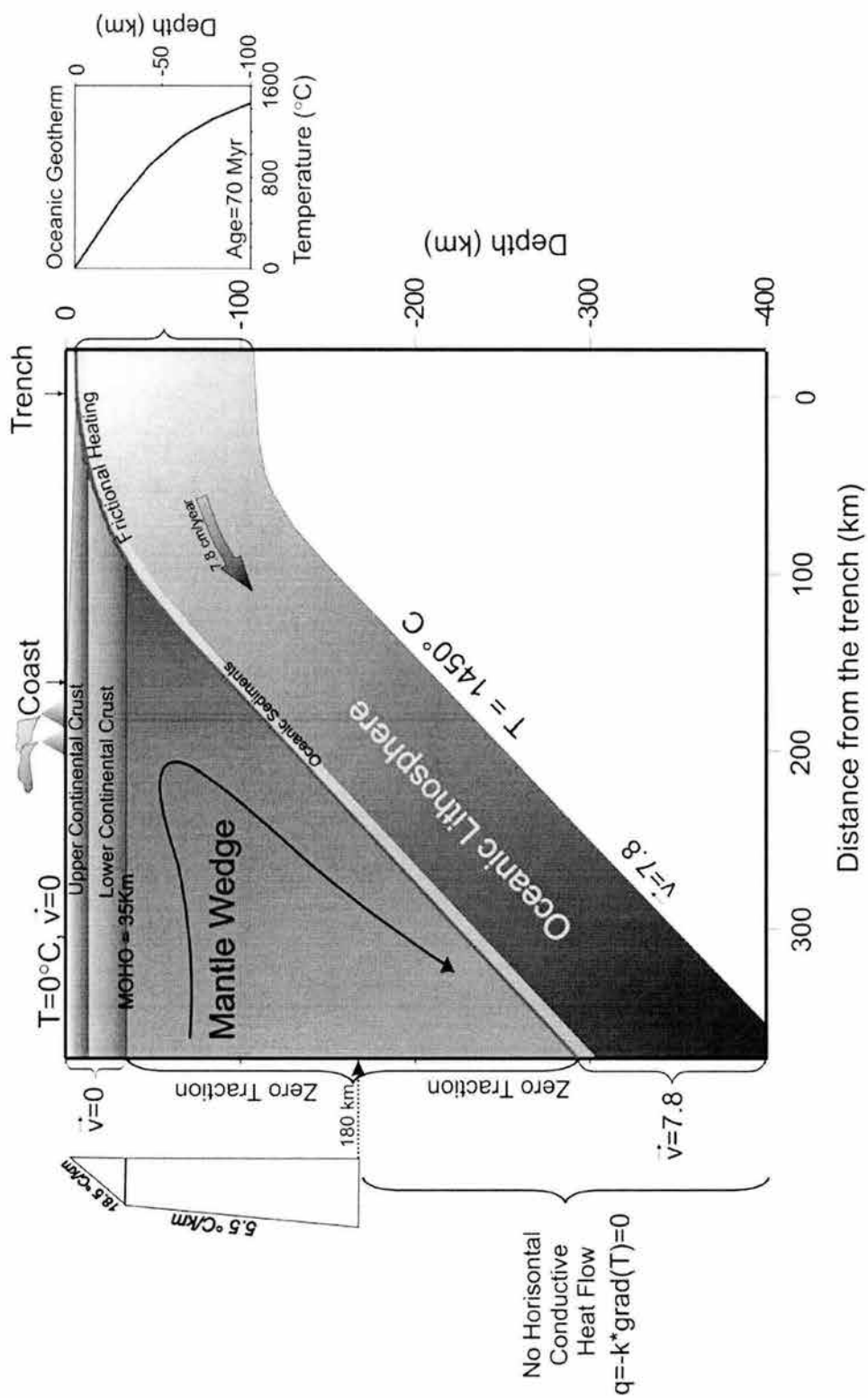
Figure 3
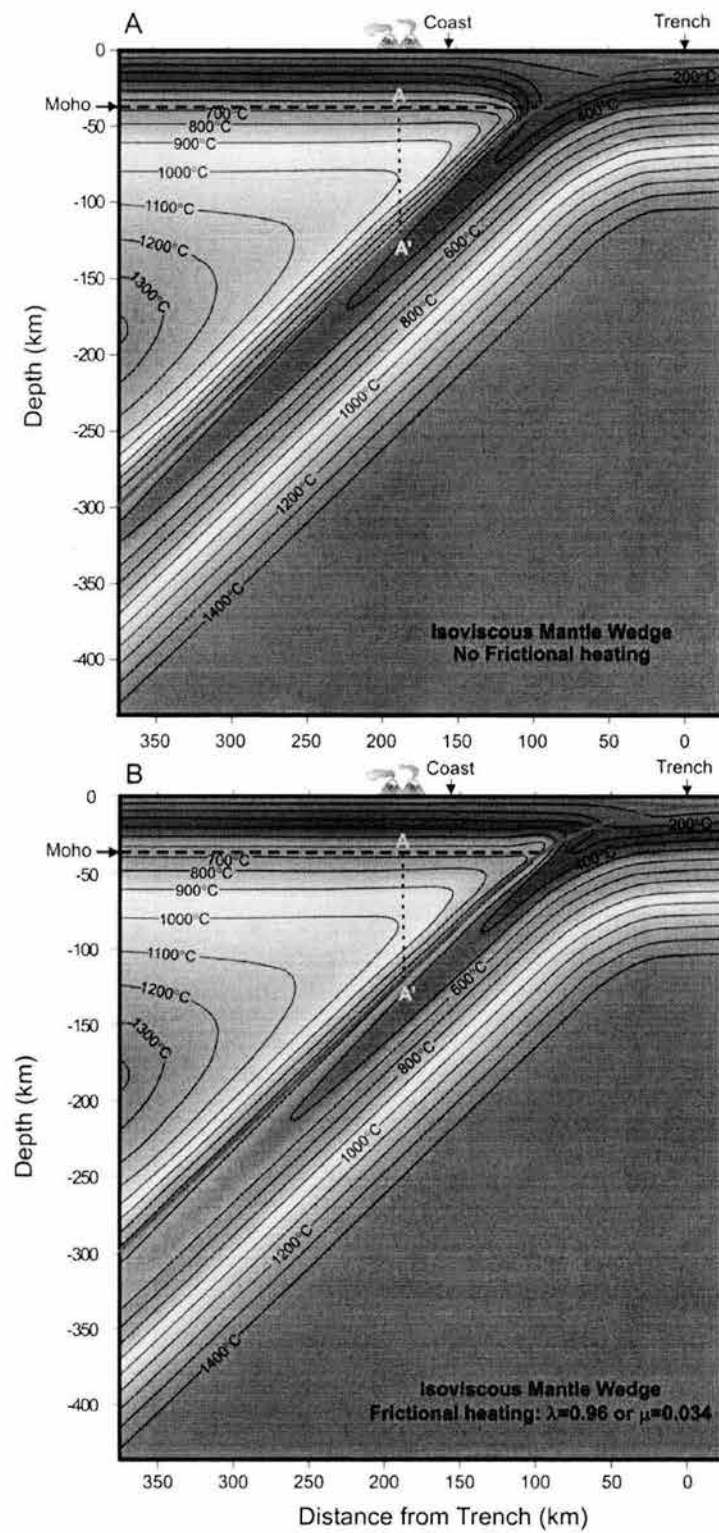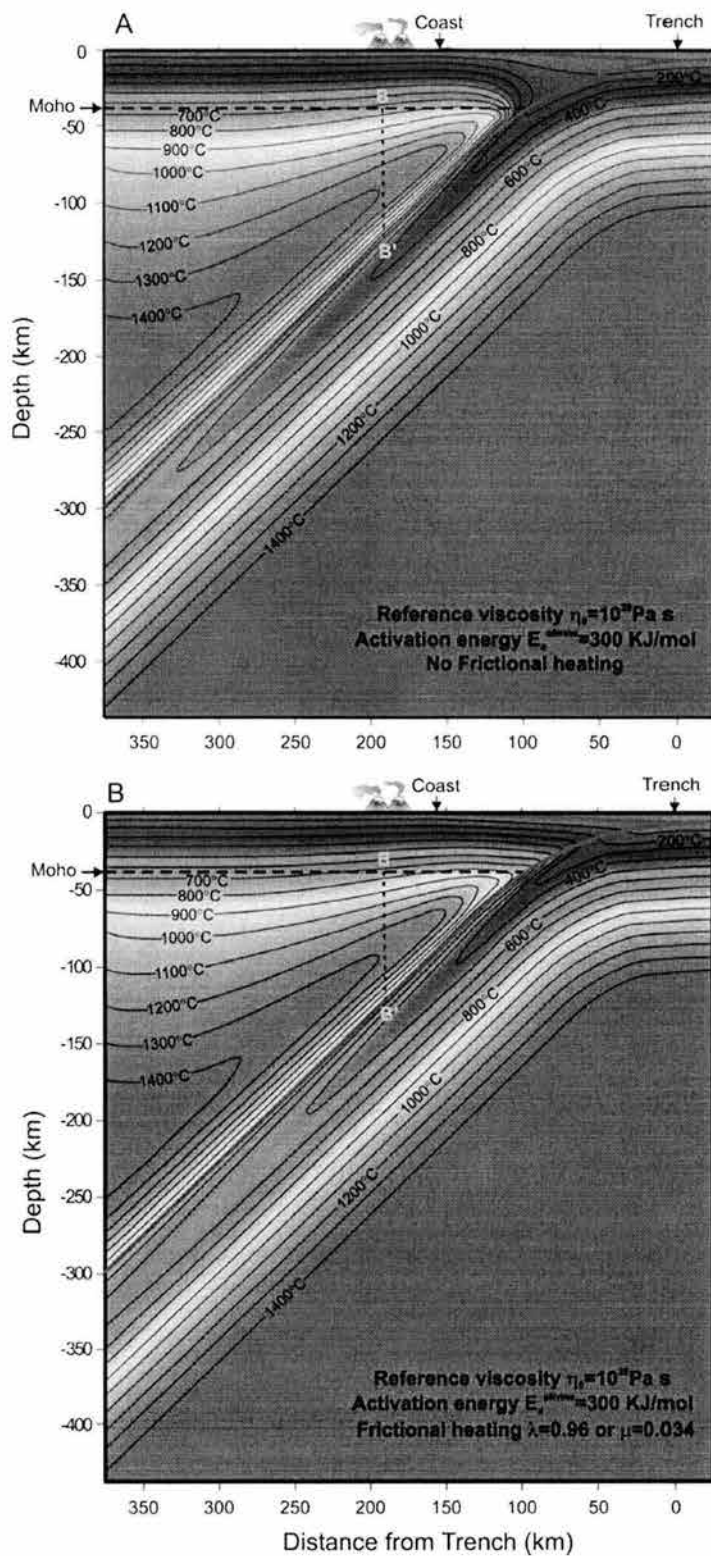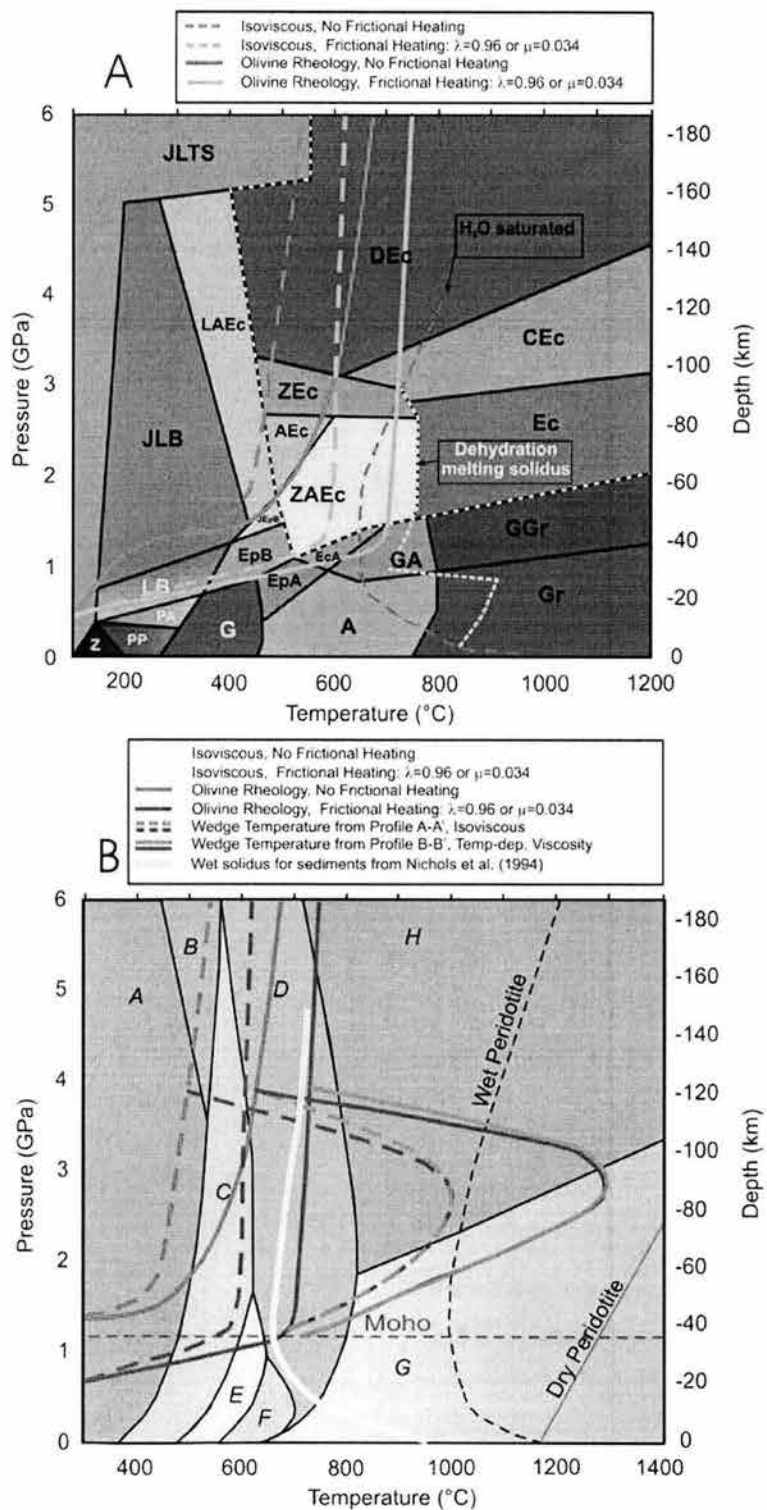
Figure 4
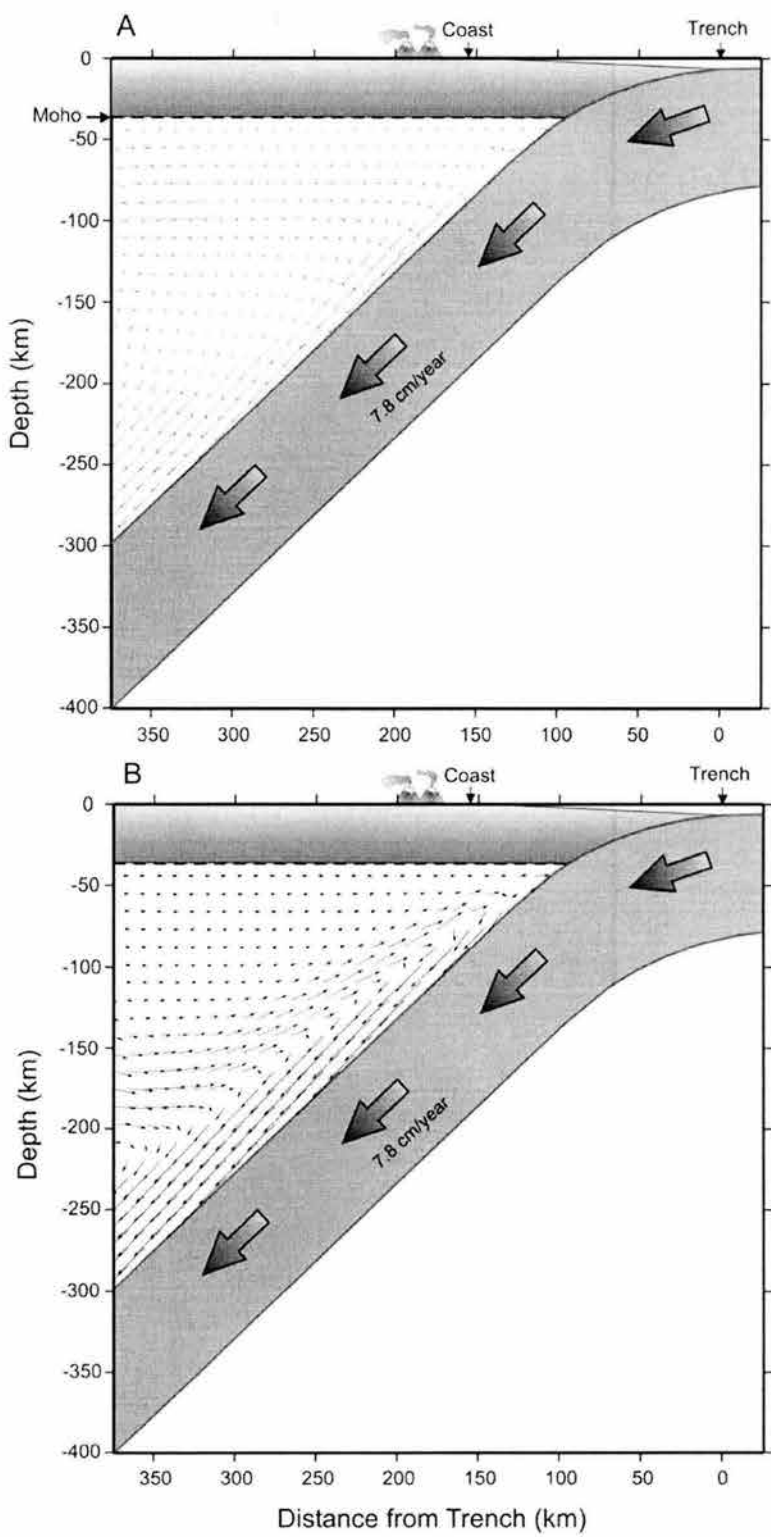
Figure 5
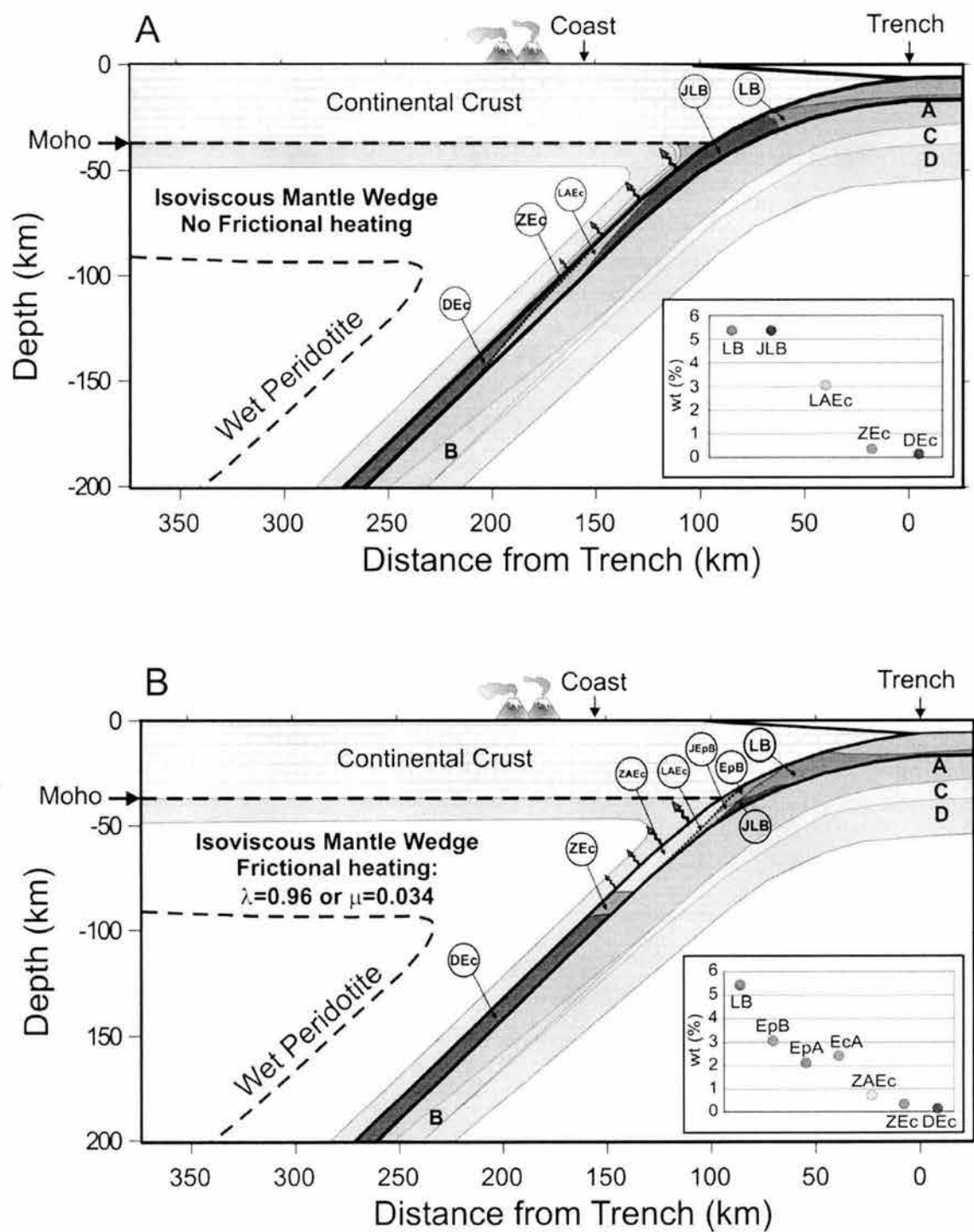
Figure 6
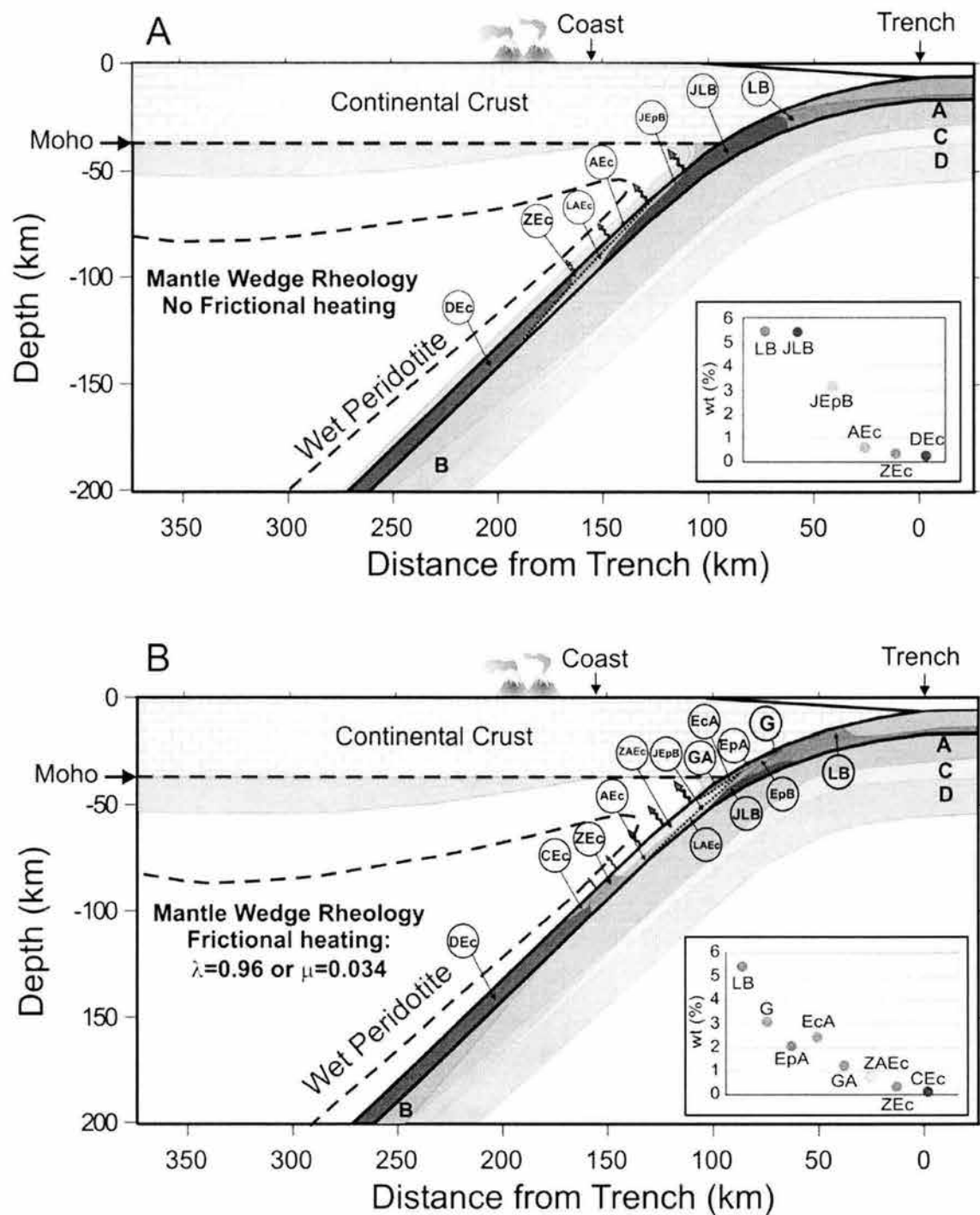
Figure 7
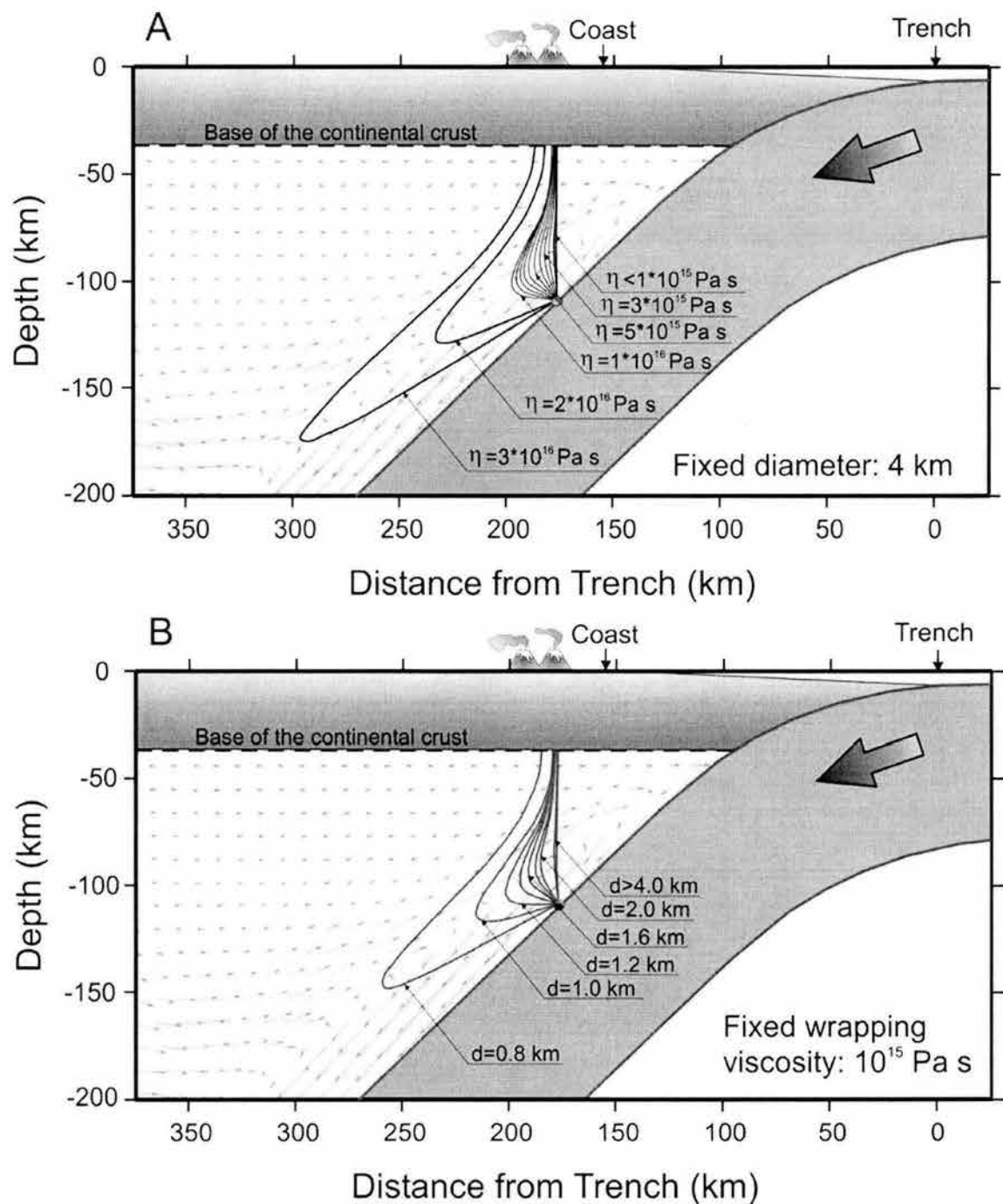
Figure 8
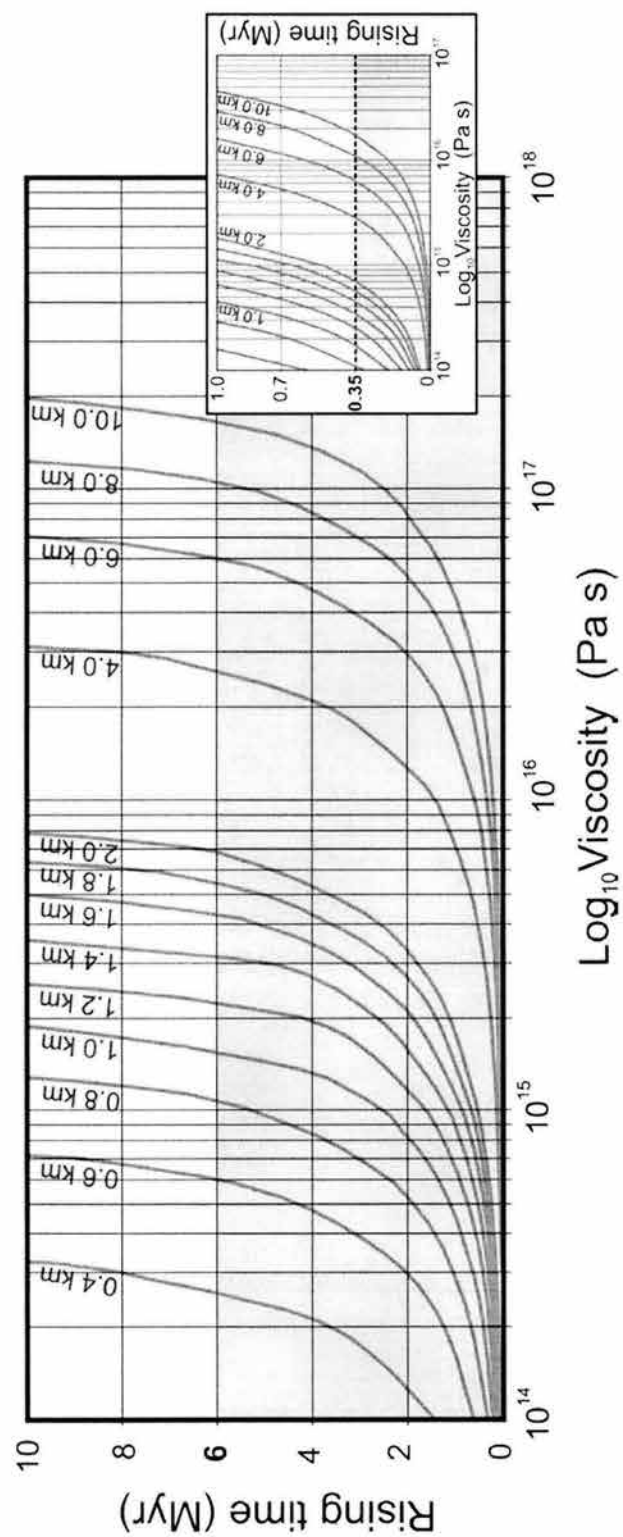
**Figure 9**
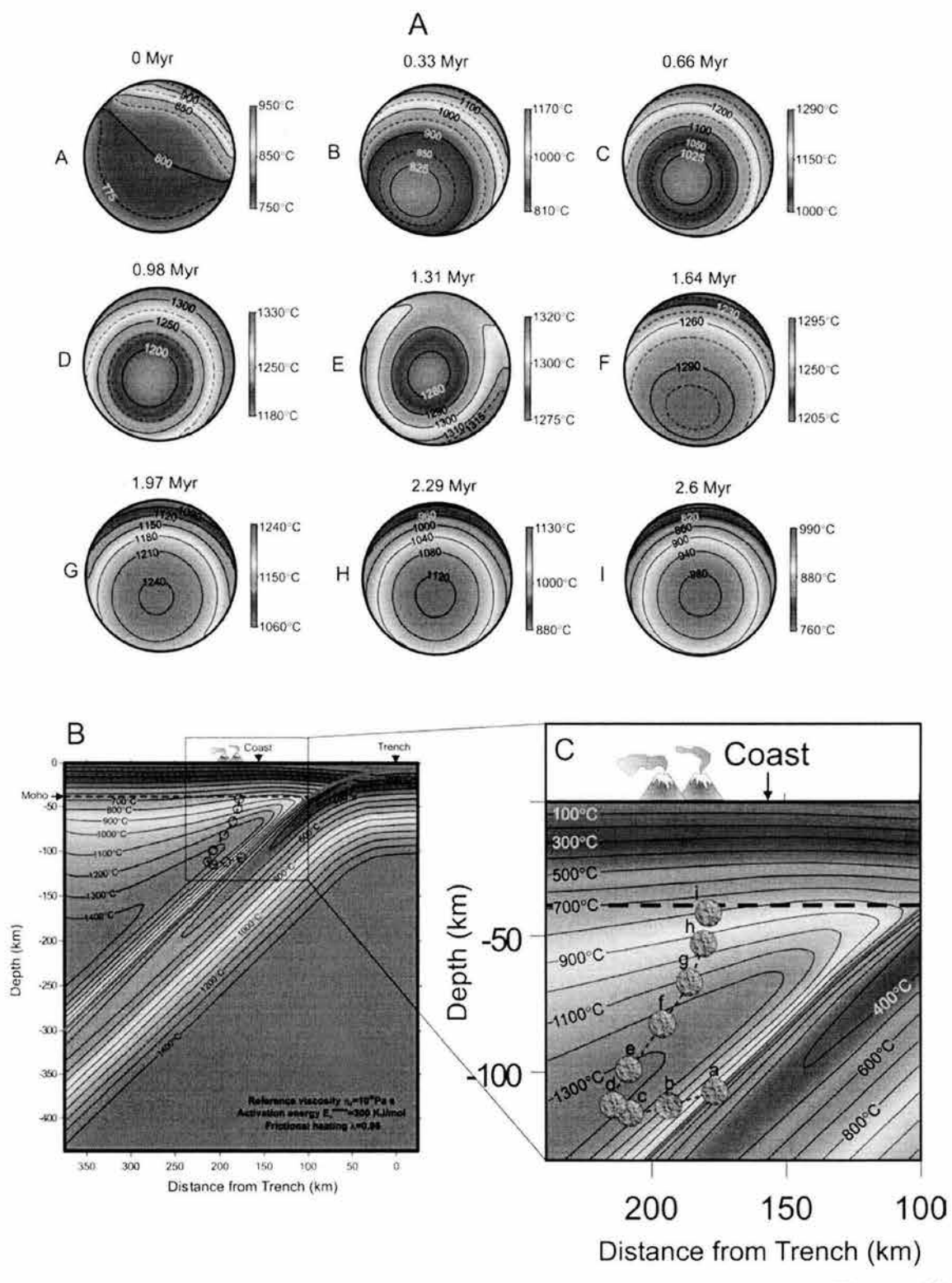
**Figure 10**
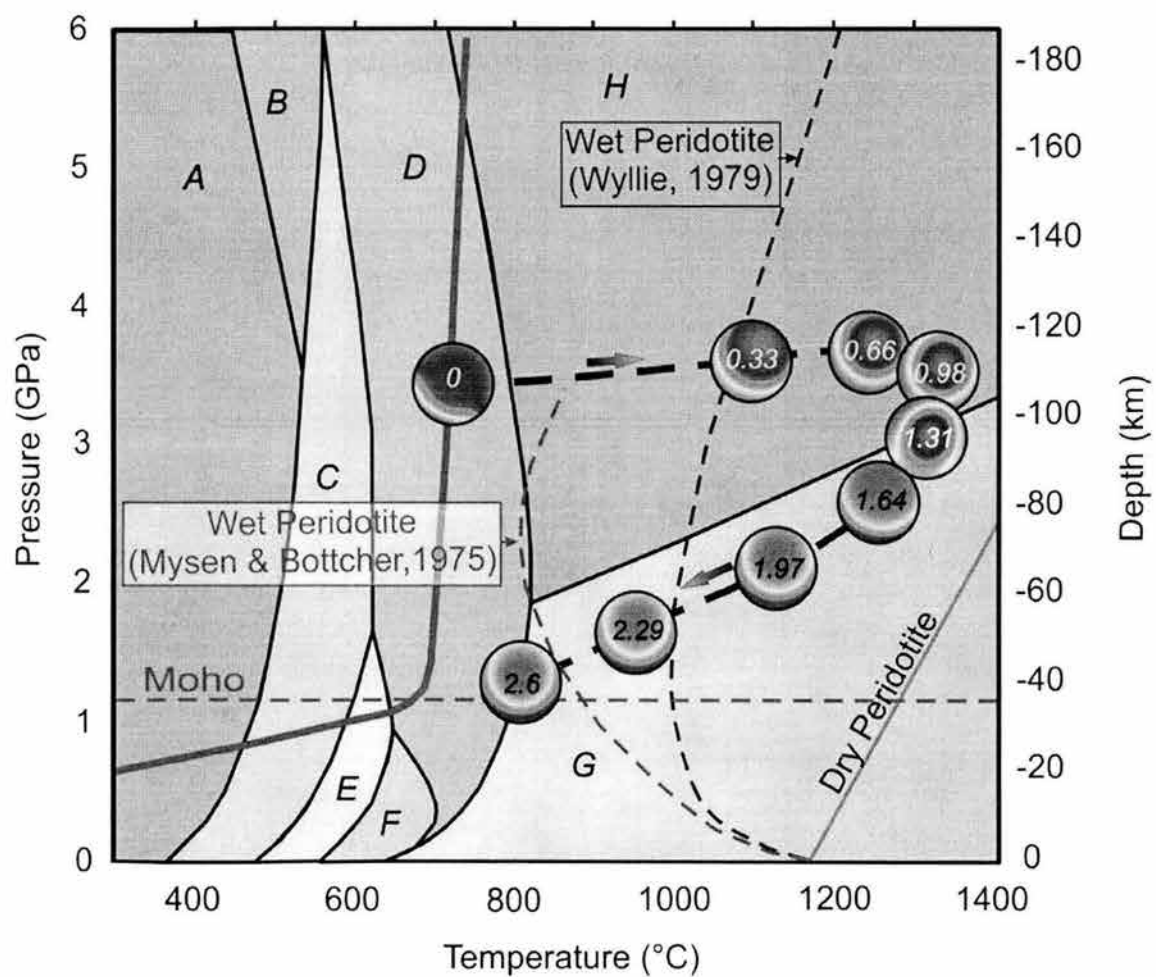
Figure 11
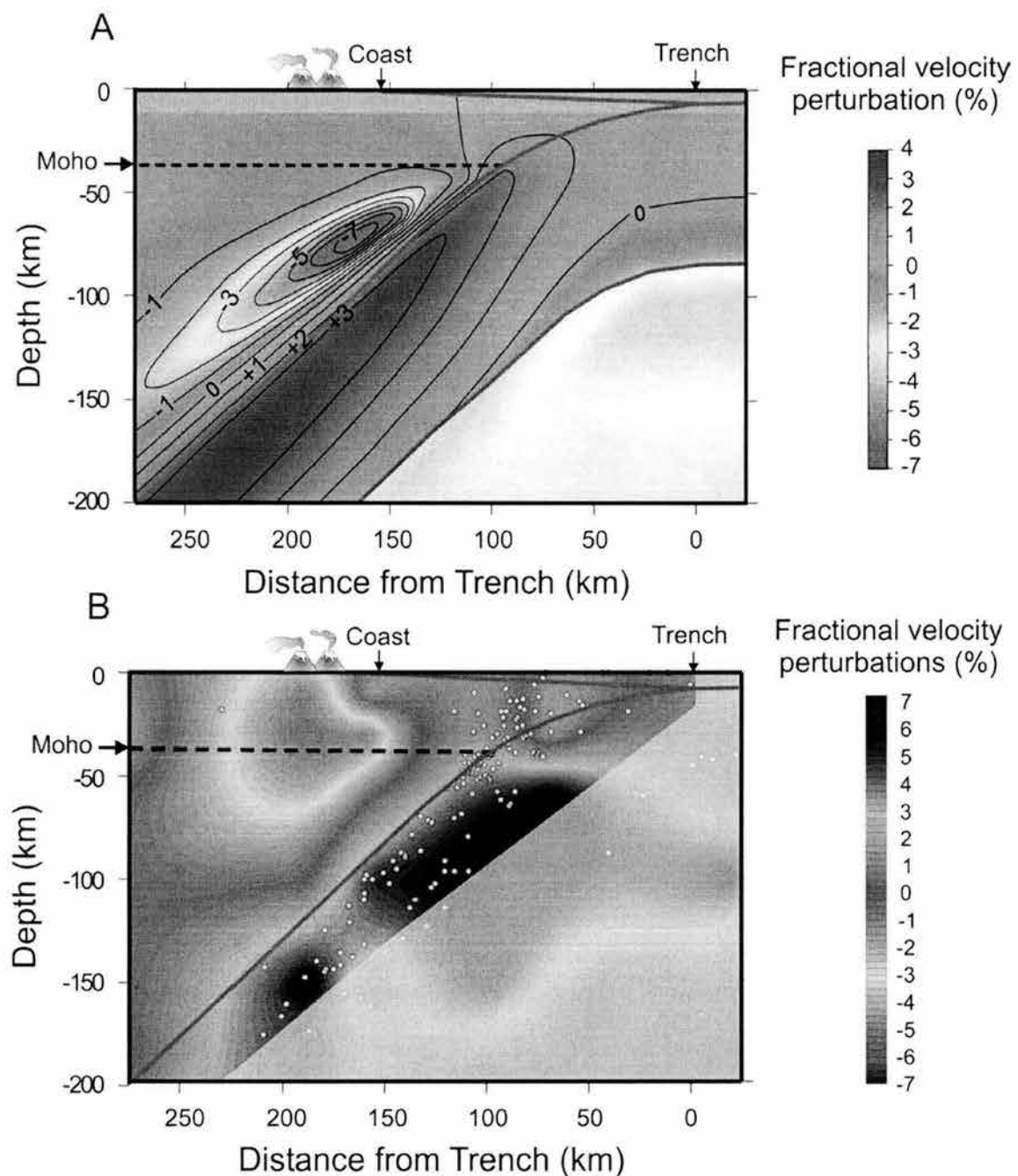
Figure 12

Figure 13

Figure 14

V. LA SÍSMICIDAD INTRAPLACA Y LOS ESFUERZOS TÉRMICOS EN LA PLACA DE COCOS DEBAJO DE LA PARTE CENTRAL DE MÉXICO

In review at Tectonophysics

INTRASLAB SEISMICITY AND THERMAL STRESS IN THE SUBDUCTED COCOS PLATE BENEATH CENTRAL MÉXICO

V.C. Manea[1], M. Manea[1],V. Kostoglodov[1], S.K. Singh[1], G. Sewell[2]

[1] Instituto de Geofisica, Universidad Nacional Autónoma de México (UNAM), México

[2] University of Texas, El Paso

ABSTRACT

With a maximum depth extent of ~ 80 km, an important particularity of the intraslab earthquakes beneath Guerrero, is their exclusively normal fault mechanism. Based on the recently developed thermal models for Guerrero subduction zone, the thermal stress due to non-uniform temperature distribution in the subducting slab is calculated using a finite element method. The calculation results revealed that the first shallow part of the subducting slab is characterized by low deviatoric compressional thermal stresses in its central part (~ 0.25 kbars). Following this part is a section where the stress field changes to an extensional behavior for the core of the slab with maximum values of ~ 0.4 kbars for the flat region and ~ 0.75 kbars deeper, where the slab bends into the asthenosphere. An important characteristic for the central Mexican subduction zone is its shallow subhorizontal plate contact; significant thermal compressional stresses (~ 0.65 kbars) arising in the upper and lower part of the slab are not consistent with the normal fault intraplate earthquake focal mechanism. Since the Cocos plate dips

into the asthenosphere at an angle of ~ 20°, pressure forces due to the induced flow in the mantle wedge are partially balanced by the gravitational body forces. A net clockwise torque might exist at the hinge point and its value is set in such a way that the compressional stresses for the flat part of the plate vanish. For the lower part of the slab, ductile behavior is assumed, the compressional stresses decreasing exponentially with depth. According to the thermal models for Guerrero, the temperature range of 700°C - 800°C is in good agreement with the maximum depth extent of the intraplate earthquakes and with the maximum extent of the tensional stresses in the subhorisontal part of the slab.

Keywords: Thermal stress, Bending stress, Mexican subduction zone, flat subduction.

INTRODUCTION

It has been accepted for some time that the cold subducted oceanic lithosphere, entering into the hotter mantle, produces significant thermal stresses that might generate intraslab earthquakes. Thermal stress distribution has been proposed as possible explanations for a double fault plane in various subduction zones as Japan and Kamchatka *(Hamaguchi et al., 1983, Gorbatov et al., 1997)*.

The thermal stress distribution of *Hamaguchi et al. (1983)* reveals very high compressional stresses up to 10 kbars for the top and bottom of the slab, and tensional stresses up to 7.5 kbars for the core of the slab. These high values are with ~ 2 order of magnitude greater than the stress drop during intraslab earthquakes (~ 0.1 kbars). These excessive values of the thermal stresses are related with temperature contrast as high as 1,000°C in the subducting slab. The bottom of the slab is likely to exhibit a ductile behavior due to high temperature, and therefore the thermal stresses induced in this region should vanish. The oversimplified mantle wedge thermal structure of *Hamaguchi et al. (1983)* is represented by a constant thermal gradient of 10°C/km up to 100 km depth and 5°C/km up to 150 km depth.

The thermo-mechanical models of the mantle wedge with temperature and/or stress dependent rheology *(Furukawa, 1993; Conder et al., 2002; Van Keken et al., 2002; van Hunen et al., 2002; Kelemen et al., 2003, Manea et al., 2004b)*, show a more complicated temperature distribution, where the temperature contrast inside the descending slab being strongly controlled by the thermal structure of the mantle wedge. Using the recently developed 2D thermal models, with strong temperature dependence viscosity in the mantle wedge, for the Mexican subduction zone *(Manea et al., 2004b)*, thermal stresses induced in the subducted slab due to non-uniform temperature distribution, are inferred using a finite element technique. Bending stresses due to concave/convex shape of the subducting slab are very difficult to determine *(Goto et al., 1985)* because they are very sensitive to the curvature of the plate that have large uncertainties in Mexico.

Slab pull of the denser subducting slab and the associated down flexure of the slab produce important deviatoric tension of up to several 100 MPa. Also, important stress concentrations and pressure variations (up to some 100 MPa), due to the shape of the subducting slab along the thrust fault, are likely to appear in this region *(Manea et al., 2004a)*. The state of stress in the slab depends also on whether the thrust fault is locked or unlocked, producing variations of the slab interior stress. Although the ridge push might be an order of magnitude smaller than the trench pull *(Turcotte and Schubert, 2002)*, the resistive forces encountered by the descending oceanic lithosphere into the mantle may compensate this difference.

The transmitted ridge push, slab pull and down bending stresses in the shallow part of the subducted slab beneath the coast, are not incorporated in the modeling here. The olivine-spinel phase change inside the slab (~ 400 km depth), might give rise to important tensional and compressional stresses up to 1 GPa *(Goto et al., 1985)*. The maximum depth extent of the present models (*Fig. 2*) is 200 km, therefore the effect of olivine-spinel phase change on the stress distribution of the subducting slab is not included here.

An important characteristic of the central Mexican subduction zone is its wide shallow subhorizontal plate interface (~ 150 km) in the central part beneath the Guerrero state and the sharp bending beneath the coast *(Kostoglodov et al., 1996)*. Another interesting distinctive feature for all the intraslab earthquakes in central Mexico is the exclusively normal fault mechanism, they usually occurring for distances starting ~ 85 km from the trench (*Fig. 1*).

Since the Cocos plate dips into the asthenosphere at an angle of ~ 20° due to basalt to eclogite phase transformation *(Manea et al., 2004a)*, pressure forces (viscosity dependent) due to the induced flow in the mantle are partially balanced by the gravitational body forces (density contrast dependent) *(Turcotte and Schubert, 2002)*.

This study aims to study the existence of exclusively normal fault intraslab earthquakes in Mexico using the superposition of thermal stress and bending stresses for the flat part of the subducted Cocos slab beneath Central Mexico.

MODELING PROCEDURE

Thermal Stresses

Using the temperature distribution of *Manea et al., 2004b (Fig. 2)*, we computed stresses in the subducting slab induced by thermal expansion. A system of 2D equations for thin plates are solved for the Guerrero cross section *(Fig. 1)* using the finite element solver PDE2D (*http://pde2d.com/*). The relevant equations in explicit form are the two coupled linear steady state PDEs:

$$
\begin{cases}
\dfrac{\partial S_{11}}{\partial x} + \dfrac{\partial S_{12}}{\partial y} = 0, \\[2mm]
\dfrac{\partial S_{12}}{\partial x} + \dfrac{\partial S_{22}}{\partial y} = 0,
\end{cases}
\text{where:}
\begin{cases}
S_{11} = E \cdot \dfrac{(e_{11} + v \cdot e_{22})}{(1-v^2)}; \\[2mm]
S_{22} = E \cdot \dfrac{(v \cdot e_{11} + e_{22})}{(1-v^2)} \\[2mm]
S_{12} = \dfrac{0.5 \cdot E \cdot e_{12}}{(1+v)},
\end{cases}
\text{and:}
\begin{cases}
e_{11} = \dfrac{\partial u}{\partial x} - \alpha \cdot T(x,y), \\[2mm]
e_{22} = \dfrac{\partial v}{\partial y} - \alpha \cdot T(x,y), \\[2mm]
e_{12} = \dfrac{\partial u}{\partial y} + \dfrac{\partial v}{\partial x},
\end{cases}
\quad (1)
$$

where:

(u,v)	-displacement vector,
$T(x,y)$	-2D temperature distribution,
$E = 1.7*10^{12}$ dyne/cm^2	-elastic modulus,
$v = 0.27$	-Poisson ratio,
$\alpha = 10^{-5}$	-coefficient of thermal expansion.

The finite element grid extends from 20 km seaward of the trench up to 600 km landward. The lower limit of the model is considered the base of the oceanic lithosphere and corresponds to the 1,150°C isotherm *(Fig. 2)*. The upper limit of the model is represented by the slab surface. The subducting plate presents two sharp bending points beneath the coast *(Kostoglodov et al., 1996)*, then follows a subhorisontal segment and finally the slab submerges into the asthenosphere at a

dip angle of ~ 20° (*Fig. 2*). The elastic parameters are considered constant in the numerical models. We use free boundary conditions (BC) at the tip of the subducting slab and also for the circumference of the model. A fixed BC at the tip of the slab increases the thermal stresses by ~ 50%, and following the conclusions of *Goto et al., 1983*, free displacement at the tip gives a better explanation for the seismicity. The grid consists of 5,000 triangle shaped elements (*Fig. 3*). The x-component (along the subducting slab) of the deviatoric stress is given by:

$$\sigma_{dx} = \frac{(2 \cdot \sigma'_x - \sigma'_y)}{3},$$

(2)

where σ'_x and σ'_y are along the plate and normal to the plate thermal stresses respectively. Because the thickness of the plate is much smaller that its length, the σ'_z is considered negligibly.

Bending Stresses

Since the Cocos plate dips into the asthenosphere at an angle of ~ 20°, suction forces due to the induced flow in the mantle are partially balanced by the gravitational body forces.

The pressure forces acting on the descending Cocos plate is calculated using the 2D viscous corner flow model of *Turcotte and Schubert, 2002*. For an oceanic plate that dips at 20° with a velocity of 5.5 cm/year, the following formula for the pressure at the top of the plate is obtained:

$$P = \frac{-8 \cdot \mu}{r} \cdot 10^{-8}$$

(3)

where:

P -flow pressure on the top of the descending slab (Pa)

μ -mantle wedge viscosity (Pa s)

r -distance along the dipping slab surface with the origin in the hinge point (m)

    The negative value of P gives the effect of suction force, which tends to lift up the slab. The lifting torque (M_P) acting on the slab is:

$$M_P = \int_0^{r_{max}} P \cdot r \cdot dr = \int_0^{r_{max}} \frac{-8 \cdot \mu}{r} \cdot 10^{-8} \cdot r \cdot dr = -8 \cdot \mu \cdot r_{max} \cdot 10^{-8} (N \cdot m) \qquad (4)$$

where:

r_{max} - the maximum plate length that contributes in transmitting the torque to the hinge point.

    The gravitational body force is calculated by:

$$Q = g \cdot h \cdot \Delta\rho \cdot \cos(20°) \ (N/m) \qquad (5)$$

where:

Q -gravitational body force (N/m)

g -gravitational acceleration (10 m/s^2)

h -elastic plate thickness (m)

$\Delta\rho$ -average density contrast over the elastic section of the slab:

$$\Delta\rho = \Delta\rho_{eclogite} \cdot \frac{h_{eclogite}}{h_{elastic\_slab}} + \Delta\rho_{peridotite} \cdot \frac{h_{peridotite}}{h_{elastic\_slab}} \qquad (6)$$

where:

$\Delta \rho_{eclogite} = \rho_{eclogite} - \rho_{peridotite} = 3,500 - 3,300 = 200 \text{ kg/m}^3$

$\Delta \rho_{peridotite} = \rho_{peridotite} - \rho_{peridotite} \, (1 - \alpha \, \Delta T) = 3,300 - 3,300 \, (1 - 10^{-5} \, 200°C) = 6.6 \text{ kg/m}^3$

$h_{eclogite}$ -eclogite layer thickness (m)

$h_{peridotite}$ -peridotite layer thickness (m)

$h_{elastic\_slab} = h_{eclogite} + h_{peridotite}$ (m)

The pulling down torque (M_Q) acting on the slab is:

$$M_Q = \int_0^{r_{max}} Q \cdot r \cdot dr = Q \cdot \frac{r_{max}^2}{2} \quad (N \cdot m) \tag{7}$$

The net torque (ΔM) at the hinge point is:

$$\Delta M = M_Q - M_P \tag{8}$$

$$\Delta \sigma = \frac{\Delta M}{I} \tag{9}$$

where:

$\Delta \sigma$ -the bending stress due to ΔM

$I = \dfrac{b \cdot h^3}{12}$ -the moment of inertia (m^4)

b -the plate unity width (1m)

Choosing a positive (clockwise) net torque at the hinge point, the thermal compressional stress at the top of the subhorisontal element of the slab (max. 0.65 kbars, see *Fig. 4-B*) might vanish.

Stress distribution in the subducting slab.

Thermal stress in subduction zones arises due to the non-uniform temperature distribution (*Fig. 2*). The results of the numerical calculations are offered in *Fig. 4*, where along plate (*Fig. 4-A*) and deviatory along plate stresses are presented (*Fig. 4-B*). The first part of the subducting plate (distances < 80 km from the trench) is characterized by compressional deviatory stresses of ~ 0.3 kbars in its central part, while tensional deviatoric stresses occur in the upper and lower part of the slab with a magnitude less than 0.3 kbars. For distances between 80 km and 115 km from the trench, the subducting plate presents a sharp bending, this being a transition region from a compressional slab core to a tensional one. Then there follows a subhorizontal sector where tensile thermal stresses are representative for the core of the slab (max ~ 0.4 kbars) and compressional stresses arise for the upper and lower parts of the slab (max. ~ 0.65 kbars close to the hinge point). Afterward, the slab bends into the asthenosphere, and the same pattern of the stresses is maintained, but with a greater magnitude of ~ 0.75 kbars due to the elevated temperature contrast (~ 400°C) in this region.

The areas of tensional and compressional stresses are located parallel with the dip of the plate. The maximum tensional stress (~ 0.75 kbars) occurs at a depth of ~ 100 km. The compressional stress in the upper part of the plate is greater than that for the lower part in about ~ 30%, these results being consistent with the conclusion of *Hamaguchi et al., 1983*. Introducing for the lower part of the slab a ductile behavior (*Turcotte and Schubert, 2002*), the bottom plate stresses reach a maximum of 0.25 kbars, and then decrease exponentially to zero (see *Fig. 5*).

The high compressional thermal stress in the upper part of the slab is not consistent with the exclusively normal fault intraslab earthquakes in central Mexico. In a recent paper of *Manea et al., 2004a*, the hinge point (270 km from the trench) is consistent with the transition of the basaltic oceanic crust to the eclogitic facies, the significant increase in density bending the slab into the asthenosphere. The cold slab dipping into the asthenosphere being denser than the surrounding

peridotite, contributes also to the gravitational torque through the elastic part of the sinking slab. With a total density contrast of $\Delta\rho$ = 60 kg/m^3, the elastic section of the plate involved in gravitational bending is delimited by the ductile behavior, therefore having a thickness of maximum 25 km (see *Fig. 6 - inset*). The net downward torque at the hinge point due to the balance between suction and gravitational forces (*Fig. 6*) might produce tensional stresses in the upper flat part of the slab, and its magnitude might compensate the thermal compression (max. ~ 0.65 kbars). In order to obtain tensile stresses at the top of the flat slab, gravitational torque must be greater than the suction torque. Along the subhorizontal part of the slab the suction force is constant and upward directed, therefore, it does not contribute to the slab bending in this flat sector. The suction torque depends on the mantle wedge viscosity and distance along dipping line, while the gravity torque is function of moment of inertia (slab elastic thickness) and distance along dipping line. Viscosities of 10^{18} Pa s up to 10^{19} Pa s are required for the mantle wedge for slab lengths up to 500 km in order to fit a tensional stress of 0.65 kbars at the top of the flat part of the slab (see *Fig. 7*).

Flat slab seismicity and stress pattern

The intraslab seismicity in Guerrero is characterized by shallow and intermediate depth intraslab normal fault earthquakes (*Fig. 1* and *Table 1*). Most of the events are confined in the subhorizontal part of the slab and a good correlation with the deviatoric tensile thermal stress is observed (*Fig. 5*). Two clusters of events, representing the background seismic activity with low magnitude, are presented also (small circles in *Fig. 2*), and appear to be related with the sharp bending-unbending of the plate in this region at ~ 80 km and ~ 110 km from the trench. The maximum depth extent of the intraslab seismicity is ~ 80 km in Mexico, being in agreement with the position of the 700°C isotherm, which might be considered as cutoff temperatures due to the transition from brittle to ductile behavior.

The subhorizontal segment of the slab is the place where the majority of the intraplate normal fault earthquakes occur. Thermal tensile (slab core) and compressional (top, bottom) stresses arise in this region, but only normal events are observed. Although thrust earthquakes have not been recorded, important deviatoric compressional thermal stresses with magnitude of ~ 0.65 kbars occur in the upper part of the slab. Introducing at hinge point a net downward torque (from the balance of suction and gravity body forces) that gives 0.65 kbars tensile stress at the top of the slab (*Fig. 8-A*), the top flat slab compression vanishes (*Fig. 8-C*). In this case, a maximum tensile stress of ~ 0.55 kbars is obtained for the core of flat slab. Between 700°C - 800°C isotherms the stress field in the slab twists from tension to compression (*Fig. 8-C*), and the lack of the compressional seismicity is well correlated with this cut off temperature range.

DISCUSSION AND CONCLUSIONS

An important individuality of the shallow and intermediate (depths of 35 - 80 km) intraslab Mexican earthquakes is their exclusively normal fault mechanism. They usually occur at a distance greater than ~ 85 km from the trench. The subhorizontal segment of the slab in Guerrero with a length of more than 150 km, comprises the greater part of the normal fault intraslab events. Although the state of stress in the subducting oceanic lithosphere is the superimposition of stress distributions with various origins, including slab pull, ridge push, tidal stresses, etc., the present study focuses on the thermal and bending stresses. Based on the new developed thermal models for Guerrero subduction zone *(Manea et al., 2004b)*, the thermal stress due to non-uniform temperature distribution in the subducting slab is calculated using a finite element technique.

The first shallow part of the subducting slab is characterized by low deviatoric compressional thermal stresses in its central part (~ 0.3 kbars) then the stress pattern is reversed: a tensional behavior for the nucleus of the slab and a compressional one for the upper and lower parts *(Fig. 4-B)*. The core of the subhorizontal part of the plate has a maximum value of thermal tension stress of ~ 0.4 kbars, while the bottom of the slab reveals a thermal compression of ~ 0.75 kbars. Although intraslab reverse earthquakes have not been recorded, important deviatoric compressional thermal stress with magnitude of ~ 0.65 kbars occurs in the upper part of the flat slab. Introducing at the hinge point a net downward torque that gives a tensile stress of 0.65 kbars at the top of the subhorizontal slab *(Fig. 8-A)*, a new stress field is obtained without compression in the upper flat segment *(Fig. 8-C)*. The lack of the compressional seimicity in the bottom part of the flat slab is consistent with the position of the 700°C - 800°C isotherms, where the stress filed toggle from tension to compression (see *Fig. 8-C-inset*). Also, the deficiency of the intraslab normal fault earthquakes in Guerrero for distances less than ~85 km from the trench is in good agreement with the onset of the tensional thermal stress pattern in the core of the subducting slab.

REFERENCES

Conder, J.A., Weins, D.A., and Morris, J., 2002. On the decompression melting structure at volcanic arcs and back-arc spreading centres. *Geophysical Research Letters, vol. 29, 17-1-17-4.*

Dean, B.W., and Drake, C.L., 1978. Focal mechanism solutions and tectonics of the Middle America arc. *Journal of Geology, vol. 86, 111-128.*

Engdahl, E. R. and Villaseñor, A., 2002. Global seismicity: 1900-1999, in Lee, W. H. K. et al. (editors), International handbook of earthquake engineering and seismology, *International Geophysics series, vol. 81A, 665- 690,*

Furukawa, F., 1993. Magmatic processes under arcs and formation of the volcanic front. *Journal of Geophysical Research, vol. 98, 8309-8319.*

González-Ruiz, J.R., 1986. Earthquake source mechanics and tectonophysics of the middle America subduction zone in Mexico, *Ph.D. Thesis, Univ. of Calif.,* Santa Cruz.

Gonzalez-Ruiz, J.R. and McNally, K.C., 1988. Stress accumulation and release since 1882 in Ometepec, Guerrero, Mexico: implications for failure mechanisms and risk assessments of a seismic gap, *Journal of Geophysical Research, vol. 93, 6297-6317.*

Gorbatov A., Kostoglodov, V., Suárez, G. and Gordeev, E., 1997. Seismicity and structure of the Kamchatka subduction zone, *Journal of Geophysical Research, vol. 102, 17,883-17,898.*

Goto, K., Hamaguchi, H., and Suzuki, Z., 1983. Distribution of stress in descending plate in special reference to intermediate and deep focus earthquakes, I. Characteristics of thermal stress distribution (the science reports of the Tohoku University, Ser. 5), *Tohoku Geophysics Journal, 29, 81-105.*

Goto, K., Hamaguchi, H., and Suzuchi, Z., 1985. Earthquake generating stresses in the descending slab. In; Kobayashi, K. and Sacks, I.S. (eds.), Structures and Processes in the Subduction Zones. *Tectonophysics, 112, 111-128.*

Hamaguchi, H., Goto, K., and Suzuki, Z., 1983. Double-planed structure of intermediate-depth seismic zone and thermal stress in the descending plate, *Journal of Physics of the Earth, 331, 329-347.*

Iglesias, A., Singh, S.K., Pacheco, J.F., and Ordaz, M., 2002. A Source and Wave Propagation Study of the Copalillo, Mexico Earthquake of July 21, 2000 (Mw=5.9): Implications for Seismic Hazard in Mexico City from Inslab Earthquakes. *Bulletin of Seismological Society of America, v.92, no. 3, pp. 1060-1071.*

Jiménez, Z. and Ponce, L., 1978. Focal mechanism of six large earthquakes in northern Oaxaca, Mexico, of the period 1928-1973. *Geofísica Internacional, vol. 17, 379-386.*

Kelemen, P.B., Rilling, J.L., Parmentier, E.M., Mehl, L., and Hacker, B.R., 2003. Thermal Structure due to Solid-State Flow in the Mantle Wedge Beneath Arcs, in Inside the Subduction Factory, *Geophysical Monograph 138*, edited by J. Eiler, AGU, Washington DC, pp. 293-311.

Kostoglodov, V., Bandy, W., Domínguez, J., and Mena, M., 1996. Gravity and seismicity over the Guerrero seismic gap, Mexico. *Geophysical Research Letters, 23, 3385-3388.*

Lay. T., Astiz, L., Kanamori, H., and Christensen, D.H., 1989. Temporal variation of large intraplate earthquakes in coupled subduction zones, *Physics of the Earth and Planetary Interiors, 54, 258-312.*

Lefevre, L.V. and McNally, K.C., 1985. Stress distribution and subduction of aseismic ridges in the Middle America subduction zone. *Journal of Geophysical Research, 90: 4495.*

Manea, V.C., Manea, M., Kostoglodov, Currie, C.A., and Sewell, G., 2004a. Thermal Structure, Coupling and Metamorphism in the Mexican Subduction Zone beneath Guerrero. *Geophysical Journal International, 158, 775–784 doi: 10.1111/j.1365 - 246X.2004.02325.x.*

Manea, V.C., Manea, M., Kostoglodov, V., Sewell, G., 2004b. (in press) Thermo-mechanical model of the mantle wedge in Central Mexican subduction

zone and a blob tracing approach for the magma transport. *Physics of the Earth and Planetary Interiors.*

Pardo, M., and Suárez, G., 1995. Shape of the subducted Rivera and Cocos plates in southern Mexico: seismic and tectonic implications. *Journal of Geophysical Research, 100, 12357-12373.*

Singh, S.K., Suárez, G., and Domínguez, T., 1985. The great Oaxaca earthquake of 15 January 1931: lithosphere normal faulting in the subducted Cocos plate. *Nature, 317, 56-58.*

Singh, S.K., and Pardo, M., 1993. Geometry of the Benioff zone and the state of stress in the overriding plate in central México. *Geophysical Research Letters, 20, 1483-1486.*

Turcotte, D.L., and Schubert, G., 2002. Geodynamics, 2nd edition. *Cambridge University Press, New York.*

van Hunen, J., van den Berg, A., and Vlaar, N., 2002. On the role of subducting oceanic plateaus in the development of shallow flat subduction. *Tectonophysics, 352, 317-333.*

van Keken, P.E., Kiefer, B., and Peacock, S.M., 2002. High resolution models of subduction zones: Implications for mineral dehydration reactions and the transport of water into deep mantle. *G-cubed, 3, 10, 20.*

Table 1.

Moderate and large normal fault intraslab events in the subducted Cocos plate for the region of interest (*Fig. 1*) (15 - 20^{0}N and 96 - 104^{0}W). If magnitude type is not given then $M = M_w$.

No. crt.	Date	Latitude (°N)	Longitude (°W)	Depth (km)	Magnitude	Azimuth	Dip	Rake	Reference
1	1928.02.10	18.26	97.99	84	6.5 M_{GR}	343	70	-117	Jiménez and Ponce (1978)
2	1931.01.15	16.34	96.87	40	7.8	270	56	-90	Singh et al. (1985)
3	1945.10.11	18.32	97.65	95	6.5 M_{GR}	343	65	-61	Jiménez and Ponce (1978)
4	1959.05.24	17.72	97.15	80	6.8	315	61	-102	Jiménez and Ponce (1978)
5	1964.07.06	18.31	100.5	55	7.3	292	38	-63	González-Ruiz et al. (1986)
6	1966.02.27	18.82	102.56	89	5.8	165	35	-107	Lefebevre & McNally (1982)
7	1966.09.25	18.12	100.96	59	5.8	290	50	-84	Pardo and Suárez (1995)
8	1967.04.13	18.12	100.4	65	5.5	314	56	-92	Pardo and Suárez (1995)
9	1967.04.14	17.2	100.43	35	5	160	48	-106	Singh & Pardo (1993)
10	1968.08.14	18.28	103.05	44	5.4	319	84	-40	Lay et al. (1989), Dean & Drake (1978), Engdahl and Villaseñor(2002)
11	1971.03.03	17.61	99.37	73	5.1	298	56	-90	Dean & Drake (1978), Lay et al. (1989), Engdahl and Villaseñor(2002)
12	1971.07.16	16.24	96.34	49	5.3	290	45	-60	Cruz & Suárez (Personal comunication)
13	1971.10.27	18.07	100.52	59	5	326	60	-90	Mota (1973)
14	1973.07.03	18.85	100.03	95	5.9	281	80	-98	Pardo and Suárez (1995)
15	1973.08.28	18	96.55	82	7.3 mb	326	50	-75	González-Ruiz et al. (1986), González-Ruiz & McNally (1988)
16	1974.01.26	18.97	103.84	51	5.2 mb	289	59	-30	Pardo and Suárez (1995)
17	1974.07.18	17.1	98.4	48	5.6 mb	243	63	174	Lefevre & McNally (1985)
18	1976.09.05	18.38	101.36	63	5.4 mb	297	64	-102	Pardo and Suárez (1995)
19	1976.09.19	17.98	100.65	62	5.5	295	54	-66	Pardo and Suárez (1995)
20	1978.07.05	18.74	100.17	59	5.5	311	47	-92	Pardo and Suárez (1995)
21	1978.09.29	18.3	102.46	63	5.5	281	33	-80	Pardo and Suárez (1995)
22	1983.12.08	18.36	102.73	54	5.6	262	40	-90	Pardo and Suárez (1995)
23	1984.06.04	17.62	98.03	62	5.3	289	45	-72	CMT Centroid Moment Tensor (Harvard catalog)
24	1985.07.04	17.55	97.08	68	5.1	318	41	-98	CMT (Harvard catalog)

25	1987.07.15	17.334	97.31	66	5.8	338	42	-65	Cruz & Suárez (Personal comunication)
26	1987.07.26	18.56	101.4	74	5.1	280	68	-93	CMT (Harvard catalog)
27	1989.08.12	18.07	101.13	47	5.3	270	71	-90	Pardo and Suárez (1995)
28	1993.08.05	17.62	97.94	54	5.2	294	39	-135	CMT (Harvard catalog)
29	1994.02.23	18.22	96.82	75	5.8	278	36	-83	CMT (Harvard catalog)
30	1994.05.23	18.19	100.2	70	6.2	273	39	-76	CMT (Harvard catalog)
31	1994.08.28	17.26	96.1	40	5.5	302	72	-89	CMT (Harvard catalog)
32	1995.12.20	18.55	100.8	78	5.3	274	61	-77	CMT (Harvard catalog)
33	1996.01.25	18.42	101.84	59	5.5	276	34	-72	CMT (Harvard catalog)
34	1996.04.01	16.42	96.06	57	5.2	306	64	-111	CMT (Harvard catalog)
35	1997.05.22	18.76	101.73	56	6.5	269	63	-96	CMT (Harvard catalog)
36	1999.06.15	18.44	97.38	61	6.9	309	40	-83	CMT (Harvard catalog)
37	1999.06.21	18.09	101.62	48	6.2	296	32	-88	CMT (Harvard catalog)
38	1999.08.15	19.16	103.23	63	5.2	295	74	-104	CMT (Harvard catalog)
39	2000.21.06	18.113	98.974	50	5.8	305	32	-80	Iglesias et al. (2002)

FIGURE CAPTIONS

Figure 1.

The position of the modeled cross-section in Guerrero. Focal mechanisms represent the intraslab normal fault events with magnitude greater than 5.0 (M_w). The thick grey line represents the 2D model cross-section. MAT - Middle American Trench.

Figure 2.

Thermal model for Guerrero with strongly temperature dependence of the viscosity from *Manea et al., 2004b*. The focal mechanisms represent the intraplate seismicity with magnitude greater than 5.0 (M_w) from *Fig. 1*.

Figure 3.

A mesh with more than 5,000 triangles is used in thermal stresses computation.

Figure 4.

(A). Thermal stresses along the subducting slab.

(B). Deviatoric thermal stresses along the subducting slab.

Figure 5.

Deviatoric thermal stresses with ductile behavior included (*Turcotte and Schubert, 2002*) at the bottom of the slab. The inset represents a cross-section through the slab at 200 km from the trench.

Figure 6.

Induced flow pressure and gravitational body force acting on the descending slab.

Figure 7.

Mantle wedge viscosities inferred from the net torque ($\Delta\sigma$ = 0.65 kbars) at the hinge point.

Figure 8.

Superimposition (C) of the bending (A) and thermal stresses (B) for the flat part of the subducting slab. The insets represent corss-sections through the slab at 200 km from the trench.
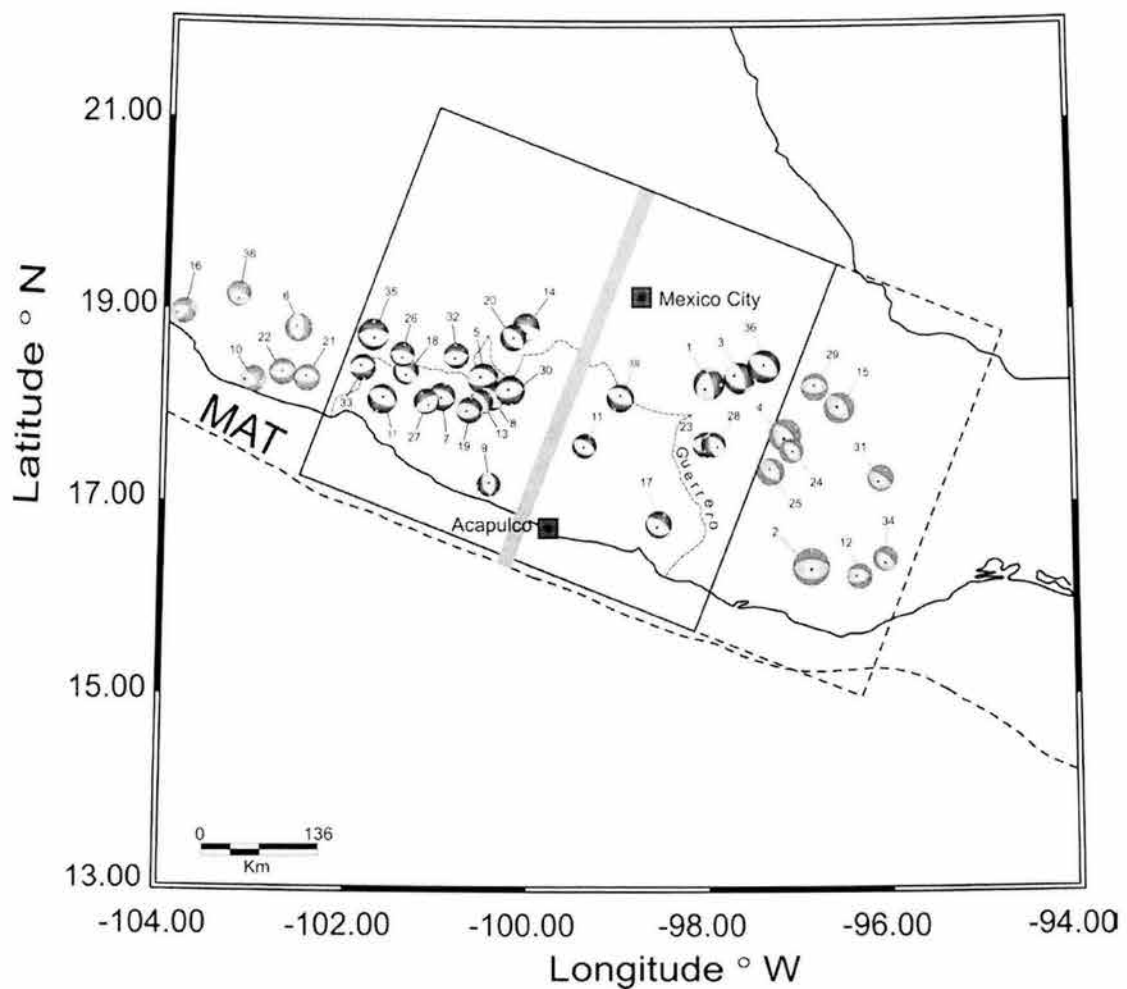
Figure 1
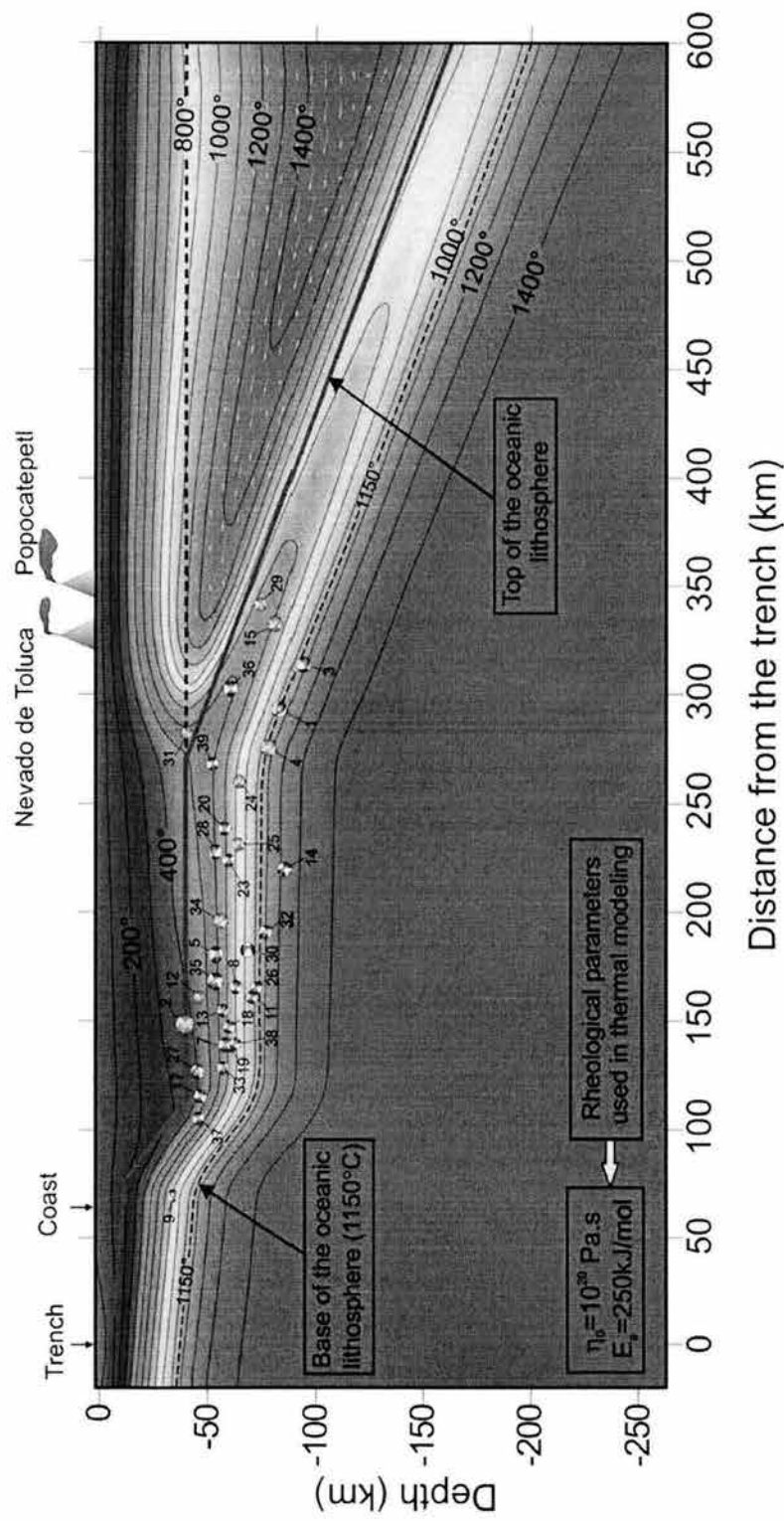
Figure 2
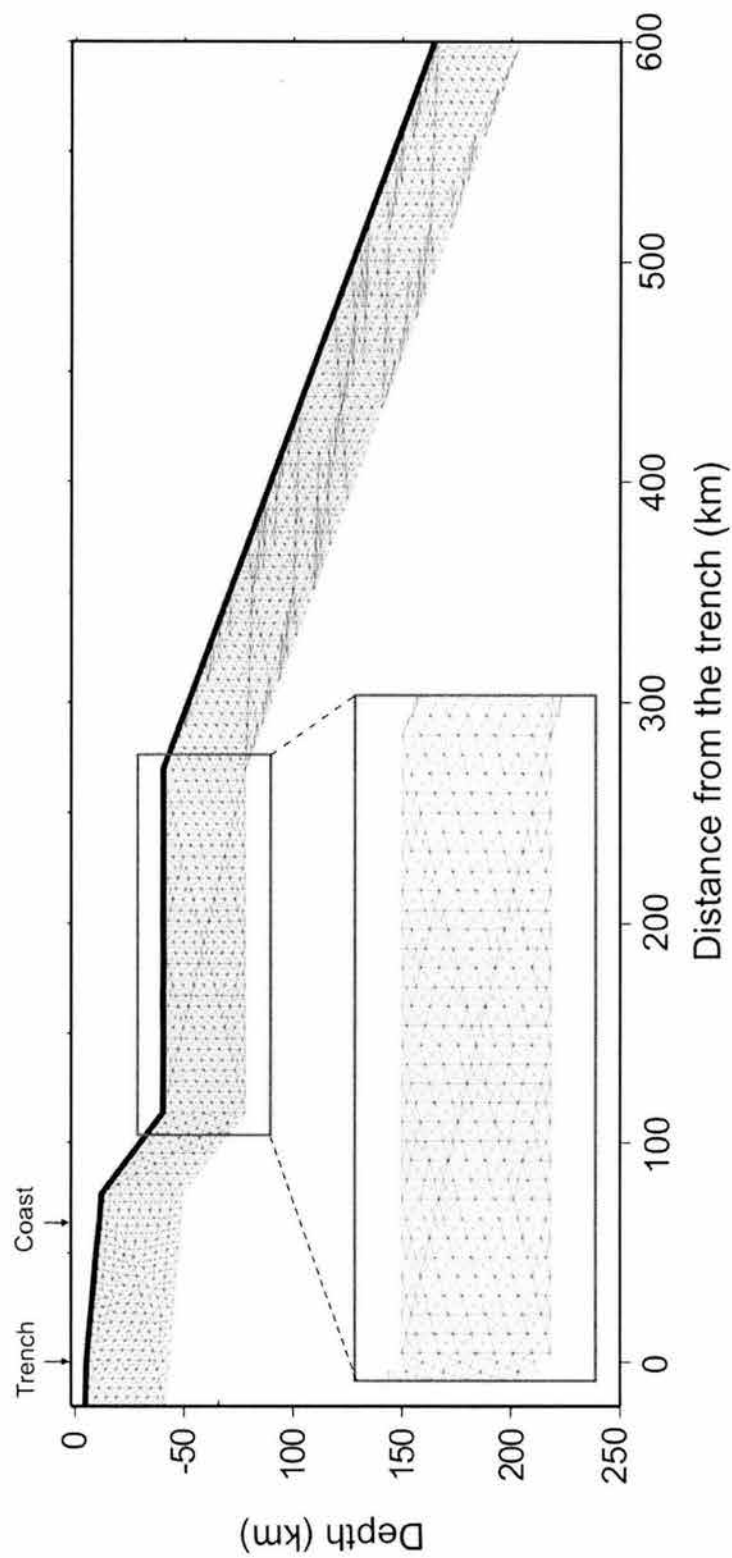
Figure 3
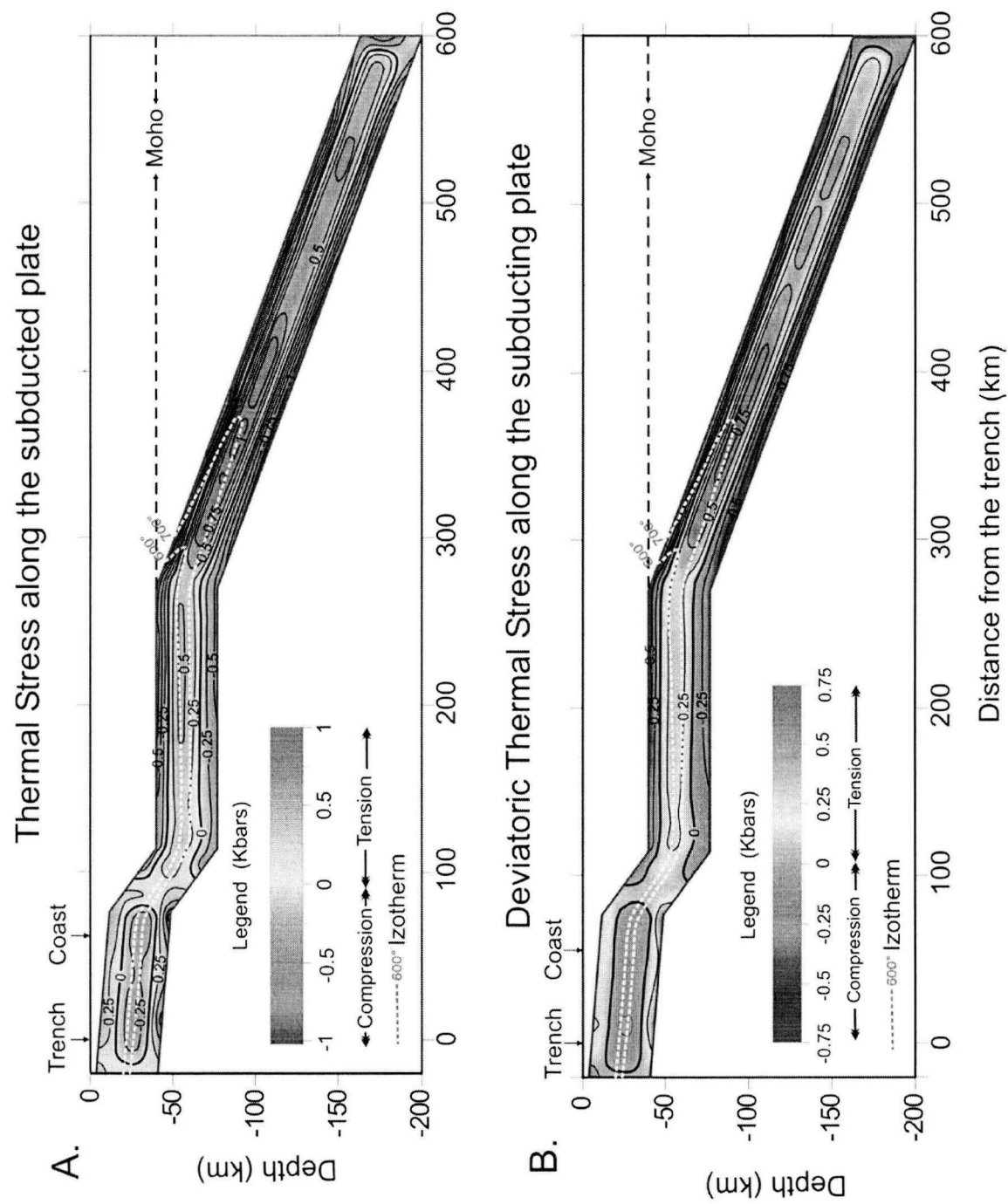
Figure 4

Deviatoric Thermal Stress along the subducting plate with ductile behavior included at the bottom of the slab
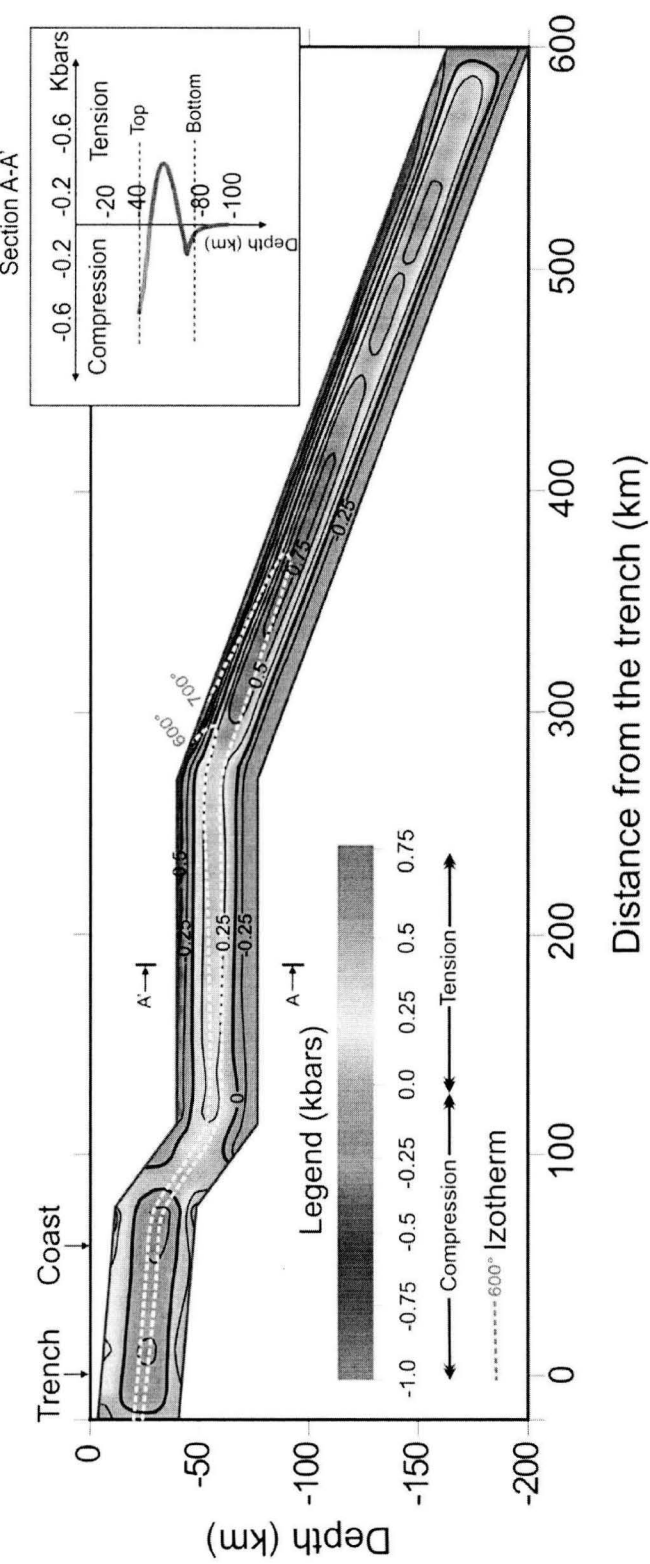
Figure 5
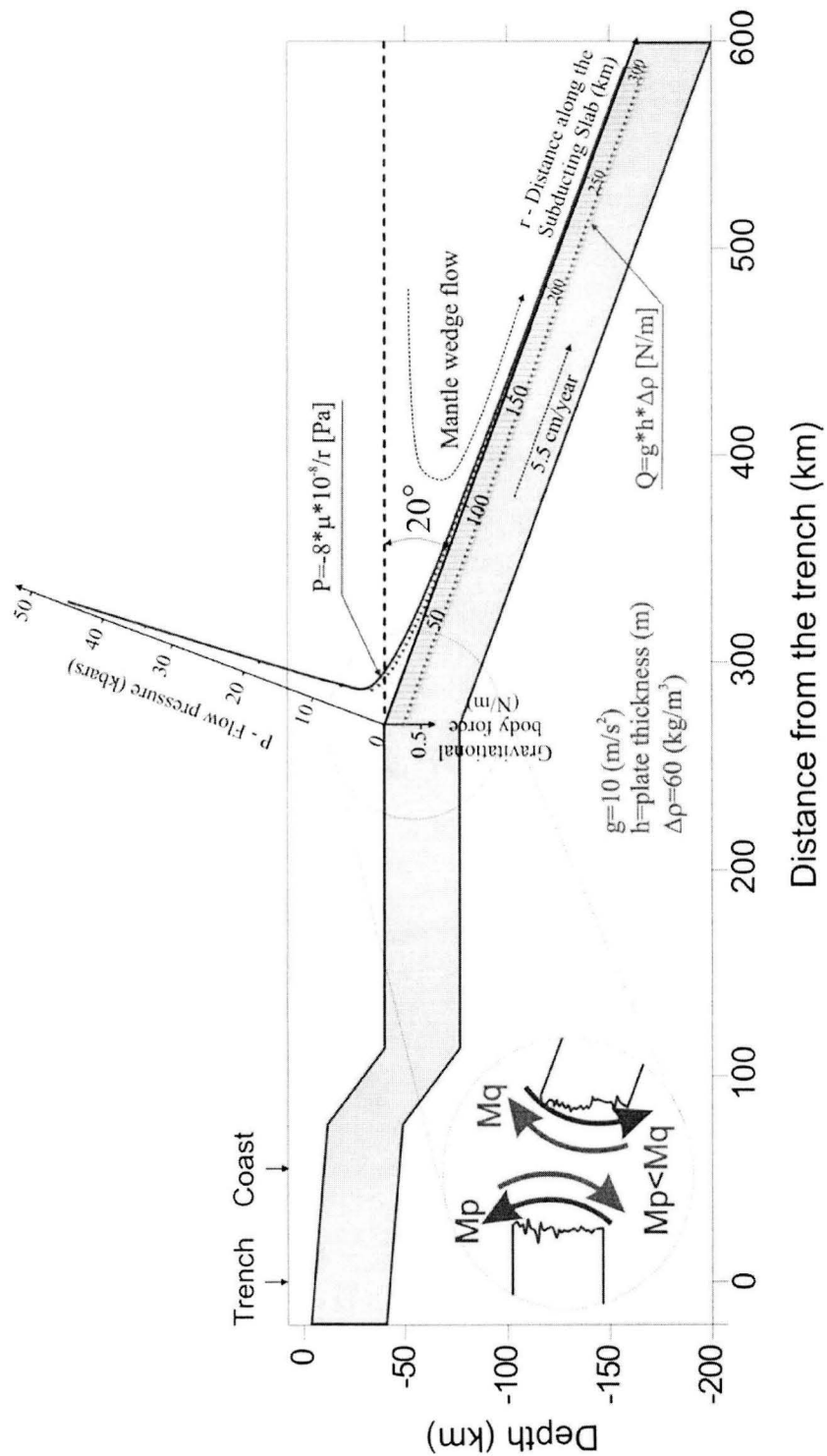
Figure 6
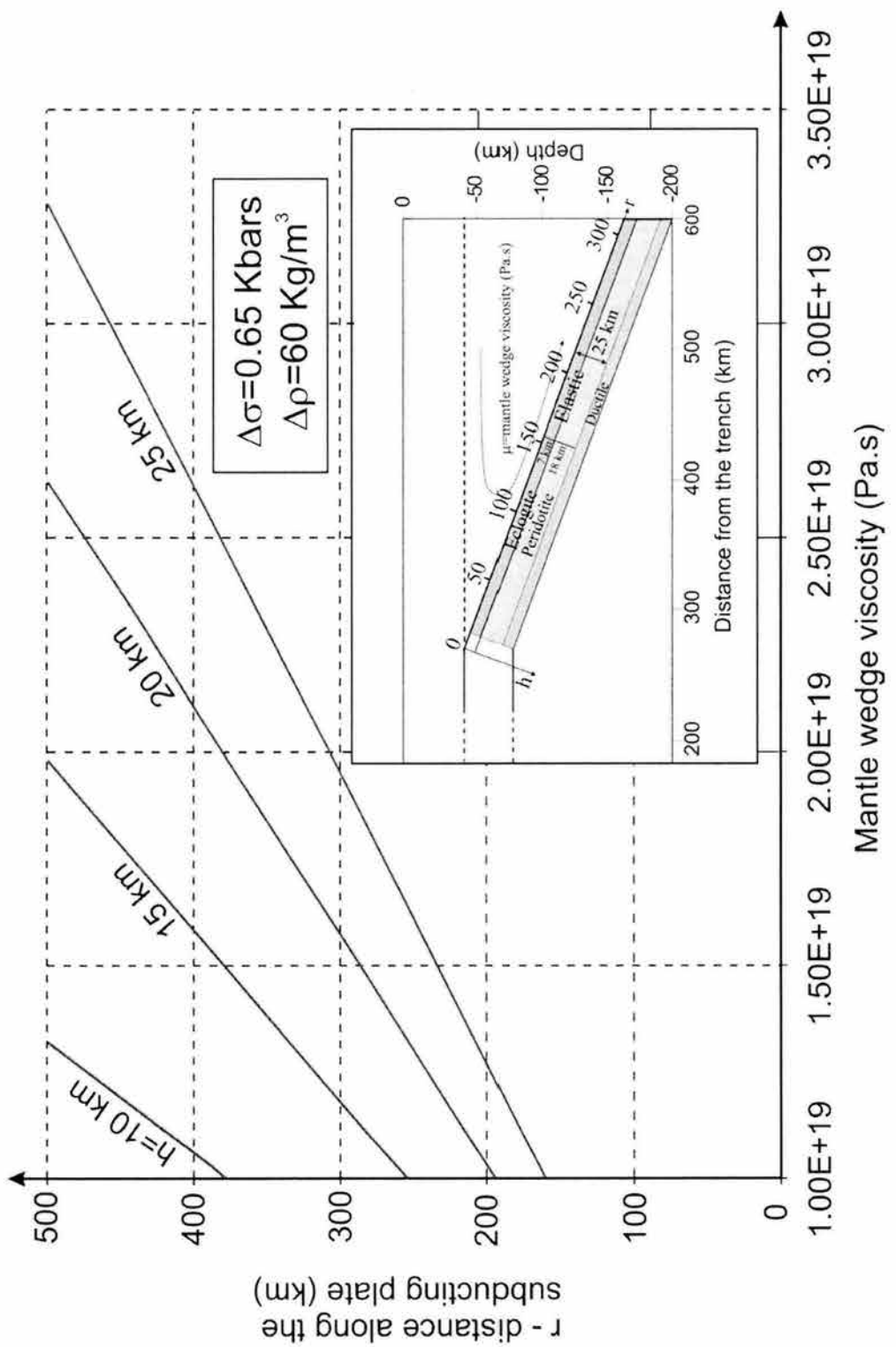
Figure 7
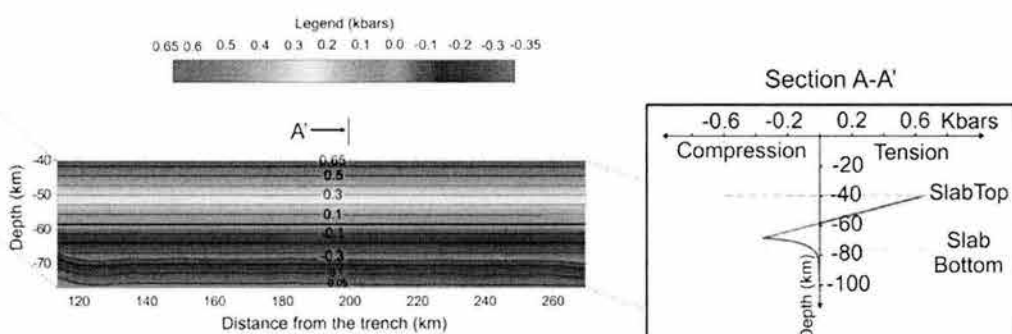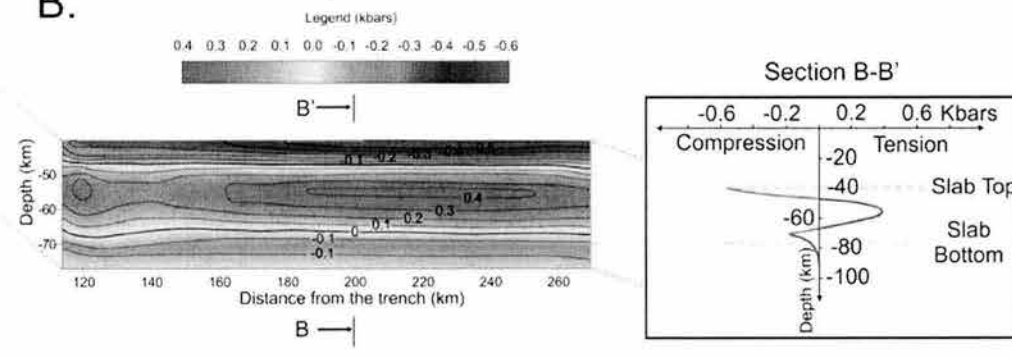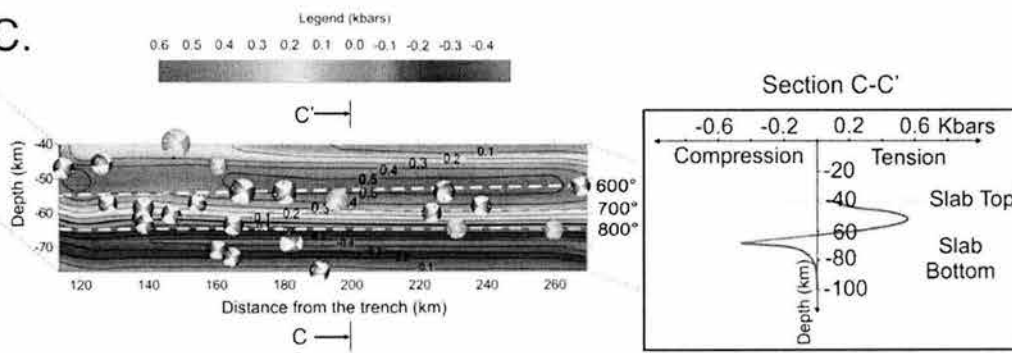
Figure 8

VI. DISCUSIÓN Y CONCLUSIONES

Las estructuras térmicas 2D de las zonas de subducción de la parte central de México y del sur de Kamchatka han sido estudiadas resolviendo un sistema de ecuaciones de Stokes y del flujo de calor con la ayuda de los elementos finitos.

Los modelos numéricos de la distribución de temperatura en el antearco de la parte central de la zona de subducción de Guerrero fueron constreñidos por: los datos de flujo de calor reportados para la superficie; la forma de la interfaz de la placa subducida deducida de los modelos de gravedad, datos de sismicidad y estimaciones recientes de la extensión del acoplamiento a lo largo de la zona de contacto entre las placas de Cocos y Norteamérica. La zona sismogénica modelada, delimitada por las isotermas de 100 °C – 150 °C y 250 °C, coincide con el ancho de la zona de ruptura de los terremotos (subduction thrust earthquakes) en Guerrero. Una pequeña cantidad de calor generada por fricción es necesaria para ajustar la extensión máxima de la zona parcialmente acoplada (la isoterma de 450 °C), de acuerdo con el ancho de la zona acoplada calculado a través de los modelos de deformación. Para ajustar la posición de la isoterma de 450 °C a una distancia de ~ 200 km de la trinchera, que corresponde a una extensión máxima del acoplamiento entre las placas, es necesario tener una interfaz subhorizontal de la placa subducida entre 115 y 270 km desde la trinchera.

El cambio en las secuencias metamórficas en la corteza oceánica subducida se relaciona con la variación del acoplamiento a lo largo del contacto entre las placas, estimado por las observaciones de las deformaciones en superficie durante el periodo intersísmico. Para el rango de temperaturas de 250°C - 450 °C y presiones de 0.6 - 1.3 GPa las facies metamórficas están representadas por jadeita-lawsonita-esquitos azules y epidot-esquitos azules. Los esquitos azules y las facies asociadas en estos rangos de presión y temperatura probablemente se comportan de manera dúctil. Este comportamiento es responsable del acoplamiento parcial de largo plazo y los eventos asísmicos esporádicos. Para temperaturas mayores a 200 °C - 300 °C las rocas preexistentes sufren cambios

marcados en su textura y mineralogía. La presión y el calor son los agentes principales del metamorfismo. El efecto del calor sobre el basalto de la placa oceánica aumenta la ductilidad y el cambio en la composición mineralógica. Las rocas metamórficas foliadas, como los esquites azules, presentan una textura aplanada que favorece el comportamiento dúctil a lo largo de la interfaz de contacto entre las placas. La deformación dúctil que resulta de los esfuerzos de cizalla, que caracterizan a la zona de subducción, es uno de los responsables del desarrollo de la anisotropía en las rocas metamórficas, como en los esquitos azules.

Nuestros modelos muestran una buena correlación entre la posición del punto de bisagra (270 km desde la trinchera) y la ocurrencia de las facies de eclogita en la corteza oceánica de la placa subducida. En estos modelos, la temperatura de 250°C coincide con la extensión máxima de la zona sismogénica (~ 82 km desde la trinchera) y con la existencia de las facies de esquitos azules y de las facies asociadas.

De acuerdo con el diagrama de fases para el MORB, la deshidratación intensiva de la corteza oceánica en subducción debe ocurrir para $T = 250$ °C - 450°C y $P = 0.6 - 1.3$ GPa, liberándose más de 2 wt% H_2O durante el cambio de fase. La ocurrencia de los eventos lentos puede estar relacionada con esta deshidratación.

Las estructuras térmicas debajo de las fajas volcánicas del México central y del sur de Kamchatka dependen de los parámetros reológicos, la viscosidad de referencia, η_0, y la energía de activación, Ea.

Para México, el diagrama de fases para minerales máficos muestra que el fundido de la corteza oceánica basaltica puede ocurrir en las profundidades de ~ 58 km para $\eta_0 = (10^{17} - 10^{20}$ Pa s) y de ~ 80 km para $\eta_0 = 10^{21}$ Pa s. Los sedimentos saturados en agua empiezan a fundirse a profundidades más someras, entre 50 y 55 km. El perfil vertical de la temperatura debajo del volcán Popocatépetl muestra temperaturas bastante grandes para fundir la peridotita hidratada.

En el rango de valores de viscosidad de referencia (10^{17} - 10^{21} Pa s), los sedimentos saturados pueden fundir a profundidades entre 45 y 50 km. La temperatura debajo del volcán Popocatépetl es superior a la del solidus de la peridotita hidratada para todo el rango de las energías de activación para olivino usadas en este estudio (150 - 350 kJ/mol).

La temperatura debajo del CVTM es superior la del solidus para peridotita hidratada, pero es más baja para la peridotita deshidratada. Esto sugiere que la hidratación de la cuña del manto por fluidos liberados de la placa subducida de Cocos es una condición necesaria para producir fundido de la peridotita del manto. Esto está de acuerdo con los resultados de nuestros modelos que muestran que la deshidratación de las rocas metamorfizadas puede ocurrir a profundidades hasta de ~ 80 km. Debido a la transformación de la zoicita y anfíbol en eclogita, ~ 0.6 wt% H_2O puede ser liberado en la cuña del manto para profundidades entre 40 - 60 km.

Los xenolitos del manto han sido encontrados en México cerca de El Peñón, sugiriendo un aporte importante de volátiles de la placa subducida de Cocos. Las rocas de composición calcialcalinas son las más comunes en el CVTM. Esta depleción ocurre probablemente debido a la cristalización de los oxidos de Fe y Ti, que inicialmente puede ser favorecida por la presencia de fluidos en el magma. La gran mayoría de las rocas calcolcalinas en el CVTM está representada por rocas con gran contenido en K_2O y Na_2O, que originalmente pueden representar el fundido parcial en la cuña del manto.

El magma con una composición félsica ha sido encontrado en el campo de volcanes mono-génicos de Chichinautzin, sugiriendo el fundido parcial de la corteza basáltica. Esto esta de acuerdo con los modelos de temperatura que muestran temperaturas > 1100 °C en la base de la corteza continental.

El modelo de transporte del magma usando el movimiento de una burbuja flotante en la cuña del manto nos puede proporcionar una herramienta sencilla para estudiar el origen del volcanismo en el CVTM. Las burbujas flotantes pueden tener su origen en la interfaz entre la placa subducida y la cuña del manto como

una consecuencia de la inestabilidad térmica y/o química. Una cierta distancia a lo largo de la interfaz es necesaria para que el magma se acumule formando una burbuja flotante. Sin duda, en este modelo la zona de salida de las burbujas ha sido elegido justamente debajo (a una profundidad de 70 km) de la estructura volcánica principal (el volcán Popocatépetl). Las burbujas con un diámetro de 10 km pueden alcanzar la base de la corteza continental en ~ 6 Ma, para una viscosidad de ~ $3 \cdot 10^{17}$ Pa s. El tiempo necesario para una burbuja de 1 km en diámetro para alcanzar la corteza continental varia entre 1000 años y 14 Ma, para viscosidades entre 10^{14} Pa s y $5 \cdot 10^{17}$ Pa s. Por lo general, el tiempo de subida para una burbuja flotante diminuye mientras el diámetro aumenta y la viscosidad disminuye.

El modelo dinámico de la trayectoria de la burbuja flotante en la cuña del manto muestra que las trayectorias más *"rápidas"* terminan en el mismo punto (debajo del volcán Popocatépetl, ~ 350 km desde la trinchera) a la base de la corteza continental. Este resultado puede ser interpretado como una posible condición de desarrollo para los estratovolcanes.

Estudios recientes muestran por lo menos dos pulsos magmáticos en un lapso de tiempo de ~ 1Ma en el volcán Nevado de Toluca. El volumen máximo de material extrudido para cada uno de estos pulsos es de ~ 3.5 km^3 (equivalente a una burbuja de ~ 2 km en diámetro). Los dos pulsos presentan una firma magmática de sedimentos fundidos (la anomalía de Ce). De acuerdo con los modelos del capitulo III de este estudio, una burbuja de 2 km diámetro alcanza la base de la corteza continental en ~ 1 Ma para una viscosidad de ~ $2 \cdot 10^{15}$ Pa s. Esta viscosidad muy baja es esencial para que las burbujas alcancen la base de la corteza continental.

El volumen promedio de los conos monogéneticos del CVTM es menor al 1 km^3, valor que corresponde a un diámetro de la burbuja de ~ 1.3 km. Si el origen de los conos monogéneticos es descrito por el modelo de la trayectoria de la burbuja flotante, la viscosidad debería ser $\eta > 5 \cdot 10^{15}$ Pa s para producir las trayectorias *"lentas"*.

Una característica principal de los terremotos intraplaca en la zona de subducción mexicana (para terremotos someros e intermedios, con profundidades entre 35 y 80 km) es su mecanismo focal normal. Estos terremotos ocurren generalmente a distancias de ~ 85 km desde la trinchera. En Guerrero hay un segmento de la placa subducida de forma subhorizontal, con una longitud de ~ 150 km, que contiene la mayoría de los eventos normales intraplaca. Aunque el estado de esfuerzos en la litósfera oceánica subducida es un conjunto de esfuerzos de varios orígenes, como el slab-pull, ridge-push, esfuerzos de mareas, etc., en este estudio se trata sólo de los esfuerzos térmicos y torsión. Usando los nuevos modelos térmicos desarrollados en el capitulo III de este estudio para la zona de Guerrero, los esfuerzos térmicos producidos por una distribución non-uniforme de la temperatura en la placa subducida de Cocos, son calculados usando la técnica de los elementos finitos.

Los resultados muestran que la primera parte somera de la placa subducida está caracterizada por esfuerzos termoelásticos desviatorios compresionales de magnitud baja (~ 0.3 kbars) en su parte central. Luego, el patrón de los esfuerzos térmicos se cambia: un comportamiento extensional para el centro de la placa y uno compresional para las partes de superior e inferior de la placa. El núcleo de la parte subhorizontal de la placa subducida tiene un valor máximo de esfuerzo termoelástico de tensión de ~ 0.4 kbars, mientras para la parte inferior de la placa, muestra unos esfuerzos termoelásticos de extensión de ~ 0.75 kbars. Incluyendo una dependencia entre los esfuerzos y la temperatura alta para la parte inferior de la placa, los esfuerzos termoelásticos de compresión de ~ 0.75 kbars desaparecen debido al comportamiento dúctil de la placa. Aunque los terremotos intraplaca con mecanismo inverso no han sido registrados, hay unos esfuerzos termoelásticos desviatorios compresionales con magnitud de ~ 0.65 kbars en la parte superior de la parte horizontal de la placa subducida. Incluyendo al punto de bisagra un momento de torsión en el sentido de las agujas del reloj que puede producir esfuerzos de tensión de 0.65 kbars en la parte superior de la placa subducida sub-horizontal, se obtiene un nuevo campo de esfuerzos, sin compresión en la parte

superior de este segmento. La falta de la sismicidad compresional en la parte inferior de la placa subducida así como la profundidad máxima de estos terremotos, de ~ 80 km, está de acuerdo con la posición de las isotermas de 700°C - 800°C. Para temperaturas mayores a este intervalo, la placa tiene un comportamiento dúctil y como consecuencia no pueden ocurrir más terremotos intraplaca.

El mismo esquema numérico utilizado para calcular los modelos termo-mecánicos para Guerrero, se usó para otra zona de subducción muy activa y antigua, la zona de subducción del sur de Kamchatka.

Los resultados muestran una temperatura > 1,300 °C y dos posibles fuentes para el fundido: los sedimentos y la peridotita de la cuña del manto debajo del frente volcánico. Una pequeña cantidad de calor producido por fricción (un coeficiente efectivo de fricción de μ = 0.034 o un esfuerzo cortante τ ~ 14 MPa) está añadida al contacto entre la Placa de Pacífico y la Península de Kamchatka. Para cantidades mayores de calor producido por fricción, el fundido de la corteza oceánica basáltica puede ocurrir, pero esto no esta de acuerdo con la falta de magmas adakíticos en el Sur de Kamchatka. El modelo térmico muestra un patrón de velocidad en la cuña del manto debajo del Moho que puede inducir una anisotropía del olivino. Esta anisotropía está de acuerdo con los estudios que muestran que los ejes anisotrópicós rápidós son perpendiculares a la trinchera en el Sur de Kamchatka.

Una deshidratación mayor de la corteza oceánica basáltica (> 5 wt% H_2O liberado) se produce debajo del arco volcánico hasta una profundidad de ~ 100 km. Como consecuencia, justamente arriba de la placa subducida (~ 5 km) puede existir una capa de peridotita y sedimentos fundidos. Esto puede producir inestabilidades térmicas y/o químicas que se pueden acumular en forma de burbujas muy cerca de la superficie de la placa subducida. Basado en esto, el modelo dinámico de la trayectoria de las burbujas en el campo de velocidades de la cuña del manto se aplica también para el sur de Kamchatka.

Para constreñir el tiempo para la subida del magma a través del manto se usan los estudios sobre los desequilibrios de las series isotópicas de U, ^{10}Be y las trazas de los elementos solubles como los isótopos de Th, Sr, y Pb. Los estudios de los desequilibrios de las series isotópicas de U proponen una subida muy rápida del magma (~ 1000 años ~ 60 m/a) desde la superficie de la placa subducida hacia la superficie a través de una red de canales. Otros estudios dan una velocidad del magma < 350 ka (o ~ 17 cm/a), deducida por los datos de los isótopos de Th, Sr, Pb. Otros estudios recientes para los desequilibrios de U-Th-Pa-Ra para Kamchatka discuten sobre la existencia de un modelo dinámico de fundido que no requiere una velocidad muy alta de subida (~ 1 m/a) dentro de la cuña del manto. Una conclusión más contradictoria proviene de los estudios del ^{10}Be que muestran un tiempo de residencia de los isótopos de Be en la cuña del manto de ~ 6 Ma antes de salir a la superficie como actividad volcánica.

Los desequilibrios de los isótopos de U-Th-Pa-Ra, Th, Sr y Pb asimismo como los estudios de ^{10}Be muestran estimaciones muy contradictorias para los tiempos necesarios para el transporte de magma en el manto desde < 350 ka hasta 6 Ma. Esta variabilidad tan alta en el transporte del magma sugiere tasas muy variables en el transporte de varios elementos y/o diferencias reales en los tiempos de transporte probablemente debido a volúmenes variables de fundido en el manto.

El modelo de las burbujas flotantes, a pesar de su simplicidad, tiene la ventaja de explicar un gran rango de tiempos de residencia del magma en la cuña del manto.

En este estudio, se predice la historia térmica de una burbuja flotante de 10 km de diámetro, que se mueve a través de la cuña del manto en un campo térmico, usando las ecuaciones de la conducción del calor. Los resultados muestran que después de ~ 1 Ma, la burbuja "fría" (~ 800°C), con un diámetro de 10 km, se mueve hacia la región más "caliente" de la cuña del manto, en donde hay temperaturas de más de 1300°C. Después de calentarse, la burbuja se mueve hacia arriba hasta la base de la corteza continental, en donde llega con un núcleo

con temperaturas > 900°C. De acuerdo con el solidus para peridotita hidratada la mayor parte del volumen de la burbuja de 10 km (T > 900°C a 1 GPa) podría ser fundido al alcanzar el Moho.

Finalmente, en este estudio, el modelo térmico para el sur de Kamchatka se usa para estimar la anomalía de velocidad en la cuña del manto. Las grandes temperaturas en la cuña del manto debajo del arco volcánico (> 1300°C) producen una anomalía de velocidad negativa muy fuerte de hasta –7% (con respecto al PREM). Por otra parte, la subducción de la placa oceánica fría produce anomalías de velocidad positivas de hasta +4%. La buena correlación que hay entre las perturbaciones en la velocidad debajo del arco volcánico (por lo menos en la magnitud) entre la imagen tomográfica de las llegadas de las ondas P (-7%) y las estimaciones de las anomalías de velocidad de este estudio (~-7%), sugiere que el modelado del campo térmico para la cuña del manto en el sur de Kamchatka ha sido satisfactorio.